

Arminda Maria Marques Almeida

A METHODOLOGICAL FRAMEWORK FOR PAVEMENT DAMAGE ESTIMATION CONSIDERING SIMULATED AXLE LOAD SPECTRA

PhD Thesis in the scientific area of Civil Engineering, speciality of Urbanism, Spatial Planning and Transports,
supervised by Professor Luis Guilherme de Picado Santos and submitted to the Faculty of Sciences and Technology
of the University of Coimbra.

July 2014



UNIVERSIDADE DE COIMBRA



FCTUC FACULDADE DE CIÊNCIAS
E TECNOLOGIA
UNIVERSIDADE DE COIMBRA

A METHODOLOGICAL FRAMEWORK FOR PAVEMENT DAMAGE ESTIMATION CONSIDERING SIMULATED AXLE LOAD SPECTRA

PhD Thesis in the scientific area of Civil Engineering, speciality of Urbanism, Spatial Planning and Transports, submitted to the Faculty of Sciences and Technology of the University of Coimbra.

Author

Arminda Maria Marques Almeida

Supervisor

Luís Guilherme de Picado Santos

Coimbra, July 2014

Part of this research work was made in the scope of the project EMSURE - Energy and Mobility for Sustainable Regions (CENTRO-07-0224-FEDER-002004).

A Methodological Framework for Pavement Damage Estimation considering Simulated Axle Load Spectra

ABSTRACT

Despite being crucial to the economic and social development of any country or region, road freight transport is one of the players responsible for environmental impact of transport increasing in the last decades. In order to minimise these impacts, heavy vehicles have been evolving. Consequently, road pavement design must keep up with it since a road pavement is designed for a foreseeable heavy traffic flow that will pass on the pavement during its considered life time.

The current pavement design procedures convert the heavy traffic flow into a number of Equivalent Standard Axle Load (ESAL) applications. In particular, the Portuguese procedure uses Aggressiveness Factors (AFs) to make that conversion. However, the Portuguese AFs have remained unchanged since at least 1995 and subsequently they are not up-to-date with the evolutions in heavy vehicles.

This thesis addresses the development of a methodological framework for AFs (and pavement damage) estimation. For that, axle load spectra are simulated by using a commercial software TruckSIM[®]. The methodological framework is applied to two case studies, a 'baseline' case study and an 'empty running' case study. For that, two pavement structures and two trucks are considered. The trucks carry different payload weights and run with different travel speeds over road profiles with different levels of roughness. In the third of a three level-hierarchical approach assumed, an application was created which allows the consideration of the degradation of the Asphalt Concrete (AC) modulus and the roughness growth along the pavement design period. It is used to quantify (a) the effect of the initial International Roughness Index (IRI) value of the road profile on the pavement damage, (b) the effect of the AC modulus degradation on the pavement damage and (c) the effect of the roughness growth on the pavement damage.

The results show that the AFs are strongly affected by the truck configuration, the pavement structure, the roughness level of the road profile and the design criterion. For example, the fatigue's AF for a specific truck running fully loaded at 60 km/h over a road profile with IRI equal to 1 m/km is 53% higher in the thinner structure. The initial IRI value and the amount of AC modulus degradation have a great effect on the pavement damage. The AC modulus degradation can increase the pavement damage, at the end of the considered life cycle, within the range of 136% to 391%. In its turn, the roughness growth can increase the pavement damage within the range of 5% to 18%. The 'empty running' case study is intended to show how the methodological framework can be applied to quantify the impact of some transport policies on the pavement damage. When the empty running percentage reduces from 25% to 0%, the pavement damage, at the end of the considered life cycle, increases by more than 26% whichever case is analysed.

These results are closely related to the flexible pavement structures, the trucks and the models considered in the analysis. However, the methodological framework developed has the advantage of being easily applied and extendable to other situations.

Keywords: flexible road pavement, pavement design, truck simulation, axle load spectra, road roughness, aggressiveness factors, pavement damage

Metodologia para Estimar o Dano em Pavimentos considerando a Simulação de Espectros de Carga

RESUMO

Apesar de ser fundamental para o desenvolvimento social e económico de qualquer região ou país, o transporte rodoviário de mercadorias é um dos responsáveis pelo crescimento do impacto ambiental dos transportes nas últimas décadas. No sentido de minimizar estes impactos, os veículos pesados têm vindo a sofrer alterações. É assim necessário que o dimensionamento de pavimentos rodoviários acompanhe essas alterações, uma vez que um pavimento é dimensionado para suportar um determinado fluxo de veículos pesados que irá solicitar o pavimento ao longo do seu tempo de vida.

Os procedimentos de dimensionamento de pavimentos correntemente usados convertem o fluxo de veículos pesados num número equivalente de aplicações de eixos-padrão. Por exemplo, o procedimento usado em Portugal utiliza fatores de agressividade para efetuar essa conversão. No entanto, estes fatores de agressividade permanecem inalterados desde pelo menos 1995, pelo que não têm acompanhado a evolução dos veículos pesados.

Esta tese apresenta o desenvolvimento de uma metodologia para estimar fatores de agressividade (e o dano em pavimentos). Neste sentido foram simulados espetros de carga por eixo usando o programa comercial TruckSIM[®]. A metodologia é aplicada a dois casos de estudo, um caso de estudo de ‘referência’ e um caso de estudo de ‘viagens sem carga’. Para tal, foram consideradas duas estruturas de pavimento e duas configurações de veículos pesados de mercadorias. Os veículos pesados podem transportar cargas com pesos diferentes e circular com velocidades de circulação diferentes sobre pavimentos com diferentes níveis de irregularidade. No terceiro dos 3 níveis da abordagem hierárquica usada, foi criada uma aplicação que permite considerar a degradação do módulo das misturas betuminosas e o aumento da irregularidade do pavimento ao longo do período de dimensionamento. Esta aplicação é usada para quantificar (a) o efeito que a irregularidade inicial do pavimento tem no dano do pavimento, (b) o efeito que a degradação do módulo das misturas betuminosas, ao longo do período de dimensionamento, tem no dano do pavimento e (c) o efeito que o aumento da irregularidade do pavimento, ao longo do período de dimensionamento, tem no dano do pavimento.

Os resultados mostram que os fatores de agressividade são fortemente afetados pelo tipo de veículo, pela estrutura do pavimento, pelo nível de irregularidade do pavimento e pelos critérios de dimensionamento considerados. Por exemplo, o fator de agressividade para o critério de fadiga e para um determinado tipo de veículo, que circula completamente cheio a 60 km/h sobre um pavimento com um Índice de Irregularidade Internacional (IRI) igual a 1 m/km, é 53% superior na estrutura delgada. O valor de IRI inicial e o modelo degradação do módulo das misturas betuminosas têm um grande efeito no dano do pavimento. A degradação do módulo pode aumentar os danos, no fim do ciclo de vida considerado, numa percentagem que pode variar entre 136% e 391%. Por sua vez, a evolução da irregularidade pode aumentar o dano do pavimento entre 5% e 18%. O caso de estudo ‘viagens sem carga’ pretende demonstrar a aplicabilidade da metodologia na quantificação do impacto que algumas políticas de transporte podem ter no dano dos pavimentos. Quando a percentagem de viagens sem carga reduz de 25% para 0%, o dano dos pavimentos, no fim do ciclo de vida considerado, aumenta em mais de 26%, seja qual for o caso analisado.

Os resultados apresentados estão intrinsecamente relacionados com as estruturas de pavimento, as configurações dos veículos pesados e os modelos considerados na análise. Contudo, a metodologia desenvolvida tem a vantagem de poder ser facilmente utilizada e de poder ser facilmente estendida a outras situações.

Palavras-chave: pavimentos rodoviários flexíveis, dimensionamento de pavimentos, simulação de veículos pesados, espectros de carga por eixo, irregularidade longitudinal, fatores de agressividade, dano em pavimentos

ACKNOWLEDGEMENTS

This work would not have been possible without the support of a few very distinguished people.

First, I would like to express my heartfelt gratitude to my supervisor, Professor Luís Guilherme de Picado Santos, for his support, pertinent advice and encouragement along the development of this thesis.

I also have to thank the people I met in the Pavement Mechanics Laboratory (*Laboratório de Mecânica de Pavimentos*) for their support during the laboratorial tests, although they are not part of this thesis.

I would also like to extend my gratitude to all of my colleagues at the Area of the Urbanism, Transports and Transportation Infrastructures for the pleasant work environment and their friendship. In addition, I thank the Department of Civil Engineering of the University of Coimbra for releasing me from my teaching responsibilities for three semesters.

Special thanks go to all of my friends with whom I socialize in my workdays as well as to my office partner, Gonçalo Correia.

I would also like to thank my family and close friends who supported me with constant love, encouragement and patience.

Last, but not least, I need to mention my appreciation and gratitude to my husband, Renato Guimarães who, although working far away from home during the last four years, is always with me.

TABLE OF CONTENTS

LIST OF FIGURES	XIII
LIST OF TABLES	XIX
LIST OF SYMBOLS	XXIII
LIST OF ABBREVIATIONS AND ACRONYMS	XXVII
1 INTRODUCTION	1
1.1 MOTIVATION AND PROBLEM OVERVIEW	1
1.2 OBJECTIVES AND METHODOLOGY	3
1.3 OUTLINE OF THE THESIS	4
1.4 REFERENCES	5
2 VEHICLE-PAVEMENT INTERACTION	7
2.1 INTRODUCTION	7
2.2 PAVEMENT ISSUES	7
2.2.1 Introduction.....	7
2.2.2 Materials characterization	8
2.2.3 Pavement response.....	14
2.2.4 Deterioration mechanisms.....	16
2.2.5 Performance prediction.....	19
2.2.6 Damage accumulation.....	22
2.3 VEHICLE ISSUES.....	23
2.3.1 Introduction.....	23
2.3.2 Vehicles, maximum authorized dimensions and weights	23
2.3.3 Traffic data used in pavement design.....	31
2.3.4 Aggressiveness factors	35
2.3.5 Pavement response for multiple axle configurations.....	38
2.3.6 Dynamic loads	40
2.3.7 Spatial repeatability.....	41
2.3.8 Payload	42
2.3.9 Overloading.....	44
2.3.10 Tyre-pavement contact.....	45
2.3.11 Suspension systems.....	54
2.4 VEHICLE SIMULATION.....	57
2.4.1 Introduction.....	57
2.4.2 Simple vehicle models	58
2.4.3 Complex vehicle models	59
2.4.4 Tyre models	61
2.4.5 Computer programs	65
2.5 MODELLING WHOLE PAVEMENT LIFE	69
2.6 REFERENCES	71
3 ROAD ROUGHNESS	81
3.1 INTRODUCTION	81
3.2 ROUGHNESS MEASUREMENT	82
3.2.1 Introduction.....	82
3.2.2 Reference devices.....	83
3.2.3 Straight edges	84
3.2.4 Profilographs.....	84
3.2.5 Response-Type Road Roughness Measurement (RTRRM) devices	85
3.2.6 Inertial profiler	85

3.2.7	<i>Further trends</i>	86
3.3	ROUGHNESS ANALYSIS	87
3.3.1	<i>Introduction</i>	87
3.3.2	<i>Roughness indices</i>	87
3.3.3	<i>Signal processing techniques</i>	94
3.4	ROAD PROFILE GENERATION	94
3.4.1	<i>Introduction</i>	94
3.4.2	<i>Procedure</i>	95
3.4.3	<i>PSD Models</i>	95
3.5	MODELS TO PREDICT PAVEMENT ROUGHNESS	98
3.5.1	<i>Introduction</i>	98
3.5.2	<i>Prediction model in the Swedish PMS</i>	98
3.5.3	<i>Mechanistic roughness model based on vehicle-pavement interaction</i>	99
3.5.4	<i>MEPDG IRI prediction model</i>	101
3.6	REFERENCES	102
4	BOUNDARY ELEMENT METHOD	105
4.1	INTRODUCTION	105
4.2	BEM FORMULATION	106
4.2.1	<i>Introduction</i>	106
4.2.2	<i>Betti's reciprocal theorem and integral equations</i>	106
4.2.3	<i>Fundamental solutions</i>	107
4.2.4	<i>Numerical implementation</i>	108
4.2.5	<i>Postprocessing</i>	111
4.2.6	<i>Integration</i>	114
4.2.7	<i>Multiple regions</i>	119
4.3	BEM IMPLEMENTATION	121
4.4	VALIDATION OF THE THREE-DIMENSIONAL BEM IMPLEMENTATION	127
4.5	OTHER BEM APPLICATIONS	129
4.5.1	<i>Linear viscoelastic materials</i>	129
4.5.2	<i>Fracture mechanics</i>	130
4.5.3	<i>Elastodynamic problems</i>	131
4.6	REFERENCES	131
5	STUDY APPROACH	135
5.1	INTRODUCTION	135
5.2	TRUCKS' DEFINITION	136
5.3	PAVEMENT STRUCTURES	141
5.4	ROAD PROFILES	144
5.4.1	<i>Generation of road profiles</i>	144
5.4.2	<i>Roughness growth</i>	148
5.5	LOAD PROFILES	151
5.6	EALFs OF THE SIMULATED TRUCKS' AXLES	155
5.7	AGGRESSIVENESS FACTORS (AFs)	157
5.8	THE THREE LEVELS OF THE STUDY APPROACH	167
5.8.1	<i>Introduction</i>	167
5.8.2	<i>Loads per axle</i>	167
5.8.3	<i>AFs of the trucks</i>	168
5.8.4	<i>'Damage' Application</i>	168
5.9	REFERENCES	171
6	CASE STUDIES AND RESULTS	173
6.1	INTRODUCTION	173
6.2	DEFINITION OF THE CASE STUDIES	173
6.2.1	<i>Introduction</i>	173
6.2.2	<i>'Baseline' case study</i>	174
6.2.3	<i>'Empty running' case study</i>	175

6.3	AGGRESSIVENESS FACTORS (AFs) AND PAVEMENT DAMAGE CALCULATION USING THE THREE LEVEL-STUDY APPROACH	176
6.3.1	Introduction	176
6.3.2	Level 1 – Study approach (Loads per axle)	176
6.3.3	Level 2 – Study approach (AFs of the trucks)	179
6.3.4	Level 3 – Study approach (‘Damage’ application)	180
6.3.5	Comparison	181
6.4	PAVEMENT DAMAGE CALCULATION USING THE ‘DAMAGE’ APPLICATION	182
6.4.1	Introduction	182
6.4.2	‘Baseline’ case study	182
6.4.3	‘Empty running’ case study	190
6.5	CONCLUDING REMARKS	193
6.5.1	‘Baseline’ case study	193
6.5.2	‘Empty running’ case study	194
6.6	REFERENCES	195
7	CONCLUSIONS AND FURTHER DEVELOPMENTS.....	197
7.1	INTRODUCTION	197
7.2	CONCLUSIONS.....	198
7.3	FURTHER DEVELOPMENTS	200
7.4	REFERENCES	201

LIST OF FIGURES

Figure 1.1 – Illustration of the trucks: (a) – lorry/truck and (b) – articulated vehicle (Eurostat et al., 2009)	2
Figure 1.2 - Outline of the thesis	5
Figure 2.1 – Back-calculated moduli reductions from BB tests carried out in ALF Mulgrave trial (Collop and Cebon, 1996).....	11
Figure 2.2 - Back-calculated moduli reductions from FWD tests carried out in ALF Mulgrave trial (Collop and Cebon, 1996).....	11
Figure 2.3 - Back-calculated moduli reductions from FWD tests carried out in ALF Callington trial (Collop and Cebon, 1996).....	11
Figure 2.4 – Modulus reduction as a function of cumulative fatigue damage calculated from BB data from the Mulgrave trial (Cebon, 1999)	13
Figure 2.5 - Modulus reduction as a function of cumulative fatigue damage calculated from FWD data from the Mulgrave trial (Cebon, 1999).....	13
Figure 2.6 - Modulus reduction as a function of cumulative fatigue damage calculated from BB data from the Callington trial (Cebon, 1999).....	13
Figure 2.7 – Stages of permanent deformation (NCHRP, 2004)	19
Figure 2.8 – Illustration of the modular concept (adapted from Åkerman and Jonsson (2007))..	27
Figure 2.9 – Summary of studies and trials	28
Figure 2.10 – Total number of vehicles and percentage by type of vehicle	29
Figure 2.11 – Percentage of the two predominant types of vehicle by axle configuration	29
Figure 2.12 – Percentage of the two predominant types of vehicle by load capacity range	30
Figure 2.13 – GVW and payload by load capacity range for the lorry/truck	30
Figure 2.14 - GVW and payload by load capacity range for the articulated vehicle	31
Figure 2.15 – Axle load spectra: (a) single axle and (b) tandem axle (Haider and Harichandran, 2009).....	33
Figure 2.16 – Bimodal mixture distributions (Haider and Harichandran, 2009).....	33
Figure 2.17 – Variation of the axle load spectra (Romanoschi et al., 2011)	34
Figure 2.18 – 80-kN Standard axle load (ESAL).....	35
Figure 2.19 – Summary of schematics for horizontal analysis locations of critical response (NCHRP, 2004).....	39
Figure 2.20 – Definition of DLC (OECD, 1998)	40
Figure 2.21 – Impact factor patterns for several types of vehicles (1 to 9) (O'Connor et al., 2000)	42
Figure 2.22 – Vehicle-kilometre percentage of empty running (OECD, 1998)	43
Figure 2.23 – Calculated load factors for the articulated vehicle with 2+3 axles	44
Figure 2.24 – Examples of dual tyre and wide base tyre (COST 334, 2001).....	46

Figure 2.25 – Tyre size parameters (COST 334, 2001)	46
Figure 2.26 – Tyres of articulated vehicles in the past, present and (possibly) future (COST 334, 2001)	47
Figure 2.27 – Tyre combinations in the articulated vehicle	47
Figure 2.28 – Static contact areas (Beer et al., 2004)	49
Figure 2.29 – Mean ratio tyre width to length as a function of load (Blab, 1999)	50
Figure 2.30 - Mean ratio tyre width to length as a function of inflation pressure (Blab, 1999)....	50
Figure 2.31 – Tyre footprints and modelled contact area of a dual-tyre assembly and a wide-base tyre (Elseifi et al., 2005).....	51
Figure 2.32 – Illustration of the five different ‘scales’ of tyre-pavement interaction (COST 334, 2001)	52
Figure 2.33 – Measured vertical contact stresses of the 315/80R22.5-tyre (Beer et al., 2005).....	53
Figure 2.34 - Measured lateral contact stresses of the 315/80R22.5-tyre (Beer et al., 2005)	54
Figure 2.35 - Measured longitudinal contact stresses of the 315/80R22.5-tyre (Beer et al., 2005)	54
Figure 2.36 – Different springs in suspension systems (Hendrickson@, 2013)	55
Figure 2.37 – Classification of the suspension systems in terms of the number of axles (Hutch@, 2013)	55
Figure 2.38 – Simple vehicle models (adapted from Cebon (1999)).....	58
Figure 2.39 – Generalized multibody vehicle model: suspension forces (F_s), tyre forces (F_t) and gravitational forces (F_g) (based on Cebon (1999)).....	61
Figure 2.40 – Four categories of possible types of approach to develop a tyre model (Pacejka, 2006)	62
Figure 2.41 – The phenomena of the tyre rolling on rough roads (adapted from Zegelaar (1998))	64
Figure 2.42 – Tyre-road interface models (Zegelaar, 1998)	64
Figure 2.43 –The Run Control screen	67
Figure 2.44 – The four main components of TruckSIM [®] (MSC, 2009b).....	68
Figure 2.45 – Model option droop-down list (from software screen).....	68
Figure 2.46 – Co-simulation of VS solver and third-party tyre model (MSC, 2009a).....	69
Figure 2.47 – COST action 333’s incremental procedure (COST 333, 1999).....	70
Figure 2.48 – WLPPM developed by Collop and Cebon (adapted from Cebon (1999))	70
Figure 3.1 – Texture categories defined by wavelengths (TCPSC@, 2014)	82
Figure 3.2 – Rod and level (Sayers and Karamihas, 1998).....	83
Figure 3.3 – Dipstick (Sayers and Karamihas, 1998)	83
Figure 3.4 – ARRB walking profilometer (ARRB@, 2014).....	84
Figure 3.5 – Rolling straight edge (Scientific@, 2014)	84
Figure 3.6 – California profilograph (Chiu et al., 2003).....	85

Figure 3.7 – Response-type systems: (a) the BPR roughometer, (b) the Mays ridemeter (Sayers and Karamihas, 1998).....	85
Figure 3.8 – Inertial profiler (Sayers and Karamihas, 1998).....	86
Figure 3.9 – Two inertial profilers in use in Portugal	86
Figure 3.10 – P3-AT autonomous robot (Chang et al., 2009)	86
Figure 3.11 – Quarter-car model and golden car parameters (Yu et al., 2006)	87
Figure 3.12 – IRI ranges for different classes of roads (adapted from Sayers and Karamihas (1998))	88
Figure 3.13 – Half-car model (Sayers and Karamihas, 1998)	90
Figure 3.14 – Full-car simulation model (Capuruço et al., 2005).....	91
Figure 3.15 – Speed-related IRI limits, considering the a_{wz} comfort levels established in ISO 2631 (Cantisani and Loprencipe, 2010).....	91
Figure 3.16 – Comparison of the IRI transfer function with a typical truck-ride transfer function both as a function of temporal frequency and as a function of spatial frequency (Prem et al., 2000b).....	92
Figure 3.17 – Used model for truck ride prediction (Prem et al., 2000b)	92
Figure 3.18 – Calculation of the RQI (MDOT, 1996).....	93
Figure 3.19 – Classification of roads (ISO 8608, 1995).....	97
Figure 4.1 – Quadratic Serendipity element	109
Figure 4.2 – Contour lines of an integration error of 10^{-3} and Gauss order of 4 (Eberwien et al., 2005).....	117
Figure 4.3 – Subelements for numerical integration when P_i is a corner node of the element (adapted from Beer et al. (2008)).....	119
Figure 4.4 - Subelements for numerical integration when P_i is a mid-side node of the element (adapted from Beer et al. (2008)).....	119
Figure 4.5 – Interaction between the BEM-Application and the GID [®] software	121
Figure 4.6 - GID problem type: BEM_applications.....	122
Figure 4.7 – The three regions/layers: AC layer, granular layer and subgrade	122
Figure 4.8 – Input file: CalculationFile.dat.....	123
Figure 4.9 – Output file: ProjectName.post.res.....	126
Figure 4.10 – Post-processing with the GID [®] software: Z-displacements	126
Figure 4.11 - Post-processing with the GID [®] software: YY-Strain.....	126
Figure 4.12 - Post-processing with the GID [®] software: ZZ-Strain.....	127
Figure 4.13 – Pavement structures	127
Figure 4.14 – Comparison between the BEM-Application and the BISAR [®] for the thin structure	128
Figure 4.15 – Comparison between the BEM-Application and the BISAR [®] for the thick structure	129
Figure 4.16 – The three modes of crack failure (adapted from Aliabadi (2002)).....	130

Figure 5.1 – Simulated vehicles.....	137
Figure 5.2 – The ‘TruckSIM Run Control’ screen for the ‘H5-Truck’.....	137
Figure 5.3 – The ‘Vehicle: Loaded Combination’ screen for the ‘H5-Truck’	138
Figure 5.4 – The ‘Vehicle: Lead Unit with 2 axles’ screen	138
Figure 5.5 - The ‘Payload: Box Shape’ screen.....	139
Figure 5.6 – Loads per axle of the ‘H5-Truck’ when fully loaded (adapted from Glaeser (2010))	139
Figure 5.7 – Tyres considered in the simulations	140
Figure 5.8 – Regression lines for tyre-pavement contact area	141
Figure 5.9 – Pavement structures.....	141
Figure 5.10 - Definition of the adapted models.....	143
Figure 5.11 – AC modulus degradation models	144
Figure 5.12 – Generated road profiles for each ISO class	145
Figure 5.13 - Generated road profiles for each ISO class (detail of the first 100 m)	145
Figure 5.14 – PSD function of each generated road profile.....	146
Figure 5.15 - Generated road profiles with specific IRI values.....	147
Figure 5.16 - Generated road profiles with specific IRI values (detail of the first 100 m).....	148
Figure 5.17 - PSD of each road profile	148
Figure 5.18 – Evolution of IRI in accordance with the mechanistic roughness model based on vehicle-pavement interaction – $IRI=f(IRI_0)$	149
Figure 5.19 - Evolution of IRI in accordance with the mechanistic roughness model based on vehicle-pavement interaction – $IRI_{i+1}=f(IRI_i)$	149
Figure 5.20 - Evolution of IRI in accordance with the prediction model of the Swedish PMS..	151
Figure 5.21 – Load profiles for each axle of a H5-Truck running fully loaded at 80 km/h over a road profile with IRI equal to 2 m/km	152
Figure 5.22 – ANOVA’s summary output for the axle 1 of the ‘H5-Truck’	153
Figure 5.23 - DLCs for the axles of the H5-Truck’s tractor.....	154
Figure 5.24 - DLCs for the axles of the H5-Truck’s semi-trailer.....	154
Figure 5.25 – DLCs for the axles of the F1-Truck	155
Figure 5.26 – Calculated EALFs for the simulated trucks’ axles (80-kN axle load)	156
Figure 5.27 - 80-kN non-standard axle load.....	157
Figure 5.28 – F1-Truck’s AFs for the thin structure.....	159
Figure 5.29 – H5-Truck’s AFs for the thin structure	159
Figure 5.30 – F1-Truck’s AFs for the thick structure	160
Figure 5.31 – H5-Truck’s AFs for the thick structure	160
Figure 5.32 – Calculated versus predicted AFs for the thin structure	162
Figure 5.33 – Calculated versus predicted AFs for the thick structure.....	163

Figure 5.34 – AFs for the thin structure considering roughness growth.....	164
Figure 5.35 – AFs for the thick structure considering roughness growth	164
Figure 5.36 – Calculated versus predicted AFs for the thin structure (IRI growth)	166
Figure 5.37 – Calculated versus predicted AFs for the thick structure (IRI growth).....	167
Figure 5.38 - Interface of the ‘Damage’ application	169
Figure 5.39 – Flowchart of the incremental procedure	170
Figure 6.1 – ‘Baseline’ case study for the thin structure.....	174
Figure 6.2 – ‘Baseline’ case study for the thick structure	175
Figure 6.3 – Comparison of the results from the three levels of the hierarchical study approach	182
Figure 6.4 – Effect of initial roughness on the damage of the thin structure ($E=E_0$ and IRI does not grow).....	183
Figure 6.5 - Effect of initial roughness on the damage of the thick structure ($E=E_0$ and IRI does not grow).....	183
Figure 6.6 – Isolated effect of the AC modulus degradation models on the damage of thin structure (IRI=0 m/km).....	184
Figure 6.7 - Isolated effect of the AC modulus degradation models on the damage of the thick structure (IRI= 0 m/km).....	185
Figure 6.8 – Degradation of the AC modulus for both structures.....	185
Figure 6.9 – Combined effect of both AC modulus degradation and initial roughness on the damage of the thin structure.....	186
Figure 6.10 – Combined effect of both AC modulus degradation and initial roughness on the damage of the thick structure.....	187
Figure 6.11 – Degradation of the AC modulus for the thin structure	188
Figure 6.12 - Degradation of the AC modulus for the thick structure	188
Figure 6.13 – Effect of roughness growth on the damage of the thin structure.....	189
Figure 6.14 – Effect of roughness growth on the damage of the thick structure.....	189
Figure 6.15 – Effect of reduction in empty running percentage on the damage of the thin structure	190
Figure 6.16 –Effect of reduction in empty running percentage on the damage of the thick structure	191
Figure 6.17 - Effect of reduction in empty running percentage on the pavement damage of the thin structure (0 % of overloaded trucks)	192
Figure 6.18 - Effect of reduction in empty running percentage on the pavement damage of the thick structure (0 % of overloaded trucks).....	192
Figure 6.19 - Pavement damage at the end of the pavement design period considering the effect of different initial roughness values and different AC modulus degradation models.....	193
Figure 6.20 - Pavement damage at the end of the pavement design period considering the effect of roughness growth during the pavement design period.....	194

Figure 6.21 - Pavement damage at the end of the pavement design period considering the effect of reduction in empty running percentage..... 195

LIST OF TABLES

Table 2.1 – JAE classification of road vehicles (adapted from Lima and Quaresma (1999)).....	24
Table 2.2 – Heavy vehicles classification according to the number and arrangement of the axles (adapted from Lima and Quaresma (1999)).....	25
Table 2.3 - Maximum authorized vehicle weights (Decree Law No. 133/2010).....	26
Table 2.4 - Maximum authorized axle weights (Decree Law No. 203/2007)	26
Table 2.5 - Maximum authorized dimensions (Decree Law No. 133/2010)	26
Table 2.6 – Traffic data of the Portuguese manual (JAE, 1995).....	32
Table 2.7 – AFs for each subclass (Lima and Quaresma, 1999).....	37
Table 2.8 – Critical pavement responses (NCHRP, 2004)	39
Table 2.9 – Density values of common commodities (OECD, 2011).....	43
Table 2.10 – Contact area sizes of some Michelin tyres (COST 334, 2001).....	48
Table 2.11 – Contact area size (‘gross and net contact area’) of some Michelin tyres (COST 334, 2001).....	48
Table 2.12 – Statistics of contact area-width measurements (Blab, 1999).....	49
Table 2.13 – Contact area of wide base tyres manufactured by Michelin (adapted from Salgado and Kim (2002)).....	50
Table 2.14 – Scales considered by the COST action 334 for tyre-pavement interaction (COST 334, 2001).....	52
Table 2.15 – Classification of the suspension systems.....	55
Table 3.1 – Road classification based on $S_k(\gamma_0)$ values (ISO 8608, 1995)	96
Table 3.2 - Road classification based on $S_k(\Omega_0)$ values (ISO 8608, 1995).....	97
Table 3.3 – Default values in the Swedish roughness prediction model (Lang, 2001).....	99
Table 3.4 – Material properties used in the roughness model development (Saleh et al., 2000)	100
Table 3.5 – Calibration factors for various climatic zones (Saleh and Mamlouk, 2002).....	101
Table 4.1 – Intrinsic coordinates of nodes.....	109
Table 4.2 – Singular integrals classification (adapted from Thöni (2009)).....	115
Table 4.3 – Number of Gauss points (Beer et al., 2008)	117
Table 4.4 – Number of Gauss points for different integration errors.....	118
Table 4.5 – Properties of the materials	127
Table 5.1 - Payload weights for the ‘H5-Truck’	139
Table 5.2 – Payload weights for the ‘F1-Truck’	139
Table 5.3 – Tyre-pavement contact areas (adapted from COST 334 (2001))	140
Table 5.4 – Widths of the tyre-pavement contact areas (adapted from COST 334 (2001)).....	140
Table 5.5 – Parameters used in the AC modulus calculation	142

Table 5.6 – AC modulus for different travel speeds	142
Table 5.7 – Materials’ characteristics	142
Table 5.8 - Wavelength ranges necessary to excite the modes of vibration at different travel speeds	144
Table 5.9 – ISO 8608 classes and corresponding IRI values	146
Table 5.10 – Some ISO 8608 classes and corresponding IRI values (Harris et al., 2010)	147
Table 5.11 – $S_u(\gamma_0)$ values of the specific road profiles	147
Table 5.12 – AADTT limits in the design lane considered for the Swedish model	150
Table 5.13 - AADTT limits in the design lane defined in the MACOPAV	150
Table 5.14 – Roughness pavement performance considered for D-class of the Swedish model	151
Table 5.15 – Roughness pavement performance considered for G-class of the Swedish model	151
Table 5.16 – Regression models for the axle loads	153
Table 5.17 – Trucks’ GVW values in tonnes	153
Table 5.18 - Tyre-pavement contact area for the simulated trucks’ axles considering an 80-kN axle load	155
Table 5.19 – Pavement damage	158
Table 5.20 – Pavement damage (AC modulus equal to 4000 MPa)	158
Table 5.21 – Regression coefficients and R-squared values for the thin structure	162
Table 5.22 – Regression coefficients and R-squared values for the thick structure	163
Table 5.23 – Regression coefficients and the R-squared values for the thin structure considering IRI growth	165
Table 5.24 – Regression coefficients and the R-squared values for the thick structure considering IRI growth	166
Table 6.1 - Percentage of different classes of trucks for two roads with different category	174
Table 6.2 – Load factor for the thin structure	175
Table 6.3 - Load factor for the thick structure	175
Table 6.4 – Definition of the empty running percentages and corresponding load factors	175
Table 6.5 – Calculated axle loads	176
Table 6.6 – Theoretical EALFs for the fatigue design criterion	177
Table 6.7 – Theoretical EALFs for the rutting design criterion	177
Table 6.8 – Number of truck passes	178
Table 6.9 – AFs of the mixed truck traffic flow for Level 1 - Study approach	178
Table 6.10 – Pavement damage for Level 1 - Study approach	179
Table 6.10 – Fatigue AFs for the thin structure	179
Table 6.11 – Rutting AFs for the thin structure	179
Table 6.12 – Fatigue AFs for the thick structure	179
Table 6.13 – Rutting AFs for the thick structure	180

Table 6.15 – AFs of the mixed truck traffic flow for Level 2 - Study approach	180
Table 6.16 - Pavement damage for Level 2 - Study approach.....	180
Table 6.9 – AFs of the mixed truck traffic flow for Level 3 - Study approach	181
Table 6.15 – Pavement damage for Level 3 - Study approach	181
Table 6.16 – Increases in the pavement damage with the AC modulus degradation.....	185
Table 6.17 – Increase ranges in the pavement damage when initial IRI value rises from 0 to 5 m/km.....	186
Table 6.18 – Definition of the empty running percentage without overloaded trucks and respective load factors	191

LIST OF SYMBOLS

- [C]** Damping matrix
[K] Stiffness matrix
[M] Mass matrix; Inertia matrix
{n} Outward normal vector
{q} Vector of generalized coordinates
{Q} Vector of generalized forces
{r} Position vector
{t} Vector of tractions
{t_n^e} Vector of tractions of the n-th node of the element e
{u} Vector of displacements
{x_n^e} Vector of displacements of the n-th node of the element e
{v_i'} Direction vector of the local coordinate system
{x} Vector of coordinates
{x_n^e} Vector of coordinates of the n-th node of the element e
a Half axle spacing
a, b, c Regression coefficients
AADT_h Annual Average Daily Heavy-Traffic
Age Pavement age
a_i Weighting factors
a_{wz} Vertical weight RMS acceleration
C Adjustment factor
c_s Suspension damping
c_t Tyre damping
D Damage
DP Design Period
E Young's modulus
E₀ Initial modulus of bituminous mixture
E_g Modulus of granular materials
E_m Modulus of bituminous mixture
E_s Modulus of subgrade
f(X_{i,j}) Uncalibrated predicted roughness value of pavement section j at age i
FC_t Area of fatigue cracking
F_g Gravitational forces
F_i External force
FI Average annual freezing index
F_s Suspension forces
F_t Tyre forces
G Modulus of elasticity in shear

- G_a** White-noise acceleration
- G_e** White-noise elevation
- g_h** Annual average growth rate of heavy-vehicles
- G_s** White-noise slope
- H** Asphalt concrete layer thickness
- h_g** Thickness of granular layer
- hⁱ** Thickness of the sublayer i
- IRI₀** Initial IRI value
- I_u** Pitch Inertia
- J** Jacobian
- k** Constant
- K** Calibration factor
- k_i** Regression coefficients
- k_{pd}** Parameter related to pavement survival probability (permanent deformation)
- k_s** Suspension stiffness; Suspension spring rate
- k_t** Tyre stiffness
- L** Element length
- m_s** Sprung mass
- m_u** Unsprung mass
- N** Number of load repetitions (cycles); Number of data points in a signal
- NE** Number of elements of the problem
- N_f** Number of repetitions to fatigue cracking
- N_n** Shape function of the n-th node
- NNE** Number of nodes per element
- N_{pd}** Number of repetitions to permanent deformation
- P** Axle load
- P** Source point
- P_a** Internal point
- pen** Penetration of bitumen
- PG1** Number of Gauss points in ξ_1 -direction
- PG2** Number of Gauss points in ξ_2 -direction
- PI** Penetration Index
- PII** Percent plasticity index of the soil
- Precip** Average annual precipitation or rainfall
- PV_{i,j}** Calibrated predicted roughness value of pavement section j at age i
- Q** Field point
- q_i** Generalized coordinate
- Q_i** Generalized force
- r** Distance between the source point P and the field point Q
- R** Distance between the source point P and the element

-
- RD** Permanent deformation
RD_a Average ruth depth
RD_g Permanent deformation (granular materials and subgrade soils)
s Scaling parameter
S_b Stiffness of bitumen
SF Site factor
S_k Spectral coefficients
t Time of loading
T Temperature; Kinetic energy
TC Length of transverse cracking
t_i Traction in the i-direction
T_{ij}(P,Q) Traction in the j-direction at point Q due to a unit point force acting in the i-direction at P
T_{rb} Softening point of bitumen
u_i Displacement in the i-direction
U_{ij}(P,Q) Displacement in the j-direction at point Q due to a unit point force acting in the i-direction at P
V_a Volume percentage of aggregates
V_b Volume percentage of bitumen
V_i Variance of elevations of profile i
W Work
w Exponent of the fitted PSD
Wp₁ Weight related to the abscissa $\xi_1(p_1)$
Wp₂ Weight related to the abscissa $\xi_2(p_2)$
x_i' Local coordinate system
X_{ij} Explanatory factors
Z_k Discrete Fourier transform of z_r
z_r Discrete time series (road profile)
- α** Model parameter
 β Model parameter
 β_i Auxiliary variables; calibration parameters
 γ Model parameter; Wavenumber (cycles/m)
 γ_0 Reference wavenumber (cycles/m)
 Γ Boundary
 δ Model parameter
 δ_i Virtual displacement
 δ_{ij} Kronecker delta
 Δ Sampling interval
 ϵ_0 Material property

- ϵ_f Fatigue strain
- ϵ'_{ij} Strains in the local coordinate system
- ϵ_{pd} Permanent deformation strain
- ϵ_{pd}^i Permanent deformation strain in sublayer i
- ϵ_r Resilient strain
- ϵ_v Average vertical resilient strain
- ρ_i Material properties
- ξ_i Local coordinate system
- σ'_{ij} Stresses in the local coordinate system
- ν Poisson's ratio
- ϕ_k Phase angles
- ω Damage parameter
- Ω Angular spatial frequency (rad/m)
- Ω_0 Reference angular spatial frequency (rad/m)

LIST OF ABBREVIATIONS AND ACRONYMS

AADT	Annual Average Daily Traffic
AADT_h	Annual Average Daily Heavy-Traffic
AASHO	American Association of State Highway Officials
AASHTO	American Association of State Highway and Transportation Officials
ABS	Antilock Brake System
AC	Asphalt Concrete
AF	Aggressiveness Factor
ALF	Accelerated Loading Facility
ANOVA	Analysis of variance
ARRB	Australian Road Research Board
BB	Benkelman Beam
BEM	Boundary Element Method
BPR	Bureau of Public Roads
CBR	California Bearing Ratio
CEC	Commission of the European Communities
CIMNE	International Centre for Numerical Methods in Engineering
CWT	Continuous Wavelet Transform
DD	Displacement Discontinuity
DEM	Discrete Element Method
DFT	Discrete Fourier Transform
DIVINE	Dynamic Interaction between Vehicles and Infrastructure Experiment
DLC	Dynamic Load Coefficient
DLI	Dynamic Load Index
DLSC	Dynamic Load Sharing Coefficient
DOF	Degrees-Of-Freedom
DWT	Discrete Wavelet Transform
EALF	Equivalent Axle Load Factor
EC	European Commission
EMS	European Modular System
ERD	Engineering Research Division
ESAL	Equivalent Standard Axle Load
ESP	Electronic Stability Programme
EU	European Union
FEM	Finite Element Method
FEP	Finite Element Program
FFT	Fast Fourier Transform
FRI	Full-car Roughness Index
FT	Fourier Transform
FTire	Flexible Structure Tyre
FWD	Falling Weight Deflectometer
GMR	General Motor Researches
GPS	Global Positioning Systems

GVW	Gross Vehicle Weight
HITL	Hardware-In-The-loop
HMA	Hot Mix Asphalt
HRI	Half-car Roughness Index
HVS	Heavy Vehicle Simulator
IDFT	Inverse Discrete Fourier Transform
INE	Instituto Nacional de Estatística (Statistics Portugal)
IRI	International Roughness Index
IRRE	International Road Roughness Experiment
ITF	International Transport Forum
JAЕ	Junta Autónoma de Estradas (former Portuguese road administration)
LHVs	Longer and Heavier Vehicles
LNEC	Laboratório Nacional de Engenharia Civil (National Laboratory of Civil Engineering)
LSC	Load Sharing Coefficient
LTPP	Long-Term Pavement Performance
MB	‘Macadame Betuminoso’
MBD	‘Mistura Betuminosa Densa’
MBS	MultiBody System
MEPDG	Mechanistic-Empirical Pavement Design Guide
MPR	Mean Panel Rating
MS-WIM	Multiple Sensor - Weight In Motion
NCHRP	National Cooperative Highway Research Program
OECD	Organisation for Economic Co-operation and Development
OTEP	Observatório Transfronteiriço Espanha/Portugal (Spain/Portugal cross-border observatory)
PI	Profile Index
PMS	Pavement Management System
ProVAL	Profile Viewing and AnaLysis
PSD	Power Spectral Density
PSI	Present Serviceability Index
PSR	Present Serviceability Rating
RMS	Root Mean Square
RN	Ride Number
RQI	Ride Quality Index
RTRRM	Response-Type Road Roughness Measurement Device
RTS	Real-Time Simulation
SPSS	Statistical Package for Social Science
SSR	Statistical Spatial Repeatability
STFT	Short-Time Fourier Transform
S-VECD	Simplified - Viscoelastic Continuum Damage
SWIFT	Short Wavelength Intermediate Frequency Tyre
TRI	Truck Ride Index
UK	United Kingdom
UMTRI	University of Michigan Transportation Research Institute

VECD Viscoelastic Continuum Damage
VPI Vehicle-Pavement Interaction
VRSPTA Vehicle-Road Surface Pressure Transducer Array
VS VehicleSim
WAVE Weight-in-motion of Axles and Vehicles for Europe
WIM Weight-In-Motion
WLPPM Whole-Life Flexible Pavement Performance Model
WT Wavelet Transform

AL Albania
AM Armenia
AT Austria
AZ Azerbaijan
BA Bosnia and Herzegovina
BE Belgium
BG Bulgaria
BY Belarus
CH Switzerland
CY Cyprus
CZ Czech Republic
DE Germany
DK Denmark
EE Estonia
EL Greece
ES Spain
FI Finland
FR France
GE Georgia
HR Croatia
HU Hungary
IE Ireland
IS Iceland
IT Italy
LT Lithuania
LU Luxembourg
LV Latvia
MD Moldova
ME Montenegro
MK The former Yugoslav Republic of Macedonia
MT Malta
NL Netherlands
NO Norway
PL Poland
PT Portugal
RO Romania

RS Serbia
RU Russia
SE Sweden
SI Slovenia
SK Slovakia
TR Turkey
UA Ukraine
UK United Kingdom
XK Kosovo

1 INTRODUCTION

1.1 MOTIVATION AND PROBLEM OVERVIEW

Freight transport is crucial to the economic and social development of any country or region. However, it also comes with environmental distresses. Therefore, a compromise between greater efficiency, higher productivity and lower environmental impacts of freight transport should be searched.

The freight transport from door-to-door by rail or water alone is limited. Consequently, the road freight transport is indispensable to the freight task. It may be used throughout, from the point of origin to the final destination, or it may serve at various links in the chain, and almost always serves as the first and the last link (OECD, 2011).

Freight transport demand has grown rapidly and will grow further as our economies recover from the current downturn, particularly the road freight transport (OECD, 2011). This puts pressure on several players such as truck industry, transporters, governments, road owners, road designers, environmentalists and citizens in general.

The introduction of Longer and Heavier Vehicles (LHVs), the increase of vehicle load factors and the decrease of empty running (unload trips) may lead to greater efficiency, higher productivity and lesser fuel consumption for the same demand. However, it can also lead to more pavement damage.

The Directive No. 96/83/EC, established in the framework of the common transport policy, harmonised the maximum authorized dimensions in national and international traffic and the maximum authorized weights in international traffic. Due to the European Union (EU) accession of Finland and Sweden, this Directive introduced a modular concept known as European Modular System (EMS). The European Commission (EC) is analysing the positive and negative impacts of allowing the use of LHVs measuring up to 25.25 m and weighting up to 60 t across the EU. LHVs are already in operation in Finland and Sweden and trials with LHVs are being planned or carried out in a number of EU countries.

Despite the successful opening-up of the transport market, there have been different developments between countries. Coherence at EU level is vital. Among the Transport White Paper's initiatives (EC, 2011), there is the adaptation of the legislation on weight and dimension to new circumstances and technologies to facilitate multimodal and intermodal transport and the reduction of the overall energy consumption and emissions.

On other direction, a pavement is designed for a foreseeable heavy traffic flow that will pass over the pavement design period. This heavy traffic flow is currently converted into a number of Equivalent Standard Axle Load (ESAL) applications using Equivalent Axle Load Factors (EALFs). Each heavy vehicle of the flow has a different impact on the pavement and on the subsequent damage.

EALFs can be either empirical or theoretical. Empirical EALFs for pavement design are presented, for instance, in the American Association of State Highway and Transportation Officials (AASHTO) guide for a range of pavement structural capacities, axle configurations and terminal serviceability values (AASHTO, 1993). They can also be determined theoretically by

using failure criteria and corresponding critical structural responses (Huang, 2004), i.e., the typical damage analysis. In 1969, Deacon (Huang, 2004) conducted a theoretical analysis of EALF considering the fatigue failure criterion with a fourth-power model. His analysis validated the EALF concept which was controversial up to that time (Ioannides and Khazanovich, 1993).

The Mechanistic-Empirical Pavement Design Guide (MEPDG) procedure, developed under the National Cooperative Highway Research Program (NCHRP) Project 1-37A, improved the consideration of traffic for the pavement design by using axle load spectra (NCHRP, 2004). It uses the distribution of axle loads directly in the mechanistic response model to calculate critical structural responses under the applied load, allowing a more detailed damage analysis. The MEPDG procedure ‘considers’, although implicitly, theoretical EALFs.

Theoretical EALFs depend on the heavy vehicles in operation, which means they evolve with time. From the statistical data disseminated by the Instituto Nacional de Estatística (INE) (Statistics Portugal) about road freight transport in Portugal every year (INE, 2012), it is possible to see that the Portuguese truck traffic fleet (goods road vehicles with a Gross Vehicle Weight (GVW) above 3,000 kg) has been evolving over the years. For example, between 1998 and 2011, the number of lorries/trucks decreased by 35% while the number of articulated vehicles increased by 46%. Figure 1.1 illustrates these two trucks. Even for the same type of vehicle, the axle configuration has been evolving. For example, between 1998 and 2011, the axle configuration 2+2 of the articulated vehicle decreased by 60% while the axle configuration 2+3 increased by 55%. There were also changes in terms of the load capacity of the vehicles.



Figure 1.1 – Illustration of the trucks: (a) – lorry/truck and (b) – articulated vehicle (Eurostat et al., 2009)

The evolution of truck traffic fleet has been accompanied with changes in tyre sizes and fitments, influencing the contact area between the tyres and the pavement and imposing a different stress state in the pavement structure, essentially nearer the pavement surface.

The Portuguese pavement design procedure (JAE, 1995) uses an Aggressiveness Factor (AF) to convert a specific foreseeable heavy traffic flow into a number of ESAL applications. An AF is defined for each traffic class which depend only on the foreseeable number of heavy vehicles that will pass over the pavement design period.

The Portuguese AFs have remained unchanged since at least 1995 and subsequently they are not keeping up with road freight industry, truck industry and transport policies.

Therefore, it is important to have a methodology for AF estimation that, at the same time, can be able to accommodate changes in road freight industry, truck industry and transport policies. This might involve the calculation of theoretical EALFs from axle load spectra which can be obtained from Weight-In-Motion (WIM) data or, when these data are unavailable, from heavy vehicle

simulations. The calculation of theoretical EALFs implies the calculation of the pavement response at the critical points defined by the deterioration mechanisms (design criteria) to prevent.

Pavement response is currently calculated by analytical methods (multilayer elastic analysis) which imply a circular contact area between the tyres and the pavement. This shape is not in agreement with the tyres that equip the heavy vehicles nowadays. To consider rectangular shape, numerical methods have to be used.

The Finite Element Method (FEM) is the most known numerical method. However, there are other numerical methods like the Boundary Element Method (BEM). The choice between the numerical methods should be adjusted to the design purposes since one method can be more suitable and efficient than the others.

It is not only the heavy vehicles in operation that affect AFs but also the road pavement itself. The thicknesses and properties of the pavement layer materials influence the pavement response which can also evolve over the pavement design period due to the degradation of the pavement properties with time and load repetition. The amount of roughness of the road pavement surface influences the magnitude of the loads applied by the vehicles to the pavement (dynamic loads) since roughness excites vehicle vibrations. The travel speed also influences the magnitude of these loads.

In order to account for all the evolutions over the pavement design period, whole pavement life should be modelled. This can be achieved by dividing the pavement life into time steps and by using an incremental procedure as recommended by the COST action 333 (COST 333, 1999).

1.2 OBJECTIVES AND METHODOLOGY

The main objective of this study is to define AFs from axle load spectra simulations for Portuguese heavy traffic conditions taking into consideration the deterioration of the pavement during its life cycle, namely related to the evolving of roughness for that period. From this, several improvements can be induced to the current way of considering pavement design in Portugal, namely by introducing in the analysis the fact that heavy traffic operations have been evolving and may continue to evolve in order to achieve a compromise between greater efficiency, higher productivity and lower environmental impacts.

To reach the objective, a methodological framework for AFs estimation and pavement damage calculation considering simulated axle load spectra (vehicle-pavement interaction) is developed. It must be able to consider the following aspects:

- Different types of heavy vehicles accommodating hence changes in the Portuguese truck traffic fleet;
- Different flexible pavement structures;
- Different design criteria;
- Road pavement surfaces with different roughness levels;
- Changes over the pavement design period (such as roughness growth and Asphalt Concrete (AC) modulus degradation) – incremental procedure.

In terms of pavement response model, the BEM is used. It was implemented and validated in the Master Thesis (Almeida (2008) and Almeida and Picado Santos (2010)), although only at two

dimensions (2D). In brief, the BEM is more effective in dealing with infinite/semi-infinite domains and with cracks (stress concentration).

The objective can be detailed into the following necessary targets:

- 3D-implementation and validation of the BEM;
- Generation of road surface profiles for specific International Roughness Index (IRI) values;
- Simulation of dynamic axle load profiles for different heavy vehicles by using a commercial software (TruckSIM[®]);
- Creation of a methodological framework to calculate mechanical-empirical AFs from pavement damage along the pavement design period and this specifying the heavy traffic flow, the travel speed of the heavy vehicles, the flexible pavement structure and the initial IRI value. The methodology should also be able to consider the roughness growth and/or the degradation of the AC modulus;
- Application of the methodological framework to a 'baseline' case study and to a case study that shows the effects of an increase of the road freight transport efficiency, translated by a reduction of empty running trips, on pavement damage.

The effect of each analysis parameter on the pavement damage shall be quantified in order to understand the specific effect.

1.3 OUTLINE OF THE THESIS

This thesis consists of seven chapters. Following this Introduction, Chapter 2 provides a review of the main topics related to vehicle-pavement interaction. A review of pavement issues as well as a review of vehicle issues is presented. In addition, some background about vehicle simulation and how to consider evolutions in pavement design during the design period is outlined. Two of the reviewed issues have its own chapter since they are important issues in this work. These are the road roughness deterioration mechanism which imposes vibrations to the vehicles, which in its turn, apply loads to the pavement structure above its static values (covered in Chapter 3) and the response model (BEM) which is used to calculate the pavement response (covered in Chapter 4).

Chapter 5 describes the study approach, i.e. describes the implementation of the methodological framework, the parameters and inputs of analyses to perform while Chapter 6 presents the case studies and the results achieved in this work.

Finally, Chapter 7 presents the main conclusions of this work regarding the use of new procedures for flexible pavement design. It finishes with considerations about the strengths and weaknesses of this work as well as with research lines for future works.

The outline of the thesis is illustrated in Figure 1.2.

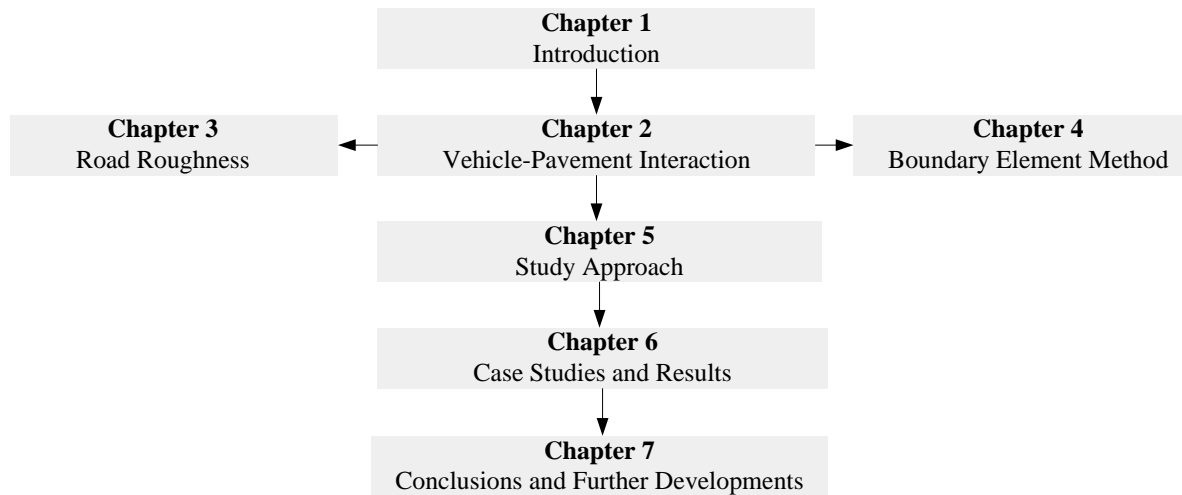


Figure 1.2 - Outline of the thesis

1.4 REFERENCES

AASHTO (1993). *AASHTO Guide for Design of Pavement Structures*. American Association of State Highway and Transportation Officials.

Almeida, A. (2008). *Modelação Estrutural de Pavimentos Rodoviários: O uso do Método dos Elementos de Fronteira (Structural Modelling of Road Pavements: The use of the Boundary Element Method)*. Master Thesis, University of Coimbra. In Portuguese.

Almeida, A. and Picado Santos, L. (2010). The use of the Boundary Element Method to Establish a Pavement Response. *2nd International Conference on Transport Infrastructures*, São Paulo, Brazil.

COST 333 (1999). *Development of New Bituminous Pavement Design Method (Final Report of the Action)*. European Commission (EC), Directorate General Transport. Belgium.

EC (2011). White Paper (Roadmap to a Single European Transport Area – Towards a competitive and resource efficient transport system). European Commission (EC), Brussels.

Eurostat, ITF and UNECE (2009). *Illustrated glossary for transport statistics*, 4th Edition. International Transport Forum, Eurostat, Economic Commission for Europe.

Huang, Y. H. (2004). *Pavement Analysis and Design*, Second Edition ed. Pearson, Prentice Hall.

INE (2012). Instituto Nacional de Estatística (Statistics Portugal). http://www.ine.pt/xportal/xmain?xpid=INE&xpgid=ine_publicacoes&PUBLICACOE_Spagenumber=1&PUBLICACOESrevista=00&PUBLICACOESstema=55488&PUBLICACOESfreeText=Estat%C3%ADsticas%20dos%20transportes. Access date: October 2012. In Portuguese.

Ioannides, A. M. and Khazanovich, L. (1993). Load equivalency concepts: a mechanistic reappraisal. *Transportation Research Record: Journal of the Transportation Research Board*, 1388, 42-51.

JAE (1995). *Manual de Concepção de Pavimentos para a Rede Rodoviária Nacional (Pavement Design Manual for the Portuguese Road Network)*. JAE (Junta Autónoma de Estradas). In Portuguese.

NCHRP (2004). *MEPDG - Guide for Mechanistic-Empirical Design of New and Rehabilitated Pavement Structures*. NCHRP (National Cooperative Highway Research Program), Transportation Research Board, National Research Council.

OECD (2011). *Moving Freight with Better Trucks: Improving Safety, Productivity and Sustainability*. Organisation for Economic Co-operation and Development (OECD) Publishing.

2 VEHICLE-PAVEMENT INTERACTION

2.1 INTRODUCTION

This chapter presents a review of the main issues related to vehicle-pavement interaction. First, pavement issues are concisely reviewed, particularly those considered in this work, such as material characterization, pavement response models, deterioration mechanisms, performance prediction and damage accumulation. Second, vehicle issues are reviewed in greater depth since they are not currently as covered as the pavement ones. This review includes type of vehicles, traffic data used in pavement design, aggressiveness of vehicles, loads carried by vehicles, loads applied by vehicles to pavements, tyre-pavement contact and types of suspension systems. Subsequently, a brief reviewing about vehicle simulation is carried out, where theoretical concepts about vehicle models are described without further detail as well as computation tools. Finally, since in real situations pavement response evolve during the design period, procedures to model whole pavement life are referred.

Although road pavements are subjected to both traffic load actions and climatic actions, this work focuses on traffic actions once the climatic ones could be simulated with enough quality by the use of simple indicators for the whole pavement life (Picado Santos, 2000).

2.2 PAVEMENT ISSUES

2.2.1 Introduction

In short, a pavement structure is designed by limiting the deterioration mechanisms at the end of its design period. This implies the definition of the deterioration mechanisms to consider in the design, the calculation of the pavement response at the deterioration mechanisms' critical locations (which requires materials characterization), the prediction of the deterioration development (by using pavement performance models) and the calculation of the accumulated damage produced by those mechanisms.

Generally, the pavement design output is based on the allowable number of Equivalent Standard Axle Load (ESAL) applications on the pavement structure during its design period without failure. Therefore, and assuming that the material properties do not change over the design period, the pavement response can be calculated only once, for the standard axle, and the accumulated damage calculated also only once, at the end of the design period, by relating the predicted number of ESAL applications (usually calculated applying an Aggressiveness Factor (AF) to the expected number of heavy traffic vehicles for the life cycle) to the allowable number of ESAL applications (given by performance models).

This section consists of a brief review of the abovementioned pavement issues. First, the characterization of the materials is presented non-exhaustively, only the properties and methods used in this work are stated. Then, methods for pavement response calculation are referred. Afterwards, the main deterioration mechanisms are described as well as the models to predict the development of them. At the end, both damage calculation and accumulation are mentioned.

2.2.2 Materials characterization

This work assumes that the pavement materials (bituminous mixtures, granular materials and subgrade soils) have linear elastic behaviour. Hence, only two material properties are required for each material, the modulus, with a similar meaning as the ‘elastic modulus’ and also referred as ‘stiffness modulus’, and the Poisson’s coefficient.

Models to calculate the modulus of the pavement materials are presented below. For bituminous mixtures, besides models to calculate the initial modulus, models to predict its degradation along the pavement life are also presented. In terms of Poisson’s coefficient, current values are used (bituminous materials: 0.35, granular materials: 0.30 and subgrade: 0.35) (Branco et al., 2005).

Bituminous mixtures

The modulus can be evaluated by laboratory tests. However, as this procedure is time consuming as well as requiring special equipment, nomographs or formulas can also be used.

The Shell International Petroleum Company (Shell, 1978) developed a nomograph that permits the determination of the modulus from knowing the stiffness of the bitumen and the volumetric composition of the mixture. Bonnaure et al. (1977) developed the formulas (2.1) and (2.2) that also permit the determination of the modulus knowing the same parameters.

For $5 \text{ MPa} < S_b < 1000 \text{ MPa}$:

$$\log E_m = \frac{\beta_4 - \beta_3}{2} (\log S_b - 8) + \frac{\beta_4 - \beta_3}{2} |\log S_b - 8| + \beta_2 \quad (2.1)$$

For $1000 \text{ MPa} < S_b < 3000 \text{ MPa}$:

$$\log E_m = \beta_2 + \beta_4 + 2.0959(\beta_1 - \beta_2 - \beta_4)(\log S_b - 9) \quad (2.2)$$

with

$$\beta_1 = 10.82 - \frac{1.342(100 - V_a)}{V_a + V_b}$$

$$\beta_2 = 8.0 + 0.00568V_a + 0.0002135V_a^2$$

$$\beta_3 = 0.6 \log \left(\frac{1.37V_b^2}{1.33V_b - 1} \right)$$

$$\beta_4 = 0.7582(\beta_1 - \beta_2)$$

where

- E_m = modulus of the bituminous mixture (MPa)
- S_b = stiffness of the bitumen (MPa)
- V_a = volume percentage of aggregates (%)

V_b = volume percentage of bitumen (%)

The stiffness of the bitumen can be determined using the Van der Poel nomograph developed by the Shell International Petroleum Company (Shell, 1978) or using the formula (2.3) developed by Ullidtz and Peattie (cited in Branco et al. (2005)).

$$S_b = 1.157 \times 10^{-7} t^{-0.368} 2.718^{-PI} (T_{rb} - T)^5 \quad (2.3)$$

where

S_b = stiffness of the bitumen (MPa)

t = time of loading (s)

PI = penetration index

$$PI = \frac{20T_{rb} + 500 \log(\text{pen}) - 1951.55}{T_{rb} - 50 \log(\text{pen}) + 120.15}$$

T_{rb} = softening point of the bitumen (°C)

pen = penetration of the bitumen (10^{-1} mm)

T = temperature of the mixture (°C)

Besides the existence of other formulas, as for example the one developed by the Asphalt Institute which is well referenced in the bibliography, only the formulas that will be used were presented.

Nevertheless, the modulus is not constant during the pavement design period because when the materials are subjected to several load repetitions which imply fatigue distress, they experiment a degradation of its properties with time and load repetition. Cracks may appear leading to a reduction of modulus that conduct to an increase in stress state within the pavement structure. Therefore, it is important to use a model to predict the modulus reduction when whole pavement life is modelled.

The Mechanistic-Empirical Pavement Design Guide (MEPDG), developed by the American Association of State Highway and Transportation Officials (AASHTO) (NCHRP, 2004), simulates the whole pavement life. It estimates the time-temperature dependent dynamic modulus from a master curve constructed at a reference temperature of 70°F ($\approx 21^\circ\text{C}$) and considers also the effect of asphalt ageing. It does not consider the reduction of modulus due to fatigue damage except for the rehabilitation design case.

The CalME is also a mechanical-empirical design method, developed by the California Department of Transportation (Caltrans), for flexible pavements that parallels the MEPDG procedure and is calibrated for California conditions (Ullidtz et al., 2006). This method expresses fatigue damage as a reduction in the modulus of the bituminous mixture – equation (2.4).

$$\log(E_m) = \delta + \frac{\alpha(1-\omega)}{1 + \exp[\beta + \gamma \log(t)]} \quad (2.4)$$

where

E_m = modulus of the bituminous mixture (MPa)

ω = damage parameter

- t = time of loading (s)
δ and α = parameters related to the minimum and the maximum E_m-values
β and γ = parameters of the model

It introduced the damage parameter (ω) to the modulus estimation model of the MEPDG procedure which is given by equation (2.5).

$$\log(E_m) = \delta + \frac{\alpha}{1 + \exp[\beta + \gamma \log(t)]} \quad (2.5)$$

Collop and Cebon (1996) developed a modulus degradation model that is capable of determining the modulus reduction of the bituminous mixtures due to cumulative fatigue damage. They used measured surface deflection bowls, from a number of test pavements, with a pavement parameter back-calculation procedure to determine the reduction in modulus of the bituminous mixtures throughout the pavement life. A semi-logarithmic relationship between the modulus reduction and the cumulative fatigue damage was achieved.

This type of relationship does not agree with an earlier one (theoretical continuum damage mechanics model) where the relationship between the modulus reduction and the cumulative fatigue damage was predicted to be linear (Collop and Cebon, 1996).

Most back-calculation procedures use a static pavement response model to reproduce the deflection bowl generated from both static and dynamic surface deflection tests. This is valid if the dynamic component of the pavement response is assumed insignificant and the resulting deflection bowl is assumed primarily due to the quasi-static response of the pavement (Collop and Cebon, 1996). Tam and Brown (1989) (cited in Collop and Cebon (1996)) compared the surface deflections bowls calculated using static and dynamic models concluding that the inertial effects are insignificant and consequently a static model could be used for back-analysis with confidence.

Collop and Cebon (1996) used data from both static or slow-moving loading tests (BB - Benkelman Beam) and transient impulsive loading tests (FWD - Falling Weight Deflectometer) carried out in the Accelerated Loading Facility (ALF) Mulgrave trial and in the ALF Callington trial by the Australian Road Research Board (ARRB). Then, they applied the VESYBACK back-calculation model (validated against other back-calculation programs) to determine the combination of moduli that give a theoretical surface deflection bowl that best matches an input measured deflection bowl. The back-calculated results showing the modulus reduction with traffic increase (fatigue-damaged) are depicted in Figure 2.1, Figure 2.2 and Figure 2.3 for BB tests carried out in ALF Mulgrave trial, FWD tests carried out in ALF Mulgrave trial and FWD tests carried out in ALF Callington trial, respectively.

The results show that the reduction in modulus as a function of load passes for each section can be approximated by a straight line on semi-logarithmic scales. The R²-values from the Callington trials are lower than those from Mulgrave trials, which may be explained by the consideration of an asphalt layer thickness equal to 100 mm in the back-calculated moduli instead of the real thickness values (not recorded). An approximation using a straight line on linear scales was also performed but with worse R²-values.

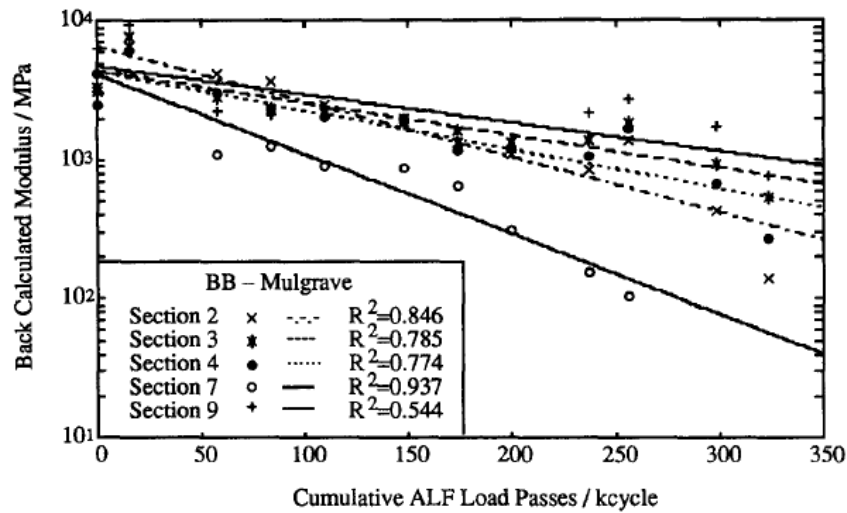


Figure 2.1 – Back-calculated moduli reductions from BB tests carried out in ALF Mulgrave trial (Collop and Cebon, 1996)

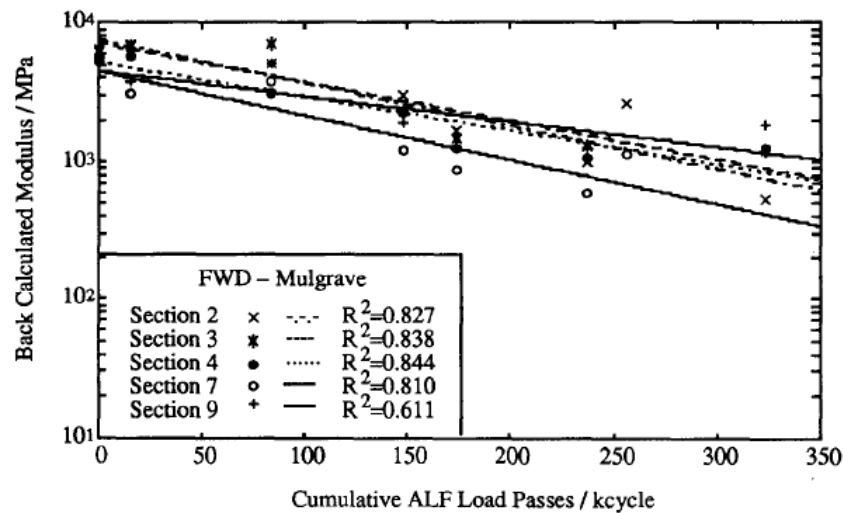


Figure 2.2 - Back-calculated moduli reductions from FWD tests carried out in ALF Mulgrave trial (Collop and Cebon, 1996)

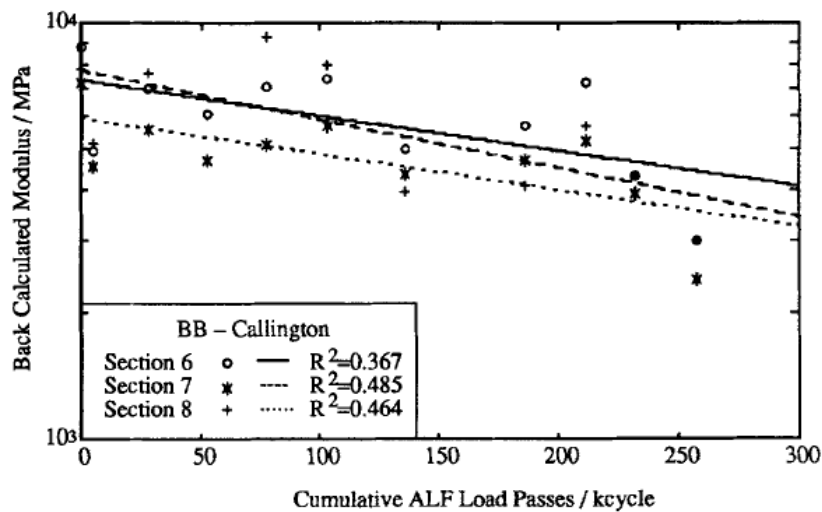


Figure 2.3 - Back-calculated moduli reductions from FWD tests carried out in ALF Callington trial (Collop and Cebon, 1996)

These relationships to predict the reduction in modulus are only useful when the same repeated load is applied. To predict that reduction for pavements under mixed traffic loading, the number of loads passing need to be transformed into cumulative fatigue damage. Collop and Cebon (1996) describe the method to obtain that transformation reaching to the relationship (2.6) between modulus reduction and cumulative fatigue damage.

$$\begin{aligned} \frac{E_m}{E_0} &= e^{-kD} & D < 1 \\ \frac{E_m}{E_0} &= \left(\frac{E_m}{E_0} \right)_c & D \geq 1 \end{aligned} \quad (2.6)$$

where

- E_m = modulus of the bituminous mixture
- E_0 = initial modulus of the bituminous mixture
- E_m/E_0 = relative modulus
- k = constant ($k = -\ln(E/E_0)_c$)
- D = damage term given by

$$D = \sum_{i=1}^j \left(\frac{N^{(i)}}{N_f^{(i)}} \right)$$

where j is the number of different strain levels considered, $N^{(i)}$ represents the number of cycles at a given level of tensile strain at the bottom of the bituminous layer and $N_f^{(i)}$ is the number of cycles to failure at that strain level

$(E_m/E_0)_c$ = critical relative modulus (when the reduction in modulus reaches this value, the bituminous mixture is assumed to have failed and the modulus is not reduced further)

Figure 2.4, Figure 2.5 and Figure 2.6 (respectively for BB data from the Mulgrave trial, FWD data from the Mulgrave trial and BB data from the Callington trial) show equation (2.6) against cumulative fatigue damage on linear scales for $(E_m/E_0)_c = 0.2$, together with the experimental data and the theoretical continuum damage mechanics model denoted as ‘Ullidtz equation’ in figures and given by relationship (2.7), where $(E_m/E_0)_c = 0.3$.

$$\begin{aligned} \frac{E_m}{E_0} &= 1 - D \left(1 - \frac{E_m}{E_0} \right)_c & D < 1 \\ \frac{E_m}{E_0} &= \left(\frac{E_m}{E_0} \right)_c & D \geq 1 \end{aligned} \quad (2.7)$$

The exponential relationship gives a better fit than the previous theoretical model based on simple continuum damage mechanics. However, it should be noted that data from a small number of studied sections were used in the analysis.

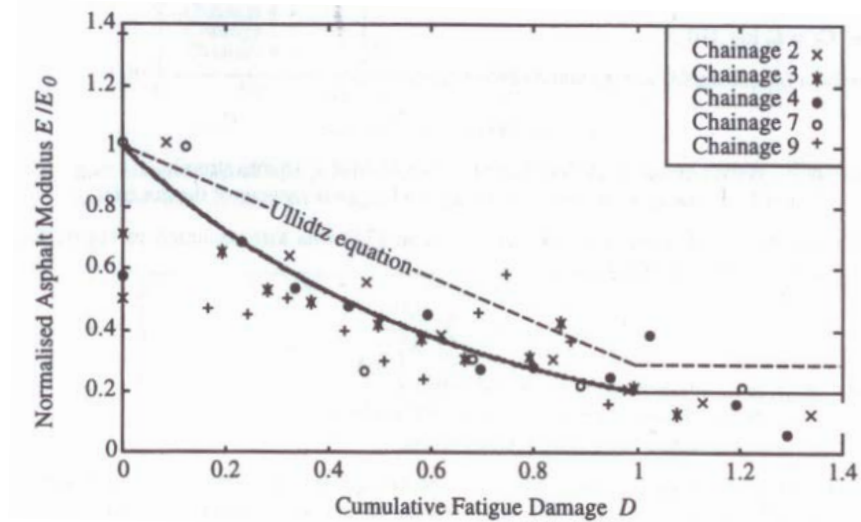


Figure 2.4 – Modulus reduction as a function of cumulative fatigue damage calculated from BB data from the Mulgrave trial (Cebon, 1999)

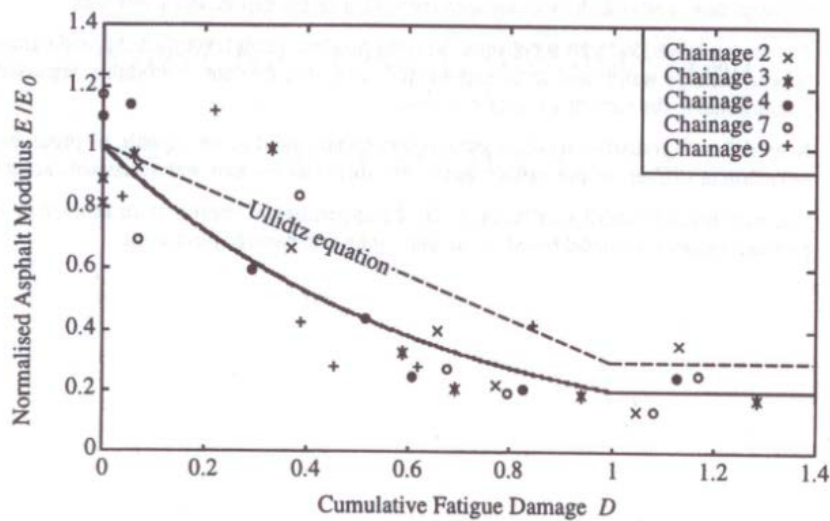


Figure 2.5 - Modulus reduction as a function of cumulative fatigue damage calculated from FWD data from the Mulgrave trial (Cebon, 1999)

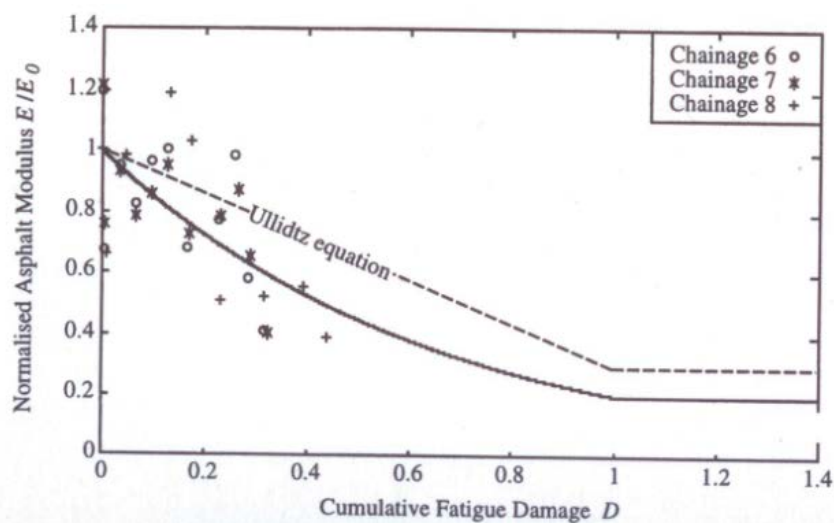


Figure 2.6 - Modulus reduction as a function of cumulative fatigue damage calculated from BB data from the Callington trial (Cebon, 1999)

Several studies have used the model developed by Collop and Cebon (1996), for example, Obrien and Taheri (2011) implemented a mechanistic-empirical approach to simulate the deterioration of a pavement taking into account the dynamic excitation of the axles, and later, Taheri et al. (2012) used the same model but considering a 3D pavement surface instead of a 2D one.

Soils and granular materials

Although these materials have non-linear behaviour in the most part of the possible stress-strain range that they are subject in a road pavement, there are simple empirical relationships which are usually used to calculate their modulus.

The modulus of the subgrade (Branco et al., 2005) is calculated as a function of the California Bearing Ratio (CBR) by equation (2.8).

$$E_s = 17.6 \times \text{CBR}^{0.64} \quad (2.8)$$

where

E_s = modulus of the subgrade (MPa)
CBR = California Bearing Ratio (%)

The modulus of the granular materials (Branco et al., 2005) is calculated as a function of the thickness of the granular layer and the modulus of the subgrade by equation (2.9).

$$E_g = k \times E_s \quad \text{with } k = 0.2 \times h_g^{0.45} \quad (2.9)$$

where

E_g = modulus of the granular materials (MPa)
 h_g = thickness of the granular layer (mm)
 E_s = modulus of the subgrade (MPa)

2.2.3 Pavement response

To assess pavement response at critical locations in the pavement structure to a wheel load, either analytical methods or numerical methods are available. The choice is essentially influenced by the analysis purpose which can address, for instance, static or non-static loads, behaviour of the materials more or less complex, contact areas between the tyres and the pavement with circular shape or not. In addition, the type of failure mechanisms to consider as well as the type of analysis (static, quasi-static or dynamic) can also influence the choice.

In relation to the type of analysis, the static analysis has been traditionally used in multilayer elastic analysis. The quasi-static analysis is based on the concept of moving the load at later positions along the pavement for each new time step and assuming the load is static at each position. No inertia or damping effects are quantified in the quasi-static analysis while in the dynamic analysis they are. Beskou and Theodorakopoulos (2011) present a comprehensive review on the subject of the dynamic response of pavements to moving loads. According to Monismith et al. (1988), quasi-static analysis is an acceptable approach for flexible pavements (cited in Yoo et al. (2006)).

A brief review of pavement response models is presented below, either using analytical or numerical methods.

Analytical methods

The theory of elasticity for solid materials (continuum mechanics) is based on equilibrium, compatibility and constitutive equations. From these, a fourth order differential equation can be derived and solved for specific boundary conditions.

In 1885, Boussinesq solved the differential equation and he found a solution for the simplest case, concentrated load applied on an elastic half-space (Huang, 2004). On the basis of Boussinesq's solution, Burmister (1943) developed the multilayer elastic theory which solved the problem of wheel load, distributed over a circular area, applied on a multilayer system, with two layers in 1943 and with three layers in 1945. The advent of computers allowed its application to systems with any number of layers. There are various commercial programs that solve this problem such as the BISAR[®] (Shell, 1988).

The COST action 333 (1999) reviewed the European pavement design methods and they concluded that the majority of the design methods are analytically based.

Methods based on the multilayer elastic theory have a number of simplified assumptions, such as the pavement materials are assumed to be linear elastic, homogeneous, continuous and isotropic. In addition, they assume that the contact area between the tyres and the pavement is circular in shape and that the loads applied by the vehicles to the pavement are static in nature.

Numerical methods

The Finite Element Method (FEM) is the most known numerical method. However, there are other numerical methods like the Discrete Element Method (DEM) and the Boundary Element Method (BEM). The choice between these numerical methods should be adjusted to the design purposes since one method can be more suitable and efficient than the others. In some cases a combination of methods can be the best choice as it allows taking the advantages of the methods reducing its disadvantages.

In general, numerical methods solve more complex problems but they are not 'user-friendly' enough and they are more time consuming. The pavement structure is discretized and the response is calculated in specific points called nodes.

Besides being the most known, the FEM is also the most employed numerical method. Various researchers have used it to model more complex material behaviours and more realistic tyre-pavement contacts. For instance, Yoo and Al-Qadi (2007) studied the effect of transient dynamic loads on flexible pavements. For that they employed a 3D finite element model (commercial software ABAQUS[®]) to calculate the dynamic response. They considered the linear viscoelastic behaviour for the bituminous mixtures and each of the tyre ribs in the tyre-pavement contact.

With DEM it is possible to model materials that consist of individual particles where a particle may roll or slide on other particles (COST 333, 1999). Therefore, grain size distribution, shape and angularity of grains, degree of compaction, stiffness of grains and coefficient of friction and cohesion between grains can be considered permitting a more realistic modelling of the pavement materials. This method has been mainly employed to simulate tests and hence to

predict material properties. For instance, Liu and You (2011) employed the DEM to simulate creep compliance tests on idealized asphalt mixtures.

The BEM is an alternative numerical method to FEM mainly when there is stress concentration or semi-infinite/infinite domains. It formulates the problem on the boundary and consequently only the boundary has to be discretised as opposed to in domain techniques, such as the FEM and the DEM which require the discretization of the domain. Birgisson et al. (2002) used the BEM to predict the viscoelastic response and crack growth in bituminous materials.

Since the BEM is employed in this work, a comprehensive description is presented in Chapter 4 – Boundary Element Method.

2.2.4 Deterioration mechanisms

Various deterioration mechanisms affect pavement performance. Interactions between them make its definition and prediction difficult. Two deterioration mechanisms are usually considered, the fatigue cracking by limiting the tensile strain at the bottom of the bituminous layers and the permanent deformation (rutting) by limiting the vertical compressive strain at the top of the subgrade.

A questionnaire in the framework of the COST action 333 (1999) had a question about the most common deterioration mechanisms observed (in a total of 12) on in-service roads in each participating country. From the answers, the deterioration mechanisms were ranked. In the top five were (1) rutting originating in the bituminous layers, (2) cracking initiated at the surface, (3) longitudinal roughness, (4) loss of skid resistance, and (5) longitudinal cracking in the wheel path. Cracking initiated at the bottom of the base course appeared on sixth and rutting in the subgrade appeared on the ninth position.

The MEPDG procedure (NCHRP, 2004) considers the permanent deformation, the fatigue cracking (both bottom-up and top-down), the thermal cracking and the roughness.

This work considers essentially three deterioration mechanisms, fatigue cracking (bottom-up cracking), permanent deformation (or rutting) and roughness. The two first mechanisms are used to calculate pavement damage (or failure), the latter one (the roughness i.e. the lack of smoothness) is considered in vehicle simulations as an excitation source which gives dynamics to simulations. The effect of the fatigue cracking mechanism on the modulus of the bituminous mixtures is also considered.

A brief description of the fatigue cracking and permanent deformation mechanisms is presented next. The roughness mechanism is further described in Chapter 3 – Road Roughness.

Fatigue cracking

Traditionally fatigue cracking initiates at the bottom of the bituminous layers in the location of the highest tensile strain, then it propagates upwards (bottom-up cracking) and becomes visible at the pavement surface as longitudinal or transversal cracks that interconnected forming alligator cracking. Consequently, the majority of fatigue cracking transfer functions used in mechanistic-empirical design is based on this concept.

However, top-down cracking has been recognized as the origin of some visible cracks at the pavement surface (Molenaar, 2007). Since then, various researchers have tried to identify key

factors and fundamental mechanisms that may lead to both fatigue cracking initiation and propagation.

Fatigue failure can be predicted following different approaches. Currently, a traditional approach to fatigue cracking performance prediction is used which employs a relationship, empirical in nature, between the tensile strain at the bottom of the bituminous layers and the allowable number of load repetitions. However, in response to the need of mechanistic models, fracture mechanics approach and continuum damage mechanics approach have also been used.

Fracture mechanics can be used to describe the critical conditions near the crack tip and capture stress redistributions resulting from crack growth while continuum damage mechanics can be used to predict crack initiation.

Myers et al. (2001) combined finite element modelling and fracture mechanics to evaluate a pavement structure with a crack at the surface (linear elastic materials). They found that the major cause of top-down cracking is due to tensile stresses resulting from vehicle-pavement interaction.

In order to achieve a promising mechanical fatigue cracking model, mechanical constitutive models for bituminous material have been developed and/or enhanced. The ViscoElastic Continuum Damage (VECD) model (Kim and Little, 1990) has been used to model bituminous materials. It ignores specific micro scale behaviours and attempts to characterise a material using macro scale observations. The VECD model predicts crack initiation by modelling damage zones and their effects on response prior to cracking. It overcomes the problem of the isolated use of the fracture mechanics approach that requires a cracked structure.

Wang et al. (2003) used micromechanics (it includes the particle configuration and the relative stiffness of mastic and aggregate particles) to investigate the causes of the top-down cracking. The results indicated that top-down cracking may initiate not only at the pavement surface but also at some distance down from the surface, that both tensile-type and shear-type cracking could initiate top-down cracking and that top-down cracking may most likely initiate when the mastic is weaker or the pavement temperature is higher.

Mun et al. (2004) studied fatigue cracking mechanisms (both bottom-up and top-down cracking) using the FEP++ Finite Element Program that employs the VECD model for asphalt layer and a nonlinear elastic model for unbound layers (the so-called VECD-FEP++ program). They demonstrated that the VECD-FEP++ program may be used to study the fatigue cracking performance.

Underwood et al. (2009) undertook a mathematical rigorous exploration to specialise the VECD model for easy prediction and characterisation using cyclic fatigue tests on cylindrical specimens resulting in the Simplified ViscoElastic Continuum Damage (S-VECD model). Then, Underwood et al. (2012) implemented the S-VECD model into the FEP++ software, showing that the S-VECD model can be used to predict the number of cycles until fatigue failure for both constant stress and constant strain loading conditions.

A NCHRP Project 1-42A (Roque et al., 2010) was undertaken to identify or develop mechanistic-based models for predicting top-down cracking in bituminous layers to improve the MEPDG procedure. In summary, two models were developed during the project, the VECD-based crack initiation model and the Hot Mix Asphalt (HMA) fracture mechanics-based crack

propagation model. Then, a fully integration of these models is recommended to form a top-down cracking performance model suitable for implementation in the MEPDG procedure.

The MEPDG procedure (NCHRP, 2004) has already considered the top-down cracking using a model that predicts the allowable number of load repetitions to fatigue cracking as a function of the tensile strain at the critical location and the bituminous modulus (traditional approach). This fatigue model is based on the original Asphalt Institute model, with some modifications and it is used for both top-down and bottom-up cracking varying only the location of the critical strain. If it is at the surface, the distress will be top-down cracking. On the other hand, if it is at the bottom of the bituminous layers, the distress will be bottom-up cracking.

As it has already been mentioned, the BEM, more specifically the Displacement Discontinuity (DD) BEM, is an attractive alternative to FEM for modelling cracks as the FEM is both complex and numerically intensive for fracture mechanics applications (Birgisson et al., 2002). As the DD-BEM only requires meshes on the boundary, the singularity at the crack tip is naturally included in it by using a representative displacement distribution around the crack tip. Birgisson et al. (2002) demonstrated the effectiveness of the method in dealing with cracks, crack propagation and viscoelasticity in bituminous materials. Then, Sangpetngam et al. (2003) implemented the HMA fracture mechanics law into the DD-BEM. The resulting HMA fracture simulator is able to model and predict HMA crack growth under general loading conditions. The DD-BEM formulation was extended into layered materials (Sangpetngam et al., 2004).

One of the key factors of the HMA fracture mechanics-based crack propagation model developed in the framework of the NCHRP Project 1-42A (Roque et al., 2010) is the pavement fracture model that uses the DD-BEM to predict load-induced tensile stresses ahead of the crack tip.

Up to now, improvements in modelling the initiation mechanism and propagation mechanism of cracks in bituminous materials were referred. However, various researchers have been carried out studies to evaluate the causes and/or effects of some issues on top-down cracking. Climatic conditions, traffic conditions, ageing, structural conditions, mixture properties and construction quality are the main causes pointed out for the initiation and propagation of top-down cracks (Freitas et al., 2005).

Freitas et al. (2003) assessed top-down cracking in Portugal. For that, specimens from a thicker pavement were evaluated. They found that construction quality is a strong cause of top-down cracking, that traffic is not one of the main responsible factors in crack progression, that ageing is an important cause of the top-down cracking mechanism and that fatigue does not appear to cause top-down cracks although it may influence crack propagation. Then, an accelerated wheel tracking device and a finite element program were used to study the effects of air voids, bitumen content and type, aggregate gradation and segregation on top-down cracking under three temperature conditions (Freitas et al., 2005). It was found that the surface cracking initiated earlier at higher temperatures, that the most influential factors were air voids (high air voids) and aggregate gradation (coarse aggregates) and that the rutted surface appears to contribute significantly to top-down cracking initiation.

Permanent deformation (or rutting)

Rutting is a surface depression in the wheels paths caused by inelastic or plastic deformations in any or all of the pavement layers and subgrade (NCHRP, 2004). These deformations are

essentially due to densification or one-dimensional compression and consolidation and due to lateral movements or plastic flow of materials from wheel loads.

Traditionally this deterioration mechanism is controlled by limiting the compressive strain at the top of the subgrade from a relationship, empirical in nature, between the compressive strain at the top of the subgrade and the allowable number of load applications. Rutting has been associated to compressive strains at the top of the subgrade because it has been assumed that pavement was both well designed and constructed, being sufficient to limit the compressive strain on the subgrade, the weaker part of the whole structure (NCHRP, 2004). However, it is clear that the total permanent deformation is a product of cumulative ruts occurring in all layers of the pavement structure. Nowadays, for instance, the MEPDG procedure (NCHRP, 2004) predicts individual layer rut depths for each layer as a function of time and traffic repetition.

There are generally three distinct stages for the permanent deformation behaviour (NCHRP, 2004), which are illustrated in Figure 2.7 and can be described as follows: (1) primary stage with high initial level of rutting predominantly associated with volumetric changes, plastic deformations decrease at increasing rate, (2) secondary stage with small rate of rutting exhibiting a constant rate of change of rutting that is also associated with volumetric changes, shear deformations increase at increasing rate, and (3) tertiary stage with high level of rutting predominantly associated with plastic (shear) deformations under no volume change condition. Only the two first stages are explicitly modelled on the MEPDG procedure.

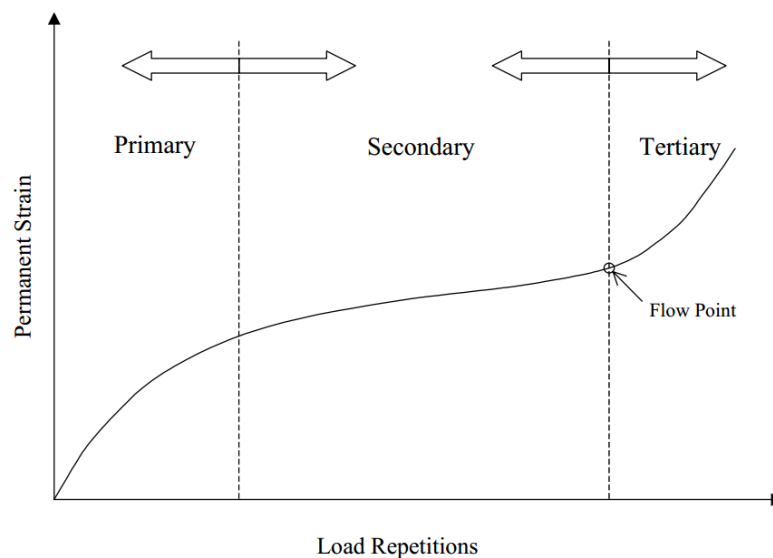


Figure 2.7 – Stages of permanent deformation (NCHRP, 2004)

This distress can be predicted using laboratory tests. The most common include the wheel-tracking test, the cyclic compression test (uniaxial and triaxial) and the repeated simple shear test at constant height (Gardete et al., 2008).

2.2.5 Performance prediction

The current design methods use some criteria to limit deterioration mechanisms. These criteria are usually expressed as a relationship between the response at deterioration mechanisms' critical points and the allowable number of load applications.

Usually two failure criteria are used, the fatigue cracking due to repeated tensile strains at the bottom of bituminous layers and the excessive permanent deformation (or rutting) controlled at the top of the subgrade. The Shell transfer functions as well as the MEPDG's prediction models are presented below for those two failure criteria.

Bottom-up fatigue cracking

To characterize the fatigue damage, numerous models can be found in the existing literature. The most commonly used model to predict the number of load repetitions to fatigue cracking is a function of tensile strain and bituminous mixture properties.

The Shell International Petroleum Company (Shell, 1978) developed a fatigue life prediction model which is typically used in Portugal for pavement design. This model was based on laboratory-controlled strain sinusoidal loading fatigue tests on different bituminous mixtures covering a large range of mixture types and test conditions. Interpreting the failure measurements, it was found that the fatigue strain for failure after a fixed number of loading applications is a function of the modulus of the bituminous mixture and the volume of the bitumen in the mixture as expressed by equation (2.10).

$$\varepsilon_f = (0.856 \times V_b + 1.08) \times E_m^{-0.36} \times N_f^{-0.2} \quad (2.10)$$

where

- ε_f = fatigue strain (horizontal tensile strain at the bottom of the bituminous layers) ($\mu\text{m}/\text{m}$)
- N_f = number of repetitions to fatigue cracking
- E_m = modulus of the bituminous mixture (Pa)
- V_b = volume percentage of bitumen (%)

From equation (2.10), a fatigue relationship, equation (2.11), is obtained.

$$N_f = \left[\frac{0.856 \times V_b + 1.08}{E_m^{0.36} \times \varepsilon_f} \right]^5 \quad (2.11)$$

The fatigue data obtained in the laboratory cannot be applied directly since in practice the field conditions of loading and spectrum of strain level are different from the laboratory ones. Therefore, correction factors should be applied as follows (Shell, 1978):

- To consider the increase in effective design life due to the transverse distribution of wheel loads over the pavement – factor of about 2.5;
- To consider the increase in effective design life due to the effects of healing and intermittent loading – factor in the range 2-10, depending on the bituminous mixture type (a lower factor for open mixtures and a higher factor for dense/rich mixtures);
- To consider the decrease in effective design life due to temperature variations in the bituminous layer – factor in the range 1-3 depending on the 'weighted' mean annual air temperature and the bituminous layer thickness (a lower correction factor for low to moderate temperatures and/or thin layers and a higher factor for higher temperatures in conjunction with thicker layers).

The MEPDG procedure (NCHRP, 2004) predicts both the top-down cracking and the bottom-up cracking using a model which relates the number of load repetitions to fatigue cracking as a

function of the tensile strain and the bituminous mixture modulus. The location of the critical strain can be either at the surface or at the bottom of the bituminous layers. The model is expressed by equation (2.12).

$$N_f = \beta_1 k_1 (\varepsilon_f)^{-\beta_2 k_2} (E_m)^{-\beta_3 k_3} \quad (2.12)$$

where

- N_f = number of repetitions to fatigue cracking
- ε_f = fatigue strain (m/m)
- E_m = modulus of the bituminous mixture (Pa)
- k_1, k_2 and k_3 = laboratory regression coefficients
- β_1, β_2 and β_3 = calibration parameters
- C = laboratory to field adjustment factor

Permanent deformation (or rutting)

The Shell International Petroleum Company also developed a permanent deformation life prediction model where the vertical compressive strain for failure after a fixed number of loading repetitions is given by equation (2.13).

$$\varepsilon_{pd} = k_{pd} \times N_{pd}^{-0.25} \quad (2.13)$$

where

- ε_{pd} = permanent deformation strain (vertical compressive strain at the top of the subgrade) ($\mu\text{m}/\text{m}$)
- N_{pd} = number of repetitions to permanent deformation
- k_{pd} = no dimensional parameter that depends of the probability of the pavement to survive this criteria, and takes the values of 2.8×10^{-2} , 2.1×10^{-2} and 1.8×10^{-2} for the probability of 50%, 85% e 95% respectively

From equation (2.13), the permanent deformation life, equation (2.14), is obtained.

$$N_{pd} = k_{pd}^4 \times \varepsilon_{pd}^{-4} \quad (2.14)$$

The MEPDG procedure (NCHRP, 2004) predicts the permanent deformation for each individual layer and then sums them as expressed by equation (2.15).

$$RD = \sum_{i=1}^{\text{Nr.Sublayers}} \varepsilon_{pd}^i h^i \quad (2.15)$$

where

- RD = permanent deformation (m)
- Nr.Sublayers = number of sublayers
- ε_{pd}^i = permanent deformation strain in sublayer i (m/m)
- h^i = thickness of sublayer i (m)

The permanent deformation of asphalt layers is predicted using the model (2.16).

$$\frac{\varepsilon_{pd}}{\varepsilon_r} = \beta_1 k_1 T^{k_2 \beta_2} N^{k_3 \beta_3} \quad (2.16)$$

where

- ε_{pd} = accumulated permanent deformation strain at N repetitions of load (m/m)
- ε_r = resilient strain of the bituminous material as a function of mixture properties (temperature and time rate of loading) (m/m)
- N = number of load repetitions
- T = temperature (°C)
- k_i = regression coefficients
- β_i = field calibration factors

On the other hand, the permanent deformation of granular materials and subgrade soils are predicted using the model (2.17).

$$RD_g(N) = \beta_1 \left(\frac{\varepsilon_0}{\varepsilon_r} \right) e^{-\left(\frac{\rho_1}{N} \right)^{\rho_2}} \varepsilon_v h_g \quad (2.17)$$

where

- RD_g = permanent deformation for the granular materials and subgrade soils (m)
- N = number of load repetitions
- ε_0, ρ_1 and ρ_2 = material properties
- ε_r = resilient strain imposed in the laboratory test (m/m)
- ε_v = average vertical resilient strain in the granular materials and subgrade soils as obtained from the primary response model (m/m)
- h_g = thickness of the granular materials and subgrade soils (m)
- β_1 = calibration factor for the granular materials and subgrade soils

2.2.6 Damage accumulation

According to performance prediction models, the pavement life is normally defined for the condition of constant strain amplitude along the pavement life (simple loading). However, in practice, the pavement is subjected to a wide spectrum of strain amplitudes (compound loading). Therefore, it is necessary to estimate the pavement life in the compound loading condition from the simple loading condition. The simplest and most widely used model is based on the linear accumulation of damage using the Miner's law.

From this law, the damage at position k on the road due to the passage of vehicles can be estimated from equation (2.18).

$$D_k = \sum_i \frac{n_i}{N_i} \quad (2.18)$$

where

- D_k = damage at position k on the road
- n_i = number of load applications with magnitude i
- N_i = allowable number of load applications with magnitude i to failure

According to this law, each load cycle consumes a small amount of pavement life and the failure occurs when the actual number of load applications equals the allowable number of load applications.

2.3 VEHICLE ISSUES

2.3.1 Introduction

This section consists of a review of the main vehicle issues. It starts with the types of heavy goods vehicles ('trucks') which can be (and are) used as well as their maximum authorized dimensions and weights. Then, traffic data used in pavement design are described. Since, besides the number of heavy goods vehicles which pass on the pavement structure during the pavement design period, the aggressiveness of them is crucial, procedures for calculating the aggressiveness of an axle, a vehicle and a mixed truck traffic flow are presented. Then, some aspects related to carried goods (payloads) and overloading are referred.

Another crucial issue is the magnitude of the loads applied by the vehicles to the pavement structure which can be complex, mainly when the vehicle is moving over rough roads, as well as the load profile pattern 'spatial repeatability' and the tyre-pavement contact. Regarding the tyre-pavement contact, it is important to define which tyres equip the vehicle, what the dimension and shape of the contact area is and what the magnitude of pressures applied on the contact area is.

At the end, suspension systems are described since they affect the magnitude of the loads and the vehicles design.

2.3.2 Vehicles, maximum authorized dimensions and weights












Road traffic comprises different types of vehicles which are grouped into eleven classes defined by the Junta Autónoma de Estradas (JAE) (the former Portuguese road administration) and they are still used as reference nowadays. Table 2.1 presents these classes.

Since the effect of light road vehicles on pavement damage is despised, only heavy road vehicles are taken into account in pavement design. The JAE classification divides the heavy road vehicles into six classes, classes F to K. The classes J and K are irrelevant in terms of the number of vehicles usually involved, therefore only the classes F, G, H and I are important for pavement design purposes.

This classification does not allow the distinction between vehicles with different number and arrangement of axles. To overcome this difficulty, the JAE and the Laboratório Nacional de Engenharia Civil (LNEC) (National Laboratory for Civil Engineering), propose a division of classes into subclasses (Lima and Quaresma, 1999). This division was based on data from an automatic counting/weighing station placed in Aveiro – Itinerário Principal nº 5 (IP5) (IP5 -

principal route) during the period of 7 June to 11 June of 1996. Table 2.2 presents that classification.

Table 2.1 – JAE classification of road vehicles (adapted from Lima and Quaresma (1999))




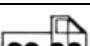







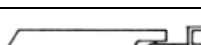
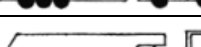


Class	Picture	Description
A		(Bi) cycles
B		Motor (bi) cycles
(Bi) cycles		Categories A + B
C		Motorcycles
D		Passenger cars with fewer than ten seats (with or without trailer)
E		Light goods vehicles with gross vehicle weight lesser than 3000 kg (with or without trailer)
Light vehicles		Categories C + D + E
F		Lorries/trucks with gross vehicle weight greater than 3000 kg
G		Lorries/trucks with gross vehicle weight greater than 3000 kg (with or without trailers)
H		Articulated vehicles Articulated vehicles with one or more trailers attached Road tractors with one or more trailers attached
I		Buses and trolley buses
J		Agricultural tractors
K		Road tractors and special purpose vehicles (bulldozers, ...)
Heavy vehicles		Categories F + G + H + I + J + K
Motor vehicles		Light + heavy vehicles
TOTAL		(Bi) cycles + light vehicles + heavy vehicles
Goods vehicles		Categories E + F + G + H

The Portuguese law (Article No. 57 of the Road Traffic Code, approved by the Decree Law No. 114/94 of 3 May) imposes that the maximum authorized vehicle weights and the maximum authorized vehicle dimensions must be defined by Regulation. The Ordinance No. 850/94 of 22 September determines these values.

Afterwards the Ordinance No. 682/96 of 21 November did some adjustments to the Regulation in order to harmonise the maximum vehicle dimensions with the Member States of the European Union (EU) according to the Directive No. 96/83/EC of 25 July. The Ordinance No. 1092/97 of 3 November transposes the Directive No. 96/83/CE into national law. Then the Ordinance No. 960/2000, published on 9 October, brings the present rules into line with technical progresses.

The Directive No. 96/83/EC, established in the framework of the common transport policy, harmonised the maximum vehicle dimensions for the circulation of road vehicles transporting goods. This Directive was amended by the Directive No. 2002/7/EC in order to harmonise the maximum vehicle dimensions for the circulation of road vehicles transporting passengers.

Table 2.2 – Heavy vehicles classification according to the number and arrangement of the axles (adapted from Lima and Quaresma (1999))

Vehicle type	Designation	
	Class	Subclass
	F	F1
		F2
		F3
		F4
Non-compliance		F5
	G	G1
		G2
		G3
Non-compliance		G4
	H	H1
		H2
		H3
		H4
		H5
		H6
Non-compliance		H7
	I	I1
		I2
Non-compliance		I3













Note: The 'non-compliance' subclasses include the vehicles that although classified in a determined class are not possible to frame in the respective subclasses.

The Decree Law No. 99/2005 of 21 June transposes into national law the amendments made to the Directive No. 96/53/EC by the Directive No. 202/7/EC and approves a new Regulation that lays down the maximum authorized weights and dimensions for road vehicles in circulation. Later, due to the importance of activities related to the transportation of woody material for the national economy, this Decree Law was altered by the Decree Law No. 131/2006 permitting the use of road trains with five-axles or more with maximum authorized vehicle weight of 60 t in these activities. The vehicles must be technically prepared for that. The Decree Law No. 203/2007 defines the maximum authorized length for these road trains. In addition, it defines the maximum authorized values for machines in circulation. Lastly, the Decree Law No. 133/2010 of 22 December permits the use of road trains with five-axles or more with maximum authorized

vehicle weight of 60 t to transport paper, paper pulp and ceramic products provided that the origin or the destination is a national port.

Table 2.3, Table 2.4 and Table 2.5 present the maximum authorized vehicle weights, the maximum authorized axle weights and the maximum authorized dimensions, respectively. Only the road vehicles transporting goods are considered.

Table 2.3 - Maximum authorized vehicle weights (Decree Law No. 133/2010)

Motor vehicles	2 axles		19 t
	3 axles		26 t
	4 axles and more		32 t
Articulated vehicles	3 axles		29 t
	4 axles		38 t
	5 axles and more		40 t – 44 t ⁽¹⁾
Road trains	3 axles		29 t
	4 axles		37 t
	5 axles and more		40 t – 44 t ⁽²⁾ – 60 t ⁽³⁾
Trailers	1 axle		10 t ⁽⁴⁾
	2 axles		18 t ⁽⁴⁾
	3 axles and more		24 t ⁽⁴⁾
Machines	Power-driven or towable machines or their combination		60 t ⁽⁵⁾

⁽¹⁾ When carrying two 20-foot (6.1 m) ISO container or one 40-foot ISO container

⁽²⁾ When carrying one 40-foot (12.2 m) ISO container

⁽³⁾ When carrying woody materials, or paper, paper pulp and ceramic products from or to a national port

⁽⁴⁾ The maximum authorized weight of the trailer may not exceed one time and half the weight of the vehicle motor with the exception of agricultural trailer

⁽⁵⁾ The maximum authorized weight of a towable machine may not exceed one time and half the weight of the road tractor

Table 2.4 - Maximum authorized axle weights (Decree Law No. 203/2007)

Single front axle		7.5 t
Single non-driving axle		10 t
Single driving axle		12 t
Tandem driving or non-driving axle, if the distance (d) between axles is	$d < 1 \text{ m}$	12 t
	$1 \leq d \leq 1.29 \text{ m}$	17 t
	$1.3 \leq d \leq 1.79 \text{ m}$	19 t
	$d \geq 1.8 \text{ m}$	20 t
Driving or non-driving tri-axle, if the distance (D) between the extreme axles is	$D < 2.6 \text{ m}$	21 t
	$D \geq 2.6 \text{ m}$	24 t

Table 2.5 - Maximum authorized dimensions (Decree Law No. 133/2010)

Length	Motor vehicle (2 axle and more)	12 m
	Trailer (1 axle and more)	12 m
	Articulated vehicle (3 axle and more)	16.5 m
	Road train	18.75 m
	Power-driven or towable machines	20 m
	Motor vehicle with semi-trailer on dolly (transportation of woody materials)	25.25 m ⁽¹⁾
Width	All vehicles	2.55 m
	Superstructures of conditioned vehicles	2.6 m
	Power-driven machines or towing machines	3 m
Height	Motor vehicles and their trailers	4 m
	Power-driven machines or towing machines	4.5 m

⁽¹⁾ The maximum dimensions of the motor vehicle and the semi-trailer may not exceed their maximum dimensions

The EU directives give general regulations for international transport within the EU. They limit the maximum authorized length to 16.5 m for articulated vehicles and to 18.75 m for road trains. They also limit the maximum authorized weight to 40 t or to 44 t in combined transport operations. However, national regulations can vary by country. The webpage of the International Transport Forum (ITF) contains information about both the permissible maximum dimensions and weights of trucks in Europe (ITF@, 2013).

The Directive 96/53/EC introduced the modular concept known as European Modular System (EMS). It allows combinations of existing units into longer and sometimes heavier vehicle combinations hereafter called Longer and Heavier Vehicles (LHVs). This concept was due to the EU access of Finland and Sweden, countries where vehicle combinations were already in use. Figure 2.8 illustrates the modular concept where it is possible to see that the volume of three EU combinations can be transported by two EMS combinations.

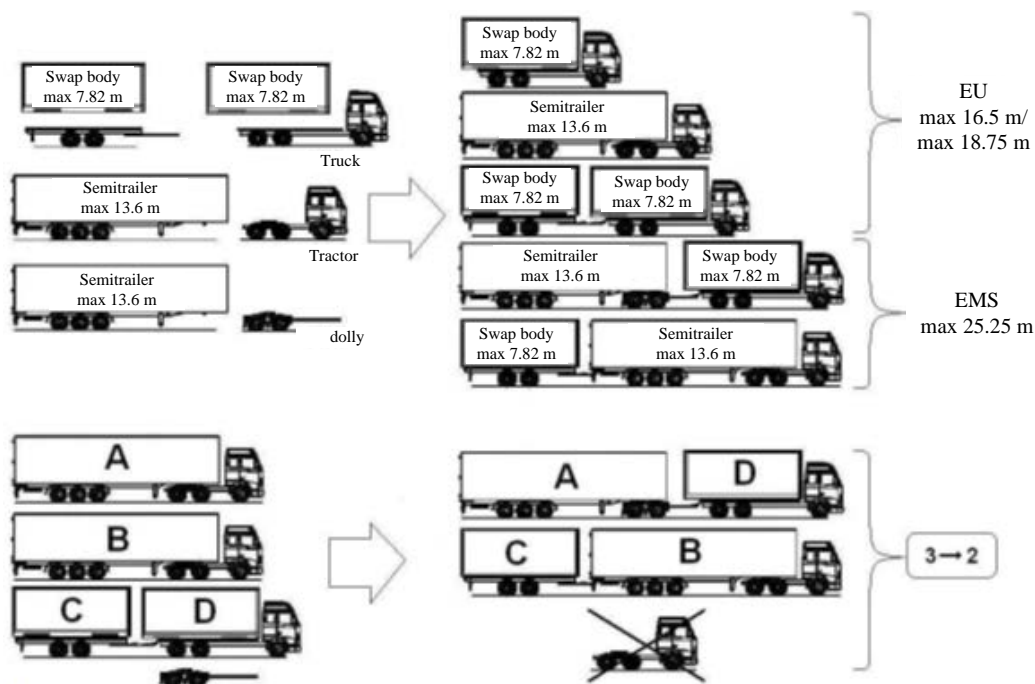


Figure 2.8 – Illustration of the modular concept (adapted from Åkerman and Jonsson (2007))

The European Commission (EC) and several EU countries have been analysing the positive and negative impacts of allowing the use of LHVs measuring up to 25.25 m and weighting up to 60 t across the EU. A lot of studies have been done to analyse these impacts such as (Ceuster et al., 2008), (Doll, 2008), (Christidis and Leduc, 2009), (Knight et al., 2008), (Knight et al., 2009) and (MDS and TRL, 2010).

LHVs are already in operation in Finland and Sweden and trials with LHVs are being planned or carried out in a number of EU countries. Figure 2.9 summarizes that.

The main concerns about LHVs are related to transport demand and modal choice, road safety, infrastructure (mainly pavements, bridges and parking facilities), emissions and energy consumption.

The main arguments cited as favourable to LHVs are the decrease of operational costs due to greater loads, the decrease of emissions, the positive impact on safety as fewer trucks are needed to transport the same amount of goods. On the other hand, the main arguments cited as unfavourable to LHVs are shifts in the freight transportation system which can lead to a transfer

from less polluting modes to the road. Hence, the reduced cost will generate more demand increasing emissions and congestion, the infrastructure could suffer greatly and if accidents occur, the damage will be higher (Ceuster et al., 2008).

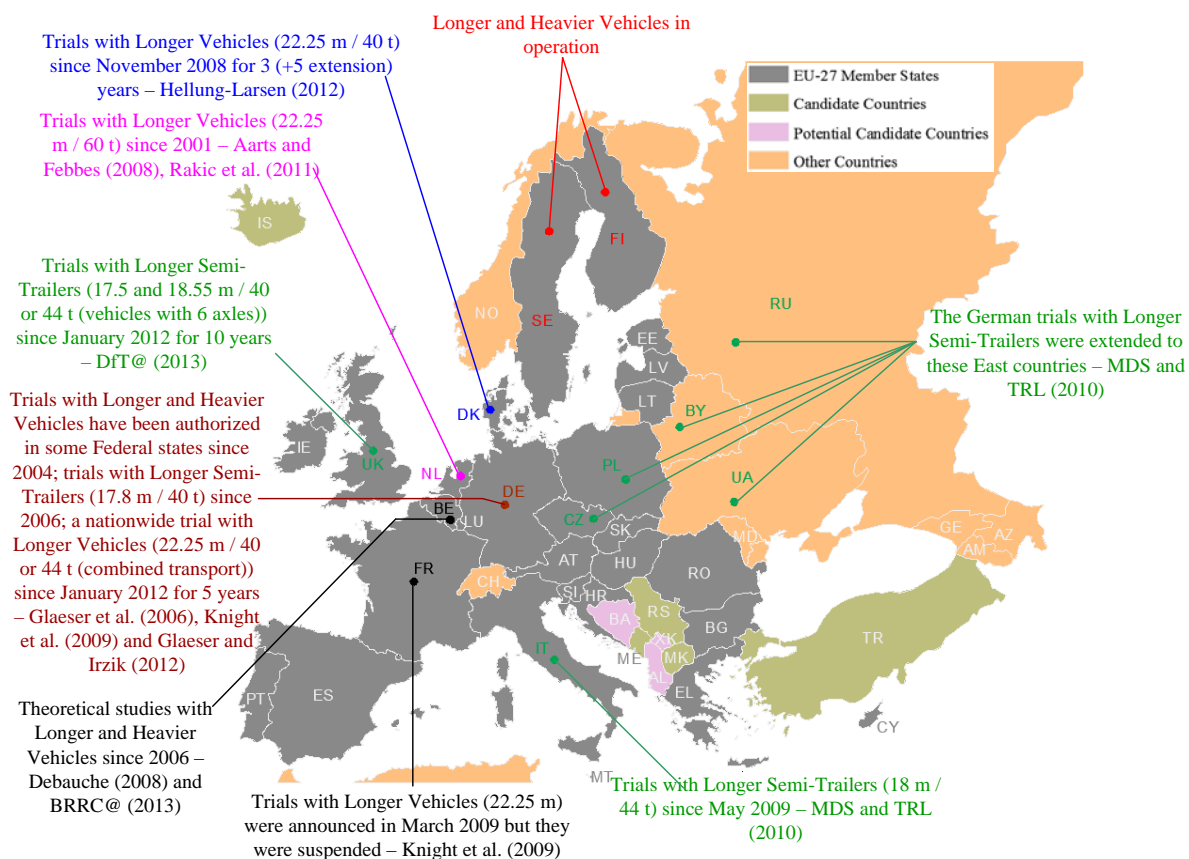


Figure 2.9 – Summary of studies and trials

In relation to the Portuguese situation, the Instituto Nacional de Estatística (INE) (Statistics Portugal) disseminates statistical data about road freight transport in Portugal every year (INE, 2012). Some of these statistical data, the most relevant to this work, are shown from Figure 2.10 to Figure 2.14. Figure 2.10 shows the total number of vehicles and the percentage by type of vehicle, Figure 2.11 shows the percentage of the two predominant types of vehicle by axle configuration, Figure 2.12 shows the percentage of the two predominant types of vehicle by load capacity range, Figure 2.13 shows the GVW and the payload by load capacity range for the lorry/truck and, finally, Figure 2.14 shows the GVW and the payload by load capacity range for the articulated vehicle. As data from 2000 to 2003 inclusive were not collected for transport operations on own-account, they are not shown in Figures.

From Figure 2.10 to Figure 2.14, the following conclusions can be drawn:

- The Portuguese road freight vehicle fleet has been changing over time. Between 1998 and 2011, the number of lorries/trucks decreased by 35%, while the number of articulated vehicles increased by 46%;
- The fleet consists basically in lorries/trucks and articulated vehicles whose predominant axle configuration is 2 axles (F1-class of Table 2.2) and 2+3 axles (H5-class of Table 2.2) respectively. In 2011, these vehicles represented 75% of the fleet;
- About 37% of lorries/trucks weigh 7.2 t, 55% of them weigh between 13 and 26 t and 8% of them weigh more than 26 t. These values correspond to the average between 1998 and 2011;

- In relation to the articulated vehicles' load capacity, a load capacity range stood out, about 46% of them weigh 40 t and this percentage has increased, it was 65% in 2011;
- About 37% of lorries/trucks carry a 3.6 t-payload, 55% of them carry payloads with weighing between 7 and 15 t and 8% of them carry payloads weighting more than 18 t;
- The most used articulated vehicles, with a load capacity of 38-40 t, carry payloads weighting 26 t in average.

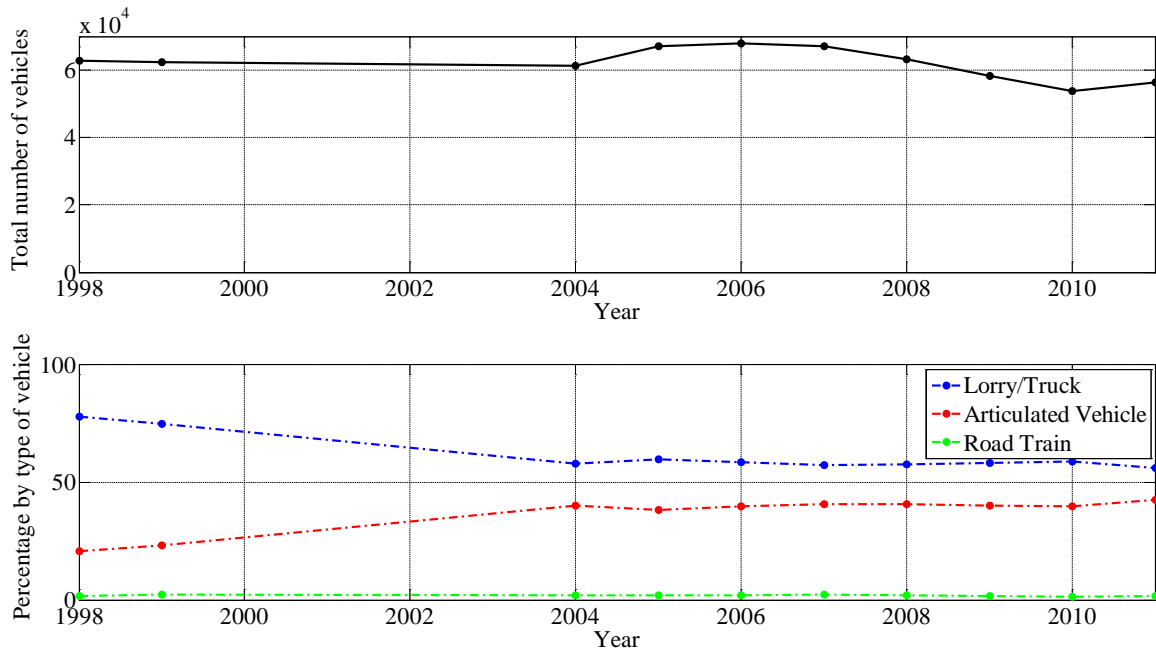


Figure 2.10 – Total number of vehicles and percentage by type of vehicle

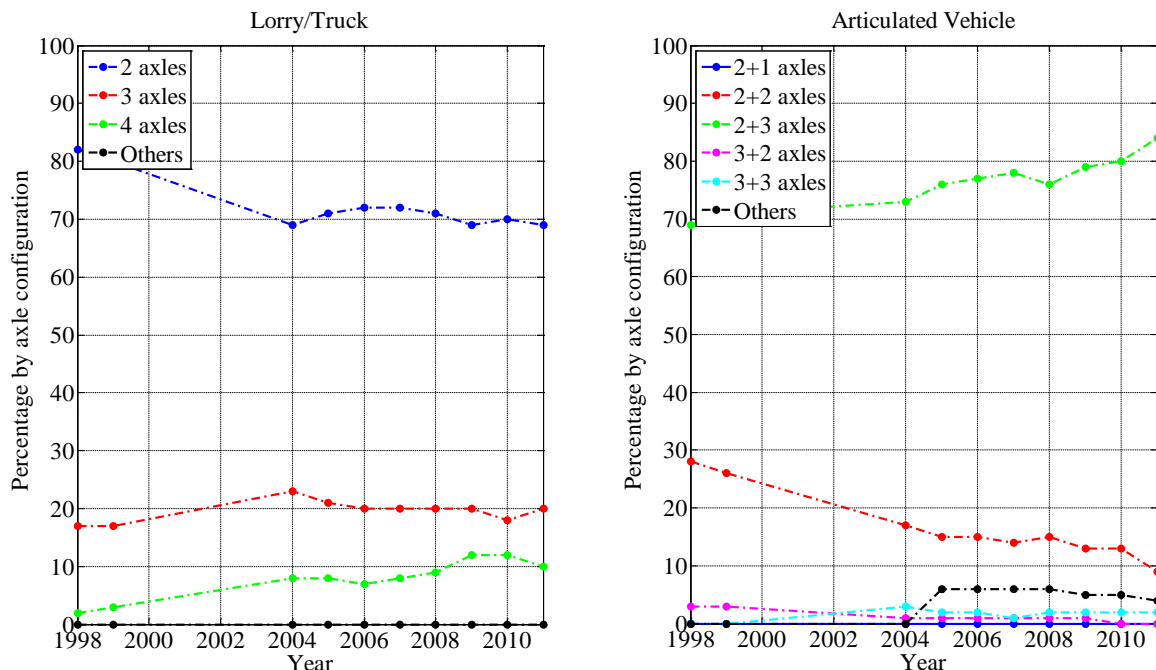


Figure 2.11 – Percentage of the two predominant types of vehicle by axle configuration

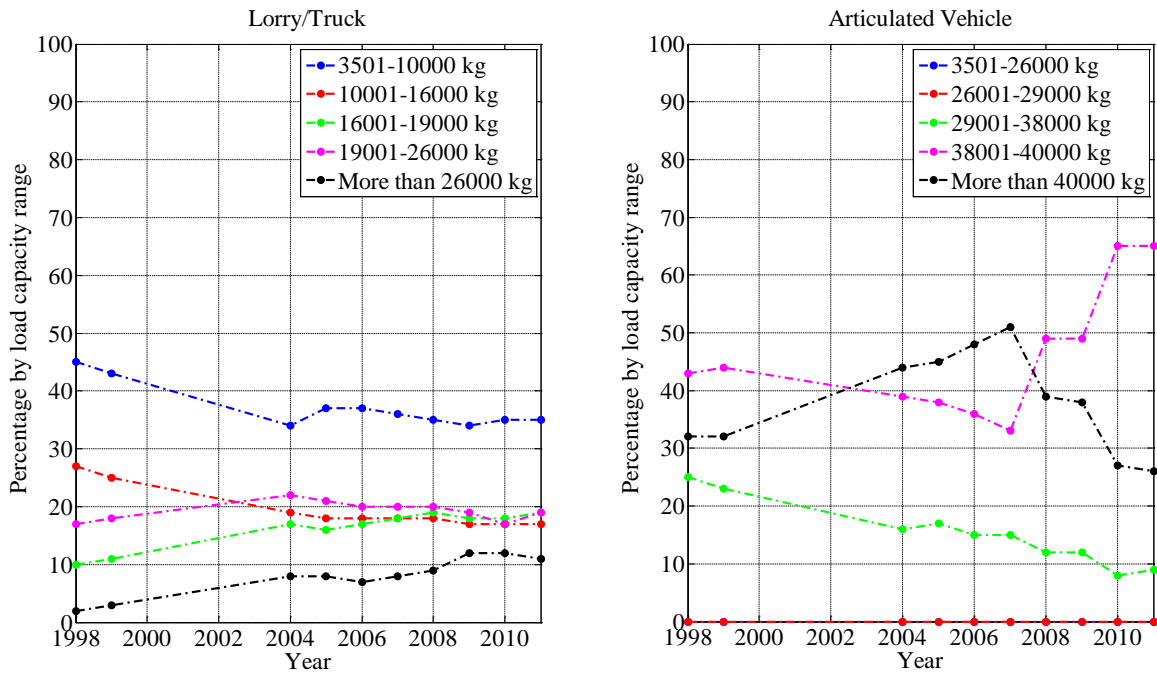


Figure 2.12 – Percentage of the two predominant types of vehicle by load capacity range

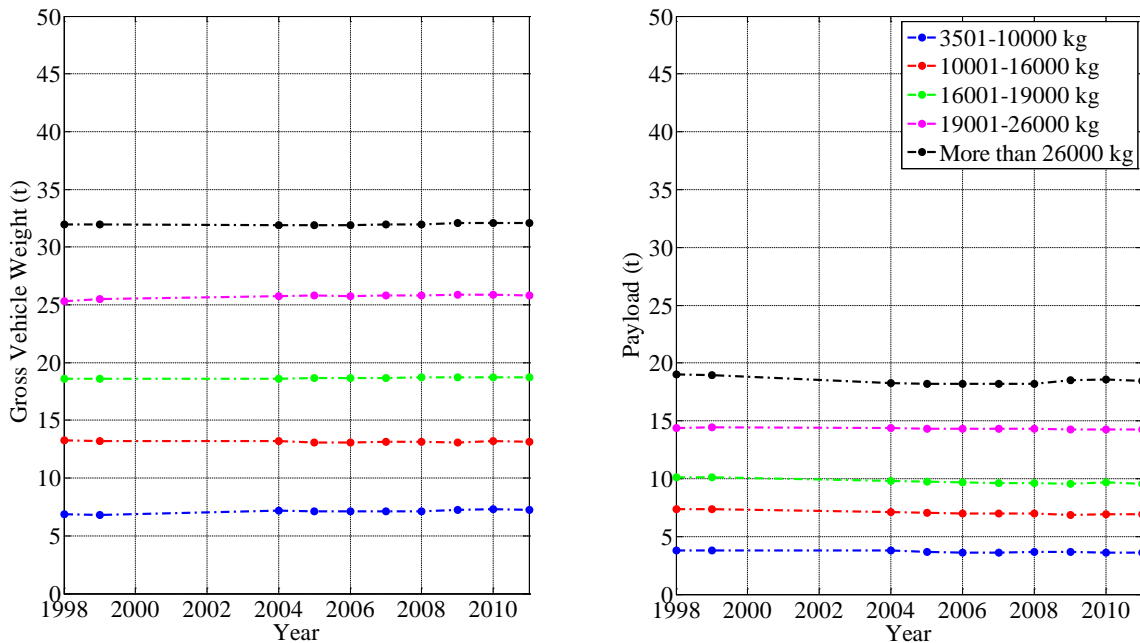


Figure 2.13 – GVW and payload by load capacity range for the lorry/truck

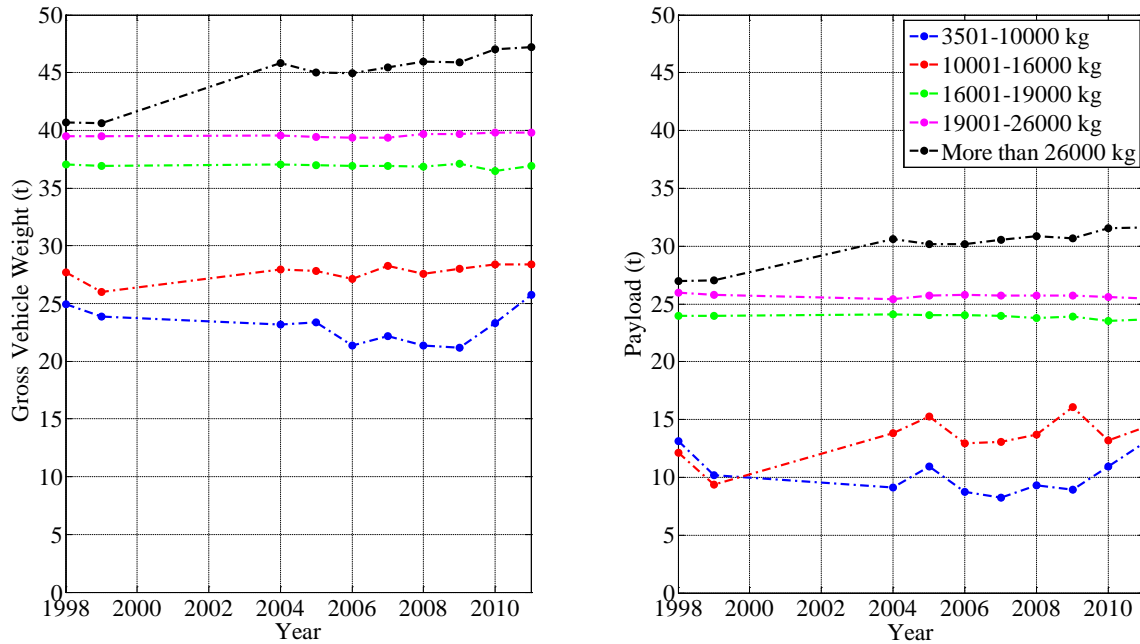


Figure 2.14 - GVW and payload by load capacity range for the articulated vehicle

2.3.3 Traffic data used in pavement design

Traffic is a key data in pavement design as it is used for estimating the loads that are applied to the pavement during its design period.

A full characterization of the traffic requires a large amount of data. The COST action 333 (1999) listed the following parameters:

- Number of heavy vehicles;
- Number of axle loads applied to the pavement;
- Dynamic axle load spectrum;
- Single, tandem and tridem axle load combinations in this spectrum;
- Load distribution within tandem or tridem axle combinations;
- Load distribution over wheels of each axle;
- Type of suspension;
- Tyre type;
- Tyre pressure;
- Contact area between tyres and pavement;
- Distribution of vertical tyre/pavement contact stress;
- Distribution of horizontal tyre/pavement shear stresses;
- Lateral distribution of the wheel loads within the traffic lane;
- Rest periods.

It is not practical to quantify some of these parameters. Therefore, the traffic data should be balanced with the pavement response model to use, the deterioration mechanisms to consider and the pavement design purpose.

Traffic counts can be categorised as follows in increasing order of accuracy (COST 333, 1999):

- Counts of total number of vehicles;
- Counts of vehicles with distinction between light vehicles and heavy vehicles;
- Counts of heavy vehicles with distribution of different types of heavy vehicles;

- Measurement of axle load spectrum, using Weight-In-Motion (WIM) systems.

A COST action 333’s questionnaire (20 countries) shows that the majority of the European countries characterise traffic by the Annual Average Daily Traffic (AADT) or by the Annual Average Daily Heavy - Traffic (AADT_h). Very often AADT is multiplied by a percentage to convert it into AADT_h. Then, the AADT_h is converted into the number of ESAL applications using AFs.

Additionally, other factors are often taken into account such as distribution of traffic in different directions, lane split, traffic growth during the pavement design period and lateral distribution.

The Portuguese manual for design of pavement structures (JAE, 1995) (hereafter called ‘MACOPAV’) calculates the cumulative number of ESAL applications by using equation (2.19). This equation converts the diversity of trucks of a Portuguese traffic flow into the number of ESAL applications by using just an AF.

$$\text{Number of ESAL applications} = \left[365 \cdot \text{AADT}_h \cdot \frac{(1 + g_h)^{DP} - 1}{g_h} \right] \cdot \text{AF} \quad (2.19)$$

where

- AADT_h = annual average daily heavy-traffic in the base year (design lane)
- g_h = annual average growth rate of heavy-traffic
- DP = design period (usually 20 years)
- AF = aggressiveness factor

This manual defines traffic classes and specifies an AF for each one. These AFs are average values from weighing stations where the occurrence of overloaded axles were taken into account, mainly in high-traffic roads. Table 2.6 presents the traffic data of MACOPAV, including the AFs.

Table 2.6 – Traffic data of the Portuguese manual (JAE, 1995)

Traffic class	AADT _h	g _h	AF	Number of ESALs (80 kN)
T ₇	<50	specific study		
T ₆	50-150	3%	2	2,000,000
T ₅	150-300		3	8,000,000
T ₄	300-500	4%	4	20,000,000
T ₃	500-800		4.5	40,000,000
T ₂	800-1200	5%	5	70,000,000
T ₁	1200-2000		5.5	100,000,000
T ₀	>2000	specific study		

The COST action 333 recommended that the traffic data for pavement design should be as comprehensive and accurate as possible, that the implementation of WIM systems should be extended and that the WIM data should be used whenever they are available. From WIM data, axle load spectra can be determined and AFs computed for the truck flow which passes (or will pass) on the pavement during its design period.

The MEPDG procedure improved the traffic data by using axle load spectra for pavement structure design (NCHRP, 2004). It does away with the ESAL concept as it uses the distribution of axle loads directly in the mechanistic model, thus allowing more detailed damage analysis.

The MEPDG procedure requires the knowledge of the axle load spectra, i.e. the distribution of the truck traffic by axle type and, within each axle type, the distribution of axle weights. To facilitate the use of this guide when the specific axle load spectra are unavailable, the MEPDG defines three hierarchical levels based on the type and amount of traffic data available: (1) site specific, (2) region specific and (3) default data or statewide averages. The difference between these levels is in terms of data quality and not in terms of the level of detail since they use the same amount and type of data.

To illustrate, Figure 2.15 shows axle load spectra for a single and a tandem axle configuration from 14 sites in different states (Long-Term Pavement Performance (LTPP) database).

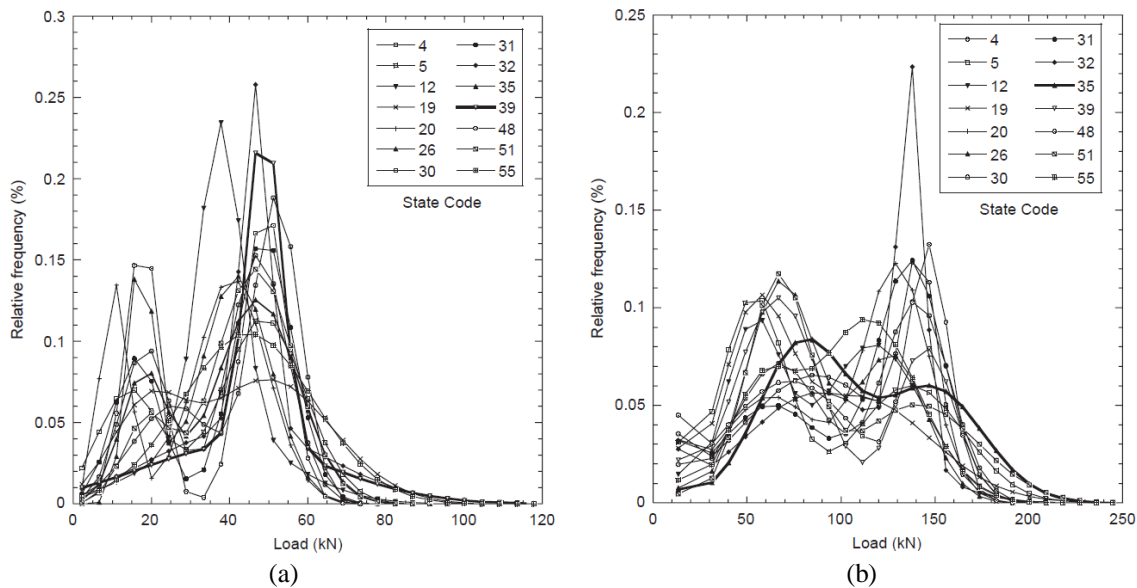


Figure 2.15 – Axle load spectra: (a) single axle and (b) tandem axle (Haider and Harichandran, 2009)

Many researchers have modelled axle load spectra as briefly outlined by Timm et al. (2005) who proposed a mixed distribution model (linear combination of lognormal and normal distributions) to characterize axle load spectra. The proposed model works very well in characterizing both single and tandem axle load distributions. Haider and Harichandran (2007) used a bimodal mixture distribution to characterize the axle load spectra. This distribution is illustrated in Figure 2.16. The parameters of the distributions can be estimated by fitting the theoretical spectra to the observed spectra.

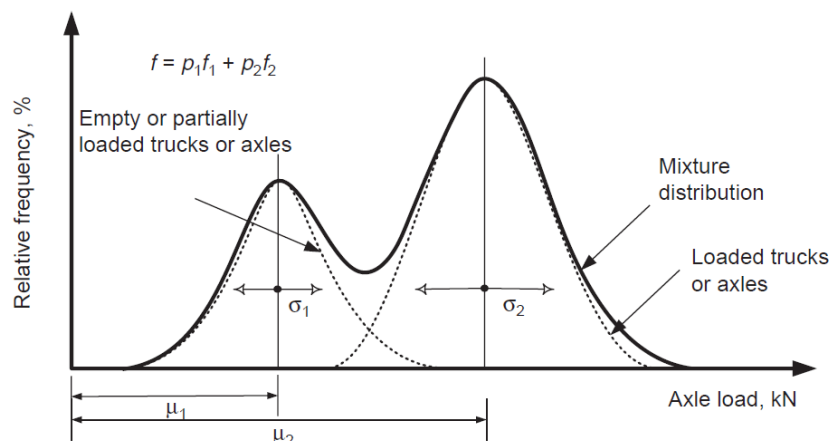


Figure 2.16 – Bimodal mixture distributions (Haider and Harichandran, 2009)

According to Haider and Harichandran (2007), it is possible to relate axle load spectra to truck GVWs and volumes, thus overcoming the non-availability of axle load data. The estimation of the axle load spectra using this type of relationships is superior to assuming the Level 3-input of the MEPDG procedure, which is the level with the poorest knowledge of traffic characteristics where regional or statewide average load distributions are used.

These researchers also related the properties of the axle load spectra to the flexible pavement performance (Haider and Harichandran, 2009). For that, they estimated properties of the bimodal mixture distributions from the five parameters defined in Figure 2.16. These estimations were then correlated with predicted flexible pavement performance (cracking, rutting and roughness). They generically concluded that higher loads appear to cause more cracking, whereas a higher number of load repetitions is more critical in developing more rutting. Roughness growth is affected by load magnitudes and traffic levels at the same time.

Romanoschi et al. (2011) in the developing process to get traffic data inputs required by the MEPDG procedure to design pavements in the New York State - USA, analysed the variability of traffic data obtained from individual stations, state average values and default values recommended by the MEPDG procedure. Figure 2.17 illustrates this variability for the axle load spectra. The results suggest that the majority of traffic data are site specific and that no state average or default values should be used in the pavement design process.

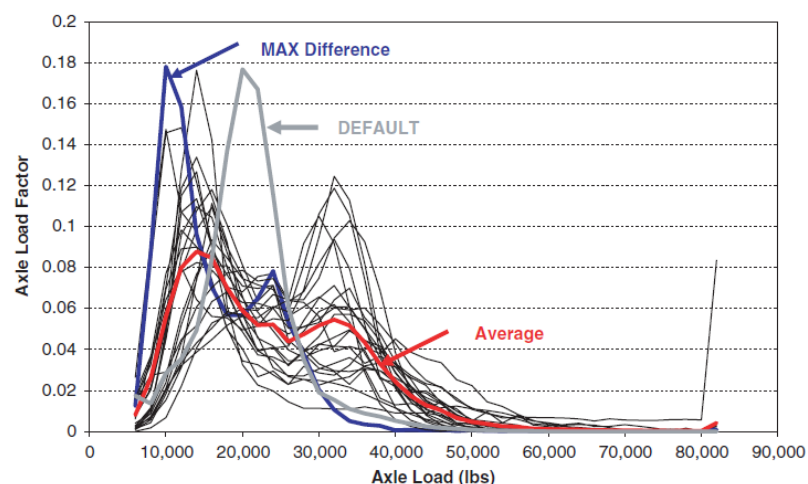


Figure 2.17 – Variation of the axle load spectra (Romanoschi et al., 2011)

Axle load spectra are defined using traffic data collected at WIM stations. Therefore, the accuracy and calibration of the WIM stations can influence the pavement design. WIM errors comprise, according to the nature of error occurrence, random errors and systematic errors. Random errors can be due to road profile (longitudinal/transverse), vehicle (speed, acceleration, tyre conditions, load, and suspension type) and environment (wind, water, and temperature). Systematic factors can be due to inadequate calibration of WIM stations.

Haider et al. (2010) investigated the impact of WIM errors on axle load spectra and quantified the effect of these errors on flexible pavement performance (cracking, rutting and roughness). Regarding previous works, they considered the reliability procedure used in the MEPDG. The results show a significant impact of WIM errors in pavement performance which is more pronounced in negative measurement bias. Nevertheless, the MEPDG reliability procedure compensates the negative measurement bias for most of the distresses, except for cracking when the negative bias is high. To prevent high negative bias, WIM systems must be calibrated periodically.

Due to the importance of accurate and reliable WIM systems, the EC supported the COST action 323 (‘Weight-in-Motion of Road Vehicles’) (COST 323, 2002) and the research project Weight-in-motion of Axles and Vehicles for Europe (WAVE) (WAVE, 2001). The main objective of the COST action 323 was to cover the need of specification for WIM systems. The WAVE project emerged from the COST action 323 with the purpose to have more advanced research on WIM.

Since the appearance of the MEPDG procedure, traffic data has been receiving considerable attention. It is important to define reliable traffic data at the beginning of the pavement design life as well as throughout the pavement design period. Hajek et al. (2011) give an overview of issues which affect forecasting of traffic loads, such as economic conditions, economic restructuring and manufacturing industries, globalization of the economy and the effect of free trade, regulatory changes in truck size and weight, changes in cargo shipping, e-commerce and improvements in truck utilization.

This subsection presented an overview of traffic data currently used. To summarize, the mixed truck traffic flow is currently converted into a number of ESAL applications. This conversion can be more or less accurate depending on the traffic data available and it is discussed in more detail in the next subsection.

2.3.4 Aggressiveness factors

A mixed truck traffic flow, which passes on the pavement structure during the design period, is composed of several types of trucks, equipped with different axles and tyres and carrying loads with different weights. Each truck causes a different damage to the road. In order to make pavement design simpler, the damage of each particular axle is converted into a number of ESAL applications through of an Equivalent Axle Load Factor (EALF). Therefore, pavement design is based on the number of ESAL applications during its design period. Figure 2.18 shows the standard axle load used in this work, which is the considered by the Shell method (Branco et al., 2005).

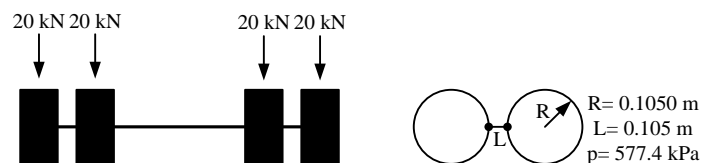


Figure 2.18 – 80-kN Standard axle load (ESAL)

Since the EALF of an arbitrary axle represents the pavement damage caused by a pass of this arbitrary axle relative to the damage caused by a pass of an ESAL, the number of ESAL applications can be computed from the knowledge of the EALFs of every axle pass on the pavement during its design period by using expression (2.20) (Huang, 2004).

$$\text{Number of ESAL applications} = \sum_{i=1}^{\text{Nr axles}} \text{EALF}_i \cdot N_i \quad (2.20)$$

where

- EALF_i = equivalent axle load factor for the *i*th-axle load
- N_i = number of passes of the *i*th-axle load during the design period

As the damage is the inverse of the number of load repetitions until failure, the EALF can be computed by the ratio of the number of passes of the ESAL to the number of passes of the *i*th-axle load during the design period using expression (2.21).

$$EALF_i = \frac{\text{Damage}_{\text{ith-axle load}}}{\text{Damage}_{\text{ESAL}}} = \frac{N_{\text{ESAL}}}{N_{\text{ith-axle load}}} \quad (2.21)$$

The fourth power law (Branco et al., 2005), developed in the Road Test conducted by the American Association of State Highway Officials (AASHO), is usually used to calculate the EALF as shown in expression (2.22).

$$EALF_i = \frac{\text{Damage}_{\text{ith-axle load}}}{\text{Damage}_{\text{ESAL}}} = \frac{N_{\text{ESAL}}}{N_{\text{ith-axle load}}} = \left(\frac{\text{Load}_{\text{ith-axle}}}{80} \right)^4 \quad (2.22)$$

However the ‘validity’ of this law is questionable particularly for current axle loads and axle configurations, tyre sizes and pressures, pavement construction, traffic volumes, all of which are significantly different from the conditions of the Road Test (Cebon, 1999).

The COST action 333 (COST 333, 1999) recommended not use the fourth power law. Instead, it is recommended to use deterioration models to calculate directly the damage caused by individual axle configurations. Therefore, expressions (2.11) and (2.14) are used to calculate the load repetitions until failure, respectively for fatigue and rutting, resulting in two mechanistic-empirical EALFs, one for fatigue, expression (2.23), and one for rutting, expression (2.24).

$$\text{Fatigue EALF}_i = \left(\frac{\text{Fatigue strain}_{\text{ith-axle load}}}{\text{Fatigue strain}_{\text{ESAL}}} \right)^5 \quad (2.23)$$

$$\text{Rutting EALF}_i = \left(\frac{\text{Rutting strain}_{\text{ith-axle load}}}{\text{Rutting strain}_{\text{ESAL}}} \right)^4 \quad (2.24)$$

Knowing EALFs, it is possible to calculate the number of ESAL applications by expression (2.20) and then the AF by expression (2.25). An AF for each failure criterion can be obtained.

$$AF = \frac{\text{Number of ESAL applications}}{\text{Number of trucks}} \quad (2.25)$$

When WIM data are available and consequently the axle load distributions or spectra can be determined, the conversion of generic axles carrying loads with different magnitudes into the number of ESAL applications can be greatly improved.

In a framework of a protocol, JAE and LNEC evaluated AFs from data collected in WIM systems (Lima and Quaresma, 1999; Lima et al., 2000). They calculated the EALF of each truck’s axle using expression (2.22), then the number of ESAL applications and finally the AF by dividing the total number of ESAL applications by the total number of trucks.


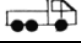
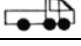
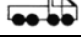
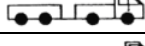

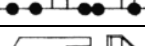
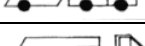
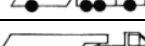
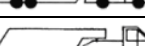
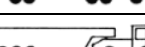
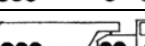
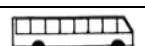
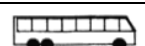

As the AF depends strongly on the power of expression (2.22), which in turns is closely related to the AASHO Road Test conditions, Lima and Quaresma (1999) analysed the AFs determined

in the FORCE project and given the design criterion used in Portugal to prevent fatigue damage, they decided to test the power 5, besides the power 4. They calculated the AF for each subclass of Table 2.2 using both powers, and they found that the AF with power 4 is higher when the weight per axle is lower, and that the AF with power 5 is higher when the weight per axle is higher. Therefore, a conservative analysis was adopted using power 5.

They also calculated the EALF of multiple axles (tandem or tridem) following two different procedures: (1) the ‘single standard axle’ procedure, where the EALF is calculated for each multiple axle’s sub-axle, and (2) the ‘multiple standard axle’ procedure, where the EALF is calculated for each multiple axle but considering as reference a multiple standard axle, the 133-kN standard axle load for tandem axles and the 182-kN standard axle load for tridem axles. Both procedures gave similar results. There were differences in the subclasses G3, H3 and H6 mainly due to an unequal distribution of the load between the sub-axles of the multiple axle. In the subclasses G3 and H6 the ‘single standard axle’ procedure gave higher truck factors (high unequal distribution) while in the subclass H3 the result was the opposite (low unequal distribution). In order to consider the unequal distribution of the load between the sub-axles of the multiple axle, the ‘single standard axle’ procedure was chosen.

Table 2.7 presents the AF for each subclass as well as the number of vehicles considered in the calculation. It is worth noting that these are average AF and that there was found a great range between the minimum and the maximum AFs. The maximum AF of each subclass is substantially greater than the representative values in the range of 25-75 per cent.

Table 2.7 – AFs for each subclass (Lima and Quaresma, 1999)

Vehicle type	Designation		Sample size	Mean AF	Minimum AF	Maximum AF
	Class	Subclass				
	F	F1	1074	1.12	0.0000	53.04
		F2	279	3.84	0.0001	74.54
		F3	16	1.04	0.0015	12.79
		F4	33	3.74	0.0019	26.40
	G	G1	61	3.45	0.0003	40.48
		G2	17	5.96	0.0851	31.13
		G3	61	7.53	0.0539	75.95
	H	H1	243	0.15	0.0000	8.56
		H2	4	0.11	0.0617	0.16
		H3	628	9.21	0.0005	102.90
		H4	20	12.02	0.0367	56.50
		H5	596	3.29	0.0010	116.80
		H6	7	3.11	0.1081	9.99
	I	I1	404	1.79	0.0610	9.01
		I2	21	0.55	0.1273	1.26

The pavement damage is based on the total number ESAL applications during the design period and on the allowable number of ESAL applications given by transfer functions. Knowing the AF of each truck of the flow, the number of ESAL applications can be calculated by expression

(2.26). Since the transfer functions depend on the failure criteria, fatigue damage and rutting damage are calculated by expressions (2.27) and (2.28), respectively.

$$\text{Number of ESAL applications} = \sum_{i=1}^{\text{No. Trucks}} AF_i \cdot N_{\text{Truck}_i} \quad (2.26)$$

$$\text{Fatigue damage} = \frac{\text{Number of ESAL applications}}{\text{Allowable number of ESAL applications}_{(\text{fatigue transfer function})}} \quad (2.27)$$

$$\text{Rutting damage} = \frac{\text{Number of ESAL applications}}{\text{Allowable number of ESAL applications}_{(\text{rutting transfer function})}} \quad (2.28)$$

2.3.5 Pavement response for multiple axle configurations

When the pavement is subjected to multiple axles (tandem, tridem, or quad), the location of the critical pavement response (maximum strain) is not clear.

The AASHTO Guide for Design of Pavement Structures (AASHTO, 1993) defines EALFs which represent the ratio of the number of repetitions of any axle load and axle configuration (single, tandem, tridem) necessary to cause the same reduction in the Present Serviceability Index (PSI) as one application of an ESAL (80-kN single axle load). The EALF for a 160-kN tandem axle load is 1.38 and the EALF for a 240-kN tridem axle load is 1.66. Therefore, a tandem axle is equivalent to 1.38 ESAL applications and a tridem axle is equivalent to 1.66 ESAL applications.

According to Branco et al. (2005), a tandem axle (P-kN) corresponds to 1.4 single axles (P/2-kN) and a tridem axle corresponds to 2.3 single axles (P/3-kN).

In its turn, Lima and Quaresma (1999) recommend to consider the multiple axle as a set of independent axles, i.e. a tandem axle corresponds to two axles, and a tridem axle corresponds to three axles, allowing hence the consideration of unequal distribution of the load between the individual axles of the multiple axle.

Gillespie et al. (1992) investigated the effects of heavy vehicle characteristics on pavement response and performance, and they concluded that two axles in a tandem suspension have the same effect as two independent axles. Consequently, a 160-kN tandem axle is equivalent to two ESAL applications. Their results are not in agreement with the AASHTO Design Guide of Pavements structures. They attributed this discrepancy to the fact that AASHTO equivalency factors are based on an empirical methodology that includes environmental factors and other variables while their methodology relates damage only to strains in the pavement structure.

As already mentioned, the MEPDG procedure classifies truck traffic by axle type (single, tandem, tridem, or quad), and within each axle type, it calculates the distribution of axle weights. Then it calculates the critical pavement responses (maximum strain for each failure criterion) for each axle configuration. As it is not possible to specify the location in which will incur the greatest damage for the different axle types, the MEPDG procedure searches for the maximum strain within the multiple axle pulses. For that, it defines analysis locations where the maximum damage could occur.

For any axle type, the MEPDG procedure uses only the single axle pulse and then it calculates the tandem, tridem and quad strain by superposition (NCHRP, 2004). This approach considers that all wheels in the gear assembly have the same load and tyre pressure.

Figure 2.19 illustrates the x-y plane analysis locations for the four axle types. Seventy x-y locations are analysed for each axle type. The depths (z) at which the calculations are performed depend on the distress type. Table 2.8 defines how the critical pavement response is estimated from the analysis locations. The simplest case is that of a single axle with dual wheels, where no superposition is required.

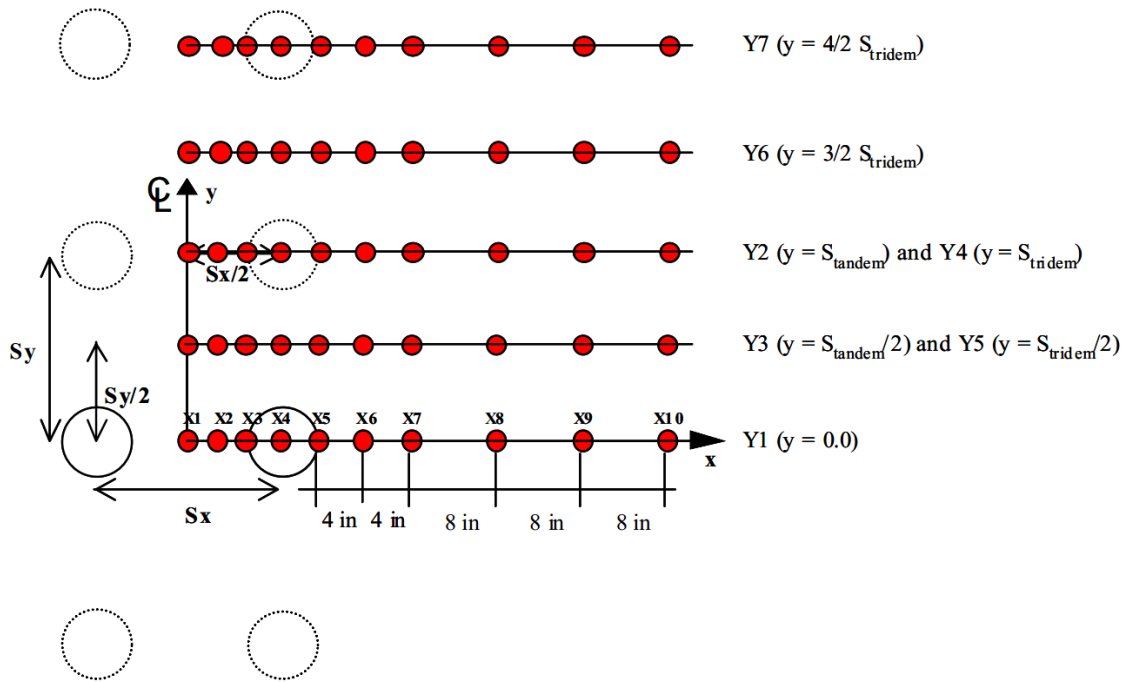


Figure 2.19 – Summary of schematics for horizontal analysis locations of critical response (NCHRP, 2004)

Table 2.8 – Critical pavement responses (NCHRP, 2004)

Single axle	Response 1 = Y1
Tandem axle	Response 1 = Y1 + Y2 Response 2 = 2 × Y3
Tridem axle	Response 1 = Y1 + 2 × Y4 Response 2 = 2 × Y5 + Y6
Quad axle	Response 1 = Y1 + 2 × Y4 + Y7 Response 2 = 2 × Y5 + 2 × Y6

The critical pavement response is significantly affected by the superposition method used as well as by the analysis locations.

Salama et al. (2007) calculated axle factors, based on rutting, due to different axle types using three procedures: (1) the MEPDG procedure, (2) a procedure that accounts for the effect of each individual axle of the multiple axle, and (3) a procedure that integrates the entire strain pulse. The axle factors were compared with results from laboratory tests. They concluded that the MEPDG procedure (procedure 1) significantly underestimates rutting prediction due to multiple axles. The calibration of the MEPDG rut models improves the results but they are still lower than the expected ones for multiple axles. On the other hand, the procedure 2 overestimates the axle

factors. The procedure 3 appears to be the best method and it shows that rutting damage is proportional to the number of individual axles of the multiple axle.

Salama and Chatti (2010) also evaluated different summation procedures to calculate the pavement damage (fatigue and rutting) caused by multiple axle configurations. Two discrete methods, peak and peak mid-way, and two continuous methods, strain area and dissipated energy, were considered as well as the MEPDG procedure. They concluded that, for fatigue damage, it is important to consider the entire strain pulse and that, for rutting damage, the peak strain method has the best agreement with the laboratory values. The MEPDG procedure underestimates the damage, both fatigue and rutting damage.

According to Zhao et al. (2012), the MEPDG procedure can be used to identify the critical location and obtain the critical response for a tandem axle, but it is inadequate for a tridem or quad axle as it underestimates the critical pavement response.

For pavement design purposes, the loads of multiple axles are mostly converted to an equivalent number of ESAL applications by summing the contributions of the individual axles (COST 334, 2001).

2.3.6 Dynamic loads

When the vehicle is not moving, the loads applied on the pavement surface by the tyres are constant. They are only due to the force of gravity. These loads are called static loads. In contrast, when the vehicle is moving along the road, road roughness excites the vehicle and it moves up and down causing dynamic variations to the loads, above and below their static values.

The magnitude of the variations depends on the vehicle dynamics, the road longitudinal profile and the travel speed. The variation generally increases with both the road roughness and the travel speed.

The Dynamic Interaction between Vehicles and Infrastructure Experiment (DIVINE) (OECD, 1998) adopted the Dynamic Load Coefficient (DLC) as a prime measure of dynamic loading. The DLC is defined as the ratio of the Root Mean Square (RMS) dynamic wheel load to the mean wheel load, where the RMS dynamic wheel load is essentially the standard deviation of the probability distribution (Figure 2.20). Therefore, DLC is the wheel load coefficient of variation. The mean value of the probability distribution reflects the constant (static) component of the wheel loading and varies with road transport regulations and other factors.

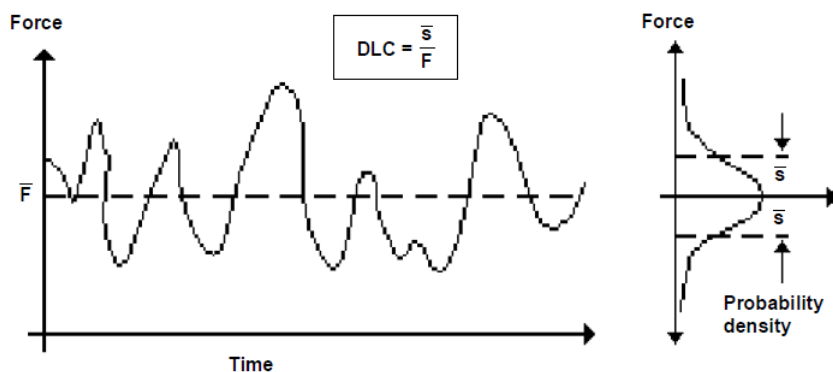


Figure 2.20 – Definition of DLC (OECD, 1998)

As a point of reference, if every axle of a truck runs perfectly over a smooth road, the theoretical DLC is zero. Maximum values of DLC have been observed in the range of 0.30-0.35 (Gillespie et al., 1992).

Impact factor is another measure of dynamic loading and it is calculated as the ratio between the dynamic load and the static load.

Dynamic loading increases pavement damage. Besides load magnitude, also the frequency content of the dynamic wheel loads is important for pavement damage.

The vibration of heavy vehicles, and hence the dynamic wheel loads, fall into two distinct frequency ranges (Cebon, 1999):

- 1.5 to 4 Hz: sprung mass bounce, pitch and roll vibration modes;
- 8 to 15 Hz: unsprung mass bounce and roll modes, ‘load-sharing’ suspension pitch modes.

At 100 km/h these modes of vibration are excited by roughness irregularities with wavelengths of 6.9 to 18.5 m and 1.9 to 3.5 m, respectively. Various experimental and theoretical studies have shown that the lower frequency sprung mass modes usually dominate the dynamic wheel loads on highways, except for vehicles which have axle group suspensions with poorly damped bogies pitching modes. These suspensions are only found on a small proportion of heavy goods vehicles (Cebon, 1999).

Dynamic wheel loads can be either measured using Multiple-Sensor WIM (MS-WIM) systems or predicted using computer simulation models. Since the end of the last century, computer simulation models have had acceptable accuracy (OECD, 1998).

2.3.7 Spatial repeatability

Usually it is assumed that damage is uniformly distributed along the pavement. However, various researchers have suggested that peak forces applied by a mixed truck traffic flow are concentrated at specific points along the pavement and termed this effect ‘spatial repeatability’ (Cebon, 1999). Spatial repeatability makes some locations along the pavement incur significantly more damage than the average and consequently the pavement life is governed by these locations.

Hahn (1985) suggested that spatial repeatability is expected in normal flows as a large portion of heavy vehicles possesses similar geometry and dynamic characteristics and tends to travel at similar highway speeds (cited in Mrad et al. (1998)).

O’Connor et al. (2000) present results of an experimental road research project showing that the same vehicle travelling several times at the same speed over a specific road profile generates impact factor patterns with strong spatial repeatability and that some different trucks of the same type (articulated vehicle with 5 axles) generate impact factor patterns with weak spatial repeatability. However, when average impact factor patterns of different trucks of the same type passing during 6 days are considered and compared with dynamic load patterns of others 6 days, they are similar, although with differences in values. Considering the total traffic flow data, the average impact factor patterns of a specific vehicle type show clear evidence of spatial repeatability and it becomes clearer as the number of considered trucks increase. The researchers

called this phenomenon ‘Statistical Spatial Repeatability’ (SSR). Figure 2.21 shows that SSR remains even when different vehicle types are considered.

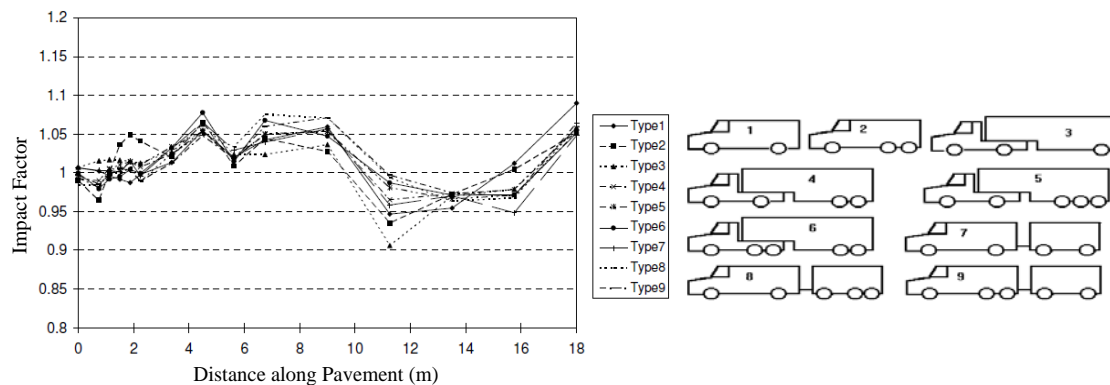


Figure 2.21 – Impact factor patterns for several types of vehicles (1 to 9) (O'Connor et al., 2000)

O'Connor et al. (2000) concluded that SSR is characteristic of a given site and is largely governed by the pavement. For a small sample of vehicles, the dimensions and the dynamic parameters of the vehicles (vehicle effect) influence strongly the impact factor and the pavement effect is suppressed. When the sample size increases, the different influences of many individual vehicles compensate and the pavement effect becomes dominant.

As patterns of SSR are a key factor in pavement design, some researchers have been developing models to predict them. Wilson et al. (2006) presents a method for predicting patterns of SSR through the use of a truck traffic flow model inferred from measurements of dynamic tyre forces using Bayesian statistics. Belay et al. (2008) also present a model to solve the same problem but they use a more direct approach which provides insights into the sensitivity of the force patterns to variations in the truck properties of the truck flow. They defined the statistical properties of the truck flow (truck flow model) by minimising the sum of squares of the differences between the theoretical and statistical measurements of the forces.

Obrien and Taheri (2011) used a computer model to predict the dynamic behaviour of a truck flow and they highlighted the importance of SSR in damage evolution during the pavement life. As pavement damage causes the road profile to change, the predicted pattern of SSR needs to be updated periodically, which is computationally very demanding. To overcome this problem, they used a numerical integration approach of forces at each point and they showed that it is sufficient to predict the changing road surface. Taheri et al. (2012) extended the previous approach to three dimensions.

2.3.8 Payload

The payload of a vehicle is limited by weight or by volume and it is the density of the carried commodities that determines which will be the case for any particular vehicle. Table 2.9 shows density values of common commodities.

The volume capacity of the European articulated vehicle (tractor-semitrailer combination) is about 100 m³ and its maximum weight is about 26 t. Dividing 26 t by 100 m³ allows knowing the density of the cargo (0.26 t/m³) which fully loaded the articulated vehicle both in terms of volume and weight. When the density of the cargo is lower than 0.26 t/m³, the payload is limited by volume. On the other hand, when the density of the cargo is higher than 0.26 t/m³, the payload is limited by weight.

Table 2.9 – Density values of common commodities (OECD, 2011)

Commodity	Density (t/m ³)
Milk, Beer, etc.	1
Fuel, Oil, Ethanol, etc.	0.6 – 0.8
Earth	1.3 – 2.0
Concrete	2.2
Briggs	1.9
Alloy	2.7
Steel	7.9
Wood (dry)	0.5 – 0.9
Rubber	1.2
Beer boxes with 20 empty bottles (0.3mx0.3mx0.4m) weigh 10	0.3
Beer boxes with 20 filled bottles (same size, but 20 kg)	0.6
Refrigerators (white goods)	0.13
Nine passenger cars, 1.5 t each, on a 100 m ³ transporter	0.135
Single dispatched items (parcels)	0.15
Plastic foam	0.04

Some European vehicles have higher volume capacity (up to 125 m³) without exceeding the permissible maximum dimensions. They are articulated vehicles with a low frame obtained by using tyres with very small diameters and the so-called ‘low-coupled’ trailers which reduce the space between the truck and the trailer (OECD, 2011). Another way to increase volume capacity is to replace the standard rigid semi-trailer axles by an independent suspension at each wheel of the semi-trailer or to use double-deck trailers. Sometimes an increase in volume capacity reduces the maximum payload weight due to an increase in unladen vehicle weight.

The efficiency of the road freight transport is closely related with the carried payload which ideally should be equal to the maximum payload, either in terms of mass or volume. This efficiency can be improved by increasing load factors - ratio between the average payload (when laden) and the maximum payload, expressed in either mass or volume terms (OECD, 2011) - and by reducing empty running. These can be achieved by improvements in the logistic chain such as the use of advanced tools with real-time information.

Figure 2.22 shows the vehicle-kilometre percentage of empty running between 2002 and 2011, including both the national and the international transport. The lowest, the highest and the average value are depicted for each country. The average empty running for all countries is about 25%. The Netherlands has the lowest value, about 15% of empty running.

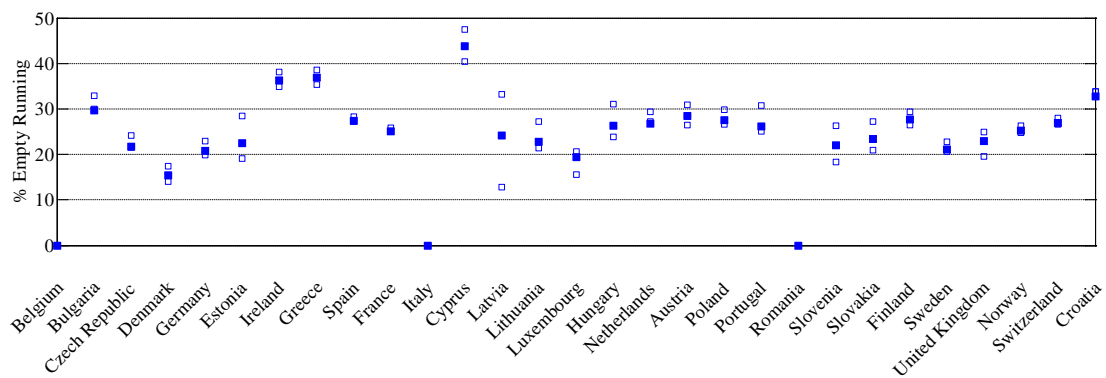


Figure 2.22 – Vehicle-kilometre percentage of empty running (OECD, 1998)

From Eurostat database in the interval 2002-2011 (Eurostat, 2013), the load factor (in mass) of the articulated vehicle with 2+3 axles was calculated dividing the tonnes-kilometre by the vehicles-kilometre and then by the maximum payload (26 t). Figure 2.23 shows these load

factors for each country. The lowest, the highest and the average value are again depicted for each country. The average load factor for all countries is about 0.70.

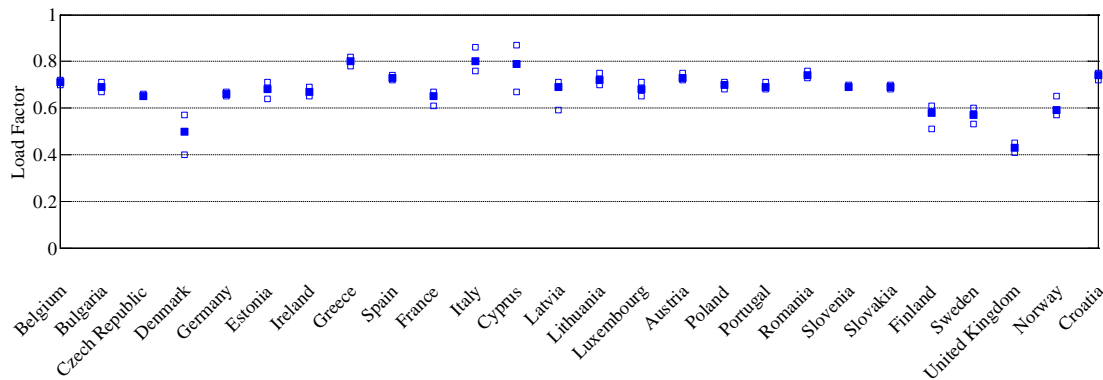


Figure 2.23 – Calculated load factors for the articulated vehicle with 2+3 axles

In addition, the efficiency of road freight transport is in its turn linked to environmental efficiency which puts more highlighting in carried payloads.

Cabotage is seen as an important, transitory step in increasing the efficiency of the market as it is seen as a way of reducing empty running after an international journey (Gleave et al., 2013). Cabotage operations means national carriage for hire or reward carried out on a temporary basis in a host Member State (EC, 2009).

A study requested by the European Parliament's Committee on Transport and Tourism analyses the European freight cabotage transport services in the EU and discusses the main changes that have occurred in the regulation of this market in recent years (Gleave et al., 2013).

The road cabotage has experienced changes in recent years. The Regulation No. 1072/2009 (EC, 2009) aimed to remove the national interpretations of the previous Regulation No. 3118/93 (EEC, 1993), thus increasing certainty in the sector. However, improvements can still be made to the Regulation particularly in relation to the interpretation of current rules and enforcement.

One of the recommendations of the study requested by the European Parliament's Committee on Transport and Tourism to ensure efficiency and reduce empty running is to consider a different approach to the '3 in 7' rule through the removal of the maximum number of cabotage operations (3) allowed in 7 days and/or a revision of the provision that requires the full unloading of international carriage before a cabotage operation (Gleave et al., 2013).

2.3.9 Overloading

Overloading is among the most important causes of the deterioration of pavement structure conducting to clear maintenance and repair costs (Sadeghi and Fathali, 2007). In addition, it deals with unfair competition between transport companies as the fraudsters can illegally gain undue competitive advantages.

The proposal for amending the Directive 96/53/EC (EC, 2013) refers that, on average, one in three vehicles checked is overloaded and these excess loads often exceed the maximum authorized weight by 10 or even 20%. It is therefore necessary to add provisions on controls and penalties to Directive 96/53/EC to re-establish compliance with the rules of competition between transporters ensuring the durability of the pavement structure.

In the framework of the proposal for amending the Directive 96/53/EC (EC, 2013), more properly in the public consultation, a group of stakeholders highlighted the relatively large number of infringements related to overloaded vehicles. The association Euro Control Route controlled 28,639 trucks in week 21 of 2012 and found 21% of them overloaded. Other evidence was found in France (March 2010) where a third of the checked vehicles were overloaded, one of them overloaded by 80%. This proposal refers that these values are in accordance with reports from Member States which have stated that 35% of the checked vehicles are overloaded.

The Observatório Transfronteiriço Espanha/Portugal (OTEP) (Spain/Portugal cross-border observatory) carried out a pilot project whose objective was to know how the freight road transport between Portugal and Spain processes (OTEP, 2004). For that, the weight per axle of vehicles was collected. In the total of loaded vehicles, 14% of them were overloaded. The intensity of overloading was analysed. Only the vehicles with maximum authorised weight of 18 t had more than 20% above the maximum. The vehicles with maximum authorised weight of 36 t and 40 t had less than 20% above the maximum.

In addition, from the report of Lima and Quaresma (1999) it is possible to verify that the measured maximum GVWs are far above the maximum authorized vehicle weights. For the two predominant types of vehicle of the Portuguese truck traffic fleet, subclass F1 and H5 of Table 2.2, the following percentages were found, 50% and 38% respectively.

Sadeghi and Fathali (2007) developed a model for ticketing the overloaded vehicles and concluded that the owners of overloaded vehicles are not paying adequate compensation for the pavement damage they are causing.

Oh et al. (2007) investigated the effects of overloaded vehicles on a truck route in Brownsville (Texas) using WIM data. To compare overloaded vehicles and legal vehicles on the basis of predicted pavement damage potential, they calculated the ratio of the life consumed from one pass of the overloaded vehicle to the corresponding life consumed due to passage of the legal vehicle. The average damage ratios were 5.30 for rutting and 4.05 for fatigue cracking at a WIM station and they were 3.40 and 2.40, respectively, at the other WIM station. These results indicate a greater potential for accelerated pavement deterioration on the route due to overloaded vehicles.

Besides increasing road damage, overloaded vehicles can deal with road safety problems since stopping a heavier vehicle requires a longer distance and collisions involving a heavier vehicle lead to more damage.

2.3.10 Tyre-pavement contact

The tyre-pavement contact can be divided into three topics: (1) tyre types and dimensions, (2) contact area, and (3) contact stresses. The most comprehensive work regarding the effects of different tyres types on pavement damage is the work carried out in the COST action 334 (2001). These three topics are described below.

Tyre types and dimensions

Vehicles are usually equipped with dual tyres and single tyres (Figure 2.24). Dual tyres have been replaced by wide single tyres in some vehicle's axles. For example, the semi-trailer axle of the articulated vehicle is currently equipped with wide single tyres instead of dual tyres.



Figure 2.24 – Examples of dual tyre and wide base tyre (COST 334, 2001)

Wide base tyres can provide cost savings to the road freight transportation industry through reduced tare weights, fuel consumption and tyre wear (COST 334, 2001). However, they are stated to produce more pavement damage than dual tyres considering the same load. Dual tyres spread the load over a wider area than wide single tyres.

Tyre sizes are coded using the following parameters which are depicted in Figure 2.25:

- S: nominal section width in millimetres
- H/S: tyre aspect (height to width) ratio in percentage
- Construction code
- Φ : nominal rim diameter in in

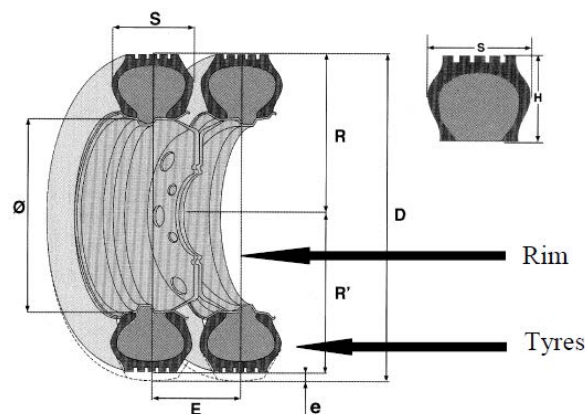


Figure 2.25 – Tyre size parameters (COST 334, 2001)

For example, the tyre code 385/65R22.5 specifies a tyre with nominal section width equal to 385 mm, tyre aspect ratio equal to 65%, radial structure and nominal rim diameter equal to 22.5 in.

The COST action 334 (2001) has identified future trends in tyre development and use in Europe which are illustrated in Figure 2.26.

According to the Serviços Comerciais para Transportes S.A. (SECTRAM) (commercial services for transport), whose mission is the marketing of goods and services in the transport sector, the Michelin brand is the tyre market leader in Portugal with 30-35% market share. Therefore, Michelin was contacted for tyre data purposes.

From these contacts it was possible to learn the most commonly used tyres in the articulated vehicle with 2+3 axles and in the lorry/truck with 2 axles. In relation to the articulated vehicle, Figure 2.27 shows the most commonly used tyre combinations. The proportion of articulated vehicles equipped with the combination 1 is 45%, with the combination 2 is 25% and with the

combination 3 is 10%. In relation to the lorry/truck, the most commonly used tyre is the 315/70R22.5, in single formation in the front axle and in dual formation in the rear axle.

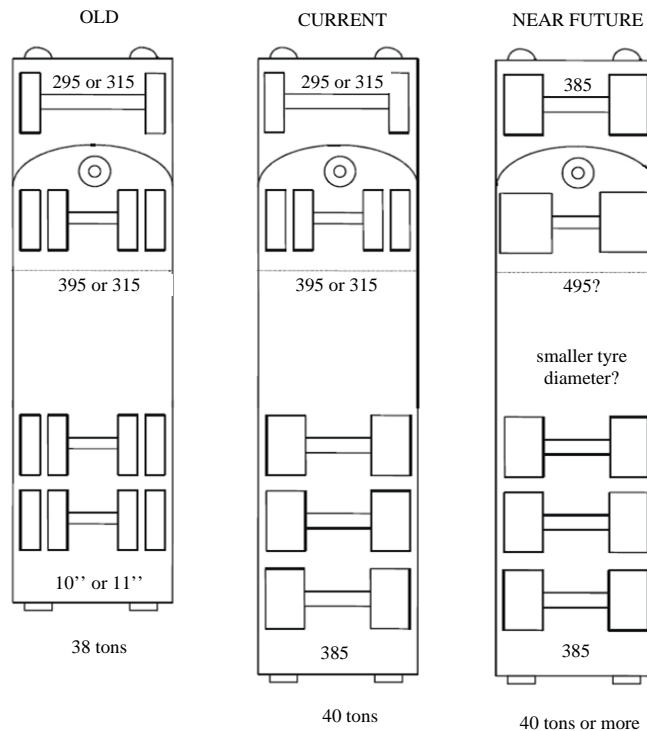


Figure 2.26 – Tyres of articulated vehicles in the past, present and (possibly) future (COST 334, 2001)

	Single tyre	Dual tyre	Wide single tyre
Combination 1	315/80R22.5	315/80R22.5	385/65R22.5
Combination 2	315/70R22.5	315/70R22.5	385/55R22.5
Combination 3	295/60R22.5	295/60R22.5	445/45R19.5

Figure 2.27 – Tyre combinations in the articulated vehicle

Contact area

The contact area is the area enclosed by the boundary of the contact between the tyre and the road. It has been common in pavement design to consider that the tyre loading is applied over a circular area with uniform contact pressure equal to the inflation pressure. The contact area is obtained normally by dividing the applied tyre load by the tyre inflation pressure.

The circular shape has been used for decades due to its simplicity when incorporated in an elastic analysis for layered flexible pavements and due to the availability of closed form solutions (analytical methods). Since the currently used simulation tools are based on a multilayered elastic theory, they are limited to circular contact areas.

For the bias-ply tyres, the shape of the contact area is approximately circular or elliptical, while for the present-day radial tyres the contact area is rather rectangular (mainly when tyre load and

inflation pressure are well matched). The contact area-width generally equals the tread width, except for strongly overinflated or ‘under-loaded’ conditions, when the width may be lesser than the tread width. The contact area-length for a certain tyre type (at constant size, manufacturer, diameter, structure) is rather constant for matching combinations of load and pressure. At overloading (or ‘under-inflation’), the length generally decreases more at the edges than in the middle, resulting in a more elliptical shape (COST 334, 2001).

Table 2.10 presents the size of contact areas for different radial tyres as well as the loads per tyre and the inflation pressures.

Table 2.10 – Contact area sizes of some Michelin tyres (COST 334, 2001)

Tyre size	Fitment	Load per tyre (kg)	Inflation pressure (bar)	Width (mm)	Length (mm)	Area (cm ²)
295/60R22.5	Dual	2250	8	258	155	399
295/60R22.5	Dual	2875	10	259	165	427
295/80R22.5	Dual	2250	7	243	170	413
315/80R22.5	Dual	2250	6.5	253	179	453
315/80R22.5	Dual	2875	8	253	193	490
385/65R22.5	Single	4500	10	284	202	574
385/65R22.5 Energy	Single	4500	10	302	193	583
495/45R22.5	Single	4500	8	425	161	686
495/45R22.5	Single	5750	10	426	173	737

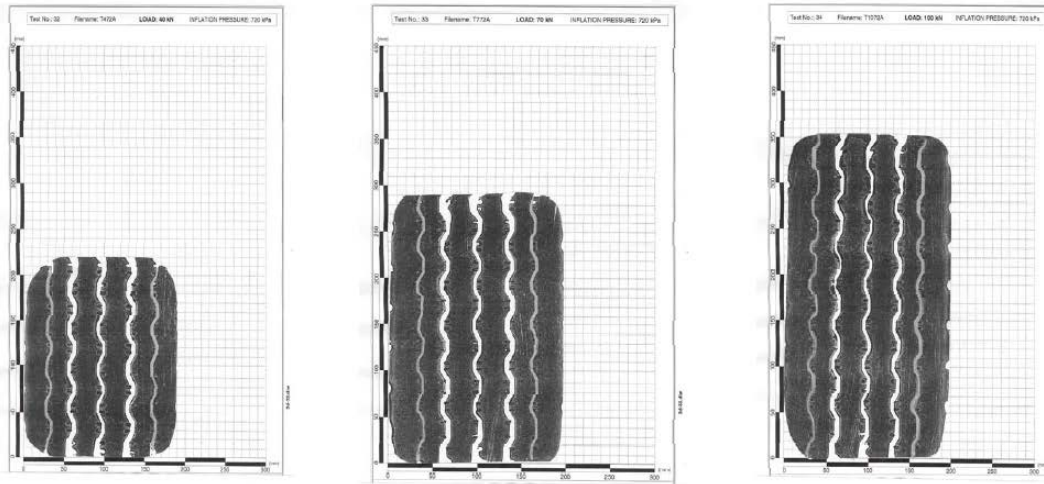
The area enclosed by the boundary of the contact between the tyre and the road (‘gross contact area’) includes both the area of tread grooves and the ‘net contact area’ between the tyre rubber and the pavement. Table 2.11 presents significant differences between the ‘gross contact area’ and the ‘net contact area’ that cannot be ignored.

Table 2.11 – Contact area size (‘gross and net contact area’) of some Michelin tyres (COST 334, 2001)

Tyre size	Fitment	Load per tyre (kg)	Inflation pressure (bar)	Max. width (mm)	Max. length (mm)	‘Gross contact area’ (cm ²)	‘Net contact area’ (cm ²)	Net/gross area (%)
295/60R22.5	Dual	2875	9.5	258	205	472	309	65.5
315/80R22.5	Dual	2875	7.5	258	247	532	351	66.1
385/65R22.5	Single	4500	9.5	283	232	579	415	71.7
385/65R22.5	Single	5750	9.5	283	256	681	505	74.1
495/45R22.5	Single	5750	9.5	427	213	709	535	75.4

Substantial differences may occur between tyres of the same nominal size but of different manufactures or even of different tyres (structure, tread pattern, materials) for the same manufacturer (COST 334, 2001).

Two-dimensional tyre contact areas were obtained during the contact stresses measurements in the South African Vehicle-Road Surface Pressure Transducer Array (VRSPTA) device (Beer et al., 2004). Measurements were performed under different loads and inflation pressures at relatively low speed ranges. Figure 2.28 depicts the static contact areas for three cases. Case 1 represents an ‘underloaded’ case, Case 2 an ‘overloaded’ case and Case 3 an ‘extremely overloaded’ case. It is clear that only the length of the tyre-pavement contact area increases with increases in load, the width remains constant.



(a) Tyre Print: Case 1: Single Loads 20 kN, 720 kPa (b) Tyre Print: Case 2: Single Load 35 kN, 720 kPa, (c) Tyre Print: Case 1: Single Load 50 kN, 720 kPa

Figure 2.28 – Static contact areas (Beer et al., 2004)

Using the VRSPTA measurements, Blab (1999) carried out a comprehensive statistical study on tyre geometry and measured contact stresses. Table 2.12 presents the statistical results for contact area-width measurements. He also concluded that, because of high lateral tyre stiffness, the contact area-width is approximately constant and relatively independent of inflation pressure and loading conditions for each of the tyre types tested. Therefore, the contact area-width can be assumed to be equal to the width of the tyre tread area of a given tyre type.

Table 2.12 – Statistics of contact area-width measurements (Blab, 1999)

Tyre type	Load range (kN)	Inflation pressure (kPa)	Sample size	Mean (m)	Standard Error	Standard deviation
Bias ply tyre (10.00-20)	26-56	420-920	141	0.211	0.0013	0.015
Radial tyre (11R22.5)	26-56	420-920	141	0.203	0.0009	0.011
Wide-base tyre (425/65R22.5)	26-106	500-760	72	0.320	0.0014	0.012

In relation to the contact area-length, Figure 2.29 and Figure 2.30 illustrate the very different longitudinal stiffness behaviour of each of the three tyre types tested, for that the mean ratio of the width and length as a function of both the applied vertical tyre load and the tyre inflation pressure are respectively plotted.

Both bias ply and radial tyre contact areas show a fairly small range for the mean width to length ratio (0.55-0.65). Taking into account that the contact area-width is more or less constant, the assumption of circular contact area shape is insufficient for these tyre types. In relation to wide base tyres, the mean ratio tyre width to length depends strongly on the applied load and presents values higher than one implying contact area-lengths lower than contact area-widths.

Salgado and Kim (2002) present some data regarding the dimensions of the contact area of wide base tyres showing also that the contact area-length is lower than the contact area-width (Table 2.13).

Numerical methods allow any shape for the contact area. Consequently, exact modelling of the contact area is feasible. Some authors use exact contact area-shape and dimension (tyre footprints) provided by manufactures (Figure 2.31).

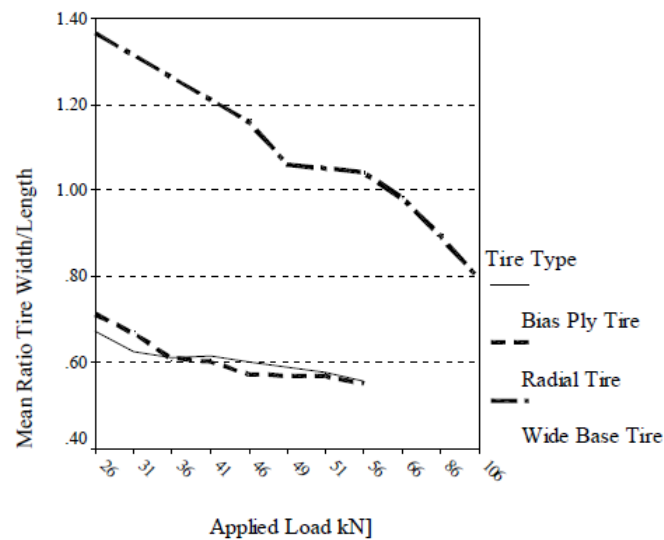


Figure 2.29 – Mean ratio tyre width to length as a function of load (Blab, 1999)

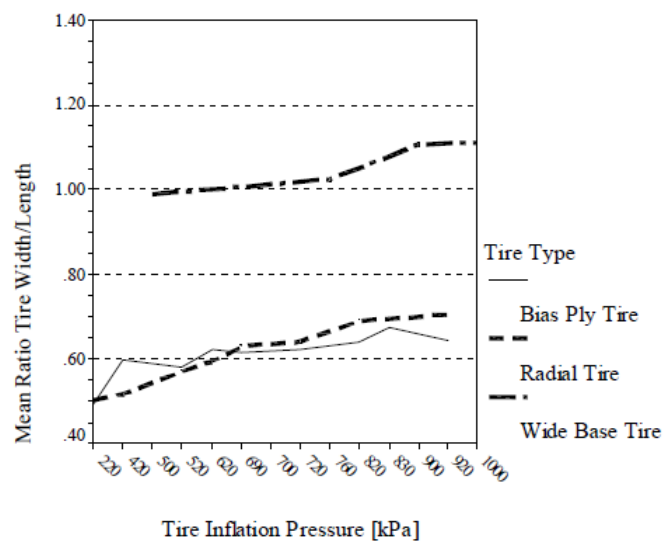


Figure 2.30 - Mean ratio tyre width to length as a function of inflation pressure (Blab, 1999)

Table 2.13 – Contact area of wide base tyres manufactured by Michelin (adapted from Salgado and Kim (2002))

Tyre	Width (cm)	Length (cm)	Ratio (width:length)	'Net contact area' (cm ²)	Maximum load (kN)	Inflation pressure (kPa)
445/65R19.5	33.3	25.9	1:0.78	522.6	46	758
385/65R22.5	28.2	23.9	1:0.85	425.2	42	862
425/65R22.5	30.5	25.9	1:0.85	460.0	51	862
445/65R22.5	38.1	28.7	1:0.75	550.3	55	827
445/65R22.5	33.3	27.4	1:0.82	527.1	55	862

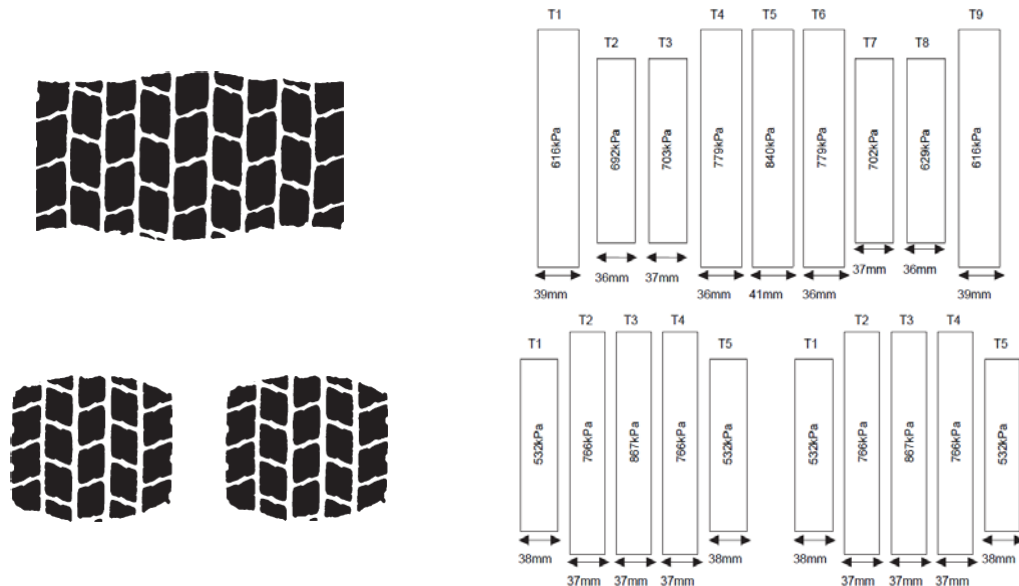


Figure 2.31 – Tyre footprints and modelled contact area of a dual-tyre assembly and a wide-base tyre (Elseifi et al., 2005)

Not only the size of the contact area is important, but also its shape. Alkasawneh et al. (2008) investigated the effect of different contact area geometries (irregular, rectangular, square, oval, circular) with different loading configurations including, non-uniform, uniform, and average pressures on the response of flexible pavements by varying the thickness of the bituminous layer. The results indicate that the use of circular contact areas with uniform contact pressure, equal to the tyre inflation pressure, can produce erroneous results that tend to overestimate the predicted fatigue life and rutting life of flexible pavements.

Contact stresses

Often, only the vertical forces are considered, but horizontal forces can also occur, due to acceleration, deceleration, steering, ascent or descent of the vehicle and/or inclination of the pavement. In addition, extra interface stresses may occur due to the deformation of tyre and pavement. These latter stresses do not generate net resultant forces at the interface (COST 334, 2001).

For tyre-pavement interaction, the COST action 334 (2001) considered five different ‘scales’, i.e. five different levels of schematisation, each with their appropriate degree of detail and accuracy. Clearly, the higher level of schematisation will have a lower degree of accuracy, but this may be sufficient for pavement design purposes. Table 2.14 describes the five ‘scales’ which are depicted in Figure 2.32.

The ‘load scale’ can consider dynamic loads. At this scale, there is no difference between tyres for equal loads. According to St. Venant’s principle, at a distance from the load, the main influencing factor for the pavement response is the magnitude of the wheel load. However, this distance may well be larger than the pavement thickness, especially for thin pavements.

The ‘tyre scale’ does not consider the size of contact area or the stress distribution on the contact area.

The ‘contact area scale’ is important for intermediate and upper pavement layers in which distresses may occur. For pavement response, not only the size of the contact area is important,

but also its shape. There will be differences in stresses in the pavement between a wide and short contact area, a square area, a circular area, or a narrow and long area (all having equal area size and vertical contact stress).

Table 2.14 – Scales considered by the COST action 334 for tyre-pavement interaction (COST 334, 2001)

Scale	Description
‘load scale’	Only the value of the net forces is considered, not the area over which they are spread, or the stress distribution within that area.
‘tyre scale’	A distinction is made whether the load is applied by a single tyre (resulting in one contact area) or by a dual tyre assembly (resulting in two separated contact areas).
‘contact area scale’	The tyre-pavement stresses are considered to be constant across the tyre-pavement contact area (decimetric scale). The considered stresses may be computed as the ratio of the different applied forces by the constant area value.
‘tread pattern scale’	The tyre-pavement stresses are considered to be constant across the tread pattern parts or ribs (centimetric scale).
‘local scale’	Millimetric gradients are considered (millimetric scale).

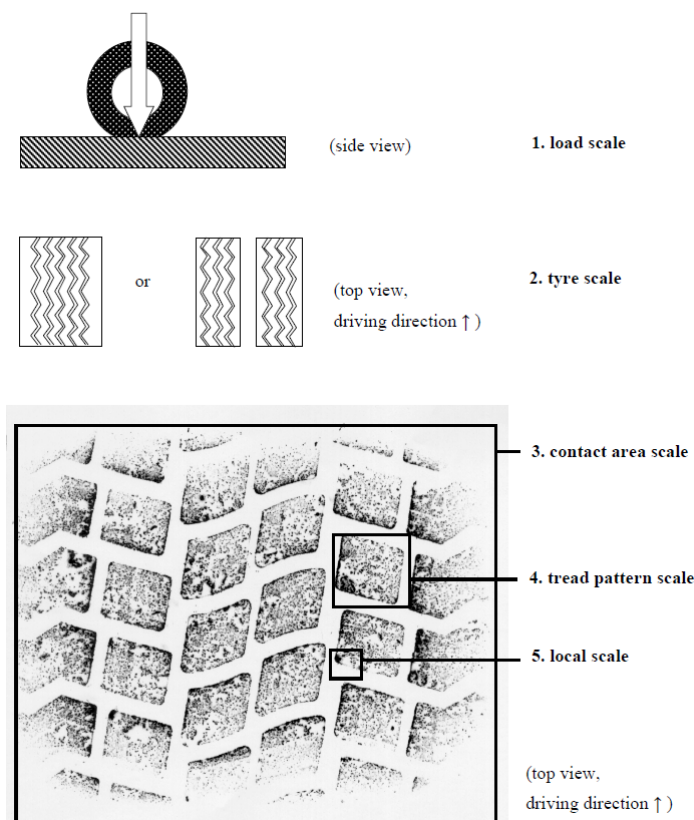


Figure 2.32 – Illustration of the five different ‘scales’ of tyre-pavement interaction (COST 334, 2001)

The ‘tread pattern scale’ has been considered in many studies. Such studies consider measurements of tyre-pavement contact stresses. Several researchers (Beer et al. (1997) and Beer and Fisher (1997)) measured the 3D tyre-pavement contact stresses under slow moving loads. These measurements were made with the VRSPTA using the Heavy Vehicle Simulator (HVS) to apply the loading. Different configurations of tyre types and several load/inflation pressures were used in the tests. The measurements showed that the vertical stress components at the moving tyre-pavement interface are not uniformly distributed and that shear stresses are also presented, both in lateral (or transverse direction) and in longitudinal direction.

The basic principle of the VRSPTA is that the loads in each tri-axial load cell pin across the tyre contact patch are measured directly. The contact stresses imposed on the road (or, in this case, on the VRSPTA surface) are calculated during the post-processing of the data (Beer and Fisher, 1997). In order to obtain an effective transfer, especially for horizontal forces, it was necessary to design the VRSPTA surface to match a surface, equivalent in friction to the ‘average’ surfacing material used on pavements. It was also necessary to assure the same stiffness of the support in the contact patch (Beer et al., 1997).

Figure 2.33, Figure 2.34 and Figure 2.35 illustrate the 3D tyre-pavement contact stresses measured for the tyre 315/80R22.5. These figures also illustrate the change in shape and magnitude in all the patterns as a function of both loading and inflation pressure. The lateral and longitudinal stresses are much lesser than the associated vertical ones.

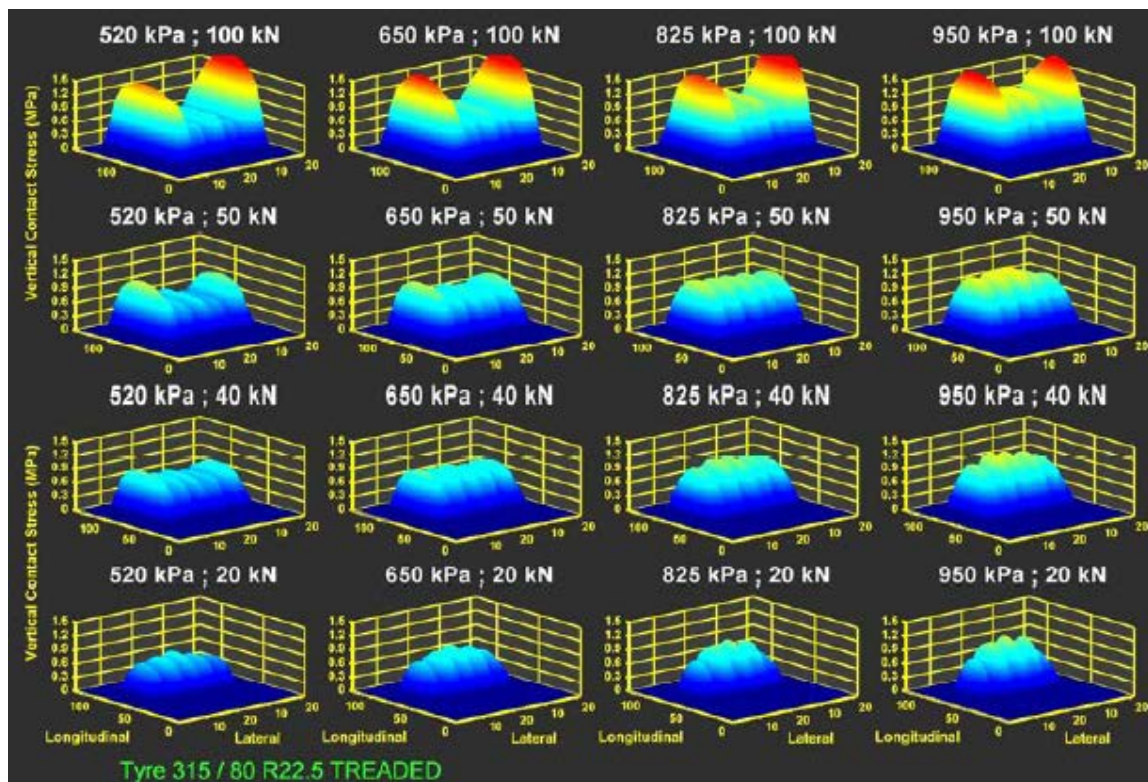


Figure 2.33 – Measured vertical contact stresses of the 315/80R22.5-tyre (Beer et al., 2005)

Since the vehicles are not channelized on the roads, the potential influence of peak stresses on the ‘tread pattern scale’ may be diminished by the multiple tyre positions on the road-way lane. It is also diminished by the fact that tyres can have different sizes, different tread patterns and can come from different manufacturers (COST 334, 2001).

The ‘local scale’ is the millimetric scale of the tyre-pavement contact. It includes local tread pattern details such as tread grooves. It is also the scale of pavement texture. The knowledge of tyre-pavement contact stresses at this scale is essentially important for tyre adherence, and thus for safety (COST 334, 2001).

The measurements carried out by Beer et al. (2005) demonstrate that the tyre-pavement contact pressure is not equal to the inflation pressure of the tyre.

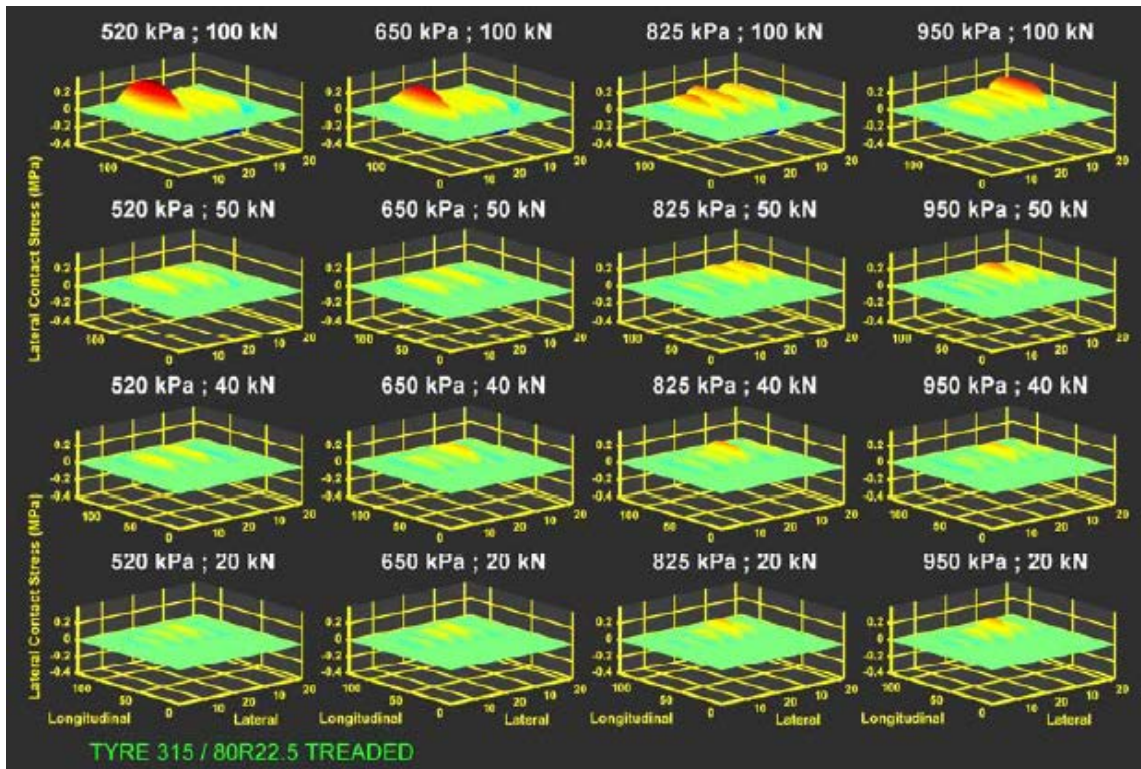


Figure 2.34 - Measured lateral contact stresses of the 315/80R22.5-tyre (Beer et al., 2005)

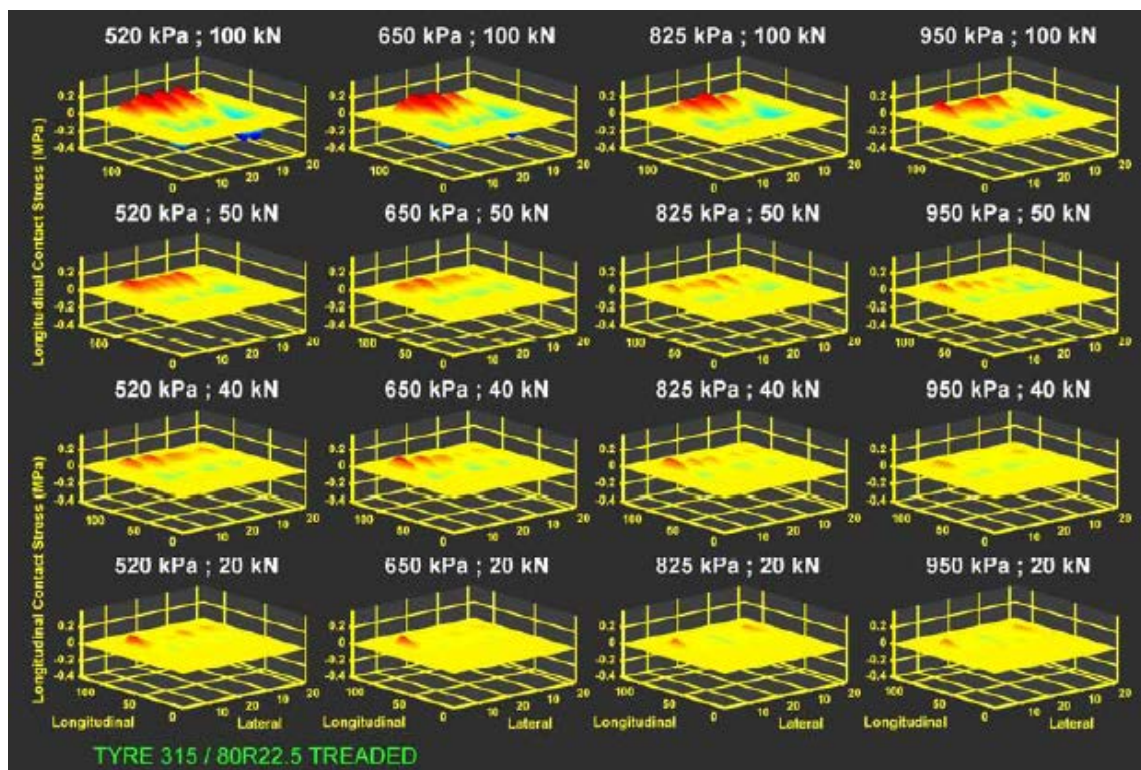


Figure 2.35 - Measured longitudinal contact stresses of the 315/80R22.5-tyre (Beer et al., 2005)

2.3.11 Suspension systems

A suspension system is an assembly of springs, shocks absorbers (dampers) and linkages that connects the vehicle body to its wheels isolating the vehicle body from road roughness which would otherwise be transferred to the driver and the freight.

There are a wide diversity of suspension systems depending on the spring element, the number of axles, the geometry (that is, the ability of opposite wheels to move independently of each other), the damper control and the load equalization in tandem and multiple axles. Table 2.15 summarizes the classification of the suspension systems.

The suspension choice is function of the truck's application, where and for what they are going to be used and what load they are going to carry. Some suspensions are better for extreme application such as construction works, while others should be lighter and/or should reduce the chassis height increasing the mass payload and/or the volume payload. Besides these, they should be road friendly and should provide good tyre-pavement contact throughout operation.

Table 2.15 – Classification of the suspension systems

Spring	Number of axles	Geometry	Damper control	Load equalization
<ul style="list-style-type: none"> • Steel • Air • Rubber 	<ul style="list-style-type: none"> • Single axle • Tandem axle • Multi axle 	<ul style="list-style-type: none"> • Dependent • Independent 	<ul style="list-style-type: none"> • Passive • Semi-active • Active 	<ul style="list-style-type: none"> • Load sharing • No load sharing

In relation to the spring, it can be a leaf or a multi-leaf spring (steel suspension), an air bar (air suspension) or a solid rubber (rubber suspension). The most current ones are the steel suspensions and the air suspensions. Figure 2.36 shows the different springs in a tandem axle. In the steel suspensions, the energy dissipation (damping) is provided by dry ('Coulomb') friction between the leaves at a number of points of contact whereas, in the air suspensions, it is provided by shock absorbers.



Figure 2.36 – Different springs in suspension systems (Hendrickson@, 2013)

In relation to the number of axles, suspension systems can be classified into single axle systems, tandem axle systems or multiple axle systems (see Figure 2.37). The tandem axle suspension depicted in Figure 2.37 assembles two single axles while the multi-leaf spring suspension depicted in Figure 2.36 uses a walking beam to link the two axles. A walking beam is particularly used for off-road applications (Cebon, 1999).

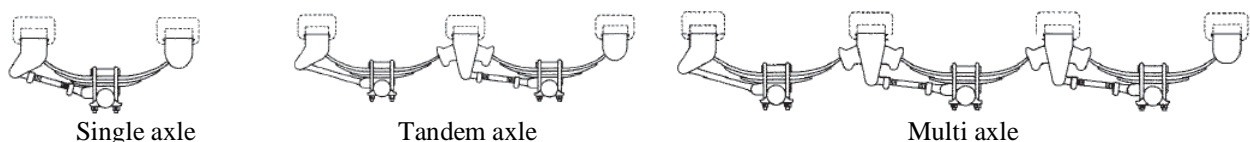


Figure 2.37 – Classification of the suspension systems in terms of the number of axles (Hutch@, 2013)

In relation to geometry, suspension systems can be either dependent suspensions (solid axles), where the axle's wheels cannot move independently, or independent suspensions, where a wheel is allowed to rise and to fall without affecting the opposite wheel. Almost all trucks are equipped with dependent suspensions.

In terms of damping control, the suspension system can be passive, semi-active or active. The passive one consists of elements that can only store or dissipate energy (dampers). As an optimal passive suspension is obtained when the spring rate is reduced to the lowest practical minimum and the linear damping coefficient is chosen to achieve the minimum road damage (Gillespie et al., 1992), damping control mechanisms have appeared. An active suspension requires an external energy source that activates a control system which will continuously control the force generated by the suspension system. A semi-active suspension provides an approximate active damping control law without the addition of large amounts of power to a suspension (Bouazara and Richard, 2001).

Finally, in terms of load equalization, some tandem and multiple axle suspensions behave like independent axles with interaction occurring only as a result of common connection to the same sprung mass (no load sharing). Others are capable to equalize the axle group load across all wheels (load sharing).

So far, an overview of the suspension systems was introduced. It is a complex topic that has been evolving. The EC (EEC, 1992) encourages the use of 'road-friendly' suspensions (air suspensions or 'equivalent' suspension systems) by providing one tonne payload incentive. Since improvements in suspension systems can deal with better truck handling, better comfort (both in terms of payload and driver) and higher transport efficiency (both in terms of payload and environmental), several researchers have been studying this topic.

Gillespie et al. (1992) evaluated the influence of single axle suspension systems (steel string suspension, air spring suspension and optimal air spring suspension) and tandem suspension systems (steel strings suspension, air strings suspension and walking-beam steel springs suspension) on pavement damage (fatigue and rutting) for different roughness levels. They concluded the following:

- The damage attributable to suspensions is much smaller than that due to road roughness;
- The damping influences greatly the performance of truck suspensions;
- The pavement damage can be reduced with developments in active suspensions;
- The air spring suspensions deal with lower pavement damage than the steel spring suspensions;
- The rutting damage is little affected by the dynamic behaviour of suspension systems;
- The walking-beam suspension is the least 'road-friendly'.

The DIVINE project (OECD, 1998) concluded that the pavement wear under steel suspension is at least 15% faster than the pavement damage under air suspension and that the magnitude of the load under an air suspension system was about half of the steel one. It defined a road-friendly suspension system as one with low spring stiffness and with a certain level of viscous damping. Those properties, which are usually found on well-designed air suspension systems, probably cannot be found on a steel suspension system.

The Directive No. 92/7/EEC of 10 February (EEC, 1992) controls the adoption of new suspensions in terms of 'road-friendliness', but have no provision for controlling the performance of suspensions in-service. Consequently, some suspension systems classified as being 'road-friendly' generate higher damage than the expected one probably due to poor maintenance.

Cole and Cebon (1991) carried out vehicle simulations to examine some of the characteristics of dynamic tyre forces generated by typical steel spring suspensions and air spring suspensions for typical highway conditions. Then, they compared the results with measurements from the

proposed EC suspension test (EEC, 1992), concluding that the ‘road-friendliness’ cannot be assessed by the simplistic parametric measurement of the proposed EC test. According to them, it is questionable whether a vehicle that passes the test will be any more ‘road friendly’ than one that fails.

Cebon (1999) recommended that a performing testing system for road-damaging potential should consist of both an initial approval test (check if the suspension is road-friendly) and an annual inspection (check if the suspension is adequately maintained).

Besides the two fundamental characteristics of the suspension systems (frequency and ratio damping) measured in the test procedure of the Directive No. 92/7/EEC of 10 February (EEC, 1992) and used to qualify the suspension system as ‘road-friendly’, the DIVINE project (OECD, 1998) recommended to evaluate the suspension systems in terms of load equalization and to use a limit for axle load equalisation performance.

The Australian specification for road-friendly suspensions nominates that ‘road-friendly’ suspensions must have static load-sharing, i.e., load-sharing when the vehicle is static, to a defined value, between axles or tyres in a multiple axle (Chen et al., 2013).

Sweatman (1983) characterized load-sharing performance by a Load-Sharing Coefficient (LSC) defined as the ratio of mean measured wheel load and mean static wheel load (cited in Gillespie et al. (1992)). The LSC is unity for perfect load sharing. On the other hand, as the load-sharing performance can be different when the truck is moving, a Dynamic Load-Sharing Coefficient (DLSC) was defined (Chen et al., 2013).

Chen et al. (2013) investigated the effects of suspension parameters and driving conditions (roughness and speed) on dynamic load-sharing of three longitudinal-connected air suspensions of a tri-axle semi-trailer. For that, they formulated a new nonlinear model of a multiple axle semi-trailer with longitudinal-connected air suspensions. The model was verified against test results with reasonable agreement. They used both load-sharing coefficients (LSC and DLSC) and concluded that the model enables a better understanding of the dynamic effects of the truck to explain changes of load-sharing with driving conditions.

2.4 VEHICLE SIMULATION

2.4.1 Introduction

Vehicle simulation process consists in three main steps: (1) modelling, to describe the physical problem, (2) formulation, to write the mathematical equations that describe the problem, and (3) calculation, to solve the mathematical equations obtaining hence the response of the problem.

The vehicle model should be problem dependent, i.e. only the relevant Degrees-Of-Freedom (DOF) of the problem have to be considered. The more complex the model is, more time is required to solve it. Therefore, models are usually a compromise between the computational cost of solving the mathematical equations and the fidelity of the models.

Vehicle models can be grouped into two categories: (1) simple vehicle models which do not account for nonlinearities of the problem and have a low number of DOF, and (2) complex

vehicle models which account, for example, for the nonlinearities of suspensions/tyres and have a high number of DOF.

Simple vehicle models can be easily simulated manually. Initially, the complex vehicle models were also simulated manually. However, the manual process becomes difficult, time-consuming and prone to errors when the number of DOF is high. In order to deal with these models, MultiBody System (MBS) analyses have been efficiently used in the formulation and calculation steps.

This section presents briefly the vehicle simulation using simple vehicle models and complex vehicle models. Then, as tyre-pavement contact is important in vehicle-pavement interaction, tyre models are described. Lastly, computer software to vehicle simulation is presented.

2.4.2 Simple vehicle models

Simple vehicle models can be used to predict dynamic tyre forces generated by heavy vehicle suspensions. This subsection refers two suspension models, a quarter-car model for single axle truck suspensions, and a walking-beam model for tandem axle truck suspensions. Both models are illustrated in Figure 2.38, (a) and (b) respectively. The quarter-car model has two masses, a sprung mass and an unsprung mass, both of which are constrained to move vertically – two DOF model. The walking-beam model has a sprung mass which is constrained to move vertically; a rigid beam which joints the two axles and is connected to the suspension spring by a pin joint at its centre; the combined beam and axle assembly is constrained to move vertically and to pitch (rotate) – three DOF model. The input of the models is the road profile elevation.

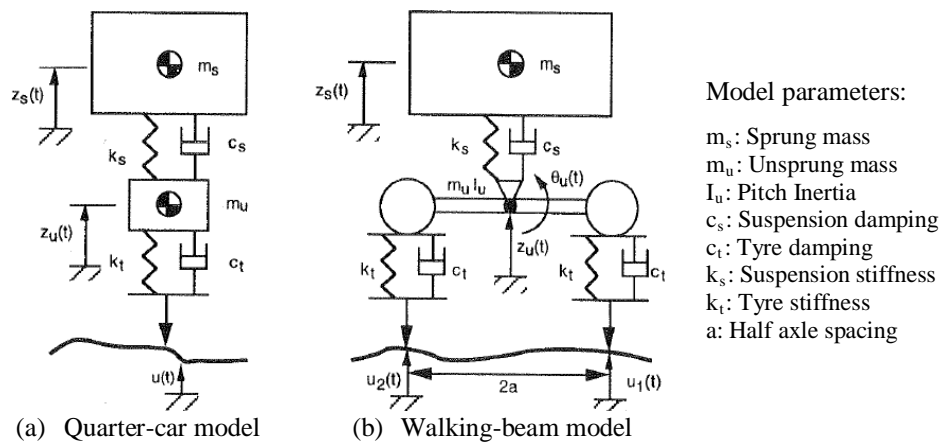


Figure 2.38 – Simple vehicle models (adapted from Cebon (1999))

The equations of motion of these simple models, derived from the application of the Newton's second law, can be written in matrix form (Cebon, 1999) - equation (2.29).

$$[M]\{\ddot{q}\} + [C]\{\dot{q}\} + [K]\{q\} = \{Q\} \quad (2.29)$$

where

- $\{q\}$ = vector of generalized coordinates
- $\{Q\}$ = vector of generalized forces
- $[M]$ = mass matrix

$[C]$ = damping matrix
 $[K]$ = stiffness matrix

For the quarter-car model (two DOF)

$$\begin{aligned} \{q\} &= \begin{Bmatrix} z_s \\ z_u \end{Bmatrix}, \quad \{Q\} = \begin{Bmatrix} 0 \\ c_t \dot{u} + k_t u \end{Bmatrix}, \quad [M] = \begin{bmatrix} m_s & 0 \\ 0 & m_u \end{bmatrix}, \\ [C] &= \begin{bmatrix} c_s & -c_s \\ -c_s & c_s + c_t \end{bmatrix}, \quad [K] = \begin{bmatrix} k_s & -k_s \\ -k_s & k_s + k_t \end{bmatrix} \end{aligned} \quad (2.30)$$

For the walking-beam model (three DOF)

$$\begin{aligned} \{q\} &= \begin{Bmatrix} z_s \\ z_u \\ \theta_u \end{Bmatrix}, \quad \{Q\} = \begin{Bmatrix} 0 \\ c_t (\dot{u}_1 + \dot{u}_2) + k_t (u_1 + u_2) \\ ac_t (\dot{u}_2 - \dot{u}_1) + ak_t (u_2 - u_1) \end{Bmatrix}, \quad [M] = \begin{bmatrix} m_s & 0 & 0 \\ 0 & m_u & 0 \\ 0 & 0 & I_u \end{bmatrix}, \\ [C] &= \begin{bmatrix} c_s & -c_s & 0 \\ -c_s & c_s + 2c_t & 0 \\ 0 & 0 & 2a^2 c_t \end{bmatrix}, \quad [K] = \begin{bmatrix} k_s & -k_s & 0 \\ -k_s & k_s + 2k_t & 0 \\ 0 & 0 & 2a^2 k_t \end{bmatrix} \end{aligned} \quad (2.31)$$

Simulations of vehicle response can be performed either in the time domain or in the frequency domain. Both simulations are described in Cebon (1999).

Various authors have used simple vehicle models to predict dynamic tyre forces. For example, Collop and Cebon (1995) used the quarter-car model in their whole-life pavement performance model.

2.4.3 Complex vehicle models

MBS dynamics has been used to model complex vehicle models which have either nonlinearities or multiple DOF or both. A MBS is formed by a set of bodies linked by kinematical relationships or joints

The equations of motion can be derived from different approaches. Since the application of the Newton's second law becomes difficult for MBS, the equations of motion will be derived from the Euler-Lagrange's equation (equation (2.32)). Newton's second law describes the motion in an inertial reference frame while the Euler-Lagrange's equation is frame indifferent.

$$\frac{d}{dt} \left(\frac{\partial T}{\partial \dot{q}_i} \right) - \frac{\partial T}{\partial q_i} = Q_i \quad (2.32)$$

where

q_i = generalized coordinate
 T = kinetic energy
 Q_i = generalized force

Computing the kinetic energy of a rigid body (equation (2.33)), equation (2.32) can be rewritten (equation (2.34)).

$$T = \frac{1}{2} \{\dot{q}\}^T [M] \{\dot{q}\} \quad (2.33)$$

$$[M] \{\ddot{q}\} = \{Q\} \quad (2.34)$$

where $[M]$ is the mass matrix.

The generalized forces are usually obtained by applying the method of virtual work. The total virtual work done by the generalized forces is given by equation (2.35).

$$\sum \delta W = \{Q\}^T \{\delta q\} \quad (2.35)$$

Introducing a compatible set of virtual displacements such that $\delta_i^{(k)}$ (k is considered to distinguish different type of forces which may act on the body) is the displacement at the point of application of external force $F_i^{(k)}$, the total virtual work is given by equation (2.36).

$$\sum \delta W = \sum_{i=1}^{n_1} F_i^{(1)} \delta_i^{(1)} + \sum_{i=1}^{n_2} F_i^{(2)} \delta_i^{(2)} + \dots + \sum_{i=1}^{n_n} F_i^{(n)} \delta_i^{(n)} \quad (2.36)$$

Combining equations (2.35) and (2.36), the equation (2.37) is obtained.

$$\{Q\}^T \{\delta q\} = \{F^{(1)}\}^T \{\delta^{(1)}\} + \{F^{(2)}\}^T \{\delta^{(2)}\} + \dots + \{F^{(n)}\}^T \{\delta^{(n)}\} \quad (2.37)$$

Relating the generalized coordinates to the virtual displacements, equation (2.37) can be rewritten resulting equation (2.38).

$$\{Q\}^T \{\delta q\} = \{F^{(1)}\}^T [Z^{(1)}] \{\delta q^{(1)}\} + \{F^{(2)}\}^T [Z^{(2)}] \{\delta q^{(2)}\} + \dots + \{F^{(n)}\}^T [Z^{(n)}] \{\delta q^{(n)}\} \quad (2.38)$$

Where $[Z^{(k)}]$ is the transformation matrix for forces of type (k).

Therefore, the generalized forces are given by equation (2.39) and subsequently the equation of motion (2.34) for each rigid body equation is given by equation (2.40).

$$\{Q\}^T = \{F^{(1)}\}^T [Z^{(1)}] + \{F^{(2)}\}^T [Z^{(2)}] + \dots + \{F^{(n)}\}^T [Z^{(n)}] \quad (2.39)$$

$$[M] \{\ddot{q}\} = [Z^{(1)}]^T \{F^{(1)}\} + [Z^{(2)}]^T \{F^{(2)}\} + \dots + [Z^{(n)}]^T \{F^{(n)}\} \quad (2.40)$$

For a generalized vehicle model, illustrated in Figure 2.39, which comprises several unsprung masses subjected to a set of generalized input ('tyre') forces $\{F_t\}$ and joined to the sprung masses by a set of connection ('suspension') forces $\{F_s\}$, the equation of motion is given by equation (2.41). $\{F_g\}$ are constant gravitational forces that act at the gravity centre of each mass.

$$[M]\{\ddot{q}\} = [S]\{F_s\} + [T]\{F_t\} + \{F_g\} \quad (2.41)$$

Where the terms $[Z^{(k)}]^{-T}\{F^{(k)}\}$ in equation (2.40) were replaced by $[S]\{F_s\}$, $[T]\{F_t\}$ and $\{F_g\}$, and all the rigid bodies were included in $[M]$. $[S]$, $[T]$ and $\{F_g\}$ contains implicitly the constraints.

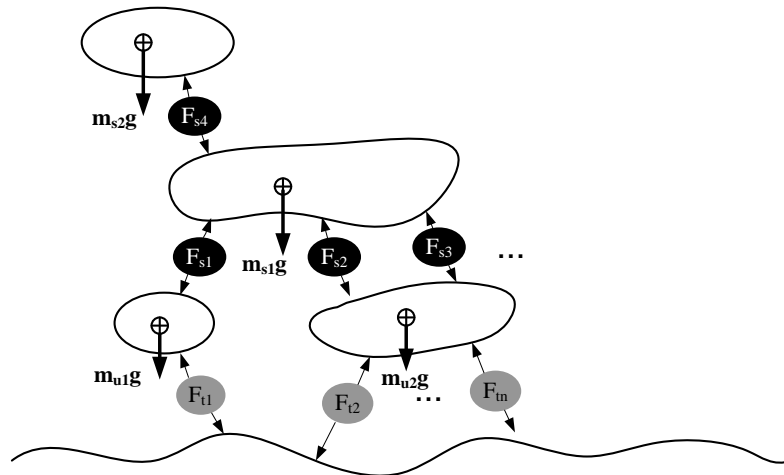


Figure 2.39 – Generalized multibody vehicle model: suspension forces (F_s), tyre forces (F_t) and gravitational forces (F_g) (based on Cebon (1999))

The motions of the various components in a vehicle can be predicted by solving the motion equation (2.41).

The dynamic simulation of MBS has received increasing attention in the last decades since it enables the analysis and design of numerous systems. Therefore, software has been developed, some of them are general-purpose and some of them are specific. In addition, software can use different approaches, both in the generation of the motion equations and in the resolution of them. For example, the motion equations can be obtained numerically or symbolically. Numerical formulation approaches produce matrices that are only valid for a given instant of time. Consequently, the equations must be reformulated at every time step of a simulation. On the other hand, symbolic formulation approaches produce sets of equations that are eternally valid and must only be generated once. Prior to simulation, the symbolic equations can also be greatly simplified in numerous ways, resulting in models that can be simulated many times faster than those modelled using a purely numerical approach. For more information see, for example, the references Roberson and Schwertassek (1988) and Blundell and Harty (2004).

Several authors have used complex models (MBS) to predict dynamic tyre forces. For example, Karamihas et al. (1995) modelled a 24-DOF 3D full vehicle model and Hasagasioglu et al. (2012) modelled a 6×2 heavy-duty commercial vehicle.

2.4.4 Tyre models

In order to analyse the vehicle dynamics it is necessary a thorough understanding of the relationship between tyres, their operating conditions, and the resulting forces and moments developed at the tyre-pavement contact.

According to Gillespie (1992), the tyre serves essentially three basic functions: (1) it supports the vertical load, while cushioning against road shocks, (2) it develops longitudinal forces for acceleration and braking, and (3) it develops lateral forces for cornering.

The tyre plays a key role in the efficiency of the vehicles. With the exception of the aerodynamic forces, all the primary control and disturbance forces applied to a vehicle are generated at the tyre-pavement contact.

Several types of mathematical tyre models have been developed during the last half century (Pacejka, 2006). For a specific purpose, there are different levels of accuracy and complexity. Figure 2.40 illustrates how the intensity of the various consequences associated with different ways of attacking the problem tends to vary. From left to right, the model is less based on full scale tyre experiments and more based on the theoretical behaviour of the physical structure of the tyre. In the middle, the model is simpler but possibly lesser accurate while at the far right the model becomes more complex and lesser suitable for application in vehicle motion simulations, being more appropriate for detailed tyre performance analysis related to its construction. At the left-hand category, there are the tyre models that describe measured tyre characteristics through tables or mathematical formulae and use certain interpolation schemes. These formulae have a given structure and possess parameters which are usually assessed with the aid of regression procedures to yields a best fit to the measured data.

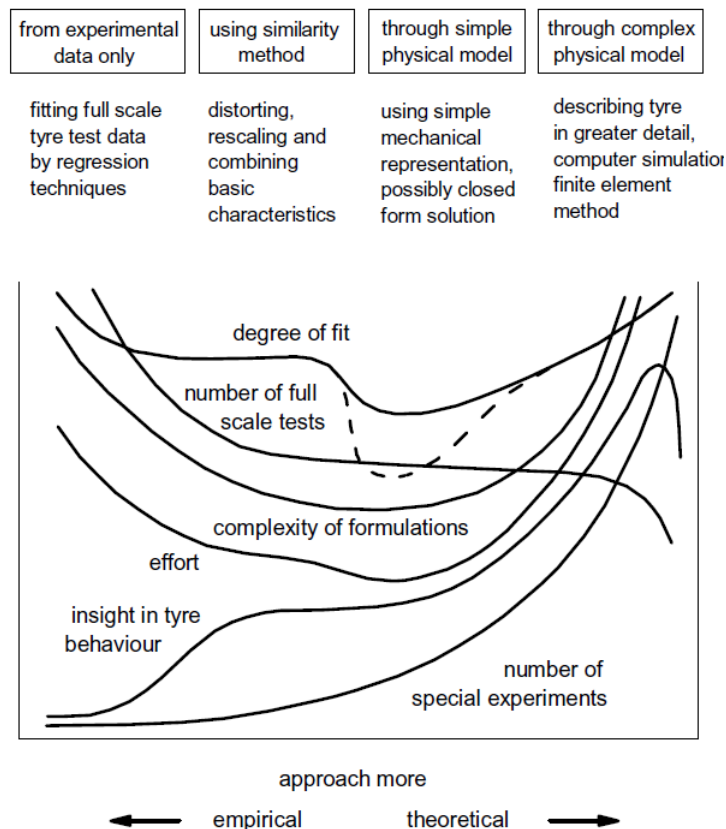


Figure 2.40 – Four categories of possible types of approach to develop a tyre model (Pacejka, 2006)

Some models have been specifically designed to represent the tyre as a vehicle component in the vehicle simulation environment (Pacejka, 2006). They are based on measured data, may contain structures that find their origin in physical models and fall in the ‘semi-empirical’ approach of

Figure 2.40. Two models are referred, the similarity method-model and the Magic Formula tyre model, which belong to the second and first categories of Figure 2.40, respectively.

Briefly, the similarity method is based on the observation that pure slip curves remain approximately similar in shape when the tyre runs at conditions which are different from the reference ones (Pacejka, 2006). This method, owing to its simplicity, is relatively fast. It is capable to represent pure slip conditions rather well including the influence of a camber angle. The description of the situation at combined lateral and longitudinal slip is qualitatively satisfactory. However, quantitatively, deviations may occur at the higher levels of the combined two slip curves.

One of the most important and widely used models is the Magic Formula tyre model. The development of this model started in the mid-eighties, and from there different versions have been introduced, extending thus the model to large camber and turn slip situations. The complete set of steady-state formulae can be found in Pacejka's book (2006). The formula is capable of producing characteristics that closely match measured curves for the side force (and if desired for the aligning torque) and for the fore and aft force as a function of their respective slip quantities: the slip angle and the longitudinal slip with the effect of vertical load and camber angle included in the parameters. An extension of the model to turn slip is also described. In general, a good agreement between computed and measured curves can be achieved with the model.

Besides steady-state behaviour models, Pacejka (2006) describes models for the physical description of the transient and oscillatory dynamic behaviour of the tyre, for instance the stretched string model and the simplified string model which can be provided with tread elements (better behaviour).

For less demanding cases (long wavelength, low frequency) the straight tangent or single contact point models may be employed (Pacejka, 2006). Such models can be used in combination with the appropriate dynamic extension that accounts for the gyroscopic couple due to lateral deflection velocity. The single point contact model due to its simple form has been and still is very popular in vehicle dynamic studies. The development of single point contact models follows essentially a different and much simpler line compared with the theoretical approach on which the string model is based. Because of its simplicity, it is possible to enhance the model to cover the full non-linear combined slip range including rolling from standstill or even change direction from rolling forwards to backwards. Camber and turn slip may also be included.

The models presented until now can only be used in long wavelength phenomena (higher than about 1.5 m). Pacejka (2006) also describes a model capable of covering situations with relatively short wavelengths (higher than about 10 cm and even shorter for modelling road obstacle enveloping properties). Situations in which combined slip occurs can be handled and the Magic Formula model can be used as the basis for the nonlinear force and moment description. The model, referred as the Short Wavelength Intermediate Frequency Tyre (SWIFT) model, was based on the work of Zegelaar (1998) and Maurice (2000) conducted at the Delft University of Technology and supported by TNO Automotive and a consortium of industries. This model can be seen as a further development of the enhanced single contact point model.

When the wavelength is shorter than two to three times the contact length and the employed tyre model is assumed to contact the road in a single point, a geometric filtering of the profile becomes necessary. The SWIFT model has a special filter that considers the envelopment properties of the tyre and the variation in effective rolling radius that occurs when the tyre rolls

over a short obstacle. Figure 2.41 shows that phenomenon, where can be seen that the response of the axle is much smoother than the shape of the actual road profile.

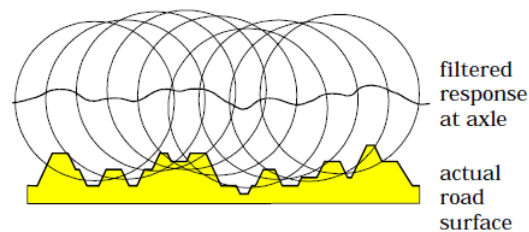


Figure 2.41 – The phenomena of the tyre rolling on rough roads (adapted from Zegelaar (1998))

There are several models which can simulate the enveloping properties of tyres on rough roads (Figure 2.46). Zegelaar (1998) gives an overview of them.

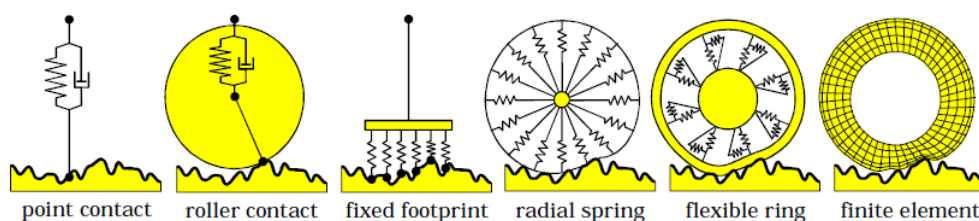


Figure 2.42 – Tyre-road interface models (Zegelaar, 1998)

The SWIFT model is a rigid ring tyre model (compact model to ensure relatively fast vehicle simulations) whose tyre-road interface is only governed by a single-point. Therefore, this model does not show explicitly the enveloping properties of the tyre rolling over rough roads. In other words, the short wavelength irregularities cannot be directly used as input in simulations using this model. In these cases, the quasi-static response of the real tyre on the actual road surface should be used as input. This quasi-static response is transferred into an effective road surface: the effective plane height, the effective road plane angle and the effective rolling radius variation (Zegelaar, 1998).

Hence, first it is necessary to transform the actual road profile into the effective road surface. The transformation is called the geometric filtering effect of the rolling tyre. Pacejka (2006) describes techniques to obtain the effective road surface. The SWIFT model uses elliptical cams to determine that surface (TNO, 2010).

The ‘TNO innovation for life’ offers two semi-empirical models (the MF-Tyre and the MF-Swift) for use in various simulation environments. Both the MF-Tyre and the MF-Swift have been developed and extensively validated using numerous measurements and experiments (TNO@, 2012). The MF-Tyre is the Delft-Tyre standard implementation of the renowned Pacejka’s Magic Formula that includes the latest developments. With the MF-Tyre, an engineer can simulate valid steady-state and transient behaviour up to 8 Hz, making it the ideal tyre model for handling and controlling prototyping analyses. Pure cornering and braking as well as combined conditions are accurately described. The robust extrapolation properties of MF-Tyre make the model suitable for the simulation of conditions that go beyond the measurement conditions (TNO@, 2012). The MF-Swift is the high frequency (100 Hz) extension of the MF-Tyre. Comparing with the MF-Tyre, the MF-Swift adds generic 3D obstacle enveloping and tyre belt dynamics to tyre-road contact force and moment simulations. Typical MF-Swift applications are in vehicle comfort analysis, suspension vibration analysis, development of vehicle control systems, such as Antilock Brake System (ABS) or Electronic Stability Programme (ESP), and handling and stability (TNO@, 2012).

The ‘cosin scientific software’ offers the Flexible Structure Tyre (FTire) model (COSIN@, 2012) which has a flexible belt provided with a large number of friction elements on tread blocks. From this model, it is possible to obtain the contact patch contour and the pressure distribution. In addition, it is suitable for a frequency range up to 200 Hz.

2.4.5 Computer programs

The motions of the various components in a vehicle can be mechanistically predicted by solving the differential equations that describe the dynamics and kinematics of its primary components (Gillespie et al., 1992). As these equations are complicated, they are solved by a process that simulates the vehicle on a computer at discrete time instants, separated by a very small ‘time step’ (Gillespie et al., 1992).

Early simulations were based on mathematical models whose equations were laboriously and meticulously derived by hand and solved using purpose-written computer programs (Prem et al., 2001).

In the late 1970s, engineers began using available computer programs, automating the process of creating mathematical models and solving differential equations (cited in Prem et al. (2001)). Generally, these programs are referred to as general-purpose multibody dynamics programs, or stated in another way they enable analysis of arbitrary multibody systems that arise in a wide range of engineering areas.

There are many computed-based packages available for simulating motions of multi-body mechanical systems such as vehicles. The Automatic Dynamic Analysis of Mechanical Systems (ADAMS[®]) package is a product of the MSC Software and it is the most widely used multibody dynamics program in the world (MSC.Software@, 2012). It was developed in the late 1970s and it has been demonstrated and verified in a wide range of engineering areas (Prem et al., 2001).

According to Gillespie et al. (1992), that studied the effects of vehicle characteristics on pavement response and performance, a computer program should deal properly with the peculiar nonlinear properties of the springs in heavy vehicle suspensions, the kinematics of the load-sharing tandem axles, and the sequential input of a single road profile into the various axles. In addition, computational efficiency is required.

However, Sayers (1999) said that ADAMS[®] and other multibody simulation programs are not designed for real-time since they employ nonlinear differential-algebraic equations, which require iterative solution methods that run. Additionally, he referred that the simulations resulting from the integration of ADAMS[®] and SIMULINK[®] run so slowly that the advantages of an interactive environment are lost.

As aforementioned, ADAMS[®] is a general-purpose program that offers a ‘complete solution’. It handles the entire simulation effort, from model description to numerical integration of equations. However, some compromises are made to achieve the generality (Sayers, 1990), namely the fact that generalized simulation codes often run slower than the specialized ones. The generalized simulation codes are written to be applied to all multibody systems. Therefore, most of the simplification techniques cannot be used. The inefficiency of the general-purpose programs make them less attractive for highly repetitive design studies and unfeasible for real-time, hardware-in-the-loop (HITL) operations (Sayers, 1990). Other weakness of them is the use

of external subroutines because they are limited to cases that were anticipated by the original programmer.

Sayers (1990) used symbolic computation to develop the AUTOSIM[®] program. It automated much of the work formerly performed by specialists in dynamics and the numerical analysis. The development time for a detailed simulation code is reduced from months to hours. The AUTOSIM is a symbolic mathematics language developed in Lisp language to AUTOMATICALLY generate SIMULATION codes.

Sayers (1999) described how the multibody symbolic code generator AUTOSIM[®] can be used to generate comprehensive vehicle dynamics models for Real-Time Simulation (RTS) applications with HITL using an ordinary computer. He also demonstrated the good adequacy of the generated code for RTS applications and showed how the same model is run using SIMULINK[®].

All of the math model solver programs in BikeSim[®], CarSim[®], and TruckSIM[®] have been produced using AUTOSIM[®]. The development of a new simulation design, called VehicleSim, started in 2005. It combines the optimization methods from AutoSim with a new simulation architecture that allows users to extend models at run-time with a variety of methods. Completed in 2007, CarSim 7 is the first product to fully use the new VehicleSim (VS) technology (MSC@, 2012). Users can modify some of the model equations of motion, add new equations with the built-in VehicleSim command language, integrate it with other software such as SIMULINK[®], LabView[®], and ETAS/ASCET, or add custom C code to work with the math model using the VehicleSim application program interface.

In the DIVINE project (1998) there was a computer simulation task that attempted to determine the ability of various computer programs to predict dynamic wheel loads and vehicle vertical response due to a defined input. Six models were analysed, abbreviated by 'Scania', 'TNO', 'Pennstate', 'Roaduser', 'FHWA' and 'Osaka' (for a full description, see the technical report). The 'Roaduser' model and the 'FHWA' model were found to be the most accurate models in estimating the wheel load of trucks for all circumstances. The 'Roaduser' model from the Roaduser Research was developed using the AUTOSIM multi-body simulation code (OECD, 1998).

Pont (2004) used the AUTOSIM[®] to simulate the response of individual vehicles to profiles with determined roughness levels. He determined the effects of variations in speed and suspension characteristics on the response and calculated transfer functions from these responses. These transfer functions were then combined for the different vehicles of the fleet, thus estimating a fleet transfer function that was fitted with a simple model. This model was then used to predict the spatial distribution of the dynamic axle loads.

The computed-based packages play an important role in the transportation system. They have been used to analyse the performance and the impact of non-standard heavy vehicles. For example, Wideberg et al. (2006) carried out a study that compares a number of stability measures of European heavy trucks with the performance of high capacity vehicle combinations in a range of the Organization for Economic Co-Operation and Development (OECD) countries. For that, they used the multibody simulation package ADAMS[®]. George et al. (1998) also used the ADAMS[®] to obtain the performance of a range of standard vehicles using a number of safety and road geometry performance-based measures. From these simulations they recommended levels or target values to be used in the assessing of non-standard vehicles.

However, some stakeholders have expressed their concerns about performance predictions from computer-based models. They may not be reliable and may substantially differ with software package and with the software's users. To address these concerns, Prem et al. (2002) compared three programs: ADAMS[®], University of Michigan Transportation Research Institute (UMTRI) constant velocity Yaw/Roll model and AUTOSIM[®]. For that, the same datasets were supplied to each consultant and identical simulations were performed using the same test manoeuvres. First of all, they carried out a literature review in order to validate the models against experimental tests. The review generally confirmed that an acceptable level of agreement, between experimental data and responses predicted with any one of the three programs, can be achieved. They concluded that, with due care, acceptable agreement between modelling packages can be achieved.

McFarlane and Sweatman (1998) discussed the use of 'Virtual Prototyping' techniques (simulation modelling and animation) in developing larger more productive combination vehicles. They used these techniques to demonstrate that new vehicle concepts are capable of having dynamic performance equivalents to the mid-range of heavy vehicles in operation.. They used the AUTOSIM technology and found a good agreement between measured and simulated performance.

Although ADAMS[®] is probably the most widely used simulation package, this work uses the TruckSIM[®] simulation package as it was generated by VehicleSim technology (successor of AUTOSIM) which usually runs significantly faster than those developed by other simulation package (Haldane and Bunker, 2002).

The TruckSIM[®] opens with a view of the Run Control screen (Figure 2.43) which permits to see the TruckSIM[®] architecture: TruckSIM[®] uses a database to define vehicles, test procedures and other data. Then, with a one click operation, a simulation can be run and the results can be seen in the animator and in the plots (800 to thousands of output variable). The results can be exported to other software. These four main components are depicted in Figure 2.44.

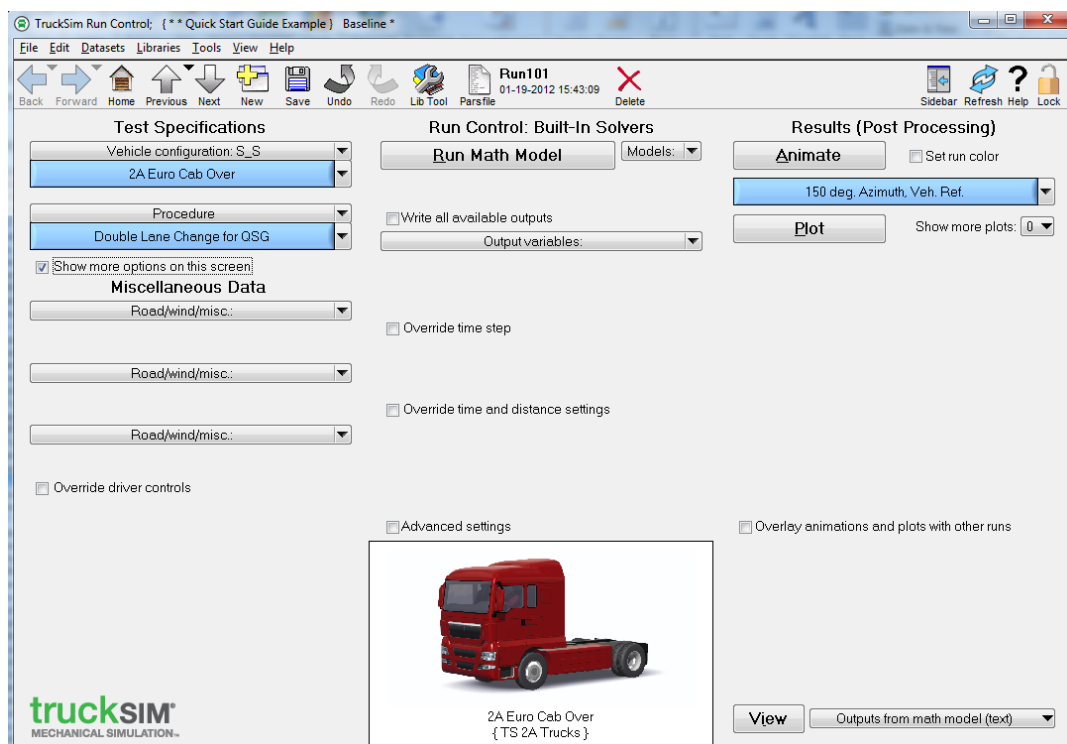


Figure 2.43 –The Run Control screen

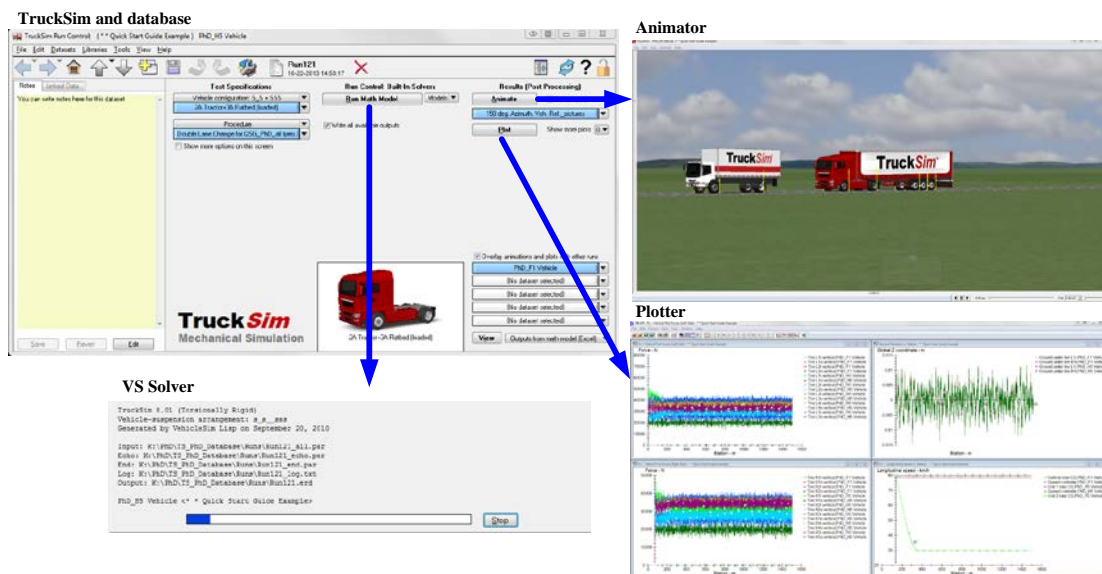


Figure 2.44 – The four main components of TruckSIM[®] (MSC, 2009b)

Next, some aspects or capabilities of the TruckSIM[®] (closer related to this work) are listed (for a full listing, see MSC (2012)):

- Road profiles are included. This provides efficient use of high-frequency measured road roughness data;
- A wide range of tractor-trailer(s) combinations is available;
- Multiple axle configurations are available;
- Dual, single and wide-base tyres are available;
- It supports many different suspension designs, using data that can be obtained from real or simulated kinematics and compliance tests;
- It includes several tyre models (Figure 2.45). It is ready to run with a table-based basic model, an extended model (more tables for camber effects), the Pacejka 5.2 version of the Magic Formula, and MF-Tyre from TNO. It is also ready to run with MF-Swift from TNO and FTire from COSIN (extra licences are required). In this case, TruckSIM[®] connects to a third-party tyre model and the tyre model built into the VS solver is disabled and all tyre forces and moments are calculated by the third-party software. Figure 2.40 shows how the VS Vehicle model of TruckSIM[®] works together with third-party tyre models. The VS vehicle model and the tyre model are implemented with separate DLL files that communicate with each other during the simulation. The VS solver simulates the entire vehicle except the wheel/tyre (above the wheel axles) and the tyre models simulates wheel/tyre dynamics including tyre/ground contact (below the wheel axles) (MSC, 2009a).

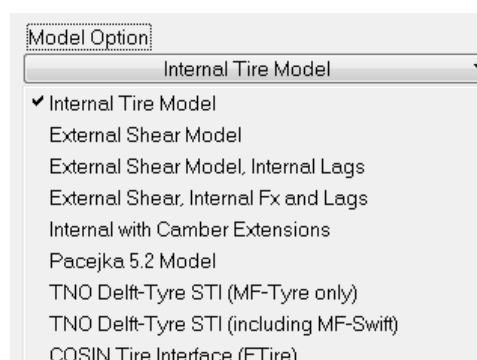


Figure 2.45 – Model option drop-down list (from software screen)

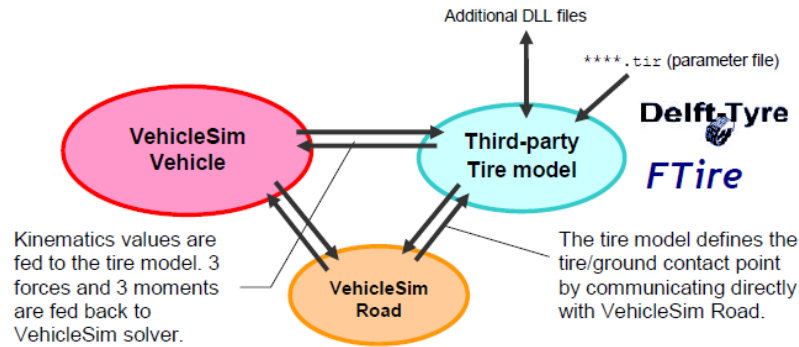


Figure 2.46 – Co-simulation of VS solver and third-party tyre model (MSC, 2009a)

2.5 MODELLING WHOLE PAVEMENT LIFE

The current pavement design methods consider that the material properties are constant over time and they calculate the pavement response only once for the standard axle (ESAL). Transfer functions are used to calculate the allowable number of ESAL applications from pavement response and then the damage is defined by relating the expected number of ESAL applications over the pavement design period (given by multiplying the expected number of trucks by an AF) with the allowable number of ESAL applications (given by transfer functions).

In these methods both the interaction between the vehicle and the pavement response and the interaction between the pavement performance and the pavement response are considered as being one-way interactions. The vehicle loads affect the pavement response but not vice-versa and the pavement response affects the pavement performance but not vice-versa. However, the pavement response has influence on the deterioration mechanisms which in turn could influence the material properties and consequently the pavement response. The roughness-deterioration mechanism could evolve during the pavement design period changing the loads applied by the vehicle to the pavement structure and consequently the pavement response.

In order to consider the abovementioned interactions, the pavement design period should be divided into a number of time increments. Within each time increment all design issues are constant, but they change between increments, the design issues of the time increment (t+1) are updated from the time increment (t).

The COST action 333 (1999) established the requirements for an European pavement design method which passes essentially by an incremental procedure. This procedure will enable changes which occur during the pavement design period as illustrated in Figure 2.47.

The MEPDG procedure (NCHRP, 2004) was the first one to include the capability to accumulate pavement damage on a monthly basis over the pavement design period.

Roebuck et al. (2012) presented the architecture of a user friendly software (Vehicle-Pavement Interaction (VPI) software - VPI@ (2013)) that can be used to model the interaction between vehicles and pavements and to assess the effects of dynamic vehicle loads and climatic factors on pavement performance. The idea is to have a modular system which allows expert users to modify or replace individual components easily with the objective to have a community of users with a common platform. The VPI software is not available yet.

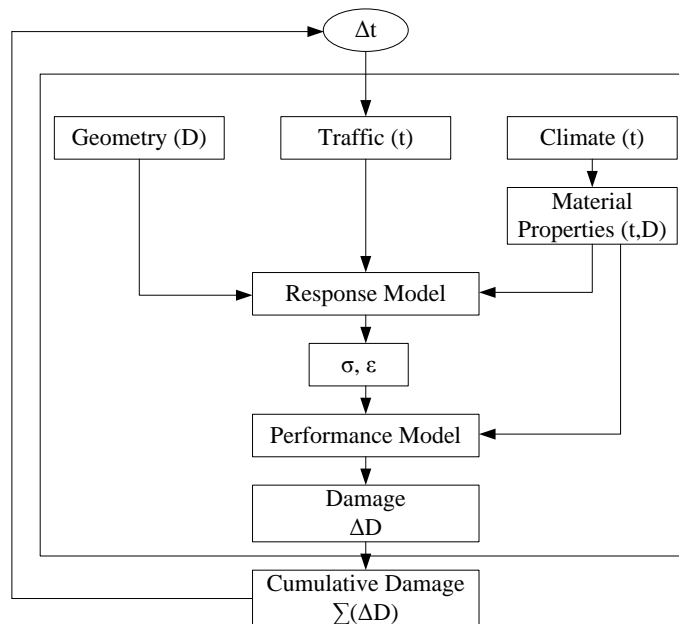


Figure 2.47 – COST action 333’s incremental procedure (COST 333, 1999)

The model implemented by the VPI software is based on the Whole-Life Flexible Pavement Performance Model (WLPPM) developed by Collop and Cebon (1995) which is depicted in Figure 2.48. In relation to previous whole-life models, this model considers the spatial repeatability of the dynamic tyre forces generated by a flow of articulated vehicles. The dynamic tyre forces were generated using a time domain vehicle simulation with a linear ‘quarter car’ vehicle model. They also considered a modulus degradation model with the form of the Collop and Cebon’s model (expression (2.6)) and updated the surface profile using rutting data.

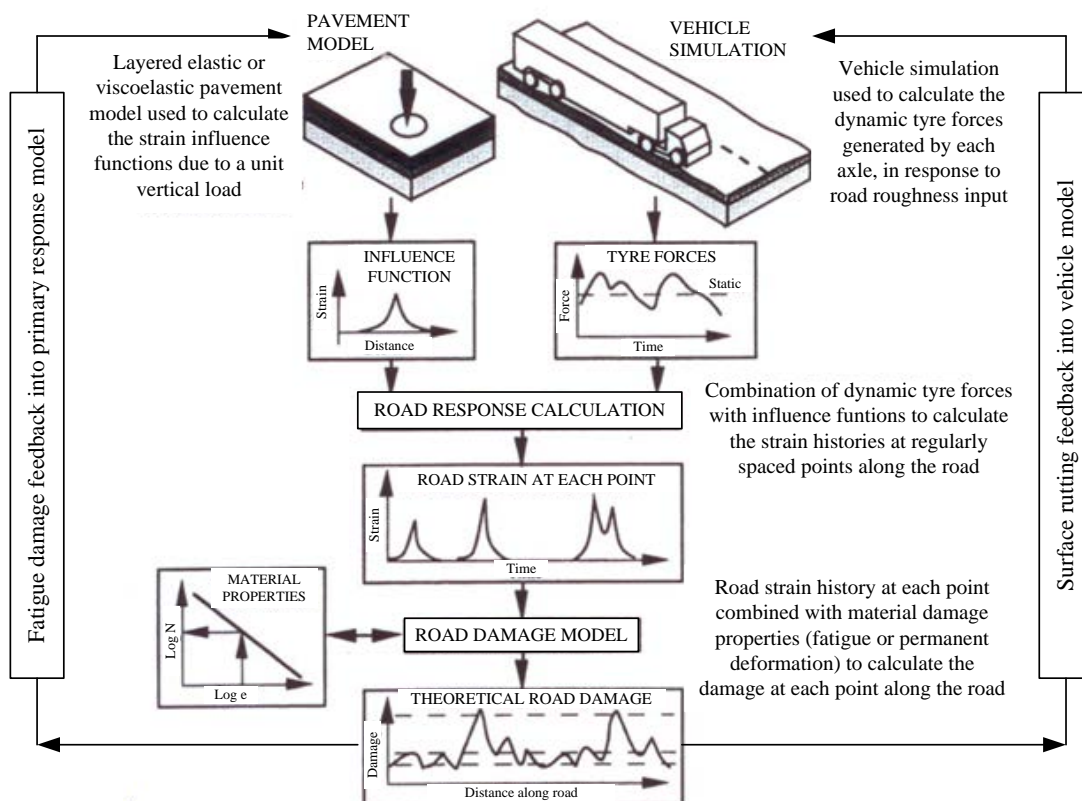


Figure 2.48 – WLPPM developed by Collop and Cebon (adapted from Cebon (1999))

Goodrum and Cebon (2010) investigated available methods (pitch-plane models and quarter car models) for generating repeatable dynamic tyre forces from axle load probability distributions with the objective of developing a calculation method capable of model the spatial repeatability of a reference vehicle flow as accurately and efficiently as possible.

2.6 REFERENCES

Aarts, L. and Febbes, G. (2008). Experiences with Longer and Heavier Vehicles in the Netherlands. *10th International Symposium on Heavy Vehicle Transportation Technology*, France.

AASHTO (1993). *AASHTO Guide for Design of Pavement Structures*. American Association of State Highway and Transportation Officials.

Åkerman, I. and Jonsson, R. (2007). *European Modular System for road freight transport – experiences and possibilities*. TFK – TransportForsK AB and KTH - Department of Transportation and urban economics. Stockholm, Sweden.

Alkasawneh, W., Oan, E. and Green, R. (2008). The Effect of Loading Configuration and Footprint Geometry on Flexible Pavement Response Based on Linear Elastic Theory. *Road Materials and Pavement Design*, 9, 159-179.

Beer, M. D. and Fisher, C. (1997). *Contact stresses of pneumatic tires measured with the Vehicle-Road Surface Pressure Transducer Array (VRSPTA) system for the University of California at Berkeley (UCB) and the Nevada Automotive Test Center (NATC)*. Division of Roads and Transport Thecnology. (CSIR), C.f.S.a.I.R. Pretoria. Confidential Contract Research Report CR-971053.

Beer, M. D., Fisher, C. and Jooste, F. J. (1997). Determination of Pneumatic Tyre/Pavement Interface Contact Stresses under Moving Loads and some Effects on Pavements with Thin Asphalt Surfacing Layers. *8th International Conference on Pavement Asphalt*, Seattle, Washington, USA.

Beer, M. D., Fisher, C. and Kannemeyer, L. (2004). Towards the Application of Stress-In-Motion (SIM) Results in Pavement Design and Infrastructure Protection. *8th International Symposium on Heavy Vehicle Weights and Dimensions*, Johannesburg, South Africa.

Beer, M. D., Sadzik, E. M., Fisher, C. and Coetzee, C. H. (2005). Tyre-Pavement Contact Stress Patterns from the Test Tyres of the Gautrans Heavy Vehicle Simulator (HSV). *24th Southern African Transport Conference (SATC 2005)*, Pretoria, South Africa.

Belay, A., O'Brien, E. and Kroese, D. (2008). Truck fleet model for design and assessment of flexible pavements. *Journal of Sound and Vibration*, 311, 1161-1174.

Beskou, N. D. and Theodorakopoulos, D. D. (2011). Dynamic effects of moving loads on road pavements: A review. *Soil Dynamics and Earthquake Engineering*, 31, 547-567.

Birgisson, B., Sangpetngam, B. and Roque, R. (2002). Predicting Viscoelastic Response and Crack Growth in Asphalt Mixtures with the Boundary Element Method. *Transportation Research Record: Journal of the Transportation Research Board*, 1789, 129-135.

Blab, R. (1999). Introducing Improved Loading Assumptions into Analytical Pavement Models Based on Measured Contact Stresses of Tires. *International Conference on Accelerated Pavement Testing*, Reno, Nevada, USA.

Blundell, M. and Harty, D. (2004). *The Multibody Systems Approach to Vehicle Dynamics*. Elsevier Butterworth-Heinemann.

Bonnaure, F., Gest, G., Gravois, A. and Uge, P. (1977). A New Method of Predicting the Stiffness of Asphalt Paving Mixtures. *Proceedings, Association of Asphalt Paving Technologists*, 46, 64-100.

Bouazara, M. and Richard, M. J. (2001). An optimization method designed to improve 3-D vehicle comfort and road holding capability through the use of active and semi-active suspensions. *European Journal of Mechanics - A/Solids*, 20, 509-520.

Branco, F., Pereira, P. and Santos, L. P. (2005). *Pavimentos Rodoviários (Road Pavements)*. ALMEDINA. In Portuguese.

BRRC@ (2013). Belgium Road Research Centre (BRRC) (European Modular Systems). http://www.brrc.be/brrc/e15/e15_00c6.php. Access date: May 2013.

Cebon, D. (1999). *Handbook of Vehicle-Road Interaction*. Taylor & Francis.

Ceuster, G. D., Breemersch, T., Herbruggen, B. V., Verweij, K., Davydenko, I., Klingender, M., Jacob, B., Arki, H. and Bereni, M. (2008). *Effects of adapting the rules on weights and dimensions of heavy commercial vehicles as established within Directive 96/53/EC*. Transport & Mobility Leuven (TML), TNO innovation for life, RWTH Aachen University, Laboratoire Central des Ponts et Chaussées (LCPC), Service d'études sur les transports, les routes et leurs aménagements (Sétra). Brussels, Belgium. TML final report for DG TREN (TREN/G3/318/2007).

Chen, Y., He, J., King, M., Liu, H. and Zhang, W. (2013). Dynamic Load-Sharing of Longitudinal-Connected Air 1 Suspensions of a Tri-Axle Semi-Trailer. *Annual Meeting of the Transportation Research Board*, Washington, D. C.

Christidis, P. and Leduc, G. (2009). *Longer and Heavier Vehicles for freight transport*. European Commission, Joint Research Centre, Institute for Prospective Technological Studies.

Cole, D. J. and Cebon, D. (1991). Assessing the Road-Damaging Potential of Heavy Vehicles. *Proceedings of the Institution of Mechanical Engineers, Part D: Journal of Automobile Engineering*, 205, 223-232.

Collop, A. and Cebon, D. (1995). Modelling Whole-Life Pavement Performance. *4th International Symposium on Heavy Vehicle Weights and Dimensions*, Ann Arbor, Michigan, USA.

Collop, A. C. and Cebon, D. (1996). Stiffness Reductions of Flexible Pavements due to Cumulative Fatigue Damage. *Journal of Transportation Engineering*, 122, 131-139.

COSIN@ (2012). FTire. <http://www.cosin.eu/imprint>. Cosin scientific software. Access date: September 2012.

COST 323 (2002). *Weight-in-Motion of Road Vehicles. Final Report of the Action*. European Commission (EC), European Cooperation in Science and Technology (COST) and Laboratoire Central des Ponts et Chaussées (LCPC). Paris.

COST 333 (1999). *Development of New Bituminous Pavement Design Method (Final Report of the Action)*. European Commission (EC), Directorate General Transport. Belgium.

COST 334 (2001). *Effects of Wide Single Tyres and Dual Tyres (Final report of the Action - version 29 November 2001 Taskgroup 3 Final Report)*. European Commission, Directorate General Transport. Belgium.

Debauche, W. (2008). Working Group on Longer and Heavier Goods Vehicles: a Multidisciplinary Approach to the Issue. *10th International Symposium on Heavy Vehicle Transportation Technology*, France.

DfT@ (2013). Providing effective regulation of freight transport. <https://www.gov.uk/government/policies/providing-effective-regulation-of-freight-transport/supporting-pages/trialling-longer-hgv-semi-trailers>. Department for Transport (DfT). Access date: May 2013.

Doll, C., D. Fiorello, E. Pastori, C. Reynaud, P. Klaus, P. Lückmann, J. Kochsiek, K. Hesse (2008). *Long-Term Climate Impacts of the Introduction of Mega-Trucks to the Community of European Railways and Infrastructure Companies (CER)*, Brussels. Fraunhofer ISI (study coordinator, Karlsruhe), TRT (Milan), NESTEAR (Gentilly), Fraunhofer-ATL (Nuremberg), Fraunhofer-IML (Dortmund). Karlsruhe.

EC (2009). Regulation (EC) 1072/2009 of the European Parliament and of the Council of 21 October 2009 on common rules for access to the international road haulage market. European Community (EC) - Official Journal of the European Union.

EC (2013). Proposal for a Directive of the European Parliament and of the Council amending Directive 96/53/EC of 25 July 1996 laying down for certain road vehicles circulating within the Community the maximum authorised dimensions in national and international traffic and the maximum authorised weights in international traffic. European Commission (EC).

EEC (1992). Council Directive 92/7/EEC of 10 February amending Directive 85/3/EEC on the weights, dimensions and certain technical characteristics of certain road vehicles. European Economic Community (EEC) - Official Journal of the European Communities.

EEC (1993). Council Regulation (EEC) No 3118/93 of 25 October 1993 laying down the conditions under which non-resident carriers may operate national road haulage services within a Member State. European Economic Community (EEC) - Official Journal of the European Communities.

Elseifi, M. A., Al-Qadi, I. L., Yoo, P. J. and Janajreh, I. (2005). Quantification of Pavement Damage Caused by Dual and Wide-Base Tires. *Transportation Research Record: Journal of the Transportation Research Board*, 1940, 125-135.

Eurostat (2013). Statistical Database - Road Transport. <http://epp.eurostat.ec.europa.eu/portal/page/portal/transport/data/database>. Access date: January 4, 2013.

Freitas, E., Pereira, P., Picado-Santos, L. and Papagiannakis, A. (2005). Effect of Construction Quality, Temperature, and Rutting on Initiation of Top-Down Cracking. *Transportation Research Record: Journal of the Transportation Research Board*, 1929, 174-182.

Freitas, E., Pereira, P. and Picado Santos, L. (2003). Assessment of Top-Down Cracking Causes in Asphalt Pavements. *Mairepav 3 - 3rd International Symposium/Maintenance and Rehabilitation of Pavements and Technological Control*, Guimarães, Portugal.

Gardete, D., Santos, L. P. and Pais, J. (2008). Permanent Deformation Characterization of Bituminous Mixtures using Laboratory Tests. *Road Materials and Pavement Design*, 9, 537-547.

George, R., Elischer, M. and Prem, H. (1998). Exemption Guide-Lines for Non-Standard Vehicles. *5th International Symposium on Heavy Vehicle Weights and Dimensions*, Australia.

Gillespie, T. D. (1992). *Fundamentals of Vehicle Dynamics*. Society of Automotive Engineers, Inc.

Gillespie, T. D., Karamihas, S. K., Cebon, D., Sayers, M. W., Nasim, M. A., Hansen, W. and Ehsan, N. (1992). *Effects of Heavy Vehicle Characteristics on Pavement Response and Performance (Final Report)*. National Cooperative Highway Research Program (NCHRP), Transportation Research Board (TRB), National Research Council. The University of Michigan - Transportation Research Institute (UMTRI). UMTRI 92-2.

Glaeser, K. P. and Irzik, M. (2012). Longer Truck Combinations in Germany - Trial Start in 2012. *12th International Symposium on Heavy Vehicle Transportation Technology*, Sweden.

Glaeser, K. P., Kaschner, R., Lerner, M., Roder, C. K., Weber, R., Wolf, A. and Zander, U. (2006). *Effects of new vehicle concepts on the infrastructure of the federal trunk road network*. Federal Highway Research Institute (bast).

Gleave, D., Frisoni, R., Dionori, F., Christoph Vollath, Tyszka, K., Casullo, L., Routaboul, C., Jarzemskis, A. and Tanczos, K. (2013). *Development and Implementation of EU Road Cabotage*. European Parliament's Committee on Transport and Tourism (Study - Provisional Version). IP/B/TRAN/FWC/2010-006/Lot1/C1/SC3.

Goodrum, W. J. and Cebon, D. (2010). Synthesising Spatially Repeatable Tyre Forces from Axle Load Probability Distributions. *11th International Symposium on Heavy Vehicle Transportation Technology*, Australia.

Haider, S. and Harichandran, R. (2009). Effect of Axle Load Spectrum Characteristics on Flexible Pavement Performance. *Transportation Research Record: Journal of the Transportation Research Board*, 2095, 101-114.

Haider, S., Harichandran, R. and Dwaikat, M. (2010). Effect of Axle Load Measurement Errors on Pavement Performance and Design Reliability. *Transportation Research Record: Journal of the Transportation Research Board*, 2160, 107-117.

Haider, S. W. and Harichandran, R. S. (2007). Relating Axle Load Spectra to Truck Gross Vehicle Weights and Volumes. *Journal of Transportation Engineering*, 133, 696-705.

Hajek, J., Billing, J. and Swan, D. (2011). Forecasting Traffic Loads for Mechanistic-Empirical Pavement Design. *Transportation Research Record: Journal of the Transportation Research Board*, 2256, 151-158.

- Haldane, M. and Bunker, D. J. (2002). *Assessing the Impacts of Multi-Combination Vehicles on Traffic Operations and Safety - A Literature Review*. Queensland Government - Department of Main Roads.
- Hasagasioglu, S., Kilicaslan, K., Atabay, O. and Güney, A. (2012). Vehicle dynamics analysis of a heavy-duty commercial vehicle by using multibody simulation methods. *The International Journal of Advanced Manufacturing Technology*, 1-15.
- Hellung-Larsen, M. (2012). Evaluation of trial with European Modular System road trains in Denmark. *12th International Symposium on Heavy Vehicle Transportation Technology*, Sweden.
- Hendrickson@ (2013). <http://europe.hendrickson-intl.com/>. Access date: January 2013.
- Huang, Y. H. (2004). *Pavement Analysis and Design*, Second Edition ed. Pearson, Prentice Hall.
- Hutch@ (2013). Hutchens Industries. <http://www.hutch-susp.com/products>. Access date: January 2013.
- INE (2012). Instituto Nacional de Estatística (Statistics Portugal). http://www.ine.pt/xportal/xmain?xpid=INE&xpgid=ine_publicacoes&PUBLICACOE_Spagenumber=1&PUBLICACOESrevista=00&PUBLICACOESTema=55488&PUBLICACOESfreeText=Estat%C3%ADsticas%20dos%20transportes. Access date: October 2012. In Portuguese.
- ITF@ (2013). International Transport Forum. <http://www.internationaltransportforum.org/IntOrg/road/dimensions.html>. Access date: 16-01-2013.
- JAE (1995). *Manual de Concepção de Pavimentos para a Rede Rodoviária Nacional (Pavement Design Manual for the Portuguese Road Network)*. JAE (Junta Autónoma de Estradas). In Portuguese.
- Karamihas, S. M., Gillespie, T. D. and Riley, S. M. (1995). Axle Tramp Contributions to the Dynamic Wheel Loads of a Heavy Truck. *4th International Symposium on Heavy Vehicle Weights and Dimensions*, USA.
- Kim, Y. R. and Little, D. N. (1990). One-Dimensional Constitutive Modeling of Asphalt Concrete. *Journal of Engineering Mechanics*, 116, 751-772.
- Knight, I., Burgess, A., Jacob, H. M. B., Irzik, M., Aarts, L. and Vierth, I. (2009). *Assessing the likely effects of potential changes to European heavy vehicles weights and dimensions*. Project TREN/B3/110/2009, Transport Research Laboratory (TRL).
- Knight, I., Newton, W., McKinnon, A., Palmer, A., Barlow, T., I McCrae, Dodd, M., Couper, G., Davies, H., Daly, A., McMahan, W., Cook, E., Ramdas, V. and Taylor, N. (2008). *Longer and/or Longer and Heavier Goods Vehicles (LHVs) - a Study of the Likely Effects if Permitted in the UK: Final Project Report (S0516/V7 (PPRO 4/012/034))*. Transportation Research Laboratory (TRL).
- Lima, H. and Quaresma, L. (1999). *Caracterização do factor de agressividade do tráfego de veículos pesados em Portugal (Characterization of the aggressiveness of heavy-vehicle traffic in Portugal)*. JAE (Junta Autónoma de Estradas) and LNEC (Laboratório Nacional de Engenharia Civil). Lisboa. In Portuguese.

- Lima, H., Quaresma, L. and Pinelo, A. (2000). Agressividade do Tráfego Pesado em Portugal - Exemplo do Itinerário Principal 5 (IP5) (Aggressiveness of heavy-vehicle traffic in Portugal - Example of the principal route number 5 (IP5)). *1º Congresso Rodoviário Português*, Laboratório Nacional de Engenharia Civil.
- Liu, Y. and You, Z. (2011). Discrete-Element Modeling: Impacts of Aggregate Sphericity, Orientation, and Angularity on Creep Stiffness of Idealized Asphalt Mixtures. *Journal of Engineering Mechanics*, 137, 294-303.
- Maurice, J. P. (2000). Short Wavelength and Dynamic Tyre Behaviour under Lateral and Combined Slip Conditions. PhD Thesis, Delft University of Technology.
- McFarlane, S. and Sweatman, P. (1998). The Development of High Productivity Long Combination Vehicles using "Virtual Prototyping". *5th International Conference on Heavy Vehicles Weights and Dimensions*, Australia.
- MDS and TRL (2010). *Longer Semi-trailer Feasibility Study and Impact Assessment* MDS Transmodal, Transport Research Laboratory (TRL). Report commissioned by Department for Transport (DfT).
- Molenaar, A. A. A. (2007). Prediction of Fatigue Cracking in Asphalt Pavements: Do we follow the Right Approach. *Annual Meeting of the Transportation Research Board*, Washington, D.C.
- Mrad, N., El-Gindy, M. and Kenis, W. (1998). *Effects of Wheel-Load Spatial Repeatability on Road Damage: A Literature Review*. Federal Highway Administration. FHWA-RD-97-036.
- MSC (2009a). *Tire Models*. Mechanical Simulation Corporation.
- MSC (2009b). *TruckSim - Quick Start Guide*. Mechanical Simulation Corporation.
- MSC (2012). *TruckSim: Math Models*. http://www.carsim.com/downloads/pdf/Math_Models_T81.pdf. Access date: January 19, 2012.
- MSC.Software@ (2012). <http://www.mscsoftware.com/Products/CAE-Tools/Adams.aspx>. Access date: 23 January 2012.
- MSC@ (2012). <http://www.carsim.com/company/ourhistory.php>. Access date: 19 January 2012.
- Mun, S., Guddati, M. and Richard Kim, Y. (2004). Fatigue Cracking Mechanisms in Asphalt Pavements with Viscoelastic Continuum Damage Finite-Element Program. *Transportation Research Record: Journal of the Transportation Research Board*, 1896, 96-106.
- Myers, L. A., Roque, R. and Birgisson, B. (2001). Propagation Mechanisms for Surface-Initiated Longitudinal Wheelpath Cracks. *Transportation Research Record: Journal of the Transportation Research Board*, 1778, 113-122.
- NCHRP (2004). *MEPDG - Guide for Mechanistic-Empirical Design of New and Rehabilitated Pavement Structures*. NCHRP (National Cooperative Highway Research Program), Transportation Research Board, National Research Council.
- O'Connor, A., O'Brien, E. J. and Jacob, B. (2000). An Experimental Investigation of Spatial Repeatability. *International Journal of Heavy Vehicle Systems*, 7, 64-81.

- O'Brien, E. J. and Taheri, A. (2011). Numerical integration approach to the problem of simulating damage in an asphalt pavement. *International Journal of Pavement Engineering*, 1-11.
- OECD (1998). *Dynamic Interaction between Vehicles and Infrastructure Experiment (DIVINE)*. Organisation for Economic Co-operation and Development (OECD). Paris, France. DSTI/DOT/RTR/IR6(98)1/FINAL.
- OECD (2011). *Moving Freight with Better Trucks: Improving Safety, Productivity and Sustainability*. Organisation for Economic Co-operation and Development (OECD) Publishing.
- Oh, J., Fernando, E. G. and Lytton, R. L. (2007). Evaluation of Damage Potential for Pavements due to Overweight Truck Traffic. *Journal of Transportation Engineering*, 133, 308-317.
- OTEP (2004). *Estudo Piloto de Pesagem de Veículos Pesados de Mercadorias nas Fronteiras entre Portugal e Espanha (Pilot Study of Weight Measurement of heavy-goods vehicles at the borders between Portugal and Spain)*. OTEP (Observatório Transfronteiriço Espanha/Portugal). In Portuguese.
- Pacejka, H. B. (2006). *Tyre and Vehicle Dynamics*, Second Edition ed. Elsevier.
- Picado Santos, L. (2000). Design Temperature on Flexible Pavements: Methodology for Calculation. *International Journal of Road Materials and Pavement Design*, 1, 355-371.
- Pont, J. d. (2004). Modelling the Dynamic Wheel Forces of the Heavy Vehicle Fleet. *8th International Symposium on Heavy Vehicle Weights and Dimensions*, Johannesburg, South Africa.
- Prem, D. H., Ramsay, E., Pont, D. J. d., McLean, D. J. and Woodroffe, J. (2001). *Comparison of Modelling Systems for Performance-Based Assessments of Heavy Vehicles (Performance Based Standards – NRTC/Austroroads Project A3 and A4)*, Working Paper. National Road Transport Commission.
- Prem, H., Pont, J. d. and Edgar, J. (2002). Comparison of Three Programs for Simulating Heavy-vehicles Dynamics. *7th International Symposium on Heavy Vehicle Weights and Dimensions*, Delft, The Netherlands.
- Rakic, B., Stegeman, J. and Kind, M. (2011). *Monitoring Traffic Safety - Longer and Heavier Vehicles*. ARCADIS and NEA. Ministry of Infrastructure and Environment (Rijkswaterstaat). The Netherlands.
- Roberson, R. E. and Schwertassek, R. (1988). *Dynamics of Multibody Systems*. Springer-Verlag.
- Roebuck, R. L., Isola, R., Goodrum, W. J., Cebon, D. and Collop, A. C. (2012). Vehicle - Pavement Interaction Modelling. *12th International Symposium on Heavy Vehicle Transportation Technology*, Sweden.
- Romanoschi, S., Momin, S., Bethu, S. and Bendana, L. (2011). Development of Traffic Inputs for New Mechanistic-Empirical Pavement Design Guide. *Transportation Research Record: Journal of the Transportation Research Board*, 2256, 142-150.
- Roque, R., Zou, J., Kim, Y. R., Baek, C., Thirunavukkarasu, S., Underwood, B. S. and Guddati, M. N. (2010). *Top-Down Cracking of Hot-Mix Asphalt Layers: Models for Initiation and*

Propagation. NCHRP - National Cooperative Highway Research Program. Final Report for NCHRP Project 1-42A.

Sadeghi, J. M. and Fathali, M. (2007). Deterioration Analysis of Flexible Pavements under Overweight Vehicles. *Journal of Transportation Engineering*, 133, 625-633.

Salama, H., Haider, S. and Chatti, K. (2007). Evaluation of New Mechanistic—Empirical Pavement Design Guide Rutting Models for Multiple-Axle Loads. *Transportation Research Record: Journal of the Transportation Research Board*, 2005, 112-123.

Salama, H. K. and Chatti, K. (2010). Evaluation of fatigue and rut damage prediction methods for asphalt concrete pavements subjected to multiple axle loads. *International Journal of Pavement Engineering*, 12, 25-36.

Salgado, R. and Kim, D. (2002). *Effects of Heavier Truck Loadings and Super-Single Tires on Subgrades*. Final Report FHWA/IN/JTRP-2002/20.

Sangpetngam, B., Birgisson, B. and Roque, R. (2003). Development of Efficient Crack Growth Simulator Based on Hot-Mix Asphalt Fracture Mechanics. *Transportation Research Record: Journal of the Transportation Research Board*, 1832, 105-112.

Sangpetngam, B., Birgisson, B. and Roque, R. (2004). Multilayer Boundary-Element Method for Evaluating Top-Down Cracking in Hot-Mix Asphalt Pavements. *Transportation Research Record: Journal of the Transportation Research Board*, 1896, 129-137.

Sayers, M. W. (1990). Symbolic Computer Methods to Automatically Formulate Vehicle Simulation Codes. PhD Thesis, University of Michigan.

Sayers, M. W. (1999). Vehicle Models for RTS Applications. *Vehicle System Dynamics*, 32, 421-438.

Shell (1978). *Shell pavement design manual - asphalt pavements and overlays for road traffic*. Shell International Petroleum Company Limited, London.

Shell (1988). *Shell pavement design method, BISAR-PC user manual*. Shell International Petroleum Company Limited.

Taheri, A., O'Brien, E. J. and Collop, A. C. (2012). Pavement damage model incorporating vehicle dynamics and a 3D pavement surface. *International Journal of Pavement Engineering*, 1-10.

Timm, D. H., Tisdale, M. and Turochy, R. E. (2005). Axle Load Spectra Characterization by Mixed Distribution Modeling. *Journal of Transportation Engineering*, 131, 83-88.

TNO (2010). MF-Tyre/MF-Swift 6.1.2.1 (Help Manual). TNO Automotive, The Netherlands.

TNO@ (2012). MF-TYRE / MF-SWIFT. http://www.tno.nl/content.cfm?context=thema&content=markt_product&laag1=894&laag2=59&laag3=351&item_id=1272&Taal=2. TNO innovation for life. Access date: September 2012.

Ullidtz, P., Harvey, J., Tsai, B.-W. and Monismith, C. (2006). *Calibration of Incremental-Recursive Flexible Damage Models in CalME Using HVS Experiments*. Report prepared for the

California Department of Transportation, Division of Research and Innovation, Office of Roadway Research. University of California, Pavement Research Center, Berkeley and Davis. UCPRC-RR-2005-06.

Underwood, B., Baek, C. and Kim, Y. (2012). Simplified Viscoelastic Continuum Damage Model as Platform for Asphalt Concrete Fatigue Analysis. *Transportation Research Record: Journal of the Transportation Research Board*, 2296, 36-45.

Underwood, B. S., Kim, Y. R. and Guddati, M. N. (2009). Improved calculation method of damage parameter in viscoelastic continuum damage model. *International Journal of Pavement Engineering*, 11, 459-476.

VPI@ (2013). Vehicle-Pavement Interaction Software. <http://vpisoftware.blogspot.co.uk/>. Access date: June 2013.

Wang, L., Myers, L., Mohammad, L. and Fu, Y. (2003). Micromechanics Study on Top-Down Cracking. *Transportation Research Record: Journal of the Transportation Research Board*, 1853, 121-133.

WAVE (2001). *Weight-in-motion of Axles and Vehicles for Europe (WAVE)*. General Report. Laboratoire Central des Ponts et Chaussées (LCPC). RTD project, RO-96-SC, 403.

Wideberg, J., Dahlberg, D. E. and Svensson, M. (2006). Study of stability measures and legislation of heavy articulated vehicles in different OECD countries. *9th International Symposium on Heavy Vehicle Weight and Dimensions*, USA.

Wilson, S. P., Harris, N. K. and O'Brien, E. J. (2006). The use of Bayesian statistics to predict patterns of spatial repeatability. *Transportation Research Part C: Emerging Technologies*, 14, 303-315.

Yoo, P. J. and Al-Qadi, I. L. (2007). Effect of Transient Dynamic Loading on Flexible Pavements. *Transportation Research Record: Journal of the Transportation Research Board*, 129-140.

Yoo, P. J., Al-Qadi, I. L., Elseifi, M. A. and Janajreh, I. (2006). Flexible pavement responses to different loading amplitudes considering layer interface condition and lateral shear forces. *The International Journal of Pavement Engineering*, 7, 73-86.

Zegelaar, P. W. A. (1998). The Dynamic Response of Tyres to Brake Torque Variations and Roas Unevennesses. PhD Thesis, Delft University of Technology.

Zhao, Y., Liu, W. and Tan, Y. (2012). Analysis of Critical Structure Responses for Flexible Pavements in NCHRP 1-37A Mechanistic-Empirical Pavement Design Guide. *Journal of Transportation Engineering*, 138, 983-990.

3 ROAD ROUGHNESS

3.1 INTRODUCTION

Road roughness is an important indicator of road condition which affects both road users (mainly ride quality, operation cost and safety) and road pavement structures (dynamic wheel loads). Therefore, it has been used as acceptance criterion for newly constructed or repaved roads. In addition, it has also been used as an indicator of pavement performance (serviceability) along its lifetime.

Serviceability is related to ride quality, which in its turn is related to road roughness. The serviceability concept was developed during the Road Test conducted by the American Association of State Highway Officials (AASHO) (Hall and Muñoz, 1999). In the Road Test, the subjective road users' opinion of serviceability was called Present Serviceability Rating (PSR) which was related to an objective index, called Present Serviceability Index (PSI). PSI can be calculated from road roughness measurements and other road pavement surface distresses.

In general, road roughness is characterized by a summary index which is usually obtained from a measured road profile. Therefore, road roughness is normally quantified using two steps. First the road profile is measured and then it is processed to calculate a roughness index.

There are several devices to measure roughness, ranging from simple devices to more complex ones. The necessity of correlation and transferability of data between them, and calibration of them to a common scale has started a long time ago. The International Road Roughness Experiment (IRRE) arose from that necessity (Sayers et al., 1986b). This experiment compared data from several devices with the objective to define a single standard roughness measurement to which all measurements could be scaled, i.e. an International Roughness Index (IRI). As road roughness can be quantified by using road profile measurements or vehicle response measurements to road roughness, the IRI had to be compatible with these two ways of measure roughness. It was defined to fulfil the following criteria: time stable, transportable, relevant and valid. Once the IRI is defined, the measurement devices (or methods) were classified into four classes: (1) precision profilers, (2) other profilers (those unable to achieve the class 1's accuracy) (3) IRI estimates from correlation equations and (4) subjective ratings and no calibrated measures.

As cited by Karamihas et al. (1999), the measurement of the true profile is an elusive goal. It implies an enormous effort of data collection to include all the wavelengths and respective amplitudes of the profile (from microtexture to roughness wavelengths). Nevertheless, most applications of road profile measurements have their own range of wavelengths.

The World Road Association - PIARC established texture categories by defining wavelength ranges (see Figure 3.1).

Therefore, for a specific purpose only the corresponding wavelength range of interest must be accurately measured. In terms of road roughness, the interesting wavelengths are those that excite vehicle vibrations, degrade ride quality, excite vehicle suspension and affect the vertical wheel loads (Karamihas, 2005).

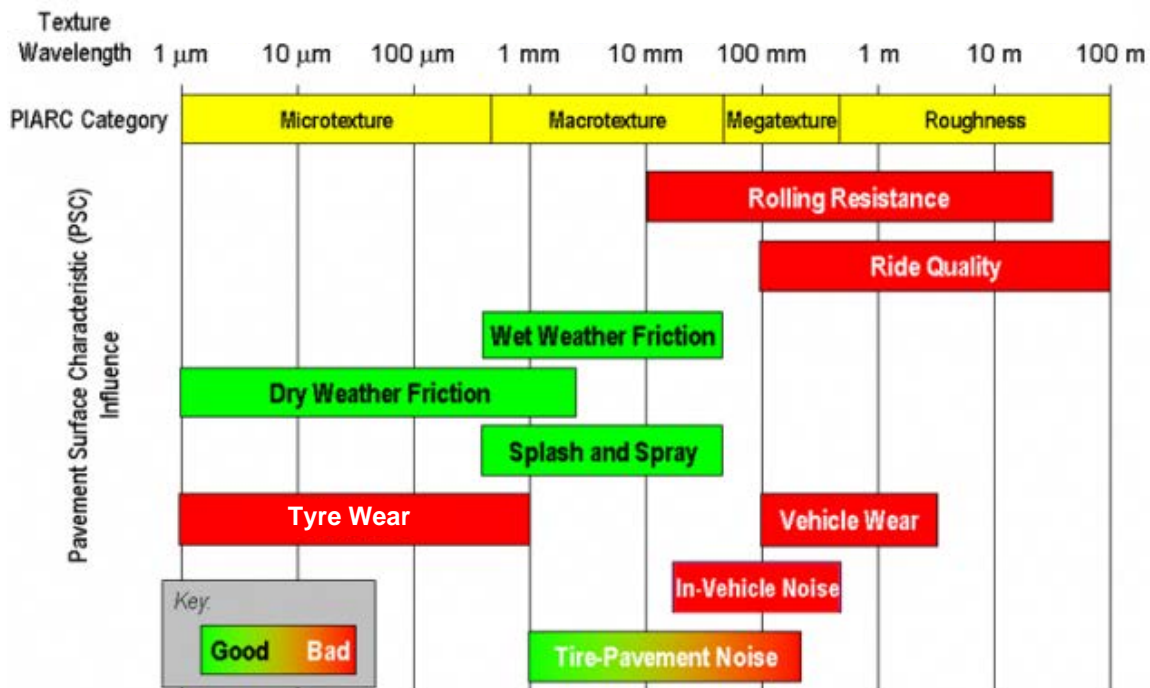


Figure 3.1 – Texture categories defined by wavelengths (TCPSC@, 2014)

This chapter begins with the presentation of roughness measurement devices, followed by two approaches of analysing roughness. One uses a summary index to define the roughness of the entire road profile, while the other one tries to extract more information of the road profile. The latter one uses signal processing techniques. Then, a procedure to generate road profiles is described. It is a crucial topic in vehicle simulation when road profile measurements are unavailable. Finally, since roughness evolves with time, models to predict roughness growth are presented.

3.2 ROUGHNESS MEASUREMENT

3.2.1 Introduction

Devices used to measure roughness have been evolving with time from static devices to high-speed devices operating at normal traffic speed. Each device has a limited range of applications for which it is valid. Therefore, its choice depends on its intended use. High-speed devices are currently used at network level while static devices are currently used at project level. Usually, accuracy requirements are higher at the project level than at the network level.

Roughness measurement can be based on road profile measurements or on vehicle response measurements to road roughness.

Next a brief description of devices is presented, namely reference devices, straight edges, profilographs, Response-Type Road Roughness Measurement (RTRRM) devices and inertial profilers. In addition, further trends are referred.

3.2.2 Reference devices

Rod and level

The device consists of a marked rod, a level that is used to establish the reference elevation and a tape used to measure the longitudinal distance (see Figure 3.2).

Measurement of long distance profiles or various profiles with this device is not practical due to the required effort. Sayers et al. (1986a) describes the procedure to measure a profile with it.

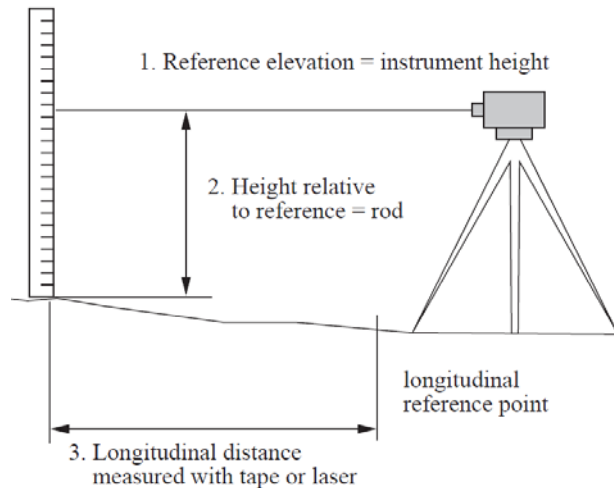


Figure 3.2 – Rod and level (Sayers and Karamihas, 1998)

The rod and level method is considered to be the most precise and accurate method for measuring profile (cited in El-Korchi et al. (2002)). Consequently, it is currently used as standard reference method.

Dipstick

The Dipstick device is faster than the rod and level one. It ‘walks’ along the line to profile. In each ‘walking step’ (usually with 305 mm in length), the difference in height of the two supports is measured by an inclinometer (see Figure 3.3).

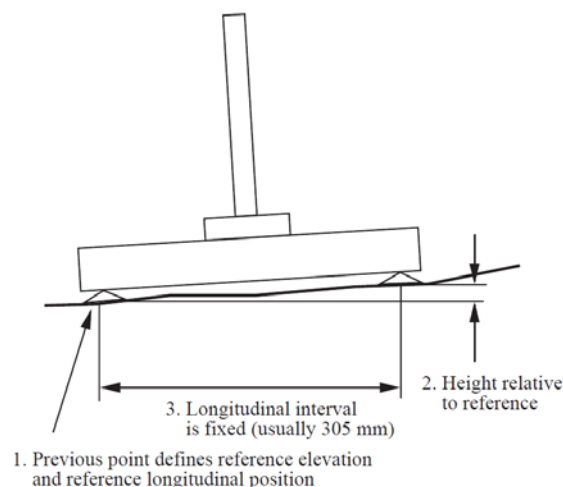


Figure 3.3 – Dipstick (Sayers and Karamihas, 1998)

Walking profilometer

The walking profilometer is similar to the Dipstick. However, the walking process is automated by the operator pushing the machine along the wheel path at walking speed. Figure 3.4 shows the Australian Road Research Board (ARRB) walking profilometer.



Figure 3.4 – ARRB walking profilometer (ARRB@, 2014)

3.2.3 Straight edges

There are conventional (sliding) and rolling straight edges, both with three meters long. The rolling straight edge, Figure 3.5, emerged from the necessity to reduce the effort to move the conventional one.

This device cannot address roughness with wavelengths longer than its span and can distort wavelengths that are harmonics of its spans. In addition, they can return misleading results when there is a high point or a depression on the road surface.



Figure 3.5 – Rolling straight edge (Scientific@, 2014)

3.2.4 Profilographs

Profilographs are ‘improved rolling straight edges’. They overcome the problem that arise from the fact that straight edges are three-contact points which can return, as above mentioned, misleading results. Profilographs have an array of wheels to establish a reference plane from which deviations are measured. The elevation is averaged for the whole array of wheels and roughness is measured as the deviation of the centre wheel from the reference (Chiu et al., 2003). As example, Figure 3.6 shows the California profilograph.



Figure 3.6 – California profilograph (Chiu et al., 2003)

3.2.5 Response-Type Road Roughness Measurement (RTRRM) devices

RTRMM devices do not measure the road profile. The roughness is measured by accumulating the deflections of a suspension which are then divided by the travelled distance (m/km). Figure 3.7 shows two examples of response-type devices. The Bureau of Public Roads (BPR) roughometer, the oldest one, is hitched to a towing vehicle while the Mays ridemeter is installed in a car.

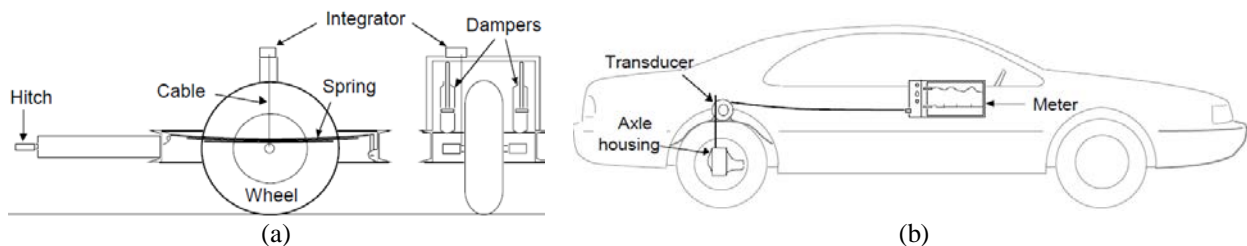


Figure 3.7 – Response-type systems: (a) the BPR roughometer, (b) the Mays ridemeter (Sayers and Karamihas, 1998)

Since this type of device depends on the host vehicle dynamics, roughness measurements are not stable with time and are not transportable.

3.2.6 Inertial profiler

The first inertial profiler was developed by the General Motor Researches (GMR) laboratories in the 1960s (Sayers and Karamihas, 1996). It consists of a vehicle with three essential transducers: an accelerometer for defining an inertial reference, a road sensing transducer(s) for measuring the height of the ground relative to the reference and a distance measuring system (see Figure 3.8).

Currently, this device is one of the most used, mainly at network level. Figure 3.9 shows two inertial profilers in use in Portugal.

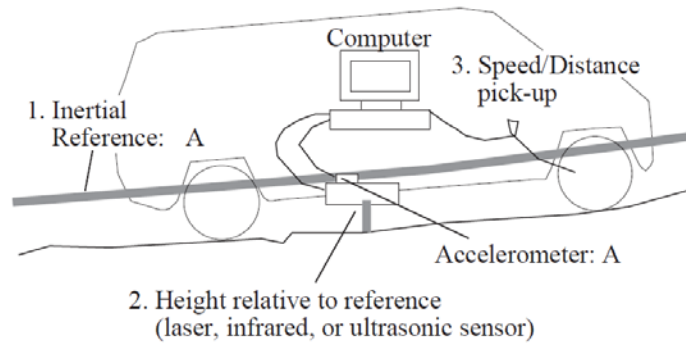


Figure 3.8 – Inertial profiler (Sayers and Karamihas, 1998)



Figure 3.9 – Two inertial profilers in use in Portugal

3.2.7 Further trends

Chang et al. (2009) tested the use of an autonomous robot (P3-AT) (Figure 3.10) to collect road profiles and calculated IRI. The P3-AT can move up to 3 km/h and is capable of measuring longitudinal profiles with 15 cm (or shorter) sampling intervals. The test was carried out indoor in a 50 m straight test path. The results were compared with results from an ARRB walking profilometer. The comparison shows a good agreement between the two devices.

According to the authors, the use of an autonomous robot will replace manually operated or driven equipment for construction purposes in the near future. They are working towards the design and implementation of an inertial navigation system using an inertial profile unit and Global Positioning Systems (GPS) with the P3-AT.

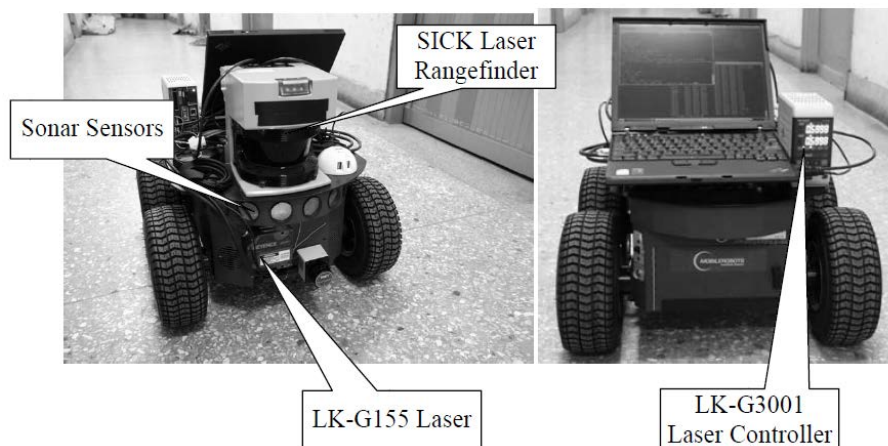


Figure 3.10 – P3-AT autonomous robot (Chang et al., 2009)

3.3 ROUGHNESS ANALYSIS

3.3.1 Introduction

Several profile indices can be computed using road profile measurements. All of them are single numerical values which attempt to quantify ride quality.

The IRI was developed to be a single standard roughness measurement for a wide range of devices, including RTRRM devices. IRI is appropriate for vehicle calibration but it may not be the most appropriated one for other applications (Sayers et al., 1986b). Consequently, there are other indices which can be better for a specific purpose. Therefore, this section presents several roughness indices, namely, the International Roughness Index (IRI), the Profile Index (PI), the Ride Number (RN), the Half-Car Roughness Index (HRI), the Full-Car Roughness Index (FRI), the Truck Ride Index (TRI), the Ride Quality Index (RQI) and the Dynamic Load Index (DLI).

The roughness indices can only give an average condition of a road profile. As inertial profilers measure road profiles with enough accuracy and the use of this device type has been growing fast, it is possible to extract more information from road profiles (which are signals). This can be done using signal processing techniques such as Fourier Transform (FT) and Wavelet Transform (WT). These two techniques are briefly referred in this section.

3.3.2 Roughness indices

International Roughness Index (IRI)

The IRI is a standard roughness index and it is the index generally used. It is used in the acceptance of new pavements as well as in pavement performance monitoring and in Pavement Management Systems (PMS). It was a product of the IRRE, whose objective was to establish a single standard roughness index (Sayers et al., 1986b).

IRI was also defined to correlate well with outputs from RTRRM devices. Therefore, the computation of IRI is based on the quarter-car model which runs along the road profile at a simulation speed of 80 km/h. The quarter-car simulation is meant to be a theoretical representation of the response-type systems in use at the time the IRI was developed. The deflection of the simulated suspension is accumulated and divided by the length of the profile giving the IRI with units of slope (m/km). The quarter-car model's parameters are referred as golden car parameters. Figure 3.11 shows the quarter-car model and the golden car parameters, where M_s is the sprung mass, M_u is the unsprung mass, K_s is the suspension spring rate, C_s is the suspension damping rate and K_t is the tyre spring rate.

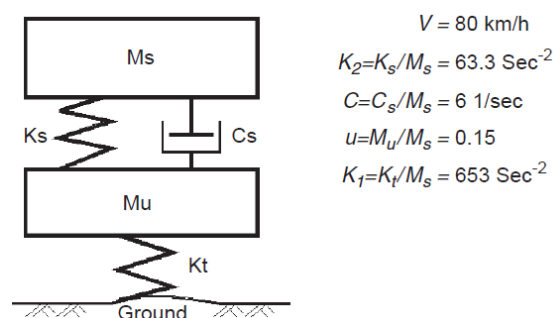


Figure 3.11 – Quarter-car model and golden car parameters (Yu et al., 2006)

The paper of Sayers (1995) is a reference document that contains the theoretical basis of the recommended IRI algorithm in detail.

IRI is a general pavement condition indicator (Sayers and Karamihas, 1998) that summarizes the roughness characteristics with impact on vehicle response. It is most appropriate when the desired measure is related to:

- Overall vehicle operating cost;
- Overall ride quality;
- Dynamic wheel loads;
- Overall surface condition.

Figure 3.12 shows IRI ranges for different classes of roads.

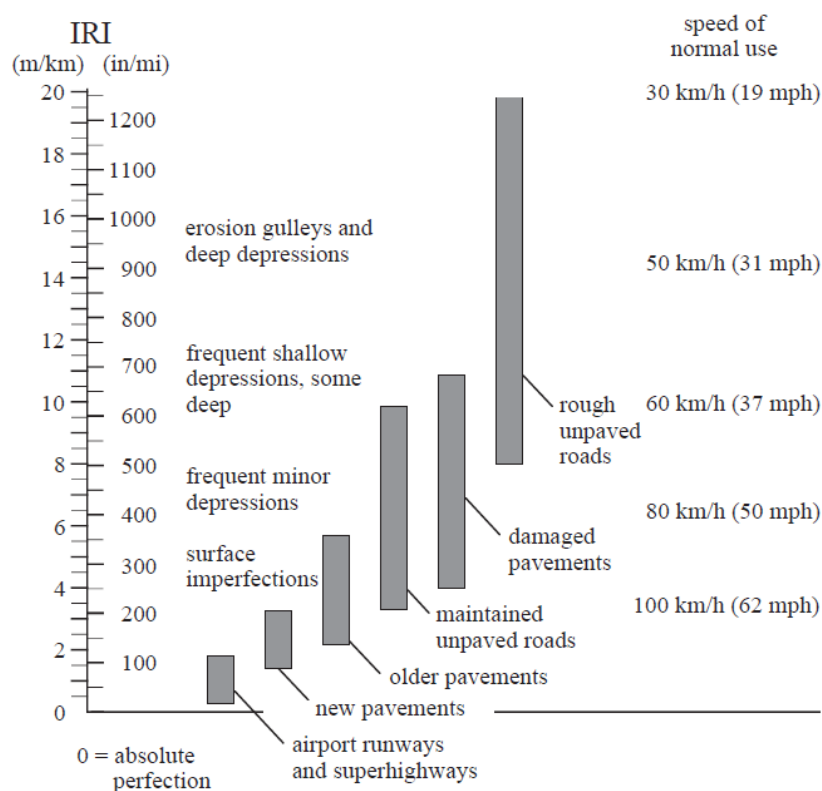


Figure 3.12 – IRI ranges for different classes of roads (adapted from Sayers and Karamihas (1998))

Hall and Muñoz (1999) developed models for estimating PSI as a function of IRI. According to the authors, their models improve other published models since their forms and coefficients were chosen to satisfy two important criteria: (a) the ability to estimate realistic values at both the low and high ends of the roughness range of values observed in practice and (b) the ability to produce good correlation between estimated and observed PSI values (using AASHO Road Test data).

Perera and Kohn (2004) evaluated the effects of speed variation in quarter-car simulations (IRI algorithm). For that, they simulated travel speeds between 60 and 120 km/h (increments of 10 km/h) over roads ranged from smooth (0.49 m/km) to rough (3.86 m/km). Eighty percent of the responses from IRI model were within ± 0.2 m/km of the IRI (simulation at 80 km/h) for simulated travel speeds between 60 and 110 km/h. However, some sections showed large differences and road users may notice differences in ride quality on such roads at different travel

speeds. Therefore, the authors recommended obtaining users' opinion and then the correlation of them with the simulated travel speed. If a better correlation is obtained for the case in which the quarter-car simulations are performed at the speed limit of the road, the speed limit should be used in the quarter-car simulation.

Believing that the same value of IRI may describe roads with quite different visual features and with differences in other profile indices, Kropáč and Múčka (2005) carried out a simulation study in which seven road profiles were considered, all having the same IRI value (2.21 m/km). They found variations in standard deviation of vertical elevation Root-Mean Square (RMS) in the range 1.48 to 7.06 and consequently they propose the standard deviation of vertical elevation RMS as an alternative profile index to the IRI.

Profile Index (PI)

The PI is determined from road profile data measured with a profilograph. It can also be determined using profilograph simulation. For example, the profile viewing and analysis software (ProVAL) simulates profilograph traces (ProVAL@, 2011).

Song and Teubert (2007) describes the PI computation procedure. It implies the definition of a blanking band. Then, the absolute values of the vertical deviations or 'scalops', outside the blanking band, are added and divided by the profile segment length. The resulting PI has units of slope (m/km).

Since some highway agencies have been measuring road profile roughness using the PI while others have used IRI, Smith et al. (2002) investigated a relationship between the IRI and the PI to make the switch between PI and IRI. They began the investigation analysing documented studies and the PI-to-IRI relationships developed by them. Three PI were considered, PI for blanking band 0.0 mm ($PI_{0.0}$), 2.5 mm ($PI_{2.5}$) and 5.0 mm ($PI_{5.0}$). They found that pavement type and climatic conditions affect significantly the PI-to-IRI relationship and consequently these variables were considered in the models development. For Asphalt Concrete (AC) pavements, they developed fifteen models for the PI-IRI relationships and eighteen models for the PI-PI relationships.

Ride Number (RN)

The RN intends to estimate (subjective) ride quality from road profile measurements on a 0 to 5 scale similar to the PSI scale, where 5 indicates a perfectly smooth road and the value decreases toward 0 as ride quality degrades.

It was developed by the National Cooperative Highway Research Project (NCHRP) in 1980s by relating road profile roughness to subjective road users' opinion (Sayers and Karamihas, 1998). Since opinions of single users tend to be unreliable, Mean Panel Ratings (MPR) are considered. Therefore, RN is an estimate of MPR.

Power Spectral Density (PSD) analyses were used to identify the wavelengths of road roughness that correlates best with MPR. Then, the profile is filtered with a band-pass filter and subsequently the filtered profile is reduced to yield a RMS slope called profile index (PI). PI is then transformed to RN using equation (3.1) (Sayers and Karamihas, 1996).

$$RN = 5e^{-160 \cdot PI} \quad (3.1)$$

If a single profile is considered, its PI is transformed directly. If profiles for both the left and right wheel tracks are processed, values for the two are averaged and then the transformation (3.1) is applied.

Half-Car Roughness Index (HRI)

The HRI is the half-car version of the IRI. The IRI processes the left wheel profile and the right wheel profile separately, obtaining an IRI value for each. Then, the two IRI values are averaged. The HRI processes a point-by-point averaged profile (see Figure 3.13).

A theoretical analyse (Sayers, 1989) gave the following limits for the relationship between the IRI and the HRI

$$0.71 \frac{IRI_{left} + IRI_{right}}{2} < HRI < \frac{IRI_{left} + IRI_{right}}{2} \tag{3.2}$$

Then, profile data were analysed by using both IRI and HRI and the relationship (3.3) was obtained.

$$HRI \approx 0.8 \frac{IRI_{left} + IRI_{right}}{2} \tag{3.3}$$

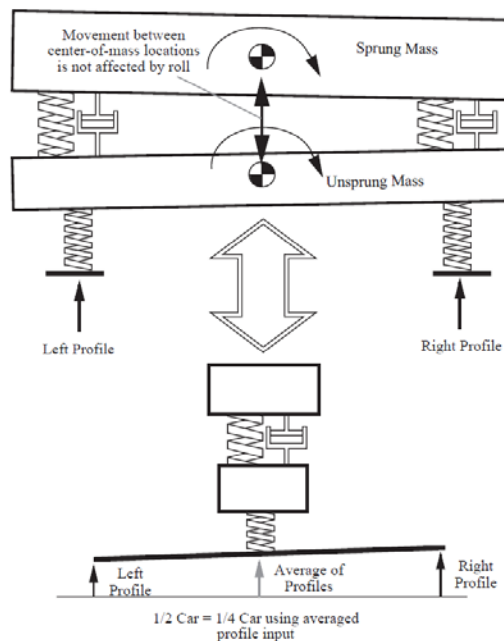


Figure 3.13 – Half-car model (Sayers and Karamihas, 1998)

Full-Car Roughness Index (FRI)

The FRI was developed by Capuruço et al. (2005). It permits the consideration of all vehicle elements related to vibration and consequently the vehicle dynamic responses for pitch, yaw, roll and bounce. Figure 3.14 shows the full-car model.

The FRI calculation is based, like the IRI and the HRI, on the quarter-car simulation. The difference is in the profile used as input. For FSI, the input profile is obtained by averaging the profile for each one of the four wheels, since the prediction of the vertical road disturbance at the

centre-of-mass locations of the sprung and unsprung masses by use of the full-car model was exactly the same as that which was obtained by averaging the profile for each one of the four wheels (Capuruço et al., 2005).

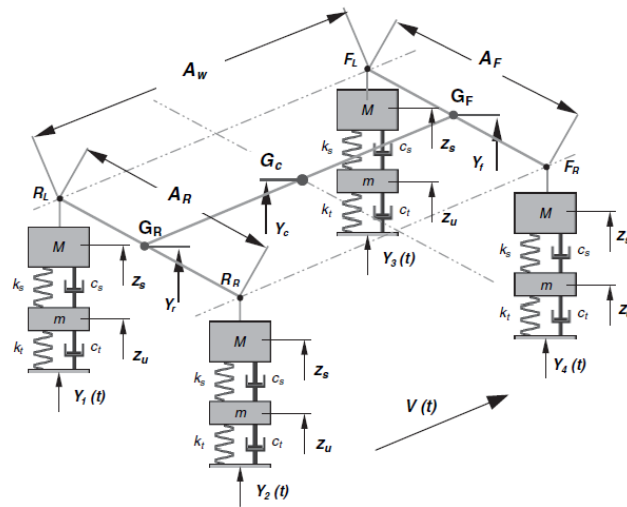


Figure 3.14 – Full-car simulation model (Capuruço et al., 2005)

In general, the FSI values are lower than the HRI values, which are in its turn lower than the IRI values (Capuruço et al., 2005). FRI is about 76% of HRI and 69% of the mean IRI and the IRI values for the left and right wheel profiles. The FSI presents lower dispersion than the other indices.

Cantisani and Loprencipe (2010) evaluated ride quality by measuring the whole body vibrations. For that, they developed a full car model which was then calibrated. With the model, dynamic simulations were carried out (80 km/h) and a synthetic index (called vertical weight RMS acceleration, a_{wz}) was calculated according to the ISO 2631-1 ('Mechanical vibration and shock - Evaluation of human exposure to whole-body vibration - Part 1: General requirements'). Comparison of a_{wz} index and IRI showed that for a fixed IRI value, the corresponding a_{wz} values have a wide variation range. Figure 3.15 presents speed-related IRI limits proposed by (Cantisani and Loprencipe, 2010), considering the a_{wz} comfort levels established in ISO 2631.

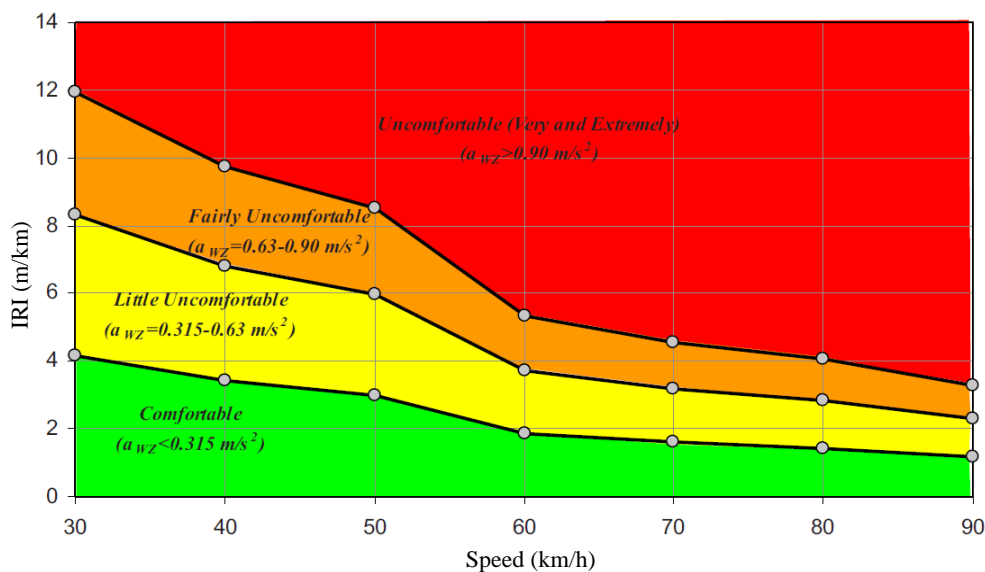


Figure 3.15 – Speed-related IRI limits, considering the a_{wz} comfort levels established in ISO 2631 (Cantisani and Loprencipe, 2010)

Truck Ride Index (TRI)

The TRI was developed to represent truck ride better than the IRI (Prem et al., 2000a). Figure 3.16 shows the necessity of a new index as it reveals the difference between the IRI and an index that may be indicative of truck ride. The IRI is sensitive to road roughness in the wavelength range 1 to 30 m, whereas the truck ride appears to be sensitive to wavelengths greater than approximately 3 m.

TRI is similar in context to the IRI but is based on a ‘quarter-truck’ model instead of a ‘quarter-car’ model. In addition, the TRI is based on a seat and driver model. Figure 3.17 shows these two models.

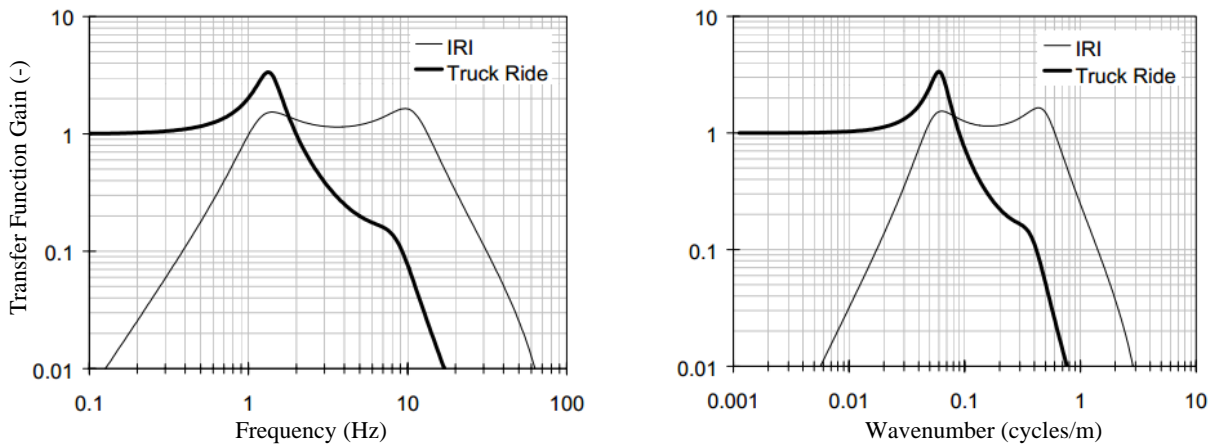


Figure 3.16 – Comparison of the IRI transfer function with a typical truck-ride transfer function both as a function of temporal frequency and as a function of spatial frequency (Prem et al., 2000b)

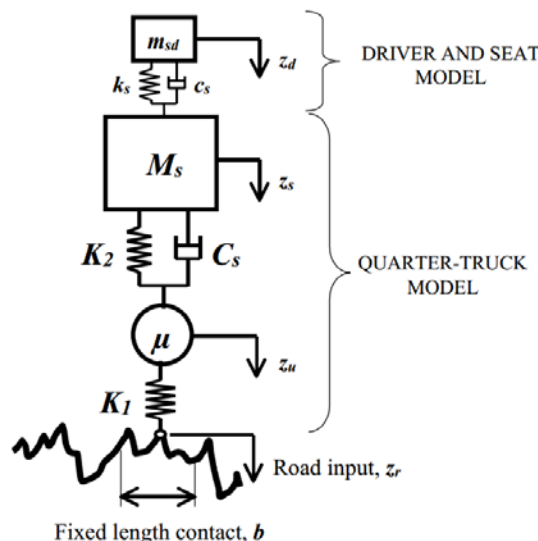


Figure 3.17 – Used model for truck ride prediction (Prem et al., 2000b)

The TRI was tested against a set of road profiles for which the users’ opinion (truck drivers and others) are known. It was found that for any particular value of IRI, the TRI covers a range of values as well as, for any particular value of TRI, the IRI covers a range of values (Prem et al., 2000a). For example, pavements with IRI equal to 3000 mm/km can have TRI values in the

range 0.2 to 2.5 m/s², and the likely reactions of truck drivers could range from ‘not uncomfortable’ to ‘extremely uncomfortable’.

Ride Quality Index (RQI)

The RQI was developed in the early 1970s by the Michigan Department of Transportation to correlate ride quality with the subjective road users’ opinion (Chatti and Lee, 2002). Psychometric tests were used for this purpose and it was found that some road components have a strong effect on users’ opinion while others have significantly less effect. Since the PSD correlated in 90 % with subjective users’ opinion, the road profile was split into three wavelength ranges: (1) 0.61 to 1.52 m, (2) 1.52 to 7.62 m, and (3) 7.62 to 15.24 m. According to the subjective users’ opinion, wavelengths shorter than 0.61 m mostly create tyre noise and those longer than 15.24 m do not disturb the vehicle suspension. Figure 3.18 shows how to calculate the RQI. The short waves have twice the effect of the intermediate waves and three times the effect of the long waves.

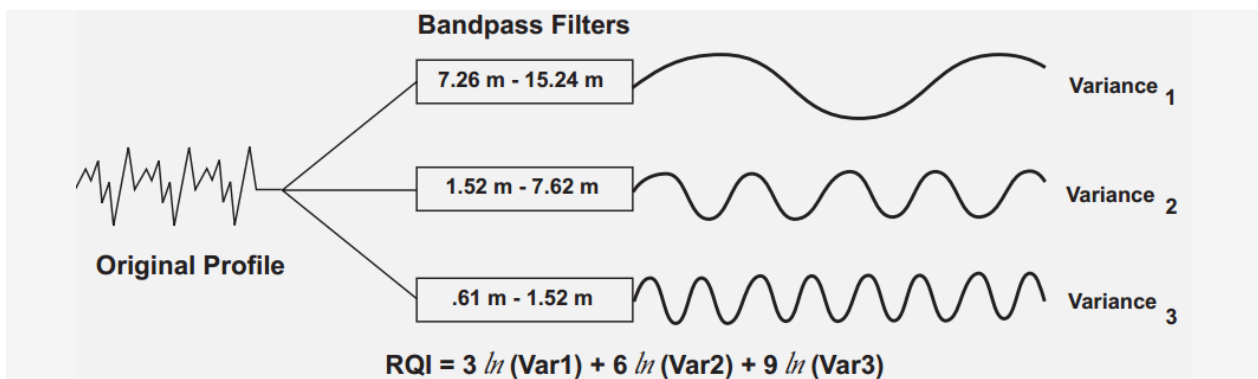


Figure 3.18 – Calculation of the RQI (MDOT, 1996)

RQI values from 0 to 30 indicates excellent ride quality, RQI values from 31 to 54 indicate good ride quality, RQI values from 55 to 70 indicate fair ride quality, and RQI values of more than 70 indicate poor ride quality (Chatti and Lee, 2002).

It is an indicator of dynamic loading. However, its development was based on passenger car response to pavement surface.

Dynamic Load Index (DLI)

In order to identify road profiles that are likely to generate high dynamic truck wheel loads, Chatti and Lee (2002) developed the DLI. The reason for that was that they found a wide range of truck dynamic load magnitudes for a given RQI value.

The vibration of heavy vehicles fall into two distinct frequency ranges: (1) vehicle bounce occurs in the frequency range 1.5 to 4 Hz and (2) axle bounce occurs in the frequency range 8 to 15 Hz. At 100 km/h, these frequencies correspond to wavelength ranges from 6.9 to 18.5 m and from 1.9 to 3.5 m, respectively. An index based in these wavelength ranges has a better correlation with truck dynamic wheel loads (from TruckSIM[®] simulations). The DLI is determined by using equation (3.4).

$$DLI = \sqrt{a_1 V_1 + a_2 V_2} \quad (3.4)$$

where

V_1 = variance of elevations of profile 1 (only waves in the wavelength range 6.9 to 18.5 m)

V_2 = variance of elevations of profile 2 (only waves in the wavelength range 1.9 to 3.5 m)

a_1 and a_2 = weighting factors

The weight-factor a_1 for V_1 was set equal to one for convenience. The weight-factor a_2 was determined to have the highest correlation between the DLI and the dynamic load of 333 pavement sections. A weighting factor of 14 was achieved.

With the DLI value, it is possible to define if a pavement profile is friendly or unfriendly in terms of truck dynamic loading. This definition can be made without running a truck simulation program.

3.3.3 Signal processing techniques

Signals (which are series of numbers) are processed mainly for two reasons (Sayers and Karamihas, 1998): (1) to improve the quality of a measurement by eliminating unwanted ‘noise’ from the data; and (2) to extract interesting information from the signal.

Two transformations can be applied to extract interesting information from a signal, namely the Fourier Transform (FT) and the Wavelet Transform (WT). The former transform extracts the frequency components of the signal by decomposing the signal into a number of sinusoids of different amplitudes, frequencies and phases. However, it loses all information on the location of a particular frequency within the signal. To overcome this problem, the short-time FT (STFT) was developed. It uses a sliding window to give information in both time and frequency domains. However, the resolution of this information is limited by the length of window which is the same for all frequencies. In contrast to the STFT, the WT adapts the length of window permitting the extraction of both information, frequency and time (or distance). Therefore, WT can be used to detect occurrences and locations of localized surface irregularities from the road profile, which is useful information for PMS.

WT is similar to FT since the original signal is approximated by adding together a series of functions with different frequencies. However, unlike the sinusoidal functions used in FT, WT uses wavelet (small wave) functions.

Wei and Fwa (2004) show how the WT can be used to detect local pavement distresses from the road profile. For a better description of WT, see, for example, the Chan’s book (Chan, 1995) and the user’s guide of the wavelet toolbox - MATLAB[®] (Misiti et al., 2013).

3.4 ROAD PROFILE GENERATION

3.4.1 Introduction

Vehicle simulations require road profiles as input. When road profile measurements are not available, road profiles can be generated to have a target spectral density.

Throughout the literature, some researchers (such as Cebon and Newland (1983), ISO 8608 (1995) and Cebon (1999)) reported that road profiles can be regarded as a stationary and ergodic stochastic process. Therefore, the profile can be described by the PSD function of the road profile elevations.

This section presents the procedure to generate road surface profiles and PSD models to define the target spectral density.

3.4.2 Procedure

Cebon (1999) presents a procedure to generate road profiles for single tracks and pairs of correlated tracks with a target spectral density. Only the generation of road profiles for single tracks is presented.

If the spectral coefficients S_k are specified, the terms Z_k of the discrete FT (DFT) can be determined from equation (3.5).

$$|Z_k| = \sqrt{S_k} \quad (3.5)$$

As $Z_k = |Z_k| e^{i\phi_k}$, equation (3.5) can be rewritten, resulting in equation (3.6).

$$Z_k = \sqrt{S_k} e^{i\phi_k} \quad (3.6)$$

For the pseudo-random sample representing a Gaussian signal, the phase angles $\{\phi_k\}$ must be randomly distributed between 0 and 2π .

The corresponding series of heights $\{z_r\}$ are determined by taking the IDFT as shown in equation (3.7).

$$z_r = \sum_{k=0}^{N-1} \sqrt{S_k} e^{i\left(\phi_k + \frac{2\pi kr}{N}\right)} \quad r=0, 1, 2, \dots, (N-1) \quad (3.7)$$

where

$$\begin{aligned} S_k &= (2\pi/N\Delta_x) S_{11}(\gamma_k) \\ S_{11}(\gamma_k) &= \text{the target spectral density} \\ \gamma_k &= (2\pi k/N\Delta_x) \text{ the wavenumber in rad/m} \\ \Delta_x &= \text{the distance interval between successive ordinates of the surface profile} \\ \{\phi_k\} &= \text{a set of independent random phase angles uniformly distributed between 0 and } 2\pi \end{aligned}$$

In addition, Cebon and Newland (1983) describe the generation procedure of more than two parallel tracks and the generation of a fully isotropic surface. These descriptions can be supported by (Newland, 1993) and (Cebon, 1999).

3.4.3 PSD Models

The road surface profile can be represented by the PSD of its vertical displacement. The PSD is a method based on FT that allows separating the road surface profile into sinusoidal components

with different wavelengths and measuring the power associated with each wavelength component.

ISO-proposed road roughness classification

The ISO 8608 (1995) aims to characterize specific road profiles in order to facilitate the division of road profiles into general classifications.

The smoothed form of the PSD may be fitted by a straight line. Equations (3.8) and (3.9) show the general form of the fitted PSD.

$$S_k(\gamma) = S_k(\gamma_0) \left(\frac{\gamma}{\gamma_0} \right)^{-w} \tag{3.8}$$

or

$$S_k(\Omega) = S_k(\Omega_0) \left(\frac{\Omega}{\Omega_0} \right)^{-w} \tag{3.9}$$

where

- γ_0 = (0.1 cycles/m) is the reference wavenumber (spatial frequency)
- Ω_0 = (1 rad/m) is the reference angular spatial frequency
- w = is the exponent of the fitted PSD

Although some literature use a two or more straight line fitting, the ISO 8608 (1995) proposes only a one-straight line fitting because its objective is the standardization of the classification and the guarantee of a unique solution, which with more than one straight line is practically impossible.

The ISO 8608 (1995) classifies roads in classes according to PSD values. Table 3.1 or Table 3.2 give the PSD values for different classes of roads in terms of the wavenumber γ or in terms of the angular spatial frequency Ω , respectively. The class limits are depicted in Figure 3.19. This classification was made by assuming a constant velocity PSD, which means that the exponent of the fitted PSD (w) is equal to 2.

Table 3.1 – Road classification based on $S_k(\gamma_0)$ values (ISO 8608, 1995)

Road class	Degree of roughness		
	$S_k(\gamma_0) (10^{-6} \text{ m}^3)$ ($\gamma_0 = 0.1 \text{ cycles/m}$)		
	Lower limit	Geometric mean	Upper limit
A	-	16	32
B	32	64	128
C	128	256	512
D	512	1024	2048
E	2048	4096	8192
F	8192	16384	32768
G	32768	65536	131072
H	131072	262144	-

Table 3.2 - Road classification based on $S_k(\Omega_0)$ values (ISO 8608, 1995)

Road class	Degree of roughness		
	$S_k(\Omega_0)$ (10^{-6} m^3) ($\Omega_0 = 1 \text{ rad/m}$)		
	Lower limit	Geometric mean	Upper limit
A	-	1	2
B	2	4	8
C	8	16	32
D	32	64	128
E	128	256	512
F	512	1024	2048
G	2048	4096	8192
H	8192	16384	-

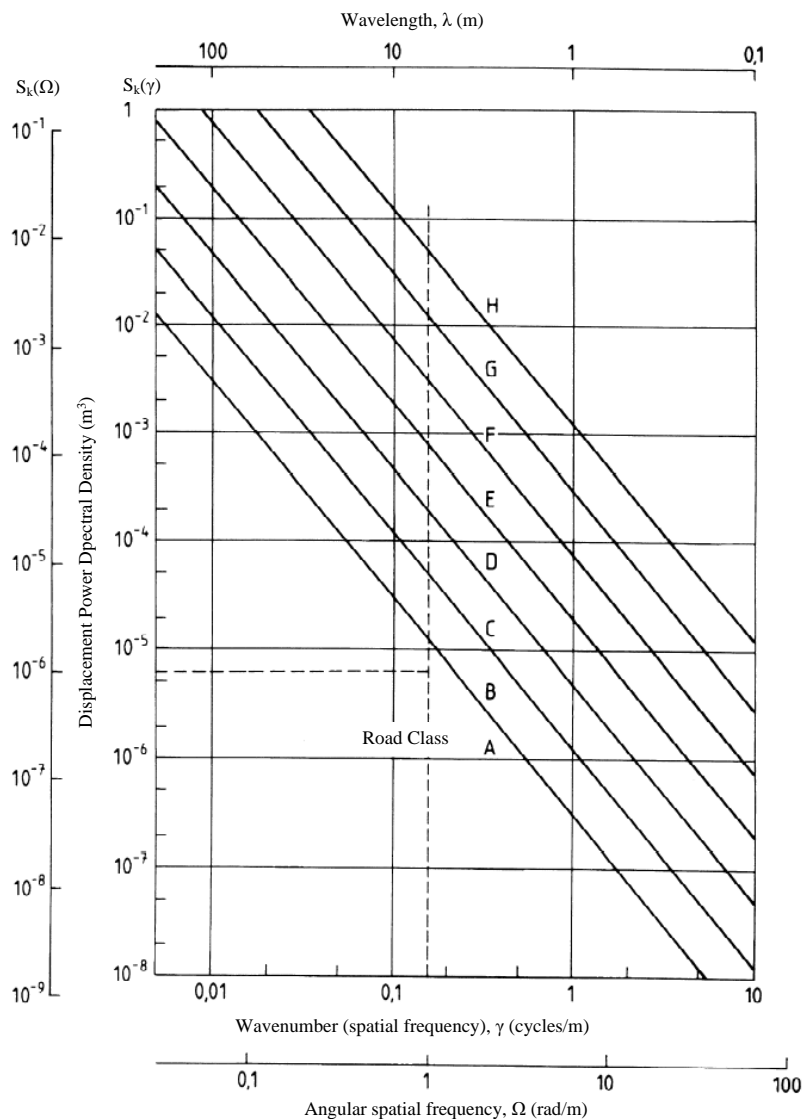


Figure 3.19 – Classification of roads (ISO 8608, 1995)

However, since the PSD is not always a straight line, the ISO 8608 (1995) gives also the displacement PSD for different classes of roads as a function of octave bands. This makes the road classification for each octave band possible. It is also conceivable to classify the road for any appropriate band of speeds. For example, in highways, and assuming that the speeds are between 70 km/h and 120 km/h, the band range 0.0221-1.4142 cycles/m (0.1388 - 8.8858 rad/m) is the most significant.

In the case of a two-track simulation, it is convenient to assume that the road surface possesses the property of isotropy, i.e. that all profiles of a given stretch of road, irrespective of orientation and location, have the same properties (ISO 8608, 1995).

Other

Sayers (1988) proposed a more general roughness model (Cebon, 1999) which uses three independent white-noise sources as shown in equation (3.9).

$$S_k(\gamma) = \frac{G_a}{(2\pi\gamma)^4} + \frac{G_s}{(2\pi\gamma)^2} + G_e \quad (3.9)$$

Where the first component, with amplitude G_a , is a white-noise acceleration that is integrated twice with respect to time; the second, with amplitude G_s , is a white-noise slope (velocity) that is integrated once with respect to time; and, the third, with amplitude G_e , is a white-noise elevation.

3.5 MODELS TO PREDICT PAVEMENT ROUGHNESS

3.5.1 Introduction

Three models to predict pavement roughness growth are presented. They are, the prediction model used in the Swedish PMS, the mechanistic roughness model developed by Saleh et al. (2000), which is based on vehicle-pavement interaction, and the prediction model of the Mechanistic-Empirical Pavement Design Guide (MEPDG) procedure.

3.5.2 Prediction model in the Swedish PMS

This model is based on roughness measurements. The total length of measurements, carried out between 1987 and 2000, is approximately 700 000 km what means that all paved roads (77 000 km) have several measurements (Lang, 2001). The total network was segmented into homogeneous sections with an average length of 300 m. Each homogeneous section is unique and is based on lane, road width, speed limit and pavement layers. For each homogeneous section it is possible to establish time series of data. Therefore, the prediction model uses a larger number of consistent measurements of roughness to calculate mean values of homogeneous sections.

The general model is the simple straight line equation (3.9).

$$\text{Prediction Condition} = \text{Initial Condition} + \text{Yearly Change} \cdot \text{Age} \quad (3.9)$$

Depending on the number of available measurements, three methods are used to establish the prediction model:

- (1) If data measurements are unavailable, the general model and default values are used.
- (2) If one or two measurements are available, the straight line equation corresponding to the prediction model is placed so that it passes through the mean value from the latest measurement. The slope of the line is determined from default values according to certain rules.

- (3) If several measurements are available, the straight line equation corresponding to the prediction model is determined by linear regression analysis. It is given greater influence to the later measurements than the earlier ones by using weight factors.

The default values were established by analyzing all available data from 1987 to 1999 for the whole country. The data were divided into climatic zones and traffic classes and statistics were calculated for them. The median values in Table 3.3 are used as default.

Table 3.3 – Default values in the Swedish roughness prediction model (Lang, 2001)

Climate zone	Traffic class	IRI initial median	IRI yearly change	IRI yearly change 90p	IRI yearly change 10p
1	A (<125)	2.70	0.08	0.41	0.02
	B (125-250)	2.55	0.07	0.37	0.01
	C (250-500)	2.28	0.06	0.30	0.01
	D (500-2000)	1.68	0.06	0.25	0.01
	E (2000-4000)	1.34	0.04	0.20	0.01
	F (4000-8000)	1.25	0.03	0.17	0.01
	G (8000-16000)	1.20	0.03	0.15	0.01
	H (>16000)	1.37	0.04	0.23	0.01
2	A (<125)	2.66	0.09	0.36	0.02
	B (125-250)	2.61	0.08	0.35	0.02
	C (250-500)	2.41	0.07	0.30	0.01
	D (500-2000)	1.86	0.06	0.28	0.01
	E (2000-4000)	1.35	0.04	0.21	0.01
	F (4000-8000)	1.25	0.04	0.21	0.01
	G (8000-16000)	1.25	0.04	0.18	0.01
	H (>16000)	1.30	0.04	0.22	0.01
3	A (<125)	2.25	0.13	0.42	0.04
	B (125-250)	2.04	0.13	0.38	0.04
	C (250-500)	1.88	0.12	0.39	0.03
	D (500-2000)	1.52	0.10	0.32	0.02
	E (2000-4000)	1.33	0.07	0.28	0.02
	F (4000-8000)	1.26	0.06	0.22	0.01
	G (8000-16000)	1.19	0.05	0.18	0.01
	H (>16000)	1.41	0.69	1.32	0.05
4	A (<125)	2.47	0.13	0.46	0.03
	B (125-250)	2.30	0.11	0.35	0.02
	C (250-500)	1.96	0.10	0.33	0.02
	D (500-2000)	1.62	0.07	0.25	0.02
	E (2000-4000)	1.43	0.06	0.26	0.02
	F (4000-8000)	1.31	0.06	0.23	0.01
	G (8000-16000)	1.30	0.07	0.22	0.02
	H (>16000)	1.29	0.06	0.13	0.01

The predicted values were compared with measured values showing a good correlation. Nevertheless, Lang (2001) suggested some further improvements to the model.

3.5.3 Mechanistic roughness model based on vehicle-pavement interaction

Saleh et al. (2000) developed a completely mechanistic model that uses vehicle dynamic analysis (COMPAS program) to estimate dynamic force profiles and finite element structural analysis (ABAQUS program) to estimate changes in road roughness for each load repetition by

calculating permanent deformation due materials-creep and plasticity at different wheel path locations.

This model takes into account that road roughness changes the magnitude of the vehicle dynamic forces applied on the pavement, and that vehicle dynamic forces change road roughness.

The model estimates roughness as a function of initial pavement roughness, pavement thickness, static axle load and number of load repetitions as shown in equation (3.10).

$$IRI = -1.415 + 2.923\sqrt{IRI_0} + 0.00129\sqrt{N} + 0.000113H - 5.485 \times 10^{-10} P^4 - 10^{-5} H\sqrt{N} + 5.777 \times 10^{-12} P^4 \sqrt{N} \quad (3.10)$$

where

- IRI = international roughness index (m/km)
- N = number of load repetitions
- P = axle load (kN)
- H = AC layer thickness (mm)
- IRI₀ = initial IRI value (m/km)

In the development of the model, a truck (three-axle tractor with a two-axle trailer) running at 100 km/h was used. It ran many times for the following variables:

- Axle load:s 67 and 80 kN;
- AC layer thicknesses: 100 and 150 mm;
- IRI values: 0.38 m/km (smooth) and 5.33 m/km (rough).

The material properties used in the model development are listed in Table 3.4.

Table 3.4 – Material properties used in the roughness model development (Saleh et al., 2000)

Material	Property	Value
AC	Modulus of elasticity	3450 MPa
	Poisson's ratio	0.3
	Initial yield stress	550 kPa
	Initial plastic strain	0
Granular base	Modulus of elasticity	550 MPa
	Poisson's ratio	0.35
	Initial yield stress	500 kPa
	Initial plastic strain	0
	Friction angle	45 degrees
Subgrade soil	Modulus of elasticity	100 MPa
	Poisson's ratio	0.4
	Initial yield stress	300 kPa
	Initial plastic strain	0
	Friction angle	30 degrees

The model does not depend on empirical observations. However, it uses theoretical assumptions that might not exactly match field constitutions as well as does not consider some factors that may affect pavement roughness, such as environmental effects, seasonal variations of material properties and specific modes of distress. Therefore, some adjustments are needed to account for these factors.

Saleh and Mamlouk (2002) present the calibration and verification of the mechanistic roughness model described above, for that 110 in-service pavement sections extracted from the LTPP database were used, 86 of which were used for calibration and the remainder ones were used for verification. The sections were taken from 4 different climatic zones (dry freeze, dry no-freeze, wet freeze and wet no-freeze). Calibration factors were determined for each climatic zone by minimizing the differences between the observed and the predicted roughness values at all ages.

The calibrated predicted roughness value of pavement section j at age i ($PV_{i,j}$) is given by equation (3.11).

$$PV_{i,j} = K \cdot f(X_{i,j}) \quad (3.11)$$

where

- K = calibration factor
- $f(X_{i,j})$ = uncalibrated predicted pavement roughness value obtained from equation (3.10)
- X = set of explanatory factors used in the development of the model (number of load repetitions, axle load, asphalt concrete layer thickness and initial IRI value)

Table 3.5 shows the calibration factors obtained for each climatic zone as well as a global calibration factor obtained from grouping all zones.

Table 3.5 – Calibration factors for various climatic zones (Saleh and Mamlouk, 2002)

Climatic zone	Dry freeze	Dry no-freeze	Wet freeze	Wet no-freeze	All zones
Calibration factor	0.745	0.757	0.712	0.689	0.730
Correlations of observed and predicted IRI values	0.913	0.865	0.855	0.889	0.879
Coefficient of determination (%)	83.2	74.7	73.0	79.0	77.2
Standard error	0.220	0.266	0.263	0.253	0.259

In order to verify the applicability of the model, a new set of 24 sections was used. The results showed a very good correlation between the predicted and observed roughness values.

3.5.4 MEPDG IRI prediction model

The development of the IRI prediction model was based on the general assumption that changes in roughness result from various distress types that must be predicted previously. Therefore, the IRI is predicted as a function of initial IRI, distresses that accumulate over time, and a site factor at the end of each analysis increment.

The general form of the model (AASHTO, 2008) is given by equation (3.12).

$$IRI = IRI_0 + 0.0150 \cdot (SF) + 0.400 \cdot (FC) + 0.0080 \cdot (TC) + 40.0 \cdot (RD_a) \quad (3.12)$$

where

- IRI = predicted IRI
- IRI_0 = initial IRI after construction
- SF = site factor (equation (3.13))

FC = area of fatigue cracking
TC = length of transverse cracking
RD_a = average rut depth

and

$$SF = \text{Age} \left[0.02003 \cdot (\text{PII} + 1) + 0.007947 \cdot (\text{Precip} + 1) + 0.000636 \cdot (\text{FI} + 1) \right] \quad (3.13)$$

where

Age = pavement age
PII = percent plasticity index of the soil
FI = average annual freezing index
Precip = average annual precipitation or rainfall

3.6 REFERENCES

AASHTO (2008). *Mechanistic-Empirical Pavement Design Guide - A Manual of Practice (Interim Edition)*. American Association for State Highway and Transportation Officials (AASHTO).

ARRB@ (2014). Walking Profiler G2. <http://www.arrb.com.au/Equipment-services/Walking-Profiler-G2.aspx>. Australian Road Research Board (ARRB). Access date: 30 January.

Cantisani, G. and Loprencipe, G. (2010). Road Roughness and Whole Body Vibration: Evaluation Tools and Comfort Limits. *Journal of Transportation Engineering*, 136, 818-826.

Capuruço, R., Hegazy, T., Tighe, S. and Zaghoul, S. (2005). Full-Car Roughness Index as Summary Roughness Statistic. *Transportation Research Record: Journal of the Transportation Research Board*, 1905, 148-156.

Cebon, D. (1999). *Handbook of Vehicle-Road Interaction*. Taylor & Francis.

Cebon, D. and Newland, D. E. (1983). Artificial Generation of a road Surface Topography by the Inverse FFT Method. *Vehicle System Dynamics*, 12, 160-165.

Chan, Y. T. (1995). *Wavelet basics*. Kluwer Academic Publishers.

Chang, J.-R., Su, Y.-S., Huang, T.-C., Kang, S.-C. and Hsieh, S.-H. (2009). Measurement of the International Roughness Index (IRI) Using an Autonomous Robot (P3-AT). *26th International Symposium on Automation and Robotics in Construction (ISARC)*, Austin, Texas, U.S.

Chatti, K. and Lee, D. (2002). Development of New Profile-Based Truck Dynamic Load Index. *Transportation Research Record: Journal of the Transportation Research Board*, 1806, 149-159.

Chiu, C.-T., Lee, M.-G. and Chen, D.-H. (2003). Study of the profile measuring using six different devices. *Symposium on Constructing Smooth Hot Mix Asphalt (HMA) Pavements*, Dallas, Texas, U.S.

- El-Korchi, T., Bacon, J., Turo, M. and Ecmecian, M. (2002). Ride Quality Assessment with Pavement Profiling Devices. *Transportation Research Record: Journal of the Transportation Research Board*, 1806, 140-148.
- Hall, K. and Muñoz, C. (1999). Estimation of Present Serviceability Index from International Roughness Index. *Transportation Research Record: Journal of the Transportation Research Board*, 1655, 93-99.
- ISO 8608 (1995). Mechanical vibration - Road surface profiles - Reporting of measured data. International Organization for Standardization (ISO).
- Karamihas, S. M. (2005). *Critical Profiler Accuracy Requirements*. University of Michigan - Transportation Research Institute (UMTRI). Final Report - UMTRI-2005-24.
- Karamihas, S. M., Gillespie, T. D., Kohn, S. D. and Perera, R. W. (1999). *Guidelines for Longitudinal Pavement Profile Measurement*. University of Michigan, Transportation Research Institute. Final Report prepared for National Cooperative Highway Research Program, Transportation Research Board, National Research Council - NCHRP Project 10-47.
- Kropác, O. and Múcka, P. (2005). Be careful when using the International Roughness Index as an indicator of road unevenness. *Journal of Sound and Vibration*, 287, 989-1003.
- Lang, J. M. (2001). Prediction Model in Swedish PMS. *5th International Conference on Managing Pavements*, Seattle, Washington, USA.
- MDOT (1996). Evaluating Pavement Surfaces: LISA and RQI. *Materials and Technology Research Record, No.79, published by Michigan Department of Transportation (MDOT), Materials and Technology Division*.
- Misiti, M., Misiti, Y., Oppenheim, G. and Poggi, J.-M. (2013). *Wavelet Toolbox for use with MATLAB (User's Guide) Version 1*. The MathWorks, Inc.
- Newland, D. E. (1993). *An introduction to Random Vibrations and Spectral Analysis*. Third Edition, Longman Scientific & Technical.
- Perera, R. and Kohn, S. (2004). Effects of Variation in Quarter-Car Simulation Speed on International Roughness Index Algorithm. *Transportation Research Record: Journal of the Transportation Research Board*, 1889, 144-151.
- Prem, H., Ramsay, E. and McLean, J. (2000a). A road profile based truck ride index (TRI). *6th International Symposium on Heavy Vehicle Weights and Dimensions*, Saskatoon, Saskatchewan, Canada, June 18 to 22.
- Prem, H., Ramsay, E. and McLean, J. (2000b). *A Road Profile Based Truck Ride Index (TRI)*. Austroads Incorporated. Sydney. Austroads Project No. BS.A.N.034 (N.BS.9704).
- ProVAL@ (2011). <http://www.roadprofile.com/>. Access date: 27 June 2011.
- Saleh, M. F. and Mamlouk, M. S. (2002). Calibration of a Pavement Roughness Model Based on Finite Element Simulation. *International Journal of Pavement Engineering*, 3, 227-238.
- Saleh, M. F., Mamlouk, M. S. and Owusu-Antwi, E. B. (2000). Mechanistic Roughness Model Based on Vehicle-Pavement Interaction. *Transportation Research Record*, 1699, 114-120.

Sayers, M. W. (1988). *Dynamic Terrain Inputs to Predict Structural Integrity of Ground Vehicles*. University of Michigan - Transportation Research Institute (UMTRI). Final Report - UMTRI-88-16.

Sayers, M. W. (1989). Two Quarter-Car Models for Defining Road Roughness: IRI and HRI. *Transportation Research Record: Journal of the Transportation Research Board*, 1215, 165-172.

Sayers, M. W. (1995). On the Calculation of International Roughness Index from Longitudinal Road Profile. *Transportation Research Record: Journal of the Transportation Research Board*, 1501, 1-12.

Sayers, M. W., Gillespie, T. D. and Paterson, W. D. O. (1986a). *Guidelines for Conducting and Calibrating Road Roughness Measurements*. World Bank Technical Paper Number 46, The World Bank, Washington, D.C., U.S.A.

Sayers, M. W., Gillespie, T. D. and Queiroz, C. A. V. (1986b). *The International Road Roughness Experiment (Establishing Correlation and a Calibration Standard for Measurements)*. World Bank Technical Paper Number Number 45, The World Bank, Washington, D.C., U.S.A.

Sayers, M. W. and Karamihas, S. M. (1996). *Interpretation of Road Roughness Profile Data*. University of Michigan - Transportation Research Institute (UMTRI). Final Report - UMTRI 96-19.

Sayers, M. W. and Karamihas, S. M. (1998). *The Little Book of Profiling: Basic Information about Measuring and Interpreting Road Profiles*. University of Michigan.

Scientific@, H. (2014). Pavement testing. http://www.hoskin.ca/catalog/index.php?main_page=product_info&products_id=1523. Access date: January 29.

Smith, K. L., Titus-Glover, L. and Evans, L. D. (2002). *Pavement Smoothness Index Relationships: Final Report*. U.S. Department of Transportation, Federal Highway Administration. FHWA-RD-02-057.

Song, I. and Teubert, C. (2007). Current California Profilograph Simulations and Comparisons. *2007 FAA Worldwide Airport Technology Transfer Conference*, Atlantic City, New Jersey, USA

TCPSC@ (2014). TheTranstec Center for Pavement Surface Characteristics - Pavement Surface Characteristics. <http://www.tcpsc.com/pavement-surface-characteristics/texture/>. Access date: January 17, 2014.

Wei, L. and Fwa, T. (2004). Characterizing Road Roughness by Wavelet Transform. *Transportation Research Record: Journal of the Transportation Research Board*, 1869, 152-158.

Yu, J., Chou, E. and Yau, J.-T. (2006). Development of Speed-Related Ride Quality Thresholds Using International Roughness Index. *Transportation Research Record: Journal of the Transportation Research Board*, 1974, 47-53.

4 BOUNDARY ELEMENT METHOD

4.1 INTRODUCTION

The Boundary Element Method (BEM) is a numerical technique based on integral equation formulation of continuous mechanic problems. There are two types of integral equation formulations. One contains, as basis unknowns, quantities with a clear physical meaning, in terms of which the known boundary conditions are given. This type is called the direct formulation. In the second type, indirect formulation, the basis unknown quantities have no physical meaning (Dominguez, 1993). This work only deals with the direct formulation, where the integral equation unknowns are displacement and traction values on the boundary.

The BEM has some clear advantages for the analysis of static and dynamic continuum mechanic problems. First of all, the problem is formulated on the boundary. Therefore, only the boundary has to be discretised as opposed to domain techniques, such as the Finite Element Method (FEM), which requires the discretization of the domain. As a consequence, the resulting system of equations is smaller in the BEM. Another consequence is that the mesh generation process, which only involves the surface, is simpler than in the domain techniques. This advantage is important in designs where the geometry changes throughout the solution process. A second characteristic of the BEM is that it produces highly accurate solutions on the boundary and in particular at any selected internal point. This feature makes the method very appropriate for problems where high accuracy is required (Dominguez, 1993).

Additionally, there is a difference between the BEM and the domain techniques that should be pointed out here because of its importance to the solution of certain dynamic problems. When dealing with infinite or semi-infinite regions, the domain techniques require a discretization that should be extend towards infinity. Obviously, the discretization has to be finished at a certain distance where an artificial boundary of some kind is located. These boundaries can be used without problems in statics. However, in dynamics, spurious reflections of waves which distort the solution of the problem take place at the artificial boundaries (Dominguez, 1993).

There is, however, a price to be paid for the above advantages. The final system of equations is non-symmetric and fully populated. The following disadvantages can also be mentioned: the use of the BEM depends on the previous knowledge of the fundamental solutions, and the BEM has difficulties in dealing with non-linear material properties. In the latter situation, the integral equations include domain integrals and the advantages of a boundary formulation vanish if extensive zones of non-linear materials exist. However, several researchers have been developed fundamental solutions and BEM methods for nonlinear problems, some of them even avoiding the domain discretization (Katsikadelis and Nerantzaki, 1999).

Beer and Watson (1992) refer to BEM and FEM as if they were not to compete with one another. Instead, they recognize the differences between them, pointing out the disadvantages as well as the advantages of each method, and do not attempt to ‘sell’ one method or the other. According to Beer and Watson, these methods complement each other since each of the methods is suited to particular problems, and for a given problem, one is generally more efficient than another. In some cases a combination of the two methods is required to analyse the problem efficiently. They summarize the suitability of each method. The FEM is more suitable for problems with a high ratio of boundary surface to volume, where boundary stresses are not of primary importance

and where the material is nonhomogeneous, behaves nonlinearly and/or contains joints and cracks. On the other hand, the BEM is more suitable for applications involving a low ratio of boundary surface to volume, a high accuracy of boundary stresses and homogeneous and linear elastic materials.

In this chapter, firstly, the BEM formulation is presented using a simpler procedure (based on the Betti's reciprocal theorem) than the one used in the Master thesis (Almeida, 2008) (based on weighted residual considerations). Secondly, a description of the BEM implementation is presented and afterwards it is validated for three-dimensional problems. In the Master thesis, only the two-dimensional BEM implementation was made and validated. Finally, the BEM application is referred for more complex problems, such as linear viscoelastic materials, fracture mechanics and elastodynamic problems.

4.2 BEM FORMULATION

4.2.1 Introduction

Different procedures have been adopted to formulate the BEM. All of them are dependent on the previous knowledge of the fundamental solutions. The procedure based on weighted residual considerations has the advantage to make the understanding of the differences between the BEM (boundary technique) and the domain techniques easier. It was the procedure adopted in the Master thesis, here a simpler one, based on the Betti's reciprocal theorem, will be outlined.

In this section, firstly the integral equation, also known as Somigliana's identity, is obtained from the Betti's reciprocal theorem. Secondly, the three-dimensional fundamental solutions for elastostatic problems are presented. Afterwards, the boundary of the problem is discretized and the procedure to calculate boundary unknowns (displacements and tractions) is described for problems with one region. Then, since an efficient evaluation of integrals is extremely important for BEM, due to the singularities of fundamental solutions, the integration topic is outlined. Finally, it is shown how to deal with multiple regions.

4.2.2 Betti's reciprocal theorem and integral equations

Consider an infinite domain with two types of 'loading', the load case number 1 corresponds to the case to solve, and the load case number 2 corresponds to the case where a unit load in the x-direction is applied at a point P (source point).

The theorem states that the work done by the load case 1 along the displacements of the load case 2 must be equal to the work done by the loads of the load case 2 along the displacements of the load case 1.

Assuming that there are no body forces acting in the domain, the theorem is given by equation (4.1).

$$\begin{aligned}
 u_x(P) = & \int_{\Gamma} \left[t_x(Q)U_{xx}(P,Q) + t_y(Q)U_{xy}(P,Q) + t_z(Q)U_{xz}(P,Q) \right] d\Gamma - \\
 & \int_{\Gamma} \left[u_x(Q)T_{xx}(P,Q) + u_y(Q)T_{xy}(P,Q) + u_z(Q)T_{xz}(P,Q) \right] d\Gamma
 \end{aligned} \tag{4.1}$$

where

- u_i = displacement in the i -direction (at point P or Q)
- t_i = traction in the i -direction (at point P or Q)
- $U_{ij}(P,Q)$ = displacement in the j -direction at point Q due to a unit point force acting in the i -direction at P
- $T_{ij}(P,Q)$ = traction in the j -direction at point Q due to a unit point force acting in the i -direction at P

Two similar integral equations can be obtained by applying a unit load in both y -direction and z -direction.

The three equations can be written in matrix notation, resulting in equation (4.2).

$$\{u(P)\} = \int_{\Gamma} [U(P,Q)] \{t(Q)\} d\Gamma - \int_{\Gamma} [T(P,Q)] \{u(Q)\} d\Gamma \quad (4.2)$$

The integral equation (4.2), also known as Somigliana's identity, is valid for any point P. Taking P on the boundary, the boundary integral equation (4.3) is obtained.

$$[C(P)] \{u(P)\} = \int_{\Gamma} [U(P,Q)] \{t(Q)\} d\Gamma - \int_{\Gamma} [T(P,Q)] \{u(Q)\} d\Gamma \quad (4.3)$$

Where the coefficients of the free term $[C(P)]$ can be determined by using the concept of rigid body motion.

4.2.3 Fundamental solutions

The fundamental solutions satisfy the governing differential equations. Merely the three-dimensional fundamental solutions are exposed.

The solution for the displacement in the j -direction at point Q due to a unit point force acting in the i -direction at point P is given by equation (4.4).

$$U_{ij}(P,Q) = \frac{1}{16\pi G(1-\nu)r} \left[(3-4\nu)\delta_{ij} + r_i r_j \right] \quad (4.4)$$

The solution for the boundary stress (traction) acting on a surface with outward normal direction $\{n\}$ is also needed. It is obtained from the displacement solution and is given by equation (4.5).

$$T_{ij}(P,Q) = -\frac{1}{8\pi(1-\nu)r^2} \left[\frac{\partial r}{\partial n} \left[(1-2\nu)\delta_{ij} + 3r_i r_j \right] + (1-2\nu)(n_i r_j - n_j r_i) \right] \quad (4.5)$$

where

- G = modulus of elasticity in shear: $G = E / [2(1+\nu)]$
- ν = Poisson's ratio
- E = Young's modulus

r = distance between source point P and field point Q
 δ_{ij} = Kronecker delta (=1 if $i=j$; =0 if $i \neq j$)
 n_i = i-component of the outward normal vector

$$r_{,i} = \frac{\partial r}{\partial x_i} = \frac{r_i}{r}$$

$$\frac{\partial r}{\partial n} = n_x r_x + n_y r_y + n_z r_z$$

The fundamental solutions tends to infinity as the distance between P and Q tends to zero. This fact will cause some problems in the integrations of the fundamental solutions.

4.2.4 Numerical implementation

In order to obtain a numerical solution of equation (4.3), the boundary of the problem is divided into elements. Consequently, integrals over a complex domain Γ are replaced by a sum of integrals over simple sub-domains Γ_e - equation (4.6). Each sub-domain corresponds to a boundary element.

$$[C(P)]\{u(P)\} = \sum_{e=1}^{NE} \left(\int_{\Gamma_e} [U(P, Q)]\{t(Q)\} d\Gamma \right) - \sum_{e=1}^{NE} \left(\int_{\Gamma_e} [T(P, Q)]\{u(Q)\} d\Gamma \right) \quad (4.6)$$

where NE is the number of elements of the problem.

For three-dimensional problems, two-dimensional boundary elements are used. For each element, a local coordinate system (ξ_1, ξ_2) is defined.

As the boundary is discretised using isoparametric elements the same interpolation is used for the geometry of the problem and for the variation of the physical quantities (displacements and tractions) – equations (4.7).

$$\{x(\xi_1, \xi_2)\} = \sum_{n=1}^{NNE} N_n(\xi_1, \xi_2) \{x_n^e\}$$

$$\{u(\xi_1, \xi_2)\} = \sum_{n=1}^{NNE} N_n(\xi_1, \xi_2) \{u_n^e\} \quad (4.7)$$

$$\{t(\xi_1, \xi_2)\} = \sum_{n=1}^{NNE} N_n(\xi_1, \xi_2) \{t_n^e\}$$

where

NNE = number of nodes per element
 N_n = shape function of the n-th node
 $\{x\}$ = vector of coordinates of a point with intrinsic coordinates (ξ_1, ξ_2)
 $\{u\}$ = vector of displacements of a point with intrinsic coordinates (ξ_1, ξ_2)
 $\{t\}$ = vector of tractions of a point with intrinsic coordinates (ξ_1, ξ_2)
 $\{x_n^e\}$ = vector of coordinates of the n-th node- of the element e
 $\{u_n^e\}$ = vector of displacements of the n-th node of the element e

$\{t_n^e\}$ = vector of tractions of the n-th node of the element e

It is necessary to specify a discrete number of nodes on the boundary. This number defines the type of interpolation: constant, linear or quadratic. For instance, a quadratic Serendipity element is shown in Figure 4.1 and the local coordinates of nodes are defined in Table 4.1.

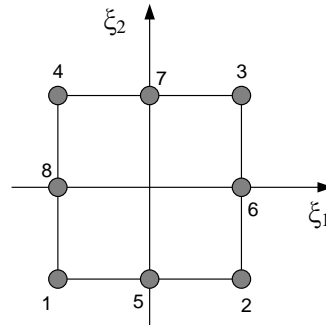


Figure 4.1 – Quadratic Serendipity element

Table 4.1 – Intrinsic coordinates of nodes

Node	ξ_1	ξ_2
1	-1	-1
2	1	-1
3	1	1
4	-1	1
5	0	-1
6	1	0
7	0	1
8	-1	0

The shape functions take the value of one at the n-th node and zero at all other nodes. For the element shown in Figure 4.1 and defined in Table 4.1, the shape functions are expressed by equations (4.8) to (4.15).

$$N_1 = \frac{1}{4}(1-\xi_1)(1-\xi_2)(-\xi_1 - \xi_2 - 1) \quad (4.8)$$

$$N_2 = \frac{1}{4}(1+\xi_1)(1-\xi_2)(\xi_1 - \xi_2 - 1) \quad (4.9)$$

$$N_3 = \frac{1}{4}(1+\xi_1)(1+\xi_2)(\xi_1 + \xi_2 - 1) \quad (4.10)$$

$$N_4 = \frac{1}{4}(1-\xi_1)(1+\xi_2)(-\xi_1 + \xi_2 - 1) \quad (4.11)$$

$$N_5 = \frac{1}{2}(1-\xi_1^2)(1-\xi_2) \quad (4.12)$$

$$N_6 = \frac{1}{2}(1-\xi_2^2)(1+\xi_1) \quad (4.13)$$

$$N_7 = \frac{1}{2}(1 - \xi_1^2)(1 + \xi_2) \quad (4.14)$$

$$N_8 = \frac{1}{2}(1 - \xi_2^2)(1 - \xi_1) \quad (4.15)$$

Substituting equations (4.7) for displacement and traction into equation (4.6), a discretization of the integral equation is obtained. Since $\{u_n^e\}$ and $\{t_n^e\}$ (nodal values) are constant with respect to the integration, they can be taken out of the integral and equation (4.6) can be rewritten as equation (4.16).

$$[C(P)]\{u(P)\} = \sum_{e=1}^{NE} \sum_{n=1}^{NNE} \{t_n^e\} \left(\int_{\Gamma_e} N_n(\xi_1, \xi_2) [U(P; \xi_1, \xi_2)] d\Gamma(\xi_1, \xi_2) \right) - \sum_{e=1}^{NE} \sum_{n=1}^{NNE} \{u_n^e\} \left(\int_{\Gamma_e} N_n(\xi_1, \xi_2) [T(P; \xi_1, \xi_2)] d\Gamma(\xi_1, \xi_2) \right) \quad (4.16)$$

The integration was changed to a sum of integrations of the product of fundamental solutions with shape functions. The integration will be analysed later in further detail.

Betti's reciprocal theorem is valid for any point P, therefore the equation (4.16) can be written for an infinite number of points P. Since the displacements and the tractions must be known on the boundary, there will be as many unknowns as the degrees-of-freedom (DOF) of the nodes. For that reason, the necessary number of equations is obtained taking P at all the nodes of the mesh (points P_i) – equation (4.17).

$$[C(P_i)]\{u(P_i)\} = \sum_{e=1}^{NE} \sum_{n=1}^{NNE} \{t_n^e\} \left(\int_{\Gamma_e} N_n(\xi_1, \xi_2) [U(P_i; \xi_1, \xi_2)] d\Gamma(\xi_1, \xi_2) \right) - \sum_{e=1}^{NE} \sum_{n=1}^{NNE} \{u_j^e\} \left(\int_{\Gamma_e} N_n(\xi_1, \xi_2) [T(P_i; \xi_1, \xi_2)] d\Gamma(\xi_1, \xi_2) \right) \quad i=1,2,3, \dots, \text{DOF-nodes} \quad (4.17)$$

Equation (4.17) can be rewritten as equation (4.18).

$$[C(P_i)]\{u(P_i)\} = \sum_{e=1}^{NE} \sum_{n=1}^{NNE} [\Delta U_{ni}^e] \{t_n^e\} - \sum_{e=1}^{NE} \sum_{n=1}^{NNE} [\Delta T_{ni}^e] \{u_n^e\} \quad (4.18)$$

where

$$[\Delta U_{ni}^e] = \int_{\Gamma_e} N_n(\xi_1, \xi_2) [U(P_i; \xi_1, \xi_2)] d\Gamma(\xi_1, \xi_2) \quad (4.19)$$

$$[\Delta T_{ni}^e] = \int_{\Gamma_e} N_n(\xi_1, \xi_2) [T(P_i; \xi_1, \xi_2)] d\Gamma(\xi_1, \xi_2)$$

For the solution of the system of equations it is convenient to replace the double sums by a matrix multiplication, resulting the system of equations (4.20) from (4.18).

$$[H]\{u\} = [G]\{t\} \quad (4.20)$$

The coefficients of the free term $[C(P_i)]$ appear in the diagonal of the matrix $[H]$. As aforementioned, these coefficients can be explicitly determined using the concept of rigid body motion. Since for a pure rigid body translation of an elastic domain there must be no change in shape of the body, the tractions applied must be zero – equation (4.21).

$$[H]\{u\} = \{0\} \quad (4.21)$$

Consequently, the diagonal terms of the matrix $[H]$ are calculated by equation (4.22).

$$h_{ii} = -\sum_{j=1}^{\text{DOF}} h_{ij} \quad (\text{for } i \neq j) \quad (4.22)$$

Once determined the diagonal of the matrix $[H]$ and introduced the boundary conditions, the system of equations (4.21) can be rearranged in order to obtain the system (4.23).

$$[X]\{x\} = \{f\} \quad (4.23)$$

where $\{x\}$ contains all the unknowns (displacements and tractions) of the problem.

4.2.5 Postprocessing

So far only the displacements and tractions values at the nodes of the boundary elements are known. However, there are other results which are of interest like stresses and strains at the boundary and at points inside the domain. These results are computed from the boundary values without approximations.

Evaluation of stresses and strains at the boundary

The most popular technique for these evaluations is the so-called traction recovery method (Gao and Davies, 2002). This method determines the tangential strains (from the displacements) at the point of interest and then, using the Hooke's law and the known tractions, determines the stresses. After that, the strains are evaluated from the determined stresses.

A local Cartesian coordinate system (x'_i) is introduced, where x'_1 and x'_2 are tangential to surface and x'_3 is directed in the normal direction. The directions of this coordinate system are defined by the vectors $\{v'_1\}$, $\{v'_2\}$ and $\{v'_3\}$ (see expressions (4.24) to (4.29)), where $\{v'_1\}$ is in the ξ_1 direction and $\{v'_3\}$ is in the normal direction.

$$\{V'_1\} = \{V_{\xi_1}\} = \frac{\partial \{x\}}{\partial \xi_1} \quad (4.24)$$

$$\{v'_1\} = \frac{1}{J_{\xi_1}} \{V'_1\} \quad (4.25)$$

$$\{V_{\xi_2}\} = \frac{\partial \{x\}}{\partial \xi_2} \quad (4.26)$$

$$\{v_{\xi_2}\} = \frac{1}{J_{\xi_2}} \{V_{\xi_2}\} \quad (4.27)$$

$$\{v_3\} = \{v_1\} * \{v_{\xi_2}\} \quad (4.28)$$

$$\{v_2\} = \{v_3\} * \{v_1\} \quad (4.29)$$

where $J_{\xi_1} = \|\{V_{\xi_1}\}\|$ and $J_{\xi_2} = \|\{V_{\xi_2}\}\|$

The relationships between x_1' , x_2' and ξ_1 , ξ_2 are given in equations (4.30).

$$x_1' = J_{\xi_1} \xi_1 + J_{\xi_2} \xi_2 \cos \theta \quad (4.30)$$

$$x_2' = J_{\xi_2} \xi_2 \sin \theta$$

Solving equations (4.30) in order to ξ_1 and ξ_2 and taking the derivatives, equations (4.31) are obtained.

$$\frac{\partial \xi_1}{\partial x_1'} = \frac{1}{J_{\xi_1}} \quad ; \quad \frac{\partial \xi_1}{\partial x_2'} = -\frac{\cos \theta}{J_{\xi_1} \sin \theta} \quad ; \quad \frac{\partial \xi_2}{\partial x_1'} = 0 \quad ; \quad \frac{\partial \xi_2}{\partial x_2'} = \frac{1}{J_{\xi_2} \sin \theta} \quad (4.31)$$

where

$$\cos \theta = \{v_1\} \cdot \{v_{\xi_2}\} \quad (4.32)$$

$$\sin \theta = \{v_{\xi_2}\} \cdot \{v_2\} \quad (4.33)$$

The strains in the local Cartesian coordinate system are given by equations (4.34) to (4.36).

$$\varepsilon_{11}' = \frac{\partial u_1'}{\partial x_1'} = \frac{\partial u_1'}{\partial \xi_1} \frac{\partial \xi_1}{\partial x_1'} + \frac{\partial u_1'}{\partial \xi_2} \frac{\partial \xi_2}{\partial x_1'} = \frac{\partial u_1'}{\partial \xi_1} \frac{\partial \xi_1}{\partial x_1'} \quad (4.34)$$

$$\varepsilon_{22}' = \frac{\partial u_2'}{\partial x_2'} = \frac{\partial u_2'}{\partial \xi_1} \frac{\partial \xi_1}{\partial x_2'} + \frac{\partial u_2'}{\partial \xi_2} \frac{\partial \xi_2}{\partial x_2'} = \frac{\partial u_2'}{\partial \xi_1} \frac{\partial \xi_1}{\partial x_2'} + \frac{\partial u_2'}{\partial \xi_2} \frac{\partial \xi_2}{\partial x_2'} \quad (4.35)$$

$$\begin{aligned} \varepsilon_{12}' &= \frac{1}{2} \left(\frac{\partial u_1'}{\partial x_2'} + \frac{\partial u_2'}{\partial x_1'} \right) = \frac{1}{2} \left(\frac{\partial u_1'}{\partial \xi_1} \frac{\partial \xi_1}{\partial x_2'} + \frac{\partial u_1'}{\partial \xi_2} \frac{\partial \xi_2}{\partial x_2'} + \frac{\partial u_2'}{\partial \xi_1} \frac{\partial \xi_1}{\partial x_1'} + \frac{\partial u_2'}{\partial \xi_2} \frac{\partial \xi_2}{\partial x_1'} \right) \\ &= \frac{1}{2} \left(\frac{\partial u_1'}{\partial \xi_1} \frac{\partial \xi_1}{\partial x_2'} + \frac{\partial u_1'}{\partial \xi_2} \frac{\partial \xi_2}{\partial x_2'} + \frac{\partial u_2'}{\partial \xi_1} \frac{\partial \xi_1}{\partial x_1'} \right) \end{aligned} \quad (4.36)$$

where

$$\frac{\partial \mathbf{u}'_1}{\partial \xi_1} = \frac{\partial \{\mathbf{u}\}}{\partial \xi_1} \cdot \{\mathbf{v}'_1\}; \quad \frac{\partial \mathbf{u}'_1}{\partial \xi_2} = \frac{\partial \{\mathbf{u}\}}{\partial \xi_2} \cdot \{\mathbf{v}'_1\}; \quad \frac{\partial \mathbf{u}'_2}{\partial \xi_1} = \frac{\partial \{\mathbf{u}\}}{\partial \xi_1} \cdot \{\mathbf{v}'_2\}; \quad \frac{\partial \mathbf{u}'_2}{\partial \xi_2} = \frac{\partial \{\mathbf{u}\}}{\partial \xi_2} \cdot \{\mathbf{v}'_2\} \quad (4.37)$$

and

$$\frac{\partial \{\mathbf{u}\}}{\partial \xi_1} = \sum_n \frac{\partial N_n}{\partial \xi_1} \{\mathbf{u}_n^e\} \quad ; \quad \frac{\partial \{\mathbf{u}\}}{\partial \xi_2} = \sum_n \frac{\partial N_n}{\partial \xi_2} \{\mathbf{u}_n^e\} \quad (4.38)$$

Using (4.34), (4.35), (4.36) and equilibrium conditions with boundary tractions (\mathbf{t}'_1 , \mathbf{t}'_2 and \mathbf{t}'_3), the stresses in the local Cartesian coordinate system are given by equations (4.39) to (4.44).

$$\sigma'_{11} = \frac{E}{1-\nu^2} (\varepsilon'_{11} + \nu \varepsilon'_{22}) + \frac{\nu}{1-\nu} \sigma'_{33} \quad (4.39)$$

$$\sigma'_{22} = \frac{E}{1-\nu^2} (\varepsilon'_{22} + \nu \varepsilon'_{11}) + \frac{\nu}{1-\nu} \sigma'_{33} \quad (4.40)$$

$$\sigma'_{33} = \mathbf{t}'_3 = \{\mathbf{t}\} \cdot \{\mathbf{v}'_3\} \quad (4.41)$$

$$\sigma'_{12} = 2G\varepsilon'_{12} \quad (4.42)$$

$$\sigma'_{23} = \mathbf{t}'_2 = \mathbf{t} \cdot \mathbf{v}'_2 \quad (4.43)$$

$$\sigma'_{13} = \mathbf{t}'_1 = \{\mathbf{t}\} \cdot \{\mathbf{v}'_1\} \quad (4.44)$$

Then the stresses are transformed into the global Cartesian coordinate system as shown in equation (4.45).

$$\sigma_{ij} = v'_{ki} v'_{nj} \sigma'_{kn} \quad (4.45)$$

where

$$\mathbf{v}' = \begin{bmatrix} v'_1(1) & v'_1(2) & v'_1(3) \\ v'_2(1) & v'_2(2) & v'_2(3) \\ v'_3(1) & v'_3(2) & v'_3(3) \end{bmatrix} \quad (4.46)$$

Evaluation of stresses and strains at internal points

The integral equation (4.2) is valid for any point P, taking point P inside the domain (point P_a), equation (4.2) is rewritten, resulting in equation (4.47).

$$\{\mathbf{u}(P_a)\} = \int_{\Gamma} [U(P_a, Q)] \{\mathbf{t}(Q)\} d\Gamma - \int_{\Gamma} [T(P_a, Q)] \{\mathbf{u}(Q)\} d\Gamma \quad (4.47)$$

The strains are determined by derivation of the displacement solution, equation (4.48), where the coefficients of $[\bar{S}]$ and $[\bar{R}]$ can be determined by the expressions (4.49) and (4.50), respectively.

$$\{\varepsilon(P_a)\} = \int_{\Gamma} [\bar{S}(P_a, Q)] \{t(Q)\} d\Gamma - \int_{\Gamma} [\bar{R}(P_a, Q)] \{u(Q)\} d\Gamma \quad (4.48)$$

$$\bar{S}_{ijk}(P, Q) = \frac{1}{16\pi G(1-\nu)r^2} \left[(1-2\nu)(r_j \delta_{ik} + r_i \delta_{jk}) - r_{,k} \delta_{ij} + 3r_{,i} r_{,j} r_{,k} \right] \quad (4.49)$$

$$\bar{R}_{ijk}(P, Q) = \frac{1}{8\pi(1-\nu)r^3} \left\{ \begin{aligned} & 3 \frac{\partial r}{\partial n} \left[\nu(r_j \delta_{ik} + r_i \delta_{jk}) + r_{,k} \delta_{ij} - 5r_{,i} r_{,j} r_{,k} \right] \\ & + (1-2\nu)(n_j \delta_{ik} - n_k \delta_{ij} + n_i \delta_{jk} + 3r_{,i} r_{,j} n_k) \\ & + 3\nu(n_j r_{,i} r_{,k} + n_i r_{,j} r_{,k}) \end{aligned} \right\} \quad (4.50)$$

The stresses are computed using the Hooke's law by equation (4.51).

$$\{\sigma(P_a)\} = \int_{\Gamma} [S(P_a, Q)] \{t(Q)\} d\Gamma - \int_{\Gamma} [R(P_a, Q)] \{u(Q)\} d\Gamma \quad (4.51)$$

where the coefficients of $[S]$ and $[R]$ can be determined by the expressions (4.52) and (4.53), respectively.

$$S_{ijk}(P, Q) = \frac{1}{8\pi(1-\nu)r^2} \left[(1-2\nu)(\delta_{ik} r_{,j} + \delta_{jk} r_{,i} - \delta_{ij} r_{,k}) + 3r_{,i} r_{,j} r_{,k} \right] \quad (4.52)$$

$$R_{ijk}(P, Q) = \frac{G}{4\pi(1-\nu)r^3} \left\{ \begin{aligned} & 3 \frac{\partial r}{\partial n} \left[(1-2\nu)r_{,k} \delta_{ij} + \nu(r_j \delta_{ik} + r_i \delta_{jk}) - 5r_{,i} r_{,j} r_{,k} \right] \\ & + (1-2\nu)(n_j \delta_{ik} + n_i \delta_{jk} + 3r_{,i} r_{,j} n_k) - (1-4\nu)n_k \delta_{ij} \\ & + 3\nu(n_j r_{,i} r_{,k} + n_i r_{,j} r_{,k}) \end{aligned} \right\} \quad (4.53)$$

All the integrals can be numerically evaluated using Gauss quadrature.

4.2.6 Integration

Due to singularities of fundamental solutions, an accurate and efficient evaluation of integrals is extremely important to BEM.

The integrands in equations (4.19) are products of fundamental solutions and shape functions. Depending on the relative position of the source points P to the boundary element over which the integration has to be carried out, three types of integrals can be identified:

- *Regular integrals*: these are integrals where the element to be integrated is far away from the source point P. The numerical evaluation of these integrals is made using Gauss quadrature.
- *Nearby-singular integrals*: these are integrals where the source point P is close to the element to be integrated but not located on it. The integral is still regular and Gauss quadrature can be used. However, an accurate and efficient integration is only possible by using special techniques such as the element subdivision technique in combination with a corresponding integration criterion.
- *Singular integrals*: these are integrals where the source point P lies on the element to be integrated and consequently the integrand becomes singular. In this case, different solutions are adopted which depend on the type of fundamental solution. These integrals can be classified according to their order of singularity and the dimension of the problem into weakly, strongly and hipersingular integrals (Table 4.2).

Table 4.2 – Singular integrals classification (adapted from Thöni (2009))

Type of singularity	Fundamental solution	Order of singularity (three-dimensional)
Weakly singular	U	1/r
Strongly singular	T, S	1/r ²
Hipersingular	R	1/r ³

Since accurate pavement responses near the boundary are important, what depends on the way integrals are evaluated, a description of the techniques used in each type of integrals is done.

Regular integrals

As already mentioned, the numerical evaluation of these integrals does not pose any difficulties. They can be evaluated by Gauss quadrature through abscissas and weights (Pina, 1995). This implies a coordinate transformation which maps element Cartesian coordinates (x, y, z) into local intrinsic coordinates (ξ_1, ξ_2). The intrinsic coordinates have values between -1 and +1.

Therefore, the integrals (4.19) can be rewritten, resulting the in integrals (4.54).

$$\begin{aligned}
 [\Delta U_{ni}^c] &= \int_{-1}^1 \int_{-1}^1 N_n(\xi_1, \xi_2) [U(P_i; \xi_1, \xi_2)] J(\xi_1, \xi_2) d\xi_1 d\xi_2 \\
 &\approx \sum_{p1=1}^{PG1} \sum_{p2=1}^{PG2} N_n(\xi_{1(p1)}, \xi_{2(p2)}) [U(P_i; \xi_{1(p1)}, \xi_{2(p2)})] J(\xi_{1(p1)}, \xi_{2(p2)}) W_{p1} W_{p2} \\
 [\Delta T_{ni}^c] &= \int_{-1}^1 \int_{-1}^1 N_n(\xi_1, \xi_2) [T(P_i; \xi_1, \xi_2)] J(\xi_1, \xi_2) d\xi_1 d\xi_2 \\
 &\approx \sum_{p1=1}^{PG1} \sum_{p2=1}^{PG2} N_n(\xi_{1(p1)}, \xi_{2(p2)}) [T(P_i; \xi_{1(p1)}, \xi_{2(p2)})] J(\xi_{1(p1)}, \xi_{2(p2)}) W_{p1} W_{p2}
 \end{aligned} \tag{4.54}$$

where

- J = Jacobian of the transformation
- PG1 = number of Gauss points in ξ_1 -direction
- PG2 = number of Gauss points in ξ_2 -direction

$$\begin{aligned} W_{p1} &= \text{weight related to the abscissa } \xi_1(p1) \\ W_{p2} &= \text{weight related to the abscissa } \xi_2(p2) \end{aligned}$$

The calculation of these integrals takes the most of the computer time needed to form the final set of equations, hence the integration should be made as economical as possible. To ensure the reliability of the final results, all integrals should be calculated with a certain, user predefined, accuracy (Bialecki et al., 1993).

Therefore, it is essential to choose an appropriate number of Gauss points. This number is usually obtained from integration criterions. In general, these integration criterions involve increasing the number of integration points as the minimum distance between the source point P and the element decreases.

The necessity of controlling the accuracy of the quadrature used in BEM has been recognized at the early stage of BEM development by Watson and co-workers (cited in Bialecki et al. (1993)). Lachat and Watson (1976) published the first integration criterion enabling to keep the integration error at a constant level (cited in Beer and Watson (1992)). However, as their criterion is based on the error estimation for the Gauss integration given by Stroud and Secrest, the use of this criterion is rather difficult (Eberwien et al., 2005) and time-consuming (Bu and Davies, 1995). Afterwards, Jun et al. (1985) simplified the criterion of Lachat and Watson illustrating the results in an easy-to-use table format. The table relates directly the ratio R/L (where R denotes the distance between the source point P and the element and L the element length) with the Gauss order required to satisfy an integration error of less than 10^{-3} . The tables were derived for integrands of the form $1/r^i$ (cited in Eberwien et al. (2005)). Bu and Davies (1995) introduced another integration criterion in which the integration error was again estimated for integrands of type $1/r^i$. They obtained a contour line with a fixed integration error (10^{-3}). The maximum distance of the contour line to the element gives the minimum ratio R/L.

Nevertheless, since the integrals consist of the product of three parts (the fundamental solution, the shape function and the Jacobian), Eberwien et al. (2005) carried out a numerical study which not only examines the integrands $1/r$ and $1/r^2$ but considers also the influence of the shape functions and the Jacobian. They investigated integrals denoted as I_{ni} (where n is the index of the shape function and i is the exponent of the distance r). The integrals were computed for a close grid of points surrounding the elements. The integration was performed numerically with a Gauss order of 25 (numerical approximation of the exact solution). The interpretation of the results was carried out in analogy to Bu and Davies, i.e. they obtained a contour line of a fixed integration error (10^{-3}) for each integral I_{ni} and Gauss order. Once more, the maximum distance of the contour line to the element gives the minimum ratio R/L. Eberwien et al. (2005) concluded that their criterion provides a significant improvement when compared with the criterion of Bu and Davies and with the criterion of Jun et al.

For instance, Figure 4.2 shows the contour lines of the integrands I_{11} , I_{21} and I_{31} . The maximum distance of the contour line to the element permits to draw the envelope. For all points on or inside the envelope, the accuracy of integration is assured.

The integration criterion of Eberwien et al. (2005) does not consider the singularity order $1/r^3$ that appears in three-dimensional problems (postprocessing) and considers only an integration error of 10^{-3} . Thöni (2009) developed an integration criterion, similar to the one developed by Eberwien et al. (2005), for the singularity order $1/r^3$ and allowing an error of integration of 10^{-3} and 10^{-4} . It is pointed out that the results obtained for the singularity order $1/r^2$ by Eberwien et al. and by Thöni differ.

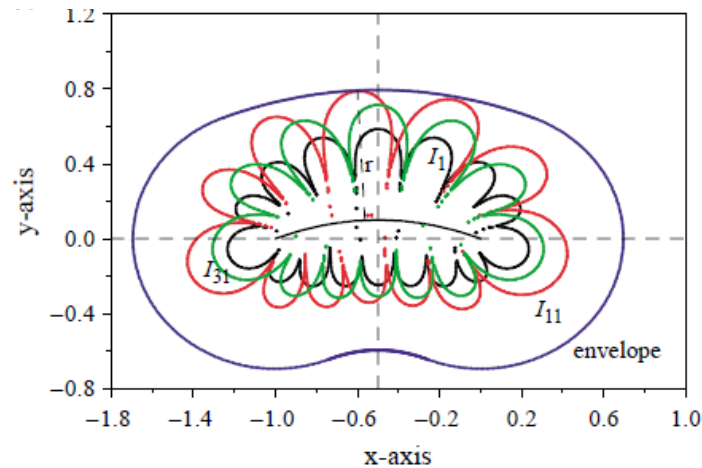


Figure 4.2 – Contour lines of an integration error of 10^{-3} and Gauss order of 4 (Eberwien et al., 2005)

Nearby-Singular Integrals

Integrals are said to be nearly-singular when the source point is very close to the element to be integrated but not located on it. Thus the integral is still regular.

It is possible to decrease the ratio R/L increasing the number of gauss points. However, the numerical integration becomes very time-consuming due to a high polynomial degree that is needed for a good approximation, especially when point moves ever more close to the element to be integrated. If a constant number of Gauss points are used, the integration error gets bigger and bigger.

Experience has shown that the minimum number of integration points should not be lower than 3 and it is more efficient to keep the maximum integration order law (Beer et al., 2008). Hence, the region of integration is subdivided so that the minimum ratio R/L is respected.

Table 4.3 shows the results for an integration error of 10^{-3} and for an element with a ratio f/L^* equal to 0.1 (where f denotes the arc rise and L^* the base length of the element) (Beer et al., 2008).

Table 4.3 – Number of Gauss points (Beer et al., 2008)

Number of Gauss points	R/L-ratio		
	$O(1/r)$	$O(1/r^2)$	$O(1/r^3)$
3	1.4025	2.3187	3.4170
4	0.6736	0.9709	1.2908

In order to use a lower integration order, the element subdivision technique is currently used. This technique was introduced by Lachat and Watson (1976) (cited in Thöni (2009)).

This work uses a recursive subdivision technique in combination with an integration criterion. This means that, first the element is subdivided for any ratio R/L higher than the values given from the integration criterion. Then, the subdivision is repeated until the criterion is fulfilled for all the subelements.

Initially the BEM was implemented using the ratios R/L shown in Table 4.3. However, the results obtained were not good enough for source points extremely close to the element to be

integrated. Since points extremely close to the boundary are crucial for pavement design, an integration criterion was developed, similar to the one developed by Eberwien et al. (2005). It takes into account integration errors lower than 10^{-3} and 10^{-4} . This new criterion was developed for a straight element (ratio f/L^* equal to 0). Table 4.4 shows the obtained results.

Table 4.4 – Number of Gauss points for different integration errors

Integration error	Number of Gauss points	R/L-ratio		
		O (1/r)	O (1/r ²)	O (1/r ³)
10 ⁻³	3	1.0800	1.8022	2.5938
	4	0.5800	0.7803	1.1715
10 ⁻⁴	3	2.0819	3.4521	5.2705
	4	0.9100	1.2632	1.7807
10 ⁻⁵	3	4.5604	6.9116	9.1626
	4	1.3900	2.0109	2.7127
10 ⁻⁶	3	8.0402	12.1201	16.0130
	4	2.0715	3.1219	4.6128
10 ⁻⁷	3	13.4904	20.2706	26.7424
	4	3.3112	5.3409	6.7812

Singular Integrals

Integrals are said to be singulars when the source point lies on the element to be integrated. The distance R is equal to zero and special integration techniques should be used to solve the singular boundary integral. The techniques vary according to the order of singularity and the dimension of the problem to be integrated. Only two-dimensional elements are considered.

For the singular boundary integrals with the displacement fundamental solution (order of singularity O(1/r)) two situations can occur:

- (1) The source point P is a node of the element but not the node n, in this situation the fundamental solution tends to infinity but the shape function tends to zero, so the product of fundamental solution and shape function may be determined using the Gauss quadrature;
- (2) The source point P is the node n of the element, in this situation a technique that splits the element into triangular subelements, described by Beer et al. (2008), is used.

For the singular boundary integrals with the traction fundamental solution (order of singularity O(1/r²)) the same two situations can occur:

- (1) The source point P is a node of the element but not the node n, in this situation the technique that splits the element into triangular subelements is also used;
- (2) The source point P is the node n of the element, in this situation the integral is evaluated indirectly by applying a traction free rigid body motion (equation (4.22)).

Figure 4.3 and Figure 4.4 show the splitting of the elements into triangular elements. For each subelement a local coordinate system is chosen in such a way that the Jacobian of the transformation approaches zero at the source point P. Gauss quadrature is then applied over two or three subelements depending if P is a corner or mid-side node. For more detailed information, see Beer et al. (2008).

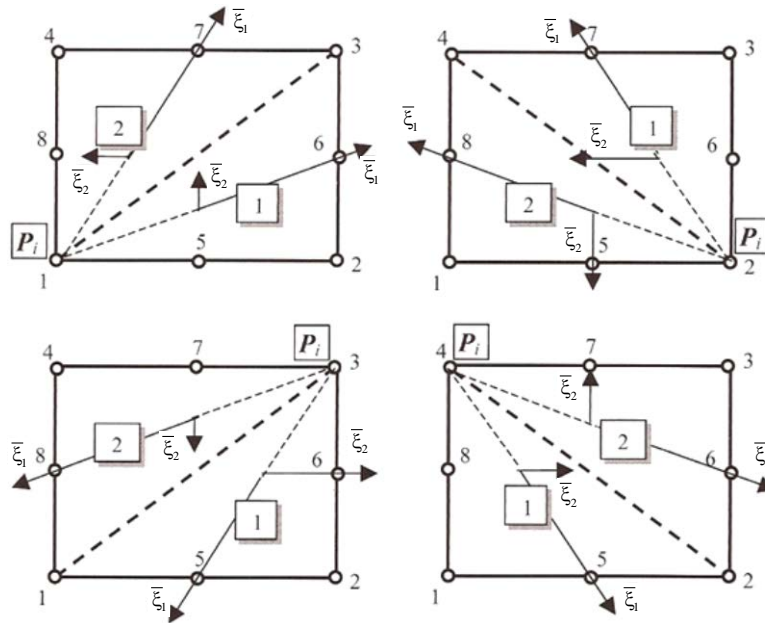


Figure 4.3 – Subelements for numerical integration when P_i is a corner node of the element (adapted from Beer et al. (2008))

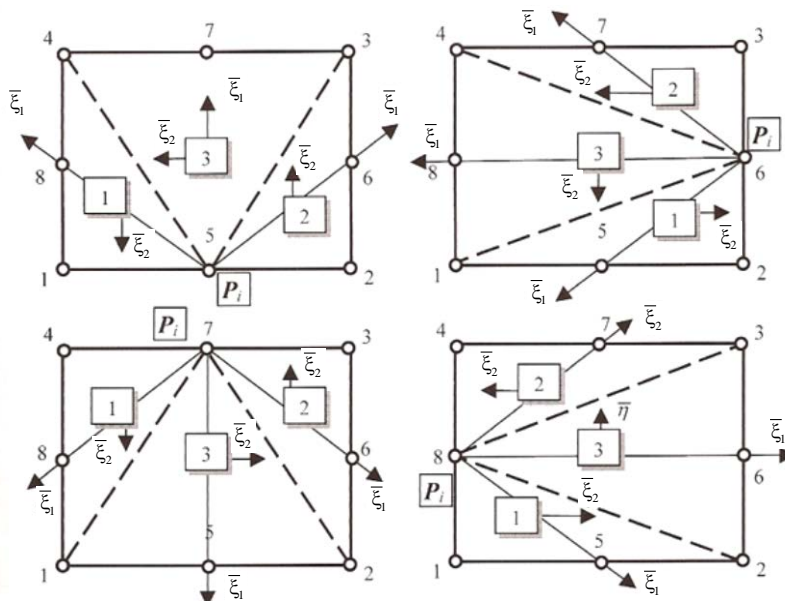


Figure 4.4 - Subelements for numerical integration when P_i is a mid-side node of the element (adapted from Beer et al. (2008))

4.2.7 Multiple regions

The description follows the reference Beer et al. (2008).

The formulation described so far is only applicable to homogeneous domains (only one region). Since the pavement structure has some layers with different properties, a new methodology is needed which is based on the fundamental solutions (4.4) and (4.5). The basic idea is to consider a number of regions equal to the number of pavement layers. Each region is treated as previously stated and has its own material properties.

As both the displacements and the tractions are not known at the interfaces between regions, there are more unknowns and consequently additional equations are required to solve the problem. These equations can be obtained from the equations of equilibrium and compatibility at the interfaces.

There are two approaches which can be taken in the implementation of the method. In the first, the assembly procedure is modified so that a larger system of equations is obtained including the additional unknowns at the interfaces. The second method is similar to the approach taken by the FEM where a ‘stiffness matrix’ of each region is constructed, the matrix coefficients are tractions due to unit displacements. The matrices for all regions are then assembled similarly to the FEM.

The second method is more efficient and may be used for coupling BEM with FEM, therefore it is the implemented one.

The problem in analysis is partially coupled, i.e. only some of the nodes of one region are connected to other regions. In this case, it is more efficient to consider only the interface nodes in the calculation of the stiffness matrix. The methodology starts by solving the problem with zero displacement values at the interface nodes and then it solves the problem where unit displacement values are applied at each interface node. The first nodes to be numbered in each region should be the interface ones.

Thereby, first the equation system (4.23) with zero displacement values at the interface nodes, system (4.55), is solved for each region.

$$[A^R] \begin{pmatrix} \{t_{int(u_{int}=0)}^R\} \\ \{u, t_{free(u_{int}=0)}^R\} \end{pmatrix} = \{f_{(u_{int}=0)}^R\} \quad (4.55)$$

Then, the system (4.56) with unit displacement value in each DOF of interface is solved for each region.

$$[A^R] \begin{pmatrix} \{t_{int(u_{int}=1)_d}^R\} \\ \{u, t_{free(u_{int}=1)_d}^R\} \end{pmatrix} = \{f_{(u_{int}=1)_d}^R\} \quad d=1, 2, 3, \dots \text{DOF of interface} \quad (4.56)$$

Once solved the systems (4.55) and (4.56), the matrices $[K]$, expression (4.57), and $[B]$, expression (4.58), of each region are constructed.

$$[K^R] = \left[\left\{ t_{int(u_{int}=1)_{d=1}} \right\} \quad \dots \quad \left\{ t_{int(u_{int}=1)_{d=DOF \text{ of interface}}} \right\} \right] \quad (4.57)$$

$$[B^R] = \left[\left\{ u, t_{free(u_{int}=1)_{d=1}} \right\} \quad \dots \quad \left\{ u, t_{free(u_{int}=1)_{d=DOF \text{ of interface}}} \right\} \right] \quad (4.58)$$

After all the region stiffness matrices $[K^R]$ have been computed, they are assembled in the equation system (4.59) which can be solved for the unknown $\{u_{int}\}$.

$$[K] \{u_{int}\} = \{f\} \quad (4.59)$$

After the interface unknown have been determined, the tractions values at the interface and both the displacement values and the tractions values at the free nodes are determined for each region by solving the system (4.60).

$$\begin{pmatrix} \{t_{int}^R\} \\ \{u, t_{free}^R\} \end{pmatrix} = \begin{pmatrix} \{t_{int(u_{int}=0)}^R\} \\ \{u, t_{free(u_{int}=0)}^R\} \end{pmatrix} + \begin{pmatrix} [K^R] \\ [B^R] \end{pmatrix} \{u_{int}^R\} \quad (4.60)$$

4.3 BEM IMPLEMENTATION

The BEM was implemented using the Microsoft® Visual Basic® 2010 Express. The created application (called BEM-Application) requires an input file and generates an output file. The GID® software (GID@, 2011), developed by the International Center For Numerical Methods In Engineering (CIMNE), is used as pre and post-processor. It generates the input file from the definition of the geometry and the mesh and by assigning the material properties. In addition, it permits the visualization of the results in the output file. Figure 4.5 shows the interaction between the BEM-Application and the GID® software.

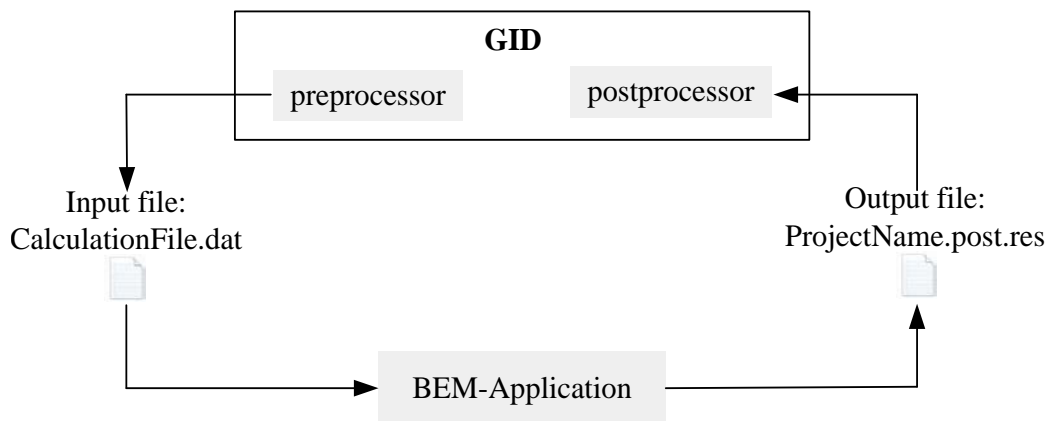


Figure 4.5 – Interaction between the BEM-Application and the GID® software

In order to create a suitable input file for the BEM-Application, a GID problem type (called ‘BEM_applications’) was created (Figure 4.6). It predefines all the information required by the user and defines the way the data is written in the input file. The BEM-Application generates the output file with the information blocks required by the GID.

Figure 4.7 presents the three modelled layers (or regions), the Asphalt Concrete (AC) layer, the granular layer and the subgrade. As can be seen from this figure, only the top boundary of the subgrade layer is modelled (semi-infinite region).

To completely illustrate the process identified on Figure 4.5, Figure 4.8 and Figure 4.9 present the input file structure and the output file structure, respectively.

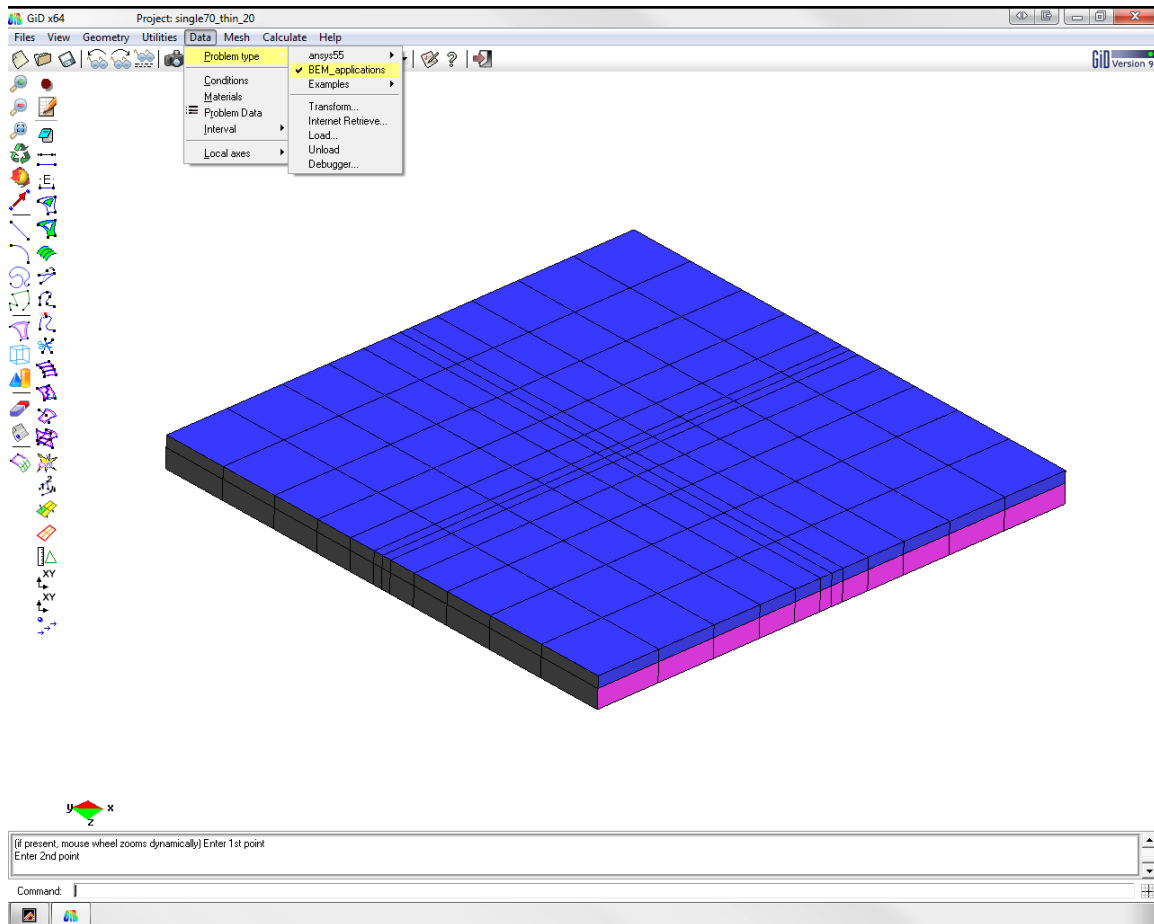


Figure 4.6 - GiD problem type: BEM_applications

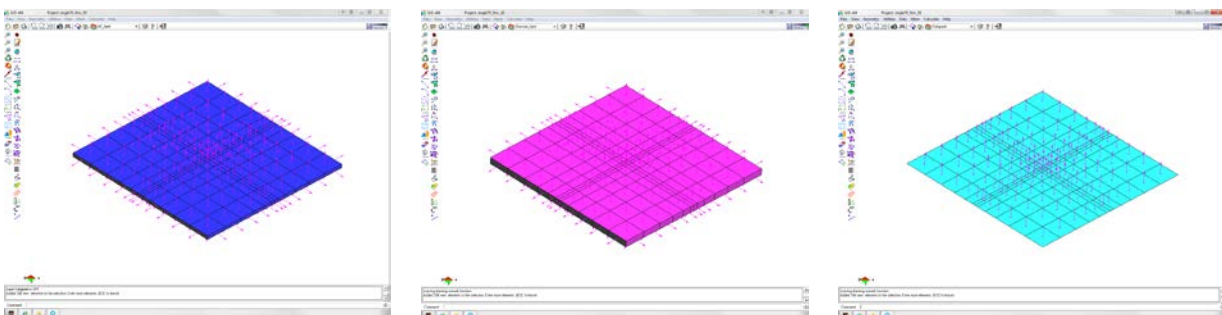


Figure 4.7 – The three regions/layers: AC layer, granular layer and subgrade

```

-----
                                Title
-----
Title: single70_thin_20
-----
Dimension of the problem [Dimension N°Nodes N°Elements N°NodesPerElement N°Regions]
3 1539 816 8 3
-----
Type of Problem [1: 2D_PlaneStrain; 2: 2D_PlaneStress; 3: 3D]
3
-----
Properties of the materials
-----
5606 0.35
200 0.30
100 0.35
-----
Type of Regions [1: Finite; 2: Semi-Infinite; 3: Infinite]
1
1
2
    
```

```

-----
Coordinates of the nodes [Node X Y Z]
-----
1 -2.61640e+00 -2.61640e+00 3.20000e-01
2 -2.61640e+00 -2.61640e+00 2.20000e-01
3 -2.61640e+00 -2.61640e+00 1.20000e-01
4 -2.61640e+00 -2.61640e+00 6.00000e-02
5 -2.61640e+00 -2.61640e+00 0.00000e+00
6 -2.61640e+00 -2.27678e+00 3.20000e-01
7 -2.27316e+00 -2.61640e+00 3.20000e-01
8 -2.61640e+00 -2.27678e+00 1.20000e-01
9 -2.27316e+00 -2.61640e+00 1.20000e-01
...
1534 2.61640e+00 2.27678e+00 0.00000e+00
1535 2.61640e+00 2.61640e+00 3.20000e-01
1536 2.61640e+00 2.61640e+00 2.20000e-01
1537 2.61640e+00 2.61640e+00 1.20000e-01
1538 2.61640e+00 2.61640e+00 6.00000e-02
1539 2.61640e+00 2.61640e+00 0.00000e+00
-----
Number of Elements per Region
-----
336
336
144
-----
Incidences of the elements [Element Incidences Material]
-----
1 1364 1393 1195 1171 1376 1312 1180 1276 1
2 1326 1364 1171 1116 1349 1276 1143 1213 1
3 1288 1326 1116 1064 1306 1213 1094 1168 1
4 1248 1288 1064 1023 1260 1168 1037 1127 1
5 1220 1248 1023 999 1229 1127 1008 1110 1
6 1171 1195 1040 981 1180 1123 1019 1088 1
7 1116 1171 981 933 1143 1088 957 1027 1
8 1064 1116 933 860 1094 1027 891 960 1
9 1023 1064 860 809 1037 960 832 918 1
10 999 1023 809 778 1008 918 787 894 1
...
814 970 819 872 1028 901 848 950 1003 3
815 1156 970 1028 1181 1076 1003 1114 1175 3
816 1350 1156 1181 1384 1261 1175 1307 1366 3
-----
Boundary Conditions -- Dirichlet BC (displacements prescribed)
-----
-- Point-Displacement (number of Nodes)
0
-- Line-Displacement (number of Elements)
0
-- Surface-Displacement (number of Elements)
0
-- Point-Displacement (List of Nodes and values)
-- Line-Displacement (List of Elements and values)
-- Surface-Displacement (List of Elements and values)
-----
Boundary Conditions -- Neuman BC (tractions prescribed)
-----
-- Point-Load (number of Nodes)
0
-- Line-Load (number of Elements)
0
-- Surface-Load (number of Elements)
4
-- Point-Load(List of Nodes and values)
-- Line-Load (List of Elements and values)
-- Surface-Load (List of Elements and values)
71 0 0 700
72 0 0 700
73 0 0 700
74 0 0 700

```

Figure 4.8 – Input file: CalculationFile.dat

```

Project: single70_thin_20
Cartesian_dimension: 3
Elasticity Problem
Quadratic Elements
Number of Nodes of System: 1539
Number of Elements of System: 816
Region 1
Finite Region
No symmetry
Youngsmodulus: 3576.0000
Poissons ratio: 0.34999999
List of Boundary Elements:
1 2 3 4 5 6 ... 333 334 335 336
Region 2
Finite Region

```

```

No symmetry
Youngsmodulus: 200.00000
Poissons ratio: 0.30000001
List of Boundary Elements:
  337  338  339  340  341  342  ...  669  670  671  672
Region      3
Infinite Region
No symmetry
Youngsmodulus: 100.00000
Poissons ratio: 0.349999999
List of Boundary Elements:
  673  674  675  676  677  678  ...  813  814  815  816
Node 1 Coor -2.62 -2.62 0.32
Node 2 Coor -2.62 -2.62 0.22
...
Node 1532 Coor 2.62 2.28 0.12
Node 1533 Coor 2.27 2.62 0.00
Node 1534 Coor 2.62 2.28 0.00
Node 1535 Coor 2.62 2.62 0.32
Node 1536 Coor 2.62 2.62 0.22
Node 1537 Coor 2.62 2.62 0.12
Node 1538 Coor 2.62 2.62 0.06
Node 1539 Coor 2.62 2.62 0.00

Incidences:
EL 1 Inci 1364 1393 1195 1171 1376 1312 1180 1276
EL 2 Inci 1326 1364 1171 1116 1349 1276 1143 1213
EL 3 Inci 1288 1326 1116 1064 1306 1213 1094 1168
EL 4 Inci 1248 1288 1064 1023 1260 1168 1037 1127
EL 5 Inci 1220 1248 1023 999 1229 1127 1008 1110
EL 6 Inci 1171 1195 1040 981 1180 1123 1019 1088
...
EL 815 Inci 1156 970 1028 1181 1076 1003 1114 1175
EL 816 Inci 1350 1156 1181 1384 1261 1175 1307 1366

POST-PROCESSED RESULTS
-----

Results at Boundary Elements:

Stress Vector (kPa): 2D-{StressXX, StressYY, StressZZ, StressXY}
                    3D-{StressXX, StressYY, StressZZ, StressXY, StressYZ, StressXZ}
Strain Vector (---): 2D-{StrainXX, StrainYY, StrainZZ, StrainXY}
                    3D-{StrainXX, StrainYY, StrainZZ, StrainXY, StrainYZ, StrainXZ}

Element: 1
Region: 1
xsi= -1.00 eta= -1.00
Stress: -0.488377E+01 0.770133E+00 0.000000E+00 -0.151553E+00 0.000000E+00
0.000000E+00
Strain: -0.144108E-02 0.693359E-03 0.402621E-03 -0.114428E-03 0.000000E+00
0.000000E+00
xsi= 1.00 eta= -1.00
Stress: -0.416670E+01 -0.167263E+00 0.000000E+00 -0.309815E+00 0.000000E+00
0.000000E+00
Strain: -0.114881E-02 0.361041E-03 0.424186E-03 -0.233921E-03 0.000000E+00
0.000000E+00
xsi= 1.00 eta= 1.00
Stress: -0.646086E+01 0.486085E+01 0.000000E+00 -0.800927E+00 0.000000E+00
0.000000E+00
Strain: -0.228248E-02 0.199165E-02 0.156600E-03 -0.604727E-03 0.000000E+00
0.000000E+00
xsi= -1.00 eta= 1.00
Stress: -0.562767E+01 0.324189E+01 0.000000E+00 -0.153781E+01 0.000000E+00
0.000000E+00
Strain: -0.189103E-02 0.145737E-02 0.233508E-03 -0.116110E-02 0.000000E+00
0.000000E+00
xsi= 0.00 eta= -1.00
Stress: -0.449775E+01 0.379970E+00 0.000000E+00 -0.278302E+00 0.000000E+00
0.000000E+00
Strain: -0.129495E-02 0.546472E-03 0.403027E-03 -0.210127E-03 0.000000E+00
0.000000E+00
xsi= 1.00 eta= 0.00
Stress: -0.493908E+01 0.247802E+01 0.000000E+00 -0.214329E+00 0.000000E+00
0.000000E+00
Strain: -0.162371E-02 0.117637E-02 0.240875E-03 -0.161826E-03 0.000000E+00
0.000000E+00
xsi= 0.00 eta= 1.00
Stress: -0.601677E+01 0.412990E+01 0.000000E+00 -0.121699E+01 0.000000E+00
0.000000E+00
Strain: -0.208676E-02 0.174378E-02 0.184677E-03 -0.918866E-03 0.000000E+00
0.000000E+00
xsi= -1.00 eta= 0.00
Stress: -0.488104E+01 0.213719E+01 0.000000E+00 -0.503652E+00 0.000000E+00
0.000000E+00
Strain: -0.157412E-02 0.107538E-02 0.268554E-03 -0.380274E-03 0.000000E+00
0.000000E+00
Element: 2

```

```

Region:      1
xsi= -1.00 eta= -1.00
Stress:     -0.329121E+01    0.114868E+01    0.000000E+00    -0.738941E+00    0.000000E+00
0.000000E+00
Strain:     -0.103279E-02    0.643346E-03    0.209700E-03    -0.557926E-03    0.000000E+00
0.000000E+00
xsi=  1.00 eta= -1.00
Stress:     -0.412069E+01    0.103721E+01    0.000000E+00    -0.521624E+00    0.000000E+00
0.000000E+00
Strain:     -0.125384E-02    0.693359E-03    0.301795E-03    -0.393843E-03    0.000000E+00
0.000000E+00
xsi=  1.00 eta=  1.00
Stress:     -0.500892E+01    0.345845E+01    0.000000E+00    -0.212847E+01    0.000000E+00
0.000000E+00
Strain:     -0.173920E-02    0.145737E-02    0.151752E-03    -0.160707E-02    0.000000E+00
0.000000E+00
xsi= -1.00 eta=  1.00
Stress:     -0.307413E+01    0.213086E+01    0.000000E+00    -0.263426E+01    0.000000E+00
0.000000E+00
Strain:     -0.106821E-02    0.896757E-03    0.923222E-04    -0.198895E-02    0.000000E+00
0.000000E+00
xsi=  0.00 eta= -1.00
Stress:     -0.372095E+01    0.105008E+01    0.000000E+00    -0.674155E+00    0.000000E+00
0.000000E+00
Strain:     -0.114331E-02    0.657833E-03    0.261411E-03    -0.509010E-03    0.000000E+00
0.000000E+00
xsi=  1.00 eta=  0.00
Stress:     -0.425281E+01    0.235706E+01    0.000000E+00    -0.118152E+01    0.000000E+00
0.000000E+00
Strain:     -0.141996E-02    0.107538E-02    0.185546E-03    -0.892090E-03    0.000000E+00
0.000000E+00
xsi=  0.00 eta=  1.00
Stress:     -0.405652E+01    0.275179E+01    0.000000E+00    -0.242524E+01    0.000000E+00
0.000000E+00
Strain:     -0.140370E-02    0.116655E-02    0.127700E-03    -0.183113E-02    0.000000E+00
0.000000E+00
xsi= -1.00 eta=  0.00
Stress:     -0.287069E+01    0.174898E+01    0.000000E+00    -0.154308E+01    0.000000E+00
0.000000E+00
Strain:     -0.973946E-03    0.770055E-03    0.109787E-03    -0.116508E-02    0.000000E+00
0.000000E+00
...
Element:    816
Region:     3
xsi= -1.00 eta= -1.00
Stress:     -0.242940E+00    -0.451287E-01    -0.855991E-01    0.268552E-01    0.741676E-01    -
0.411839E+00
Strain:     -0.197186E-02    0.698601E-03    0.152251E-03    0.725091E-03    0.200253E-02    -0.111197E-
01
xsi=  1.00 eta= -1.00
Stress:     -0.504983E+00    -0.232112E-01    -0.135914E+00    0.130433E+00    0.108570E+00    -
0.252535E+00
Strain:     -0.449289E-02    0.201103E-02    0.489539E-03    0.352170E-02    0.293139E-02    -0.681844E-
02
xsi=  1.00 eta=  1.00
Stress:     -0.553725E+00    0.139093E-01    -0.179080E+00    0.589274E-01    0.276078E-01    -
0.267055E+00
Strain:     -0.495915E-02    0.270391E-02    0.985555E-04    0.159104E-02    0.745411E-03    -0.721049E-
02
xsi= -1.00 eta=  1.00
Stress:     -0.285185E+00    -0.550936E-01    -0.111960E+00    0.166531E-01    0.205895E-01    -
0.439301E+00
Strain:     -0.226716E-02    0.839070E-03    0.713743E-04    0.449633E-03    0.555917E-03    -0.118611E-
01
xsi=  0.00 eta= -1.00
Stress:     -0.372286E+00    -0.535106E-01    -0.866297E-01    0.767227E-01    0.578925E-01    -
0.175994E+00
Strain:     -0.323237E-02    0.107110E-02    0.623993E-03    0.207151E-02    0.156310E-02    -0.475184E-
02
xsi=  1.00 eta=  0.00
Stress:     -0.535228E+00    -0.777803E-02    -0.160557E+00    0.957338E-01    0.714049E-01    -
0.259149E+00
Strain:     -0.476311E-02    0.235747E-02    0.294952E-03    0.258481E-02    0.192793E-02    -0.699702E-
02
xsi=  0.00 eta=  1.00
Stress:     -0.410779E+00    -0.329322E-01    -0.108392E+00    0.358686E-01    0.811526E-02    -
0.183884E+00
Strain:     -0.361316E-02    0.148778E-02    0.469069E-03    0.968451E-03    0.219112E-03    -0.496487E-
02
xsi= -1.00 eta=  0.00
Stress:     -0.272847E+00    -0.561488E-01    -0.107245E+00    0.228075E-01    0.500011E-01    -
0.416318E+00
Strain:     -0.215660E-02    0.768835E-03    0.790368E-04    0.615802E-03    0.135003E-02    -0.112406E-
01
Internal Results:
Displacement Vector (mm): 2D-{ux, uy}
                          3D-{ux, uy, uz}

```

Stress Vector (kPa): 2D-{StressXX, StressYY, StressZZ, StressXY}
 3D-{StressXX, StressYY, StressZZ, StressXY, StressYZ, StressXZ}
 Strain Vector (---): 2D-{StrainXX, StrainYY, StrainZZ, StrainXY}
 3D-{StrainXX, StrainYY, StrainZZ, StrainXY, StrainYZ, StrainXZ}

Coordinates - Displacement Components - Stress Components - Strain Components

Figure 4.9 – Output file: ProjectName.post.res

Once again, with the objective to illustrate, Figure 4.10, Figure 4.11 and Figure 4.12 present the post-processing with the GID[®] software, i.e., the results in the output file for Z-displacements, YY-Strains, ZZ-Strains, respectively.

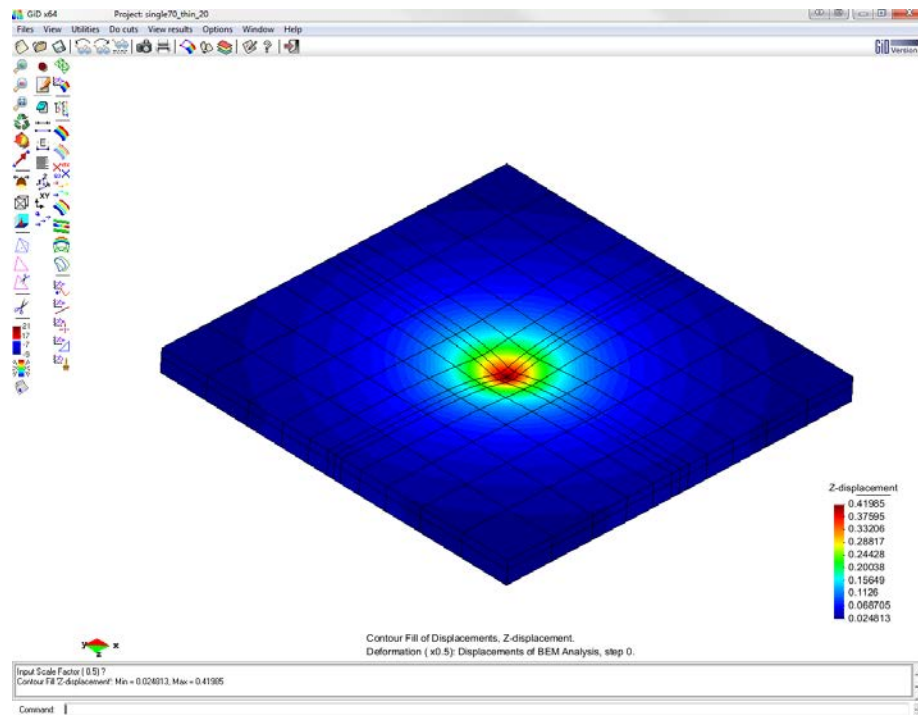


Figure 4.10 – Post-processing with the GID[®] software: Z-displacements

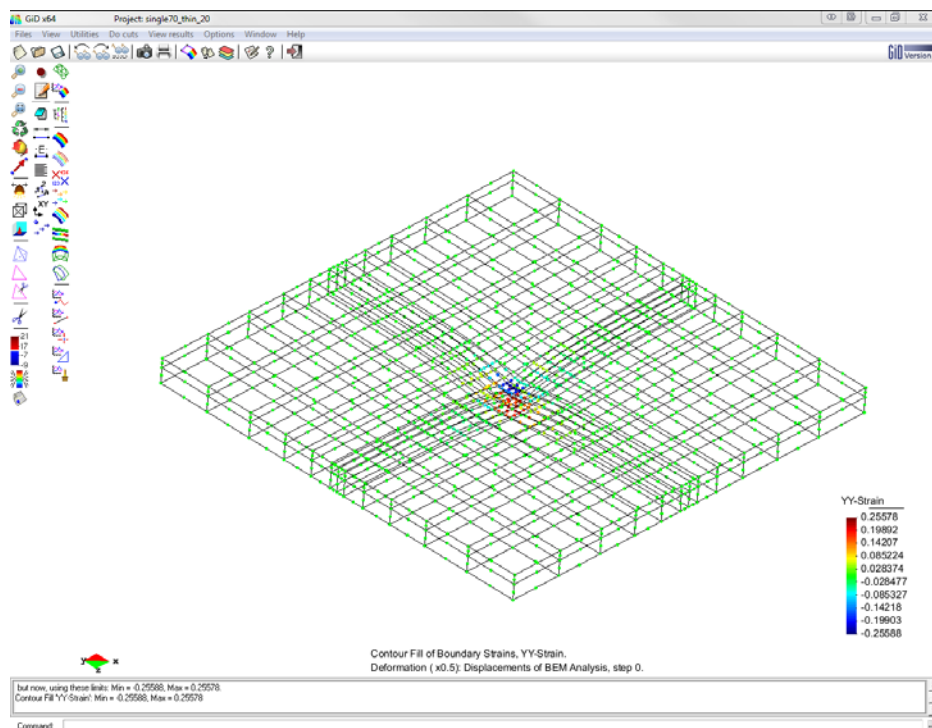


Figure 4.11 - Post-processing with the GID[®] software: YY-Strain

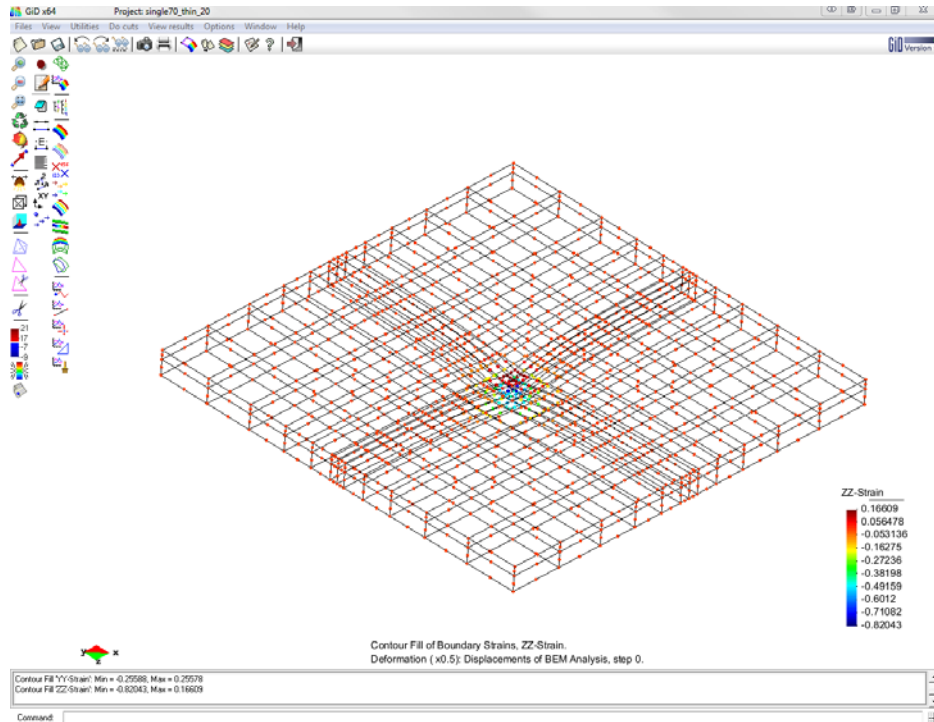


Figure 4.12 - Post-processing with the GID® software: ZZ-Strain

In relation to the Master thesis (Almeida, 2008), the three-dimensional BEM was implemented as well as some improvements in terms of integration were made (mentioned in the previous section). In addition, improvements were made in terms of data pre- and post-processing by a better use of the GID® software as seen in this section.

4.4 VALIDATION OF THE THREE-DIMENSIONAL BEM IMPLEMENTATION

In the Master thesis only the implementation and validation of the two-dimensional BEM was made (Almeida, 2008). Consequently, the three-dimensional BEM implementation ought to be validated. For that, the pavement structures used in the Master thesis were considered. Figure 4.13 shows the pavement structures and Table 4.5 presents the properties of the materials.

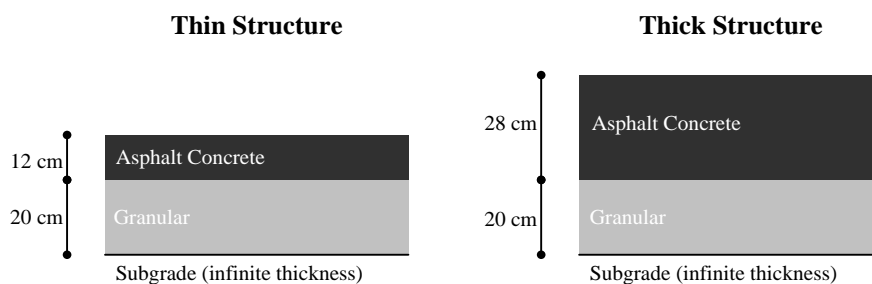


Figure 4.13 – Pavement structures

Table 4.5 – Properties of the materials

Layer	Modulus (MPa)	Poisson's ratio
Asphalt Concrete	4658	0.35
Granular	200	0.30
Subgrade	100	0.35

In terms of load applied on the pavement surface and tyre-pavement contact area, the ones defined in the Master thesis were also used, i.e., a vertical load equal to 42 kN and a contact area equal to 425.6 cm². On the basis of this definition was the following data for the tyre 385/65R22.5: contact area equal to 425.6 cm² and ratio width:length equal to 1:0.85.

The validation consists in comparing the BEM results from the BEM-Application with the results of the stress-strain computation software from the Shell pavement design method, called BISAR[®] (Shell, 1988), which has an analytical formulation. Therefore, a circular contact area is considered, whose radius is defined to have the same vertical stress as the used in the Master thesis (987 kPa).

Figure 4.14 and Figure 4.15 compare the results from both the BEM-Application and the BISAR[®] for the thin structure and the thick structure, respectively.

The results show an excellent agreement between the two applications, validating hence the three-dimensional BEM implementation. As stated in the BEM formulation (postprocessing), the internal points are computed from the boundary values without approximations, resulting an exact representation of the strains curves from BISAR[®] even near the boundaries. The exact representation near the boundaries was achieved by the integration improvements implemented. In order to have this representation with FEM a very close mesh will be essential.

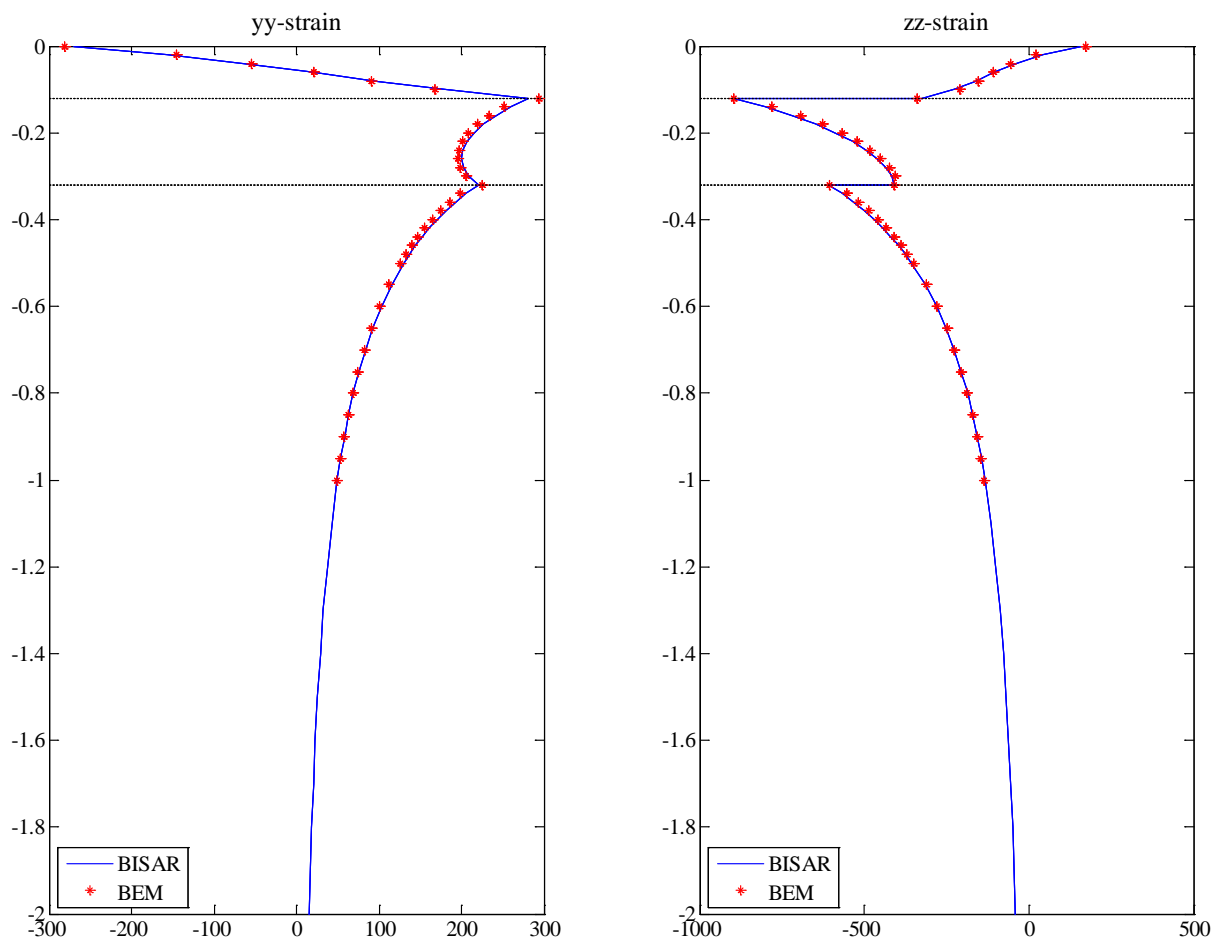


Figure 4.14 – Comparison between the BEM-Application and the BISAR[®] for the thin structure

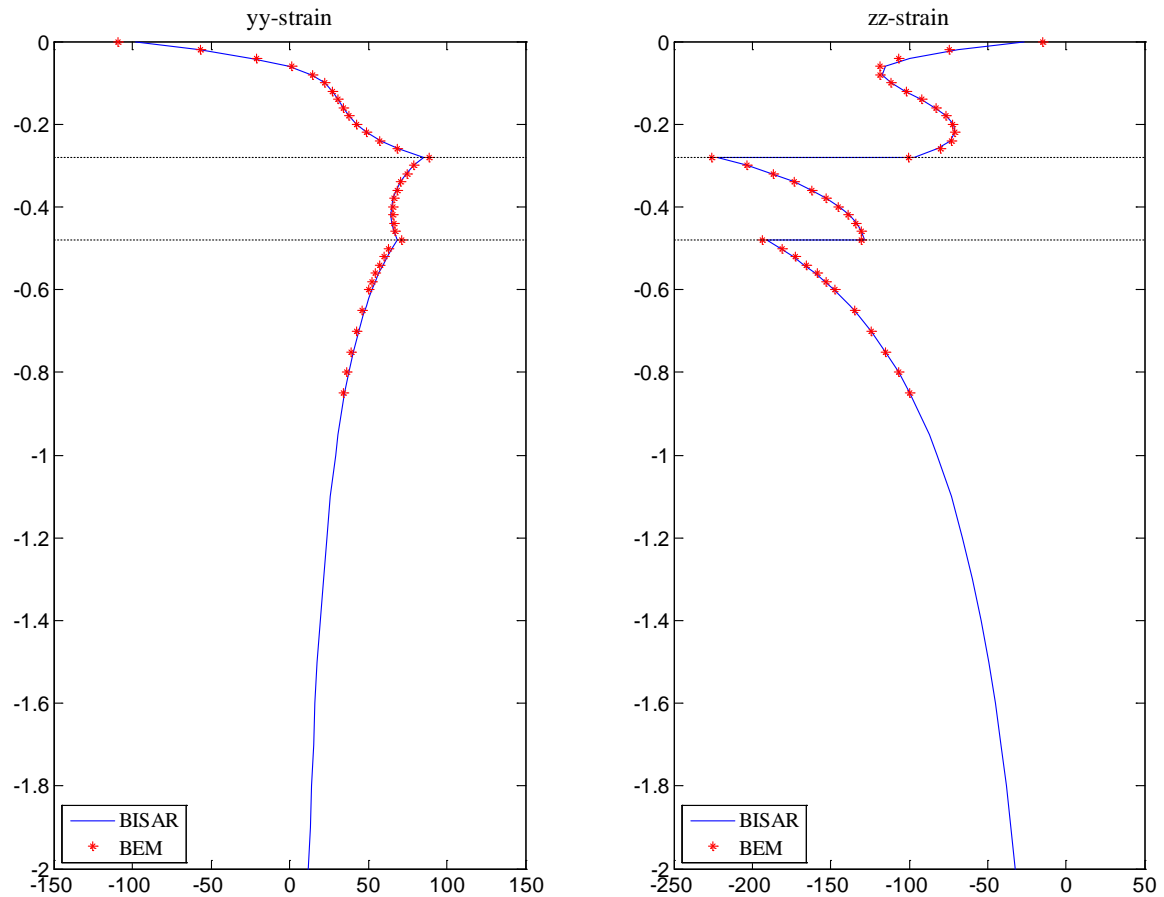


Figure 4.15 – Comparison between the BEM-Application and the BISAR® for the thick structure

4.5 OTHER BEM APPLICATIONS

4.5.1 Linear viscoelastic materials

There are two main approaches for analysing linear viscoelastic material by BEM. One of the approaches uses the elastic-viscoelastic correspondence principle to obtain an ‘elastic problem’, which is then solved in the Laplace transformed domain and the resulting solution is inverted to obtain the solution in time domain. The other approach implies the BEM formulation in the time domain and the boundary integral equation is solved by a step-by-step time integration scheme. The last approach requires viscoelastic fundamental solutions which may not be available for the specific problem. There is a third approach which aims to take the advantages of the previous ones, solving the problem in the time domain but using Laplace transforms of the fundamental solutions.

Since the BEM has been widely used, several researchers have been working in the development of fundamental solutions and procedures to increase its application range. For example, in terms of linear viscoelastic materials, Kusama and Mitsui (1982) developed and validated a method for analysing linear viscoelastic materials by BEM. They used the elastic-viscoelastic correspondence principle and a numerical procedure for the inversion of the Laplace transform. Gaul and Schanz (1999) carried out a comparative study of boundary element approaches to calculate the transient response of viscoelastic material in semi-infinite regions. González and Abascal (2004) achieved a validated fundamental solution for the steady state regime of a load that moves with a constant speed over a linear viscoelastic material. Until

then, there were no fundamental solutions for that specific problem. They applied the elastic-viscoelastic correspondence principle to the linear fundamental solutions.

Wang and Birgisson (2007) applied the BEM to model the quasi-static behaviour of asphalt pavements. They used the Displacement Discontinuity (DD) BEM which expresses the unknown in terms of discontinuous displacements (elemental displacements, i.e., displacements along and normal to the boundary element) instead of displacements in absolute terms. The BEM formulation was made in the time domain and the boundary integral equation solved by a step-by-step time integration scheme.

4.5.2 Fracture mechanics

The BEM is especially advantageous in fracture mechanics since it has the ability to follow the path of a growing crack with limited remeshing. The remeshing can consist in the addition of extra elements to the previous crack tip with no changes on the remaining mesh. Furthermore, the BEM deals with stress concentration problems more accurately than the FEM.

However, the presented BEM formulation cannot be used in fracture mechanics as the coincidence of cracks nodes results in a singular system of equations. To overcome this difficulty, some techniques have been developed. The two most used techniques are the DD method and the dual method.

In the DD method, only one of the crack boundaries is discretized. Then, the displacement boundary integral equation is applied to the nodes on the outer boundary and the traction boundary integral equation is applied to the nodes on the crack boundary. This method considers new unknown variables, the normal and tangential displacement differences between the two crack boundaries.

In the dual method, the two crack boundaries are discretized and a non-singular system of equations can be obtained by using two different boundary integral equations for the coincident nodes. The displacement integral equation is applied to both the nodes on the outer boundary and the nodes on one of the crack boundaries, and the traction integral equation is applied to the nodes on the other crack boundary. The unknown variables are displacements and tractions.

Stress intensity factors are used to describe fracture mechanics since they characterize in a simple way the complex stress field immediately around the crack. There are three intensity factors, one for each of the three modes of fracture mechanics shown in Figure 4.16.

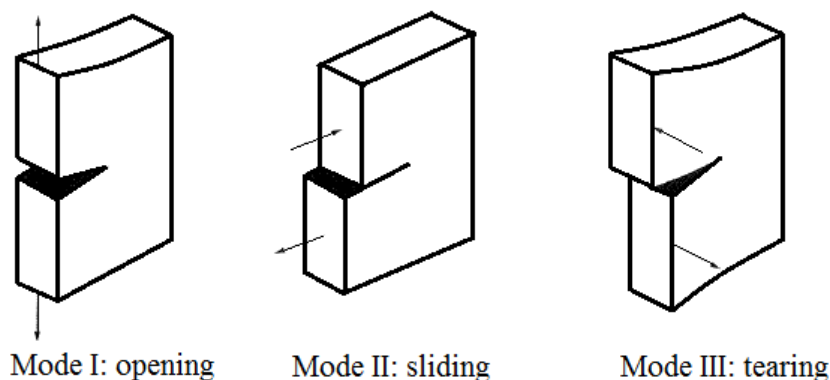


Figure 4.16 – The three modes of crack failure (adapted from Aliabadi (2002))

There are several methods to evaluate the intensity factors using the BEM such as the ones based on the quarter-point elements, path independent integrals, energy methods, subtraction of singularity method and the weight function methods. Aliabadi (2002) describes these methods.

Birgisson et al. (2002) predicted the viscoelastic response and the crack growth in asphalt mixtures using the BEM, more precisely the DD method. Sangpetngam et al. (2003) developed a crack growth law based on viscoelastic fracture mechanics which is capable to describe both the crack initiation and the crack propagation in asphalt mixtures. Then, Sangpetngam et al. (2004) extended the previous formulation to layered materials.

4.5.3 Elastodynamic problems

The BEM has the advantage of satisfying implicitly the radiation condition for infinite or semi-infinite regions. In its turn, domain methods, like FEM, require a discretization which should extend towards infinity. However, as it is not possible, an artificial boundary is defined. This boundary can be used without problems in statics, but in dynamics it ought to have appropriate boundary conditions to avoid wave reflection (transmitting boundary conditions).

Elastodynamic problems are usually solved by one of the following boundary element methods: the time domain method, the Laplace (or Fourier) transform method or the dual reciprocity method, which are very briefly summarized next. The time domain method uses elastodynamic fundamental solutions (time-dependents) requiring both time and space integrations. The Laplace (or Fourier) transform method transforms the fundamental solutions requiring only (complicated) space integrations. The latter method, dual reciprocity method, uses the elastostatic fundamental solutions (time-independents) requiring only time integrations. The first two methods require considerable knowledge of mathematics and mechanics (Tosecký et al., 2008). The dual reciprocity method transforms the domain integral into boundary integrals.

Aliabadi (2002) presents, although briefly, a comparison of these three methods. The time domain method is the most time consuming and the most general of the three methods. The Laplace (or Fourier) transform is usually the most accurate while the dual reciprocity method is possibly the least accurate of the three methods. Nevertheless, dual reciprocity method is the simplest and fastest of the three.

Beskos wrote two papers (Beskos (1987) and Beskos (1997)) that review extensively the boundary elements in elastodynamic. Therefore, they are suggested for a better comprehension and learning of this topic as well as the Dominguez's book (Dominguez (1993)).

4.6 REFERENCES

Aliabadi, M. H. (2002). *The Boundary Element Method, Volume 2: Applications in Solids and Structures*. John Wiley & Sons, Ltd.

Almeida, A. (2008). *Modelação Estrutural de Pavimentos Rodoviários: O uso do Método dos Elementos de Fronteira (Structural Modelling of Road Pavements: The use of the Boundary Element Method)*. Master Thesis, University of Coimbra. In Portuguese.

Beer, G., Smith, I. and Duenser, C. (2008). *The Boundary Element Method with Programming - For Engineers and Scientists*. Springer Wien New York.

- Beer, G. and Watson, J. O. (1992). *Introduction to Finite and Boundary Element Methods for Engineers*. John Wiley & Sons, England.
- Beskos, D. E. (1987). Boundary element methods in dynamic analysis. *Applied Mechanics Reviews*, 40, 1-23.
- Beskos, D. E. (1997). Boundary element methods in dynamic analysis: Part II (1986-1996). *Applied Mechanics Reviews*, 50, 149-197.
- Bialecki, R. A., Dallner, R. and Kuhn, G. (1993). Minimum distance calculation between a source point and a boundary element. *Engineering Analysis with Boundary Elements*, 12, 211-218.
- Birgisson, B., Sangpetngam, B. and Roque, R. (2002). Predicting Viscoelastic Response and Crack Growth in Asphalt Mixtures with the Boundary Element Method. *Transportation Research Record: Journal of the Transportation Research Board*, 1789, 129-135.
- Bu, S. and Davies, T. G. (1995). Effective evaluation of non-singular integrals in 3D BEM. *Advances in Engineering Software*, 23, 151-128.
- Dominguez, J. (1993). *Boundary Elements in Dynamics*. Computational Mechanics Publications.
- Eberwien, U., Duenser, C. and Moser, W. (2005). Efficient calculation of internal results in 2D elasticity BEM. *Engineering Analysis with Boundary Elements*, 29, 447-453.
- Gao, X.-W. and Davies, T. D. (2002). *Boundary Element Programming in Mechanics*. Cambridge University Press.
- Gaul, L. and Schanz, M. (1999). A comparative study of three boundary element approaches to calculate the transient response of viscoelastic solids with unbounded domains. *Computer Methods in Applied Mechanics and Engineering*, 179, 111-123.
- GID@ (2011). The personal pre and post processor. <http://gid.cimne.upc.es/>. CIMNE (The International Center for Numerical Methods in Engineering). Access date: 10 February 2011.
- González, J. A. and Abascal, R. (2004). Linear viscoelastic boundary element formulation for steady state moving loads. *Engineering Analysis with Boundary Elements*, 28, 815-823.
- Katsikadelis, J. T. and Nerantzaki, M. S. (1999). The boundary element method for nonlinear problems. *Engineering Analysis with Boundary Elements*, 23, 365-373.
- Kusama, T. and Mitsui, Y. (1982). Boundary element method applied to linear viscoelastic analysis. *Applied Mathematical Modelling*, 6, 285-290.
- Pina, H. (1995). *Métodos Numéricos (Numerical Methods)*. McGraw-Hill, Portugal. In Portuguese.
- Sangpetngam, B., Birgisson, B. and Roque, R. (2003). Development of Efficient Crack Growth Simulator Based on Hot-Mix Asphalt Fracture Mechanics. *Transportation Research Record: Journal of the Transportation Research Board*, 1832, 105-112.

Sangpetngam, B., Birgisson, B. and Roque, R. (2004). Multilayer Boundary-Element Method for Evaluating Top-Down Cracking in Hot-Mix Asphalt Pavements. *Transportation Research Record: Journal of the Transportation Research Board*, 1896, 129-137.

Shell (1988). *Shell pavement design method, BISAR-PC user manual*. Shell International Petroleum Company Limited.

Thöni, K. (2009). Error-Controlled Adaptive Analysis of Non-Linear Problems using the Boundary Element Method. PhD Thesis, Graz University of Technology.

Tosecký, A., Koleková, Y., Schmida, G. and Kalinchukb, V. (2008). Three-dimensional transient half-space dynamics using the dual reciprocity boundary element method. *Engineering Analysis with Boundary Elements*, 32, 597-618.

Wang, J. and Birgisson, B. (2007). A time domain boundary element method for modeling the quasi-static viscoelastic behavior of asphalt pavements. *Engineering Analysis with Boundary Elements*, 31, 226-240.

5 STUDY APPROACH

5.1 INTRODUCTION

This chapter presents the study approach to define a methodological framework for pavement damage estimation considering simulated axle load spectra.

The TruckSIM[®] computer software allows simulation of trucks for different values of the following variables: truck configuration, payload weight or truck's Gross Vehicle Weight (GVW), travel speed and International Roughness Index (IRI) value of the road profile. From simulations, axle load profiles are obtained for each truck axle and then axle load spectra can be defined. The knowledge of these simulated axle load spectra makes the pavement design more mechanistic since critical pavement responses to each axle load can be analytically or numerically computed. These pavement responses depend on design criterion and pavement structure.

Once the critical pavement responses are known, the theoretical Equivalent Axle Load Factors (EALFs) can be computed. There is an EALF for each design criterion and pavement structure. For a specific situation and truck, the truck's overall Aggressiveness Factor (AF) is obtained by summing all the EALFs (defined for each axle of the truck).

If AFs of several trucks of the Portuguese truck traffic fleet are known for several situations, the pavement design can be based on the number of Equivalent Standard Axle Load (ESAL) applications for each situation and consequently the pavement response can be analytically computed using, for example, the BISAR[®] computer software (Shell, 1988).

It should be mentioned that although the estimation of the pavement damage is based on the number of ESAL applications, they are calculated using theoretical EALFs which is equivalent to considering the axle load spectra in the same way as the Mechanical-Empirical Pavement Design Guide (MEPDG) (NCHRP, 2004).

The study approach consists essentially in the following steps:

- (a) Definition of a mixed truck traffic flow over the pavement design period;
- (b) Simulation of the axle load spectra by using the TruckSIM[®];
- (c) Calculation of AFs for the trucks of the mixed truck traffic flow;
- (d) Calculation of the AF of the mixed truck traffic flow;
- (e) Calculation of the number of ESAL applications;
- (f) Calculation of the pavement damage.

As some pavement designers may not have the necessary resources to apply this study approach, a hierarchical approach is defined to facilitate its use. It encompasses three levels, representing different levels of flexibility for the pavement designers. These three levels are defined as follows:

- (1) The knowledge of the axle loads for each simulated truck as a function of the IRI-value of the road profile, the travel speed of the truck and the GVW of the truck;

- (2) The knowledge of the AFs for each simulated truck as a function of the IRI-value of the road profile, the travel speed of the truck and the GVW of the truck. These AFs are both design criterion-specific and pavement structure-specific;
- (3) The use of an application to calculate the AF for a mixed truck traffic flow and the pavement damage through the pavement design period.

Using level (1), the pavement designers can consider any pavement structure and any design criterion. However, this level requires the calculation of the critical pavement responses which should be done preferentially by using numerical methods. Numerical methods deal with specificities that cannot be dealt with analytical methods like the BISAR®.

Using level (2), the pavement designers only need to calculate the critical pavement responses due to an ESAL application (analytical methods). However, AFs for different pavement structures and design criteria are required.

Finally, using level (3), the pavement designers have an application to calculate the AFs and the pavement damage. Its practical applicability depends on the number of simulated trucks as well as on the number of pavement structures considered.

From level (1) to (3), the pavement design becomes easier although less flexible. For example, the level (1) can be applied to different pavement structures while the level (3) can only be applied to the pavement structures modelled in the application. However, the pavement damage estimation with the level (1) requires several calculations while that the pavement damage estimation with the level (3) is automatic.

To fulfil the aforementioned steps of the study, this chapter deals with the following actions. It starts with the definition of the truck configurations to simulate. The payload weights and the trucks' tyres are also defined, including the tyre-pavement contact. Then, road profiles are generated for specific IRI-values. Once the trucks are defined and the road profiles are generated, simulations are carried out and axle load profiles are obtained. Dynamic Load Coefficients (DLCs) of them are determined and regression models to estimate axle loads are developed. In order to calculate critical pavement responses imposed by axle loads, pavement structures are defined. From these responses, theoretical EALFs are calculated as well as AFs for the simulated trucks. With the calculated AFs, regression models are defined to predict them. At the end, the three levels of the study approach are described. In level (3) an application is developed, which can consider changes in the Asphalt Concrete (AC) modulus and in IRI-value of the road profile over the pavement design period. With the objective of understanding the importance of tyre-pavement contact, EALFs for each axle of the simulated trucks are presented.

This work considers only two trucks, two pavement structures and two design criteria. Nevertheless, it can be easily extended to other situations.

5.2 TRUCKS' DEFINITION

In order to have a reasonable representation of the Portuguese truck traffic fleet, a lorry/truck with 2 axles (F1-subclass of Table 2.2) and an articulated vehicle with 2+3 axles (H5-subclass of Table 2.2) were simulated. The use of these two vehicles can be justified by Figure 2.10 to Figure 2.14. In 2011, these two trucks represented 75% of the Portuguese truck traffic fleet. Hereafter, they are referred as 'F1-Truck' and 'H5-Truck', respectively. The F1-Truck's GVW is

19 t and the H5-Truck's GVW is 40 t. Figure 5.1 shows both vehicles which were built from the TruckSIM[®]'s library.



Figure 5.1 – Simulated vehicles

TruckSIM[®] defines the simulation parameters for the considered trucks through a set of screens with graphics, tables and values. Figure 5.2 shows the first screen that the user encounters when opens the TruckSIM[®]. It gives access to all aspects of simulation such as truck definition, road definition, driver controls and outputs.

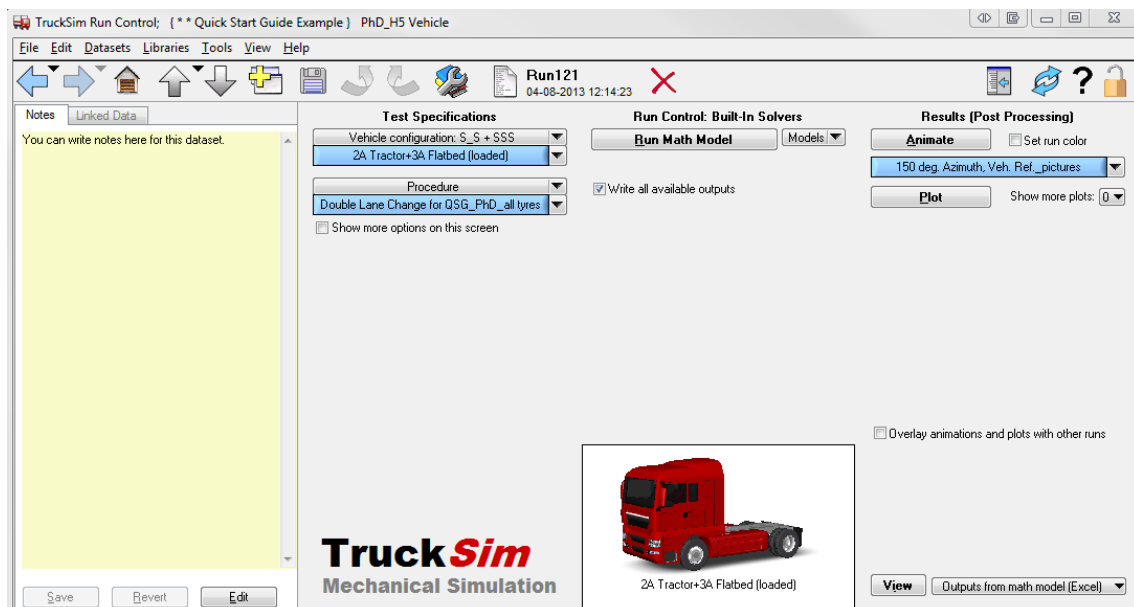


Figure 5.2 – The ‘TruckSIM Run Control’ screen for the ‘H5-Truck’

Firstly, appropriate vehicle configurations are selected using the screen shown in Figure 5.3. For example, the ‘H5-Truck’ has a lead unit with 2 axles and a trailer with 3 axles. When vehicle measurements cannot be available, TruckSIM[®] has default values for all parameters. From this screen, the user can see the available options to characterize both the lead unit and the trailer. Figure 5.4 shows the screen with these options for the lead unit. The majority of default values were used because they are typical of these kinds of vehicles and because there are not available measurements. The most interesting parameters to this work are related to tyres and suspensions. In relation to tyres, the current tyres that equip the ‘F1-Truck’ and ‘H5-Truck’ in Portugal were selected. In relation to suspensions, the default ones were left since they are representative of the current trucks in operation.

VehicleSim (VS) math models in TruckSIM[®] support many different suspension designs, using data that can be obtained from real or simulated kinematics and compliance (K&C) tests. This approach means that details of a specific design (linkage geometry, bushing properties, etc.) are not needed, because the behaviour of the suspension as it affects vehicle response is captured with more generic system-level parameters and nonlinear tables. This approach reduces the number of suspension

models to just a few types, based on fundamental kinematical behaviour. TruckSIM[®] has math models for two basic suspension types: independent and solid axle.

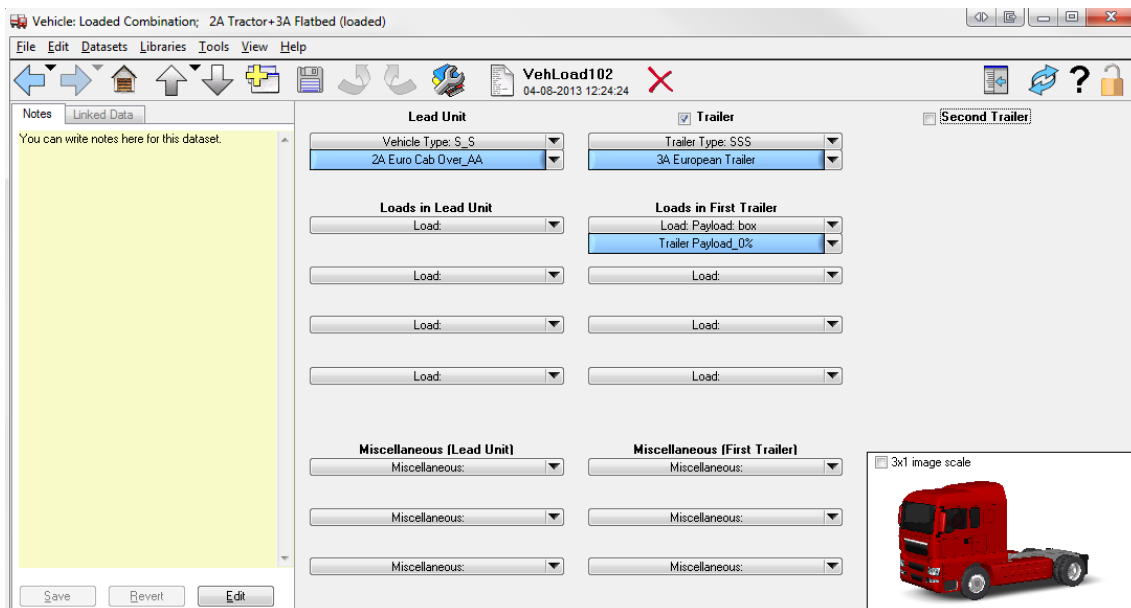


Figure 5.3 – The ‘Vehicle: Loaded Combination’ screen for the ‘H5-Truck’

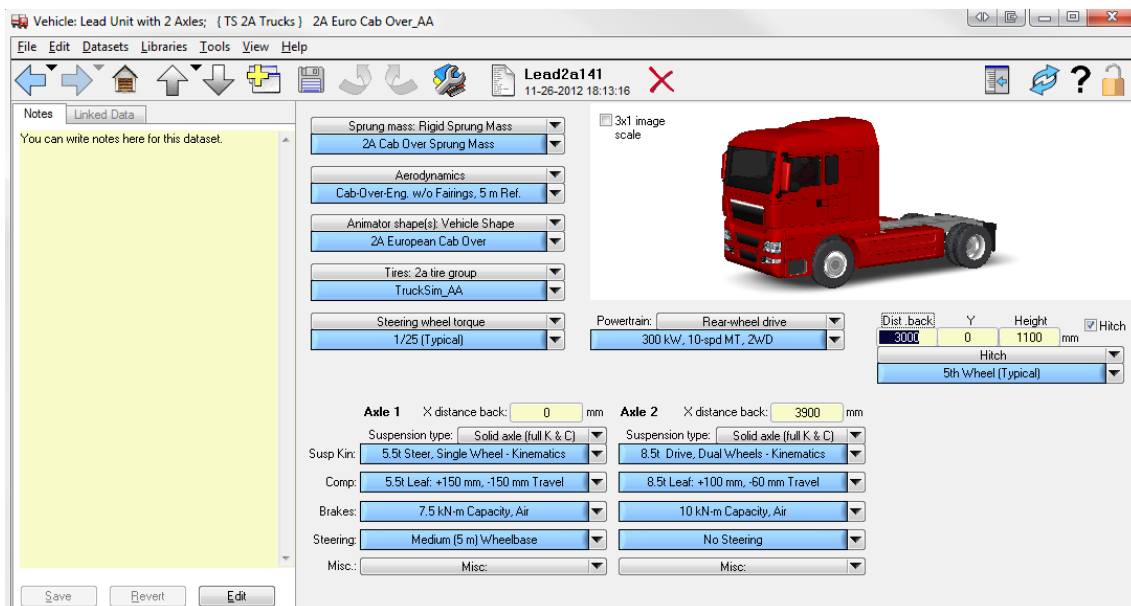


Figure 5.4 – The ‘Vehicle: Lead Unit with 2 axles’ screen

In terms of payloads, they can be modelled with different dimensions and weights. In addition, it is possible to choose the payload location and consequently it is possible to consider different payload distributions on the truck. For example, Figure 5.5 shows a payload with box shape defined by dimensions and weight. It is the payload of the ‘H5-Truck’ running with the legal limits (40 t in mass).

By changing the payload weight, empty-trucks to overloaded-trucks can be simulated. Table 5.1 and Table 5.2 present the payload weights considered in this work. In addition, these tables present the loads per axle which were obtained from the TruckSIM[®] considering the trucks running over a smooth pavement surface (IRI equal to 0 m/km). In this case, the loads are essentially due to the action of gravity since the obtained load profiles are constant and as a result they can be denoted as ‘static loads’. The loads per axle of the ‘H5-Truck’ when fully loaded (payload equal

to 26.0 t) are in agreement with values from literature, as for instance in the Glaeser (2010)'s work (see Figure 5.6).

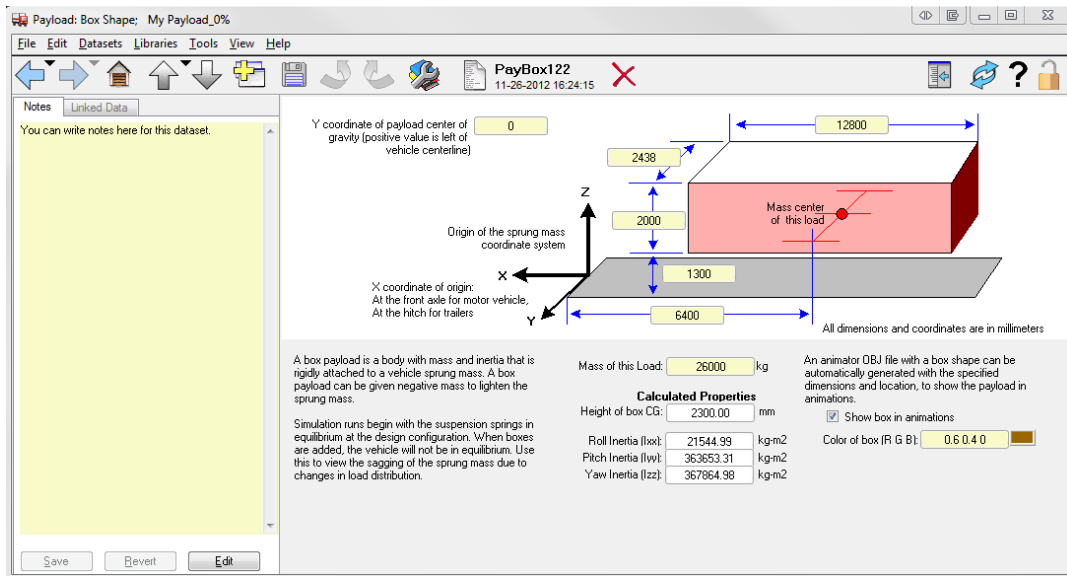


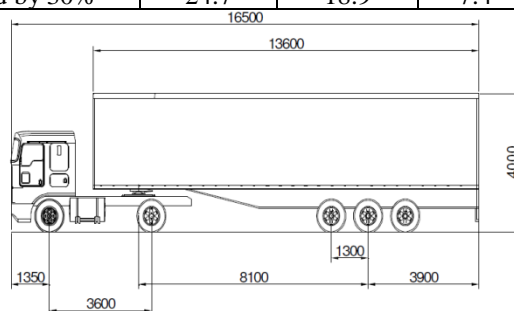
Figure 5.5 - The 'Payload: Box Shape' screen

Table 5.1 - Payload weights for the 'H5-Truck'

Load case	GVW (t)	Payload (t)	Load per axle (t)				
			axle 1	axle 2	axle 3	axle 4	axle 5
Fully Loaded	40.0	26.0	6.5	11.6	7.7	7.3	6.9
Empty	14.0	0.0	4.5	4.7	1.9	1.6	1.3
Underloaded by 10%	36.0	22.0	6.2	10.5	6.8	6.4	6.0
Underloaded by 20%	32.0	18.0	5.9	9.5	5.9	5.5	5.2
Underloaded by 30%	28.0	14.0	5.6	8.4	5.0	4.6	4.3
Overloaded by 10%	44.0	30.0	6.8	12.7	8.6	8.2	7.7
Overloaded by 20%	48.0	34.0	7.1	13.7	9.5	9.0	8.6
Overloaded by 30%	52.0	38.0	7.4	14.8	10.4	9.9	9.4

Table 5.2 – Payload weights for the 'F1-Truck'

Load case	GVW (t)	Payload (t)	Load per axle (t)	
			axle 1	axle 2
Fully Loaded	19.0	14.0	6.5	11.6
Empty	5.8	0.0	4.5	4.7
Underloaded by 10%	17.1	11.3	6.2	10.5
Underloaded by 20%	15.2	9.4	5.9	9.5
Underloaded by 30%	13.3	7.5	5.6	8.4
Overloaded by 10%	20.9	15.1	6.8	12.7
Overloaded by 20%	22.8	17.0	7.1	13.7
Overloaded by 30%	24.7	18.9	7.4	14.8



LADEN (t)	6.5	11.5	22.0	40.0
-----------	-----	------	------	------

Figure 5.6 – Loads per axle of the 'H5-Truck' when fully loaded (adapted from Glaeser (2010))

In addition to changes in payload weights, simulations are carried out for different travel speeds (40, 60, 80 and 100 km/h) and for different road surface profiles (from smooth to rough ones). The road surface profiles are defined later.

The tyre-pavement contact area (both its shape and dimension) is a crucial aspect from the point of view of pavement design. Before defining the contact area, it is necessary to define the truck tyres which have been changing over time.

The ‘H5-Truck’ is equipped with the tyres that have already been referred (Combination 1 of Figure 2.27). For the F1-Truck, some contacts with one of the main tyre manufacturers as well as with one of the main freight distribution companies were made. The tyres dimension and arrangement for both simulated trucks can be seen in Figure 5.7.



Figure 5.7 – Tyres considered in the simulations

The report of COST action 334 (2001) presents values in practice for the tyre-pavement contact areas of the considered tyres. These values depend on the axle load and are presented in Table 5.3. The widths of the tyre-pavement contact areas are presented in Table 5.4.

Table 5.3 – Tyre-pavement contact areas (adapted from COST 334 (2001))

Axle load (t)	Contact area (cm ²)				
	315/80R22.5 (dual)	385/65R22.5 (single)	315/80R22.5 (single)	315/70R22.5 (dual)	315/70R22.5 (single)
6	-	-	537	-	502
7	-	555	548	-	512
8	467	564	559	496	-
9	475	578	-	505	-
10	482	-	-	513	-
11.5	488	-	-	521	-
13	500	-	-	-	-

Table 5.4 – Widths of the tyre-pavement contact areas (adapted from COST 334 (2001))

315/80R22.5 (dual)	385/65R22.5 (single)	315/80R22.5 (single)	315/70R22.5 (dual)	315/70R22.5 (single)
247	285	247	253	253

From the values of Table 5.3, regression lines (Figure 5.8) were calculated which were then extrapolated and used to obtain different lengths for the tyre-pavement contact areas. The widths of the tyre-pavement contact areas are kept constant. In other words, for each tyre, the length of the contact area is calculated as a function of the axle load and then rounded to the nearest integer, while the width of the contact area is always the same.

For dual tyres, the total width is taken as twice the footprint width of the individual tyres plus the spacing between the footprints of the duals. This spacing was assumed to be 100 mm as considered in the COST action 334 (2001).

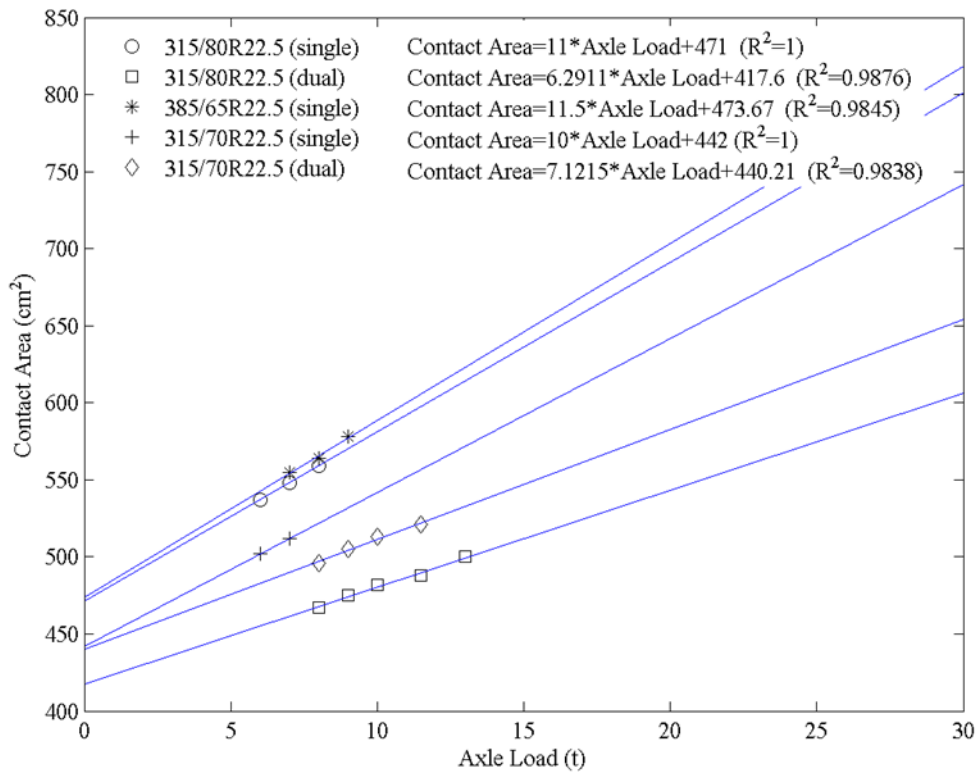


Figure 5.8 – Regression lines for tyre-pavement contact area

5.3 PAVEMENT STRUCTURES

Two pavement structures are considered, a thin structure and a thick structure. Both structures are depicted in Figure 5.9. The AC thickness of the thin structure corresponds to the T6-traffic class of the MACOPAV, while the AC thickness of the thick structure corresponds to the T1-traffic class of that manual (JAE, 1995).

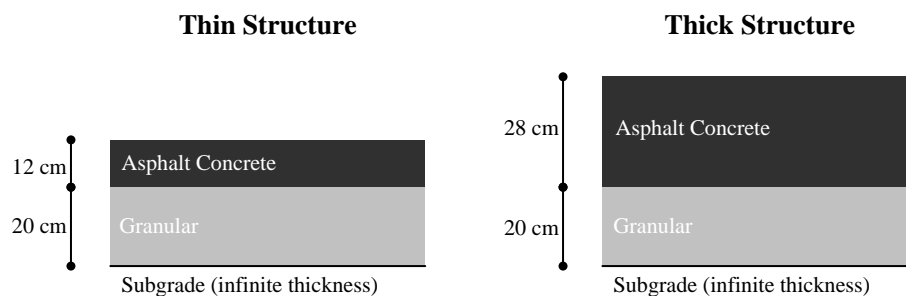


Figure 5.9 – Pavement structures

The materials behaviour was assumed to be linear elastic. Therefore only two materials' characteristics are needed. They are the modulus and the Poisson's ratio.

The AC modulus was calculated by the expression (2.1) or by the expression (2.2) considering the variables presented in Table 5.5. These variables were defined to have approximately a thin structure with the characteristics of a binder course (AC 20 bin – MBD) and a thick structure with the characteristics of a base course (AC 20 base – MB). Since the volume percentage of bitumen has a great influence on fatigue performance, the target values of 12% and 9.5% were defined for the thin and thick structure, respectively.

Table 5.5 – Parameters used in the AC modulus calculation

	Thin structure	Thick structure
Aggregate density (kg/m ³)	2530	
Bitumen density (kg/m ³)	1030	
Bitumen content (% of aggregate mass)	5.8	4.5
Void content (%)	3.5	5.0
Voids in mineral aggregate (%)	15.5	14.5
Volume percentage of bitumen (V _b) (%)	12.0	9.5
Volume percentage of aggregate (V _a) (%)	84.5	86.4
Bitumen grade	35/50	
Temperature (°C)	25	
Travel speeds (km/h)	40/60/80/100	

As travel speed influences the pavement response, different AC modulus are considered, one for each travel speed. Table 5.6 presents the AC modulus and Table 5.7 presents the remaining characteristics.

Table 5.6 – AC modulus for different travel speeds

Vehicle speed (km/h)	AC modulus (MPa)	
	Thin structure	Thick structure
40	4470	5327
60	4942	5837
80	5306	6229
100	5606	6550

Table 5.7 – Materials’ characteristics

Layer	Modulus (MPa)	Poisson’s ratio
AC	function of both structure and travel speed (Table 5.6)	0.35
Granular	200	0.30
Subgrade	100	0.35

As already mentioned, the pavement structure degrades over the design period as result of several load repetitions and consequently there is a gradual reduction in the AC modulus.

In order to better understand the pavement damage progression with AC modulus degradation, besides the AC modulus degradation model developed by Collop and Cebon (1996), two models adapted from that model were considered.

The Collop and Cebon’s model is given by equation (2.6) and the considered critical relative modulus was 0.2 resulting in a k equal to 1.609. The two adapted models correspond to smaller reductions in the AC modulus, for example if, in a time increment, the original model conducts to a ΔE reduction in AC modulus, the adapted models correspond to a $\Delta E/2$ reduction and a $\Delta E/4$ reduction in AC modulus and they are termed ‘50%-Adapted Model’ and ‘25%-Adapted Model’, respectively (see Figure 5.10). The model developed by Collop and Cebon is termed ‘Original Model’.

The adapted models were defined using exponential trend lines adjusted to the AC modulus values as shown in Figure 5.10. Then, the adapted models were extrapolated to critical AC modulus and the equations (5.1) and (5.2) were obtained for the ‘50%-Adapted Model’ and for the ‘25%-Adapted model’, respectively. All of the AC degradation models are depicted in Figure 5.11.

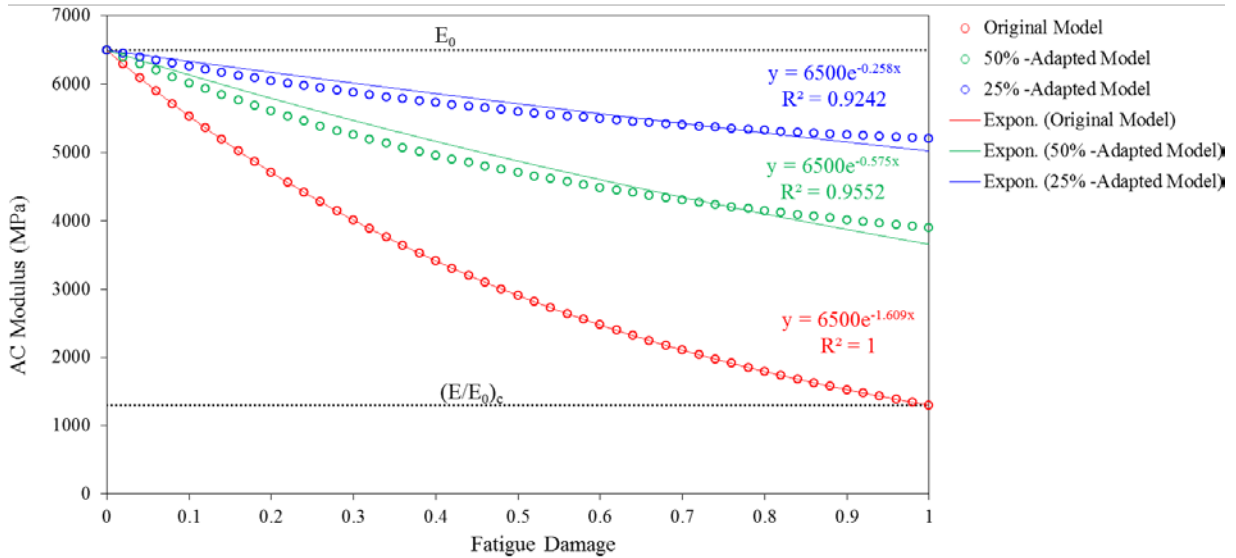


Figure 5.10 - Definition of the adapted models

$$\frac{E_m}{E_0} = e^{-0.575D_{50\%}} \quad D_{50\%} < 1$$

$$\frac{E_m}{E_0} = \left(\frac{E_m}{E_0} \right)_c \quad D_{50\%} \geq 1$$

, where $D_{50\%} = \frac{D}{2.80}$ (5.1)

$$\frac{E_m}{E_0} = e^{-0.258D_{25\%}} \quad D_{25\%} < 1$$

$$\frac{E_m}{E_0} = \left(\frac{E_m}{E_0} \right)_c \quad D_{25\%} \geq 1$$

, where $D_{25\%} = \frac{D}{6.24}$ (5.2)

where

- E_m = modulus of the bituminous mixture
- E_0 = initial modulus of the bituminous mixture
- E_m/E_0 = relative modulus
- D = damage term given by

$$D = \sum_{i=1}^j \left(\frac{N^{(i)}}{N_f^{(i)}} \right)$$

where j is the number of different strain levels considered, $N^{(i)}$ represents the number of cycles at a given level of tensile strain at the bottom of the bituminous layer and $N_f^{(i)}$ is the number of cycles to failure at that strain level

$(E_m/E_0)_c$ = critical relative modulus (when the reduction in modulus reaches this value, the bituminous mixture is assumed to have failed and the modulus is not reduced further)

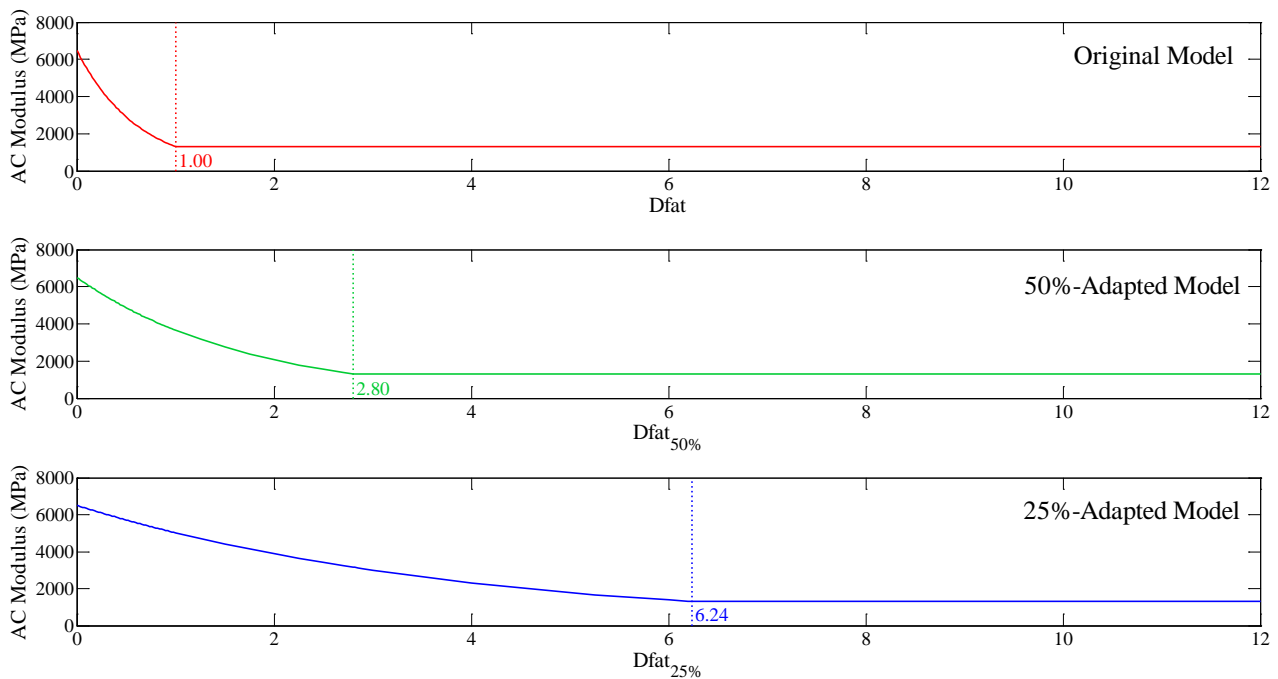


Figure 5.11 – AC modulus degradation models

5.4 ROAD PROFILES

5.4.1 Generation of road profiles

As already mentioned, the vibration of heavy vehicles, and hence the dynamic axle loads, fall into two distinct frequency ranges (Cebon, 1999):

- 1.5 to 4 Hz: Sprung mass bounce, pitch and roll vibration modes;
- 8 to 15 Hz: Unsprung mass bounce and roll modes, ‘load-sharing’ suspension pitch modes.

In order to excite these modes of vibration, roughness irregularities with wavelengths from 0.1 to 50 m were considered. This encompasses every wavelength range necessary to excite those modes of vibration at the travel speeds considered in this work (40, 60, 80 and 100 km/h) as listed in Table 5.8. Theoretically, the 0.1-50 m wavelength range allows exciting modes of vibration from 0.67 to 27.8 Hz at the 10-120 km/h speed range.

Table 5.8 - Wavelength ranges necessary to excite the modes of vibration at different travel speeds

Frequency range	40 km/h	60 km/h	80 km/h	100 km/h
1.5 – 40Hz	2.8 – 7.4 m	4.2 – 11.1 m	5.6 – 14.8 m	6.9 – 18.8 m
8 – 15 Hz	0.7 – 1.4 m	1.1 – 2.1 m	1.5 – 2.8 m	1.9 – 3.5 m

The road profiles were generated using the procedure described in Chapter 3. For that, an application in Matlab® (M-file) was created (MATLAB®, 2012). Profiles with 1500 m in length were generated such that the first 500 m can be ignored from the vehicle simulation, considering hence load profiles with 1000 m in length.

The spectral composition of the road profiles follows the specified in the ISO 8608 (ISO 8608, 1995). In order to generate profiles with specific IRI values, first it was necessary to obtain a relationship between the displacement Power Spectral Density (PSD) (S_k) and the IRI. For that

road profiles were generated for each ISO 8608 class considering the geometric mean value of S_k .

Figure 5.12 shows the profiles generated (a detail of the first 100 m is shown in Figure 5.13), Figure 5.14 shows the corresponding displacement PSD (blue are the non-smoothed and green are the smoothed; the red lines depict the limits of ISO classes) and Table 5.9 shows the computed IRI values. The relationship between the displacement PSD (S_k) and the IRI is given by expression (5.3).

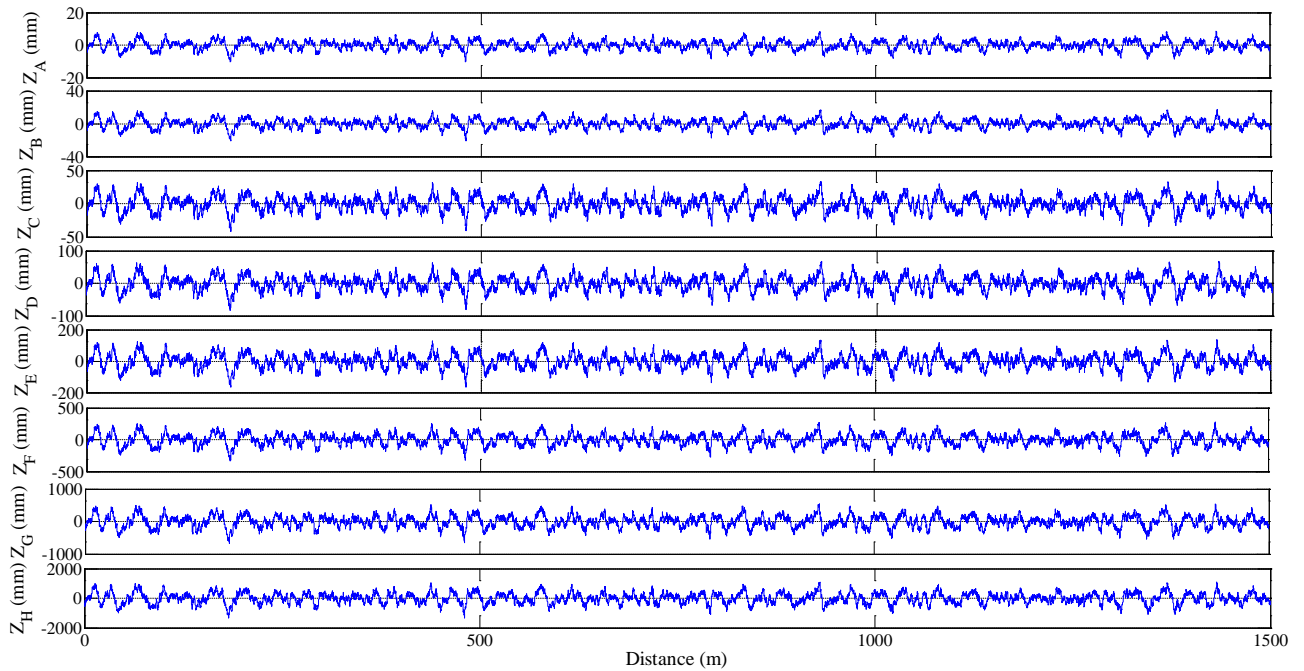


Figure 5.12 – Generated road profiles for each ISO class

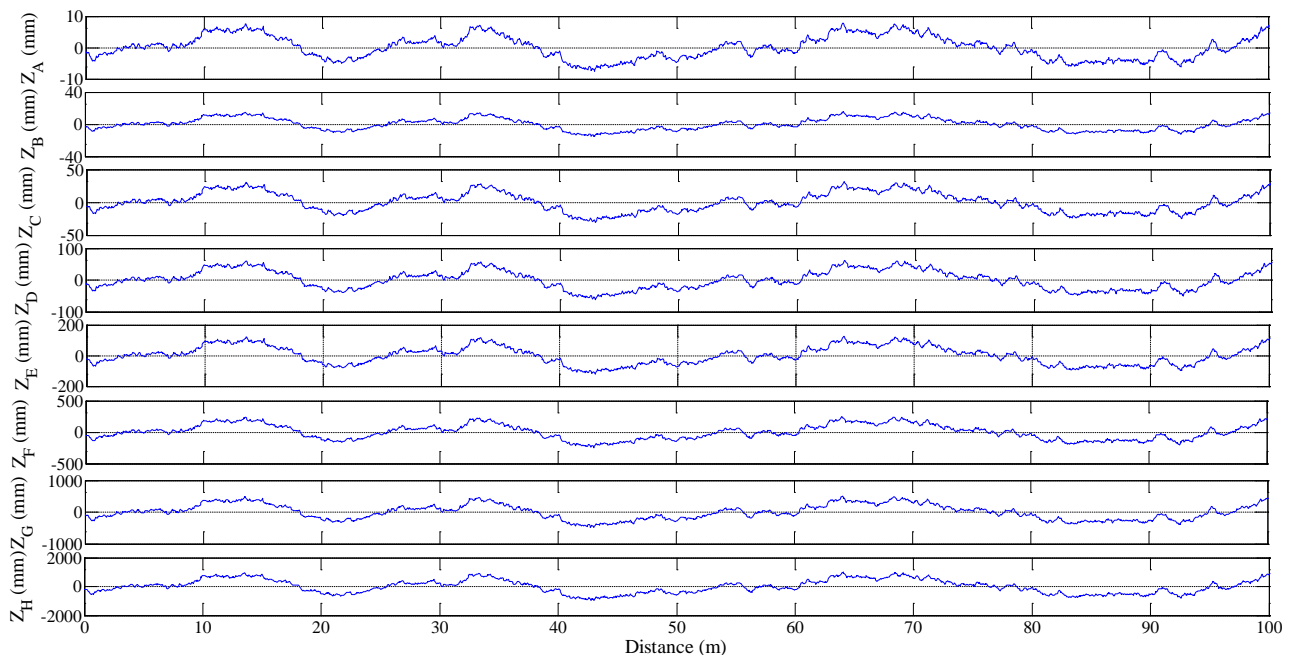


Figure 5.13 - Generated road profiles for each ISO class (detail of the first 100 m)

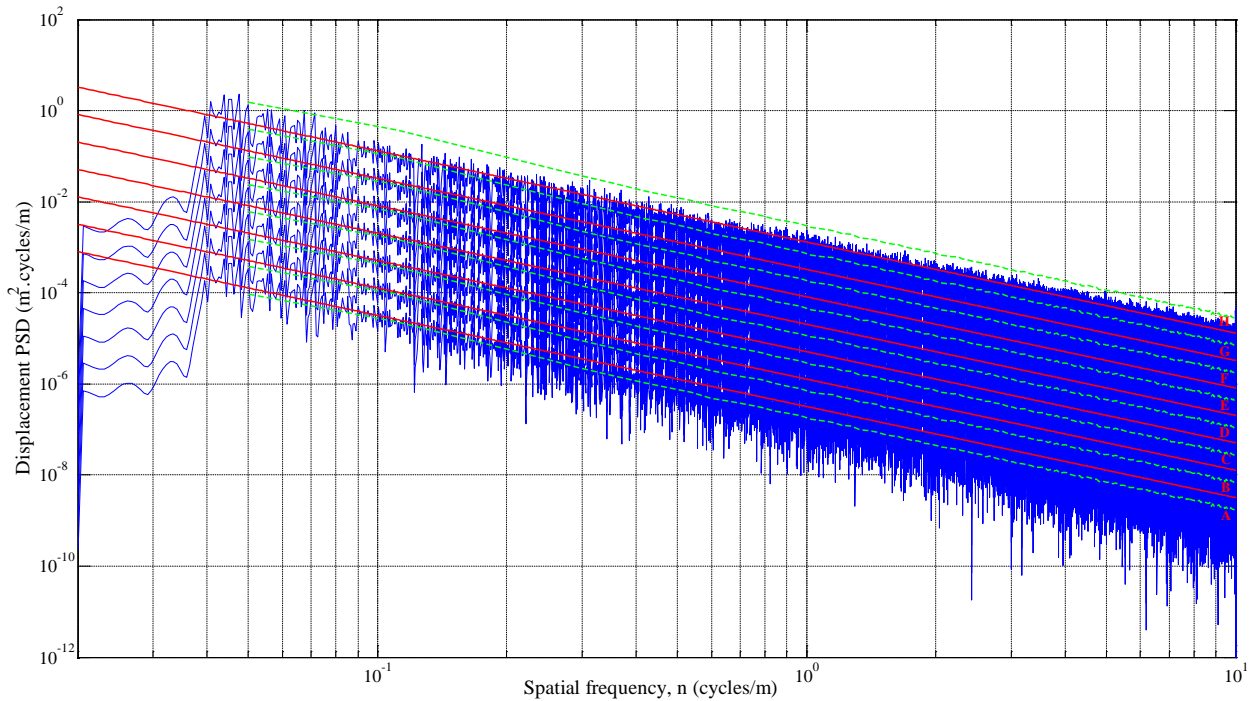


Figure 5.14 – PSD function of each generated road profile

Table 5.9 – ISO 8608 classes and corresponding IRI values

ISO class	$S_k(\gamma_0)$ (m ³)	IRI (m/km)
A	16×10^{-6}	2.15
B	64×10^{-6}	4.29
C	256×10^{-6}	8.58
D	1024×10^{-6}	17.16
E	4096×10^{-6}	34.33
F	16384×10^{-6}	68.66
G	65536×10^{-6}	137.32
H	262144×10^{-6}	274.64

$$\text{IRI(m / km)} = 0.5369 \cdot \left[S_k (\gamma_0) / 1 \times 10^{-6} \right]^{0.4999} \quad (R^2 = 1.0) \quad (5.3)$$

The IRI values were computed using an engineering software application, called ProVAL (Profile Viewing and AnaLysis). ProVAL is freeware and can be downloaded from the internet (ProVAL@, 2011). It supports, among others files, the ERD file format (ERD@, 2011) which is a standard file format used for storing numbers in tabular form, with labels to support automated plotting and processing. It was developed by the Engineering Research Division (ERD) of the University of Michigan Transportation Research Institute (UMTRI).

At first sight, the computed IRI values seem quite high even knowing that the ISO 8608 deals with roads, streets and highways, and off-road terrain. Thus, it was critical to validate these values before to generate the specific profiles of this work. Harris et al. (2010) generated road profiles considering the ISO 8608 and specified the corresponding IRI values. Table 5.10 shows these values that are in accordance with the calculated ones, except the profile 3.

Ngwangwa et al. (2010) also generated road profiles considering the ISO 8608 and specified the corresponding IRI values. They generated four profiles belonging to classes A, C, D and F and specified the following IRI values, 2.5, 10.0, 19.9 and 79.8 m/km.

Once the developed application is validated, road profiles with specific IRI values are generated. Five IRI values were chosen: 1, 2, 3, 4 and 5 m/km. IRI values from 1.2 to 5.9 m/km (average value: 2.5 m/km) were found to be representative of the Portuguese road network (Luz, 2011). Table 5.11 lists the displacement PSD values and Figure 5.15 depicts the road profiles (a detail of the first 100 m is shown in Figure 5.16). The related non-smoothed (blue) and smoothed (green) PSD of each road profile are shown in Figure 5.17 as well as the lower and upper limits of the PSD (red) defined in the ISO 8608 for each road class.

Table 5.10 – Some ISO 8608 classes and corresponding IRI values (Harris et al., 2010)

Profile	ISO class	$G_d(n_0)$ ($m^3/cycle$)	IRI (m/km)
1	A	8×10^{-6}	1.04
2	A	16×10^{-6}	2.19
3	B	64×10^{-6}	3.02
4	B/ C	128×10^{-6}	6.23
5	C	256×10^{-6}	8.43

Table 5.11 – $S_u(\gamma_0)$ values of the specific road profiles

IRI (m/km)	$S_u(\gamma_0)$ (m^3)	ISO class
1	3.5×10^{-6}	A
2	13.9×10^{-6}	A
3	31.2×10^{-6}	A/B
4	55.5×10^{-6}	B
5	86.8×10^{-6}	B

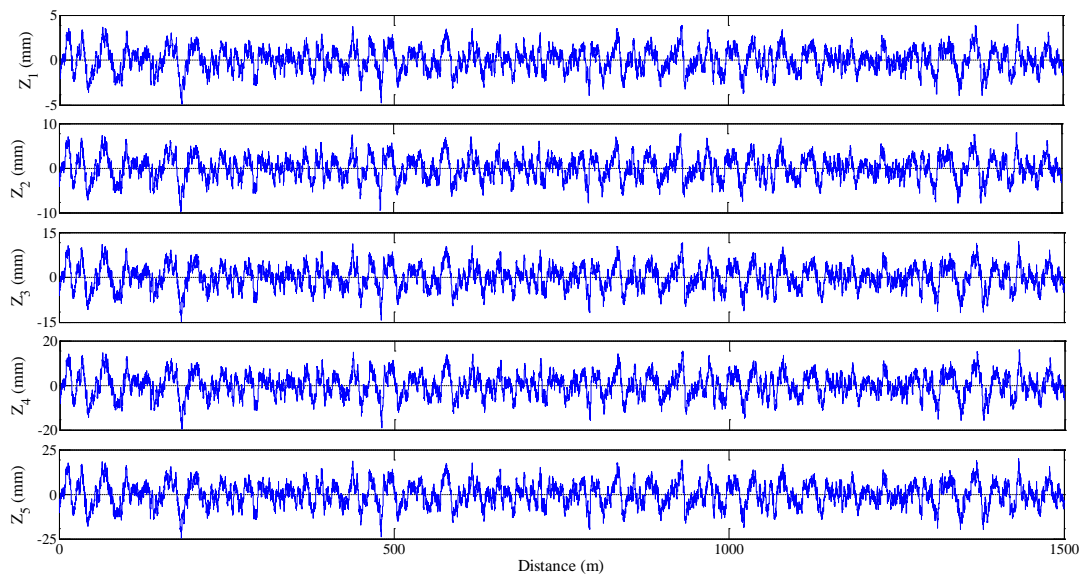


Figure 5.15 - Generated road profiles with specific IRI values

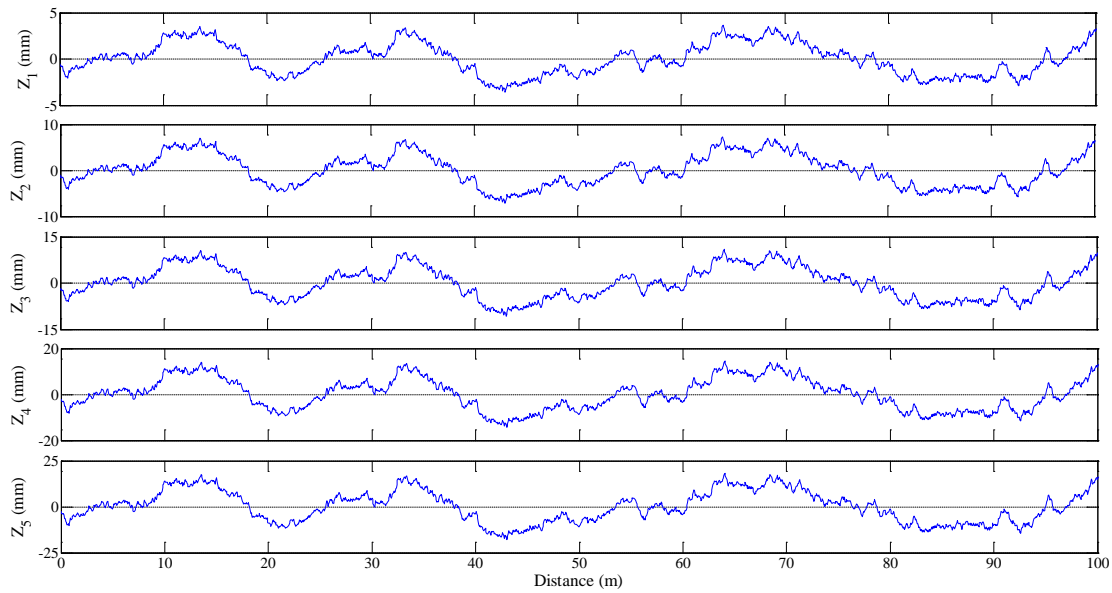


Figure 5.16 - Generated road profiles with specific IRI values (detail of the first 100 m)

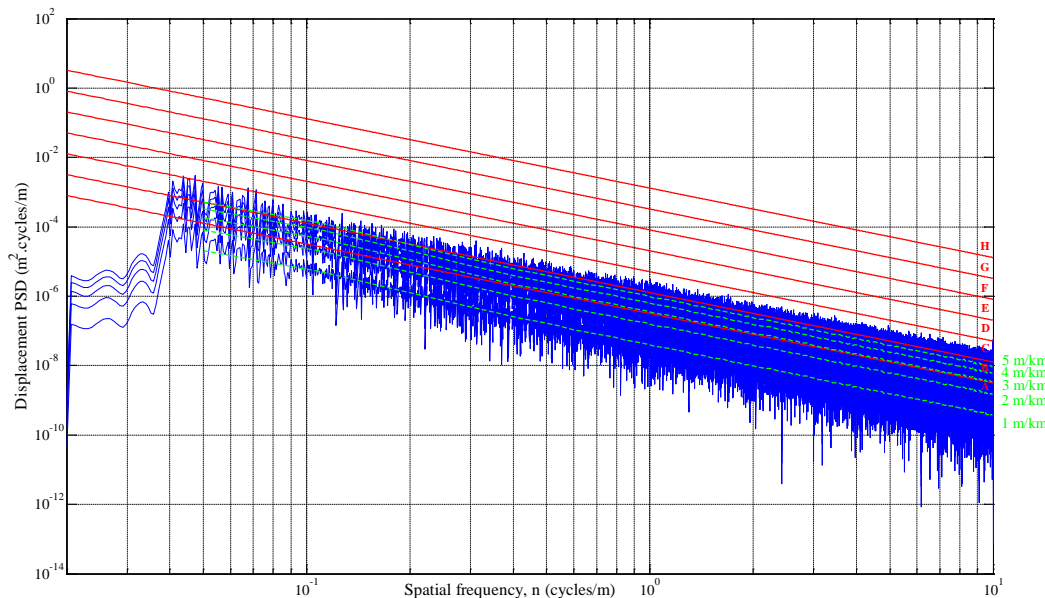


Figure 5.17 - PSD of each road profile

5.4.2 Roughness growth

Three models to predict roughness growth were described in Chapter 3, they are: (1) the prediction model of the Swedish Pavement Management System (PMS), (2) the mechanistic roughness model based on vehicle-pavement interaction, and (3) the prediction model of the MEPDG procedure.

Apparently, the mechanistic roughness model based on vehicle-pavement interaction would be the most interesting one for this work. It is a mechanistic model in which the predicted IRI-value is function of the initial IRI-value, the bituminous layer thickness, the axle load and the number of load repetitions – equation (3.10). However, due to the variables considered in its development (AC layer thickness equal to 100 mm and 150 mm), it can only be applied to the thin structure (AC layer thickness equal to 120 mm).

On the other hand, in the prediction model of the MEPDG procedure, the predicted IRI-value depends on various distress types that should be previously predicted, but they are not considered in this work. The prediction model of the Swedish PMS can be applied to both the thin and the thick structure. Nevertheless, it does not consider the influence of the axle load in the same way as the mechanistic roughness model.

The first approach to consider roughness growth was to use the mechanistic roughness model based on vehicle-pavement interaction in the thin structure and the prediction model of the Swedish PMS in both the thin and the thick structure. Over time the mechanistic roughness model based on vehicle-pavement interaction has appeared to be not as much promising as it was expected to be.

Figure 5.18 shows the evolution of the IRI-value in accordance with the mechanistic roughness model based on vehicle-pavement interaction. The most increase in the IRI-value occurs in the first year, then (from the first year to the end of pavement design period) that increase is about 6%. Such evolution does not correspond to reality. Even considering in each time step the previous IRI-value instead of the initial IRI-value, the evolution does not correspond to reality, on the contrary, it is further from reality, as can be seen in Figure 5.19.

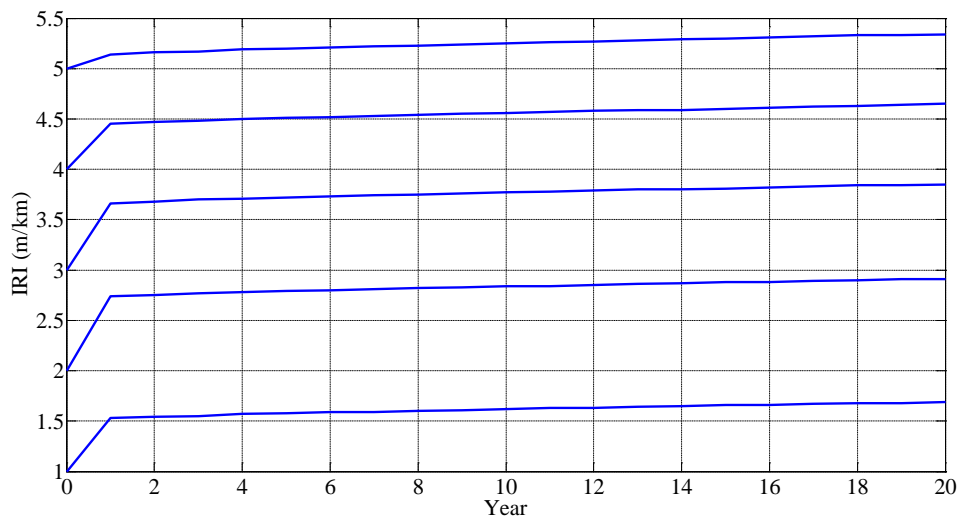


Figure 5.18 – Evolution of IRI in accordance with the mechanistic roughness model based on vehicle-pavement interaction – $IRI=f(IRI_0)$

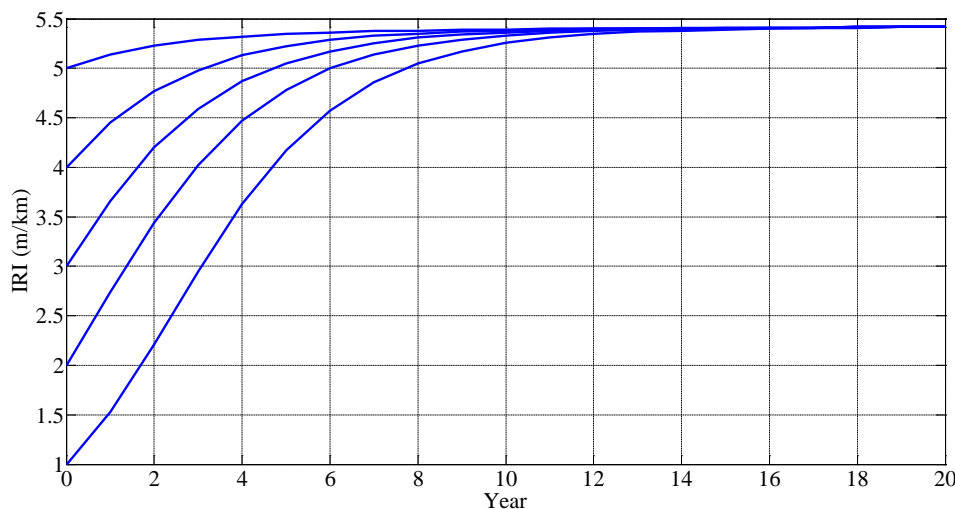


Figure 5.19 - Evolution of IRI in accordance with the mechanistic roughness model based on vehicle-pavement interaction – $IRI_{i+1}=f(IRI_i)$

Therefore, and because the main purpose of this work is to identify how much the increase in damage due to IRI growth is, only the prediction model of the Swedish PMS is used. It defines pavement performance for four climatic zones and eight traffic classes. The climate zone 1 is in the southern part of Sweden while the climate zone 4 is in the northern part. Despite the northern zones have a humid and snowy climate which greatly differs from Portuguese climate, average values from the 4 climatic zones were considered. This option can be justified by the fact that the values from the 4 climatic zones are of the same order of magnitude (see Table 5.14 and Table 5.15) and by the fact that the consideration of average values is enough to fulfil the purpose of this work, that is, to quantify the increase in damage due to IRI growth.

Lang (2001) defined the traffic classes using Annual Average Daily Traffic (AADT) limits. However, a comparison of these limits with the MACOPAV ones (JAE, 1995) indicates that it is necessary to consider a percentage of trucks. Since no information was found for this percentage, it was defined to have similar traffic classes in the Swedish PMS model and in the MACOPAV. Therefore, a percentage of 12% was used as well as the consideration that the traffic is in the design lane. Table 5.12 and Table 5.13 present the Annual Average Daily Heavy-Traffic (AADT_h) limits in the design lane considered for the Swedish PMS model and the defined ones in the MACOPAV, respectively.

The thin structure (AC layer thickness equal to 120 mm) is subjected to an AADT_h of 100 which corresponds to the T6-class of the MACOPAV and to the D-class of the Swedish model. On the other hand, the thick structure (AC layer thickness equal to 280 mm) is subjected to an AADT_h of 1600 which corresponds to the T1-class of the MACOPAV and to the G-class of the Swedish model.

Table 5.12 – AADTT limits in the design lane considered for the Swedish model

Class	Lower limit	Upper limit
A	0	15
B	15	30
C	30	60
D	60	240
E	240	480
F	480	960
G	960	1920
H	1920	

Table 5.13 - AADTT limits in the design lane defined in the MACOPAV

Class	Lower limit	Upper limit
T7	0	50
T6	50	150
T5	150	300
T4	300	500
T3	500	800
T2	800	1200
T1	1200	2000
T0	2000	

The roughness pavement performance for each climate zone and for the mean of the four climate zone is defined in Table 5.14 and Table 5.15, respectively for the thin and thick structure. Figure 5.20 shows the corresponding IRI growth along the pavement design period.

Table 5.14 – Roughness pavement performance considered for D-class of the Swedish model

Climate zone	IRI initial median	IRI yearly change	IRI yearly change 90p	IRI yearly change 10p
1	1.68	0.06	0.25	0.01
2	1.86	0.06	0.28	0.01
3	1.52	0.10	0.32	0.02
4	1.62	0.07	0.25	0.02
Mean	1.67	0.07	0.28	0.02

Table 5.15 – Roughness pavement performance considered for G-class of the Swedish model

Climate zone	IRI initial median	IRI yearly change	IRI yearly change 90p	IRI yearly change 10p
1	1.20	0.03	0.15	0.01
2	1.25	0.04	0.18	0.01
3	1.19	0.05	0.18	0.01
4	1.30	0.07	0.22	0.02
Mean	1.24	0.05	0.18	0.01

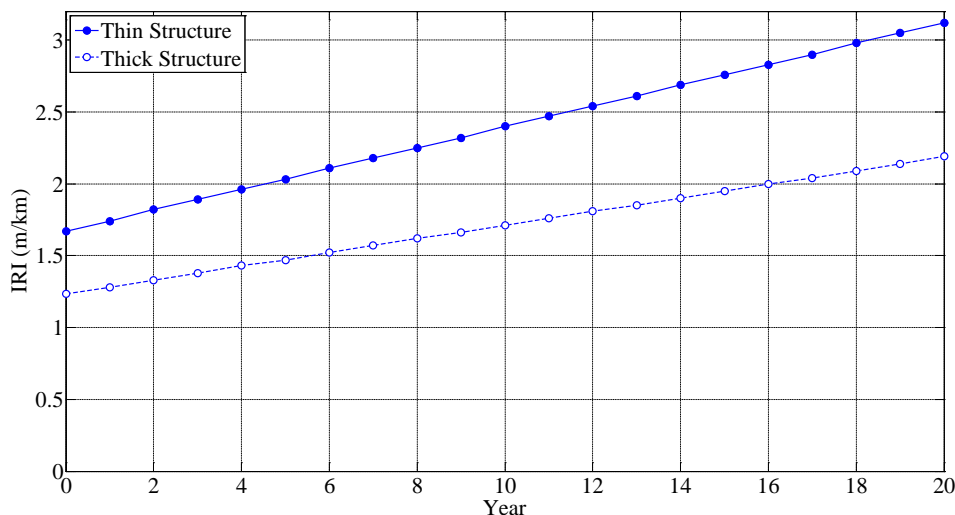


Figure 5.20 - Evolution of IRI in accordance with the prediction model of the Swedish PMS

5.5 LOAD PROFILES

The road profiles generated on the previous section were used as input in the vehicle simulations carried out by using the TruckSIM[®] computer software. This work considers the following variables in vehicle simulation:

- Two trucks: F1-Truck and H5-Truck;
- Eight payload weights resulting trucks: fully loaded; empty; underloaded by 10, 20 and 30%; and overloaded by 10, 20 and 30%;
- Four travel speeds: 40, 60, 80 and 100 km/h;
- Six roughness levels: IRI equal to 0, 1, 2, 3, 4 and 5 m/km.

The values of the variables were chosen to cover a broad range of situations. The two trucks represent, as already mentioned, the majority of the trucks in the Portuguese truck traffic fleet

nowadays. With the eight payloads, empty trucks, not fully loaded trucks and overloaded trucks up to 30% can be simulated, allowing the creation of truck traffic flows with different load factors. The four travel speeds were chosen in order to consider roads with different categories (main road, secondary road, national road and so on) as well as the fact that some truck classes can run more in a determined road category than in others. In relation to the roughness levels, some of them are theoretical mainly because they are referred to being initial profiles. However, as already mentioned, IRI values from 1.2 to 5.9 m/km (average value: 2.5 m/km) have been found in the Portuguese road network during pavement condition evaluations (Luz 2011).

Therefore a total of 384 TruckSIM® simulations were performed, one for each combination of these variables. In each run, a load profile for each axle of the simulated truck is obtained. As an example, Figure 5.21 shows the axle load profiles of the H5-Truck running fully loaded at 80 km/h over a road profile with IRI equal to 2 m/km. The red line depicted in this figure represents the 85th percentile that corresponds to the load used in this work.

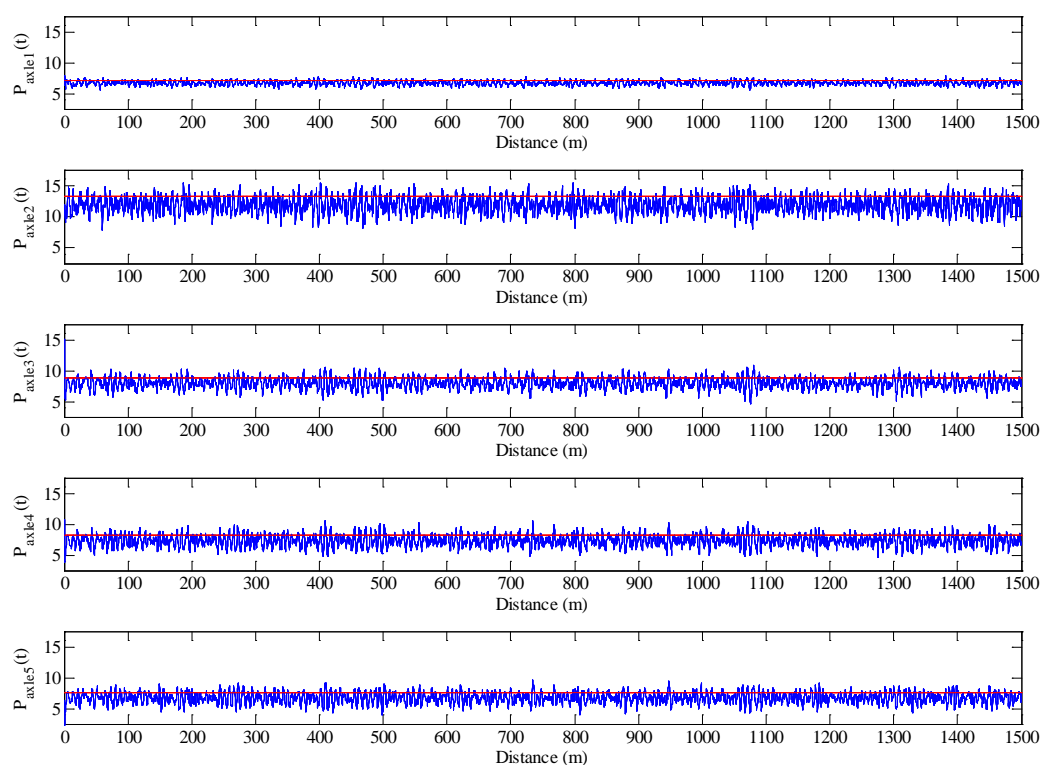


Figure 5.21 – Load profiles for each axle of a H5-Truck running fully loaded at 80 km/h over a road profile with IRI equal to 2 m/km

The loads of each axle are statistically analysed by a multiple linear regression technique, defining hence a regression model that explains the variation of the axle loads in terms of the road roughness, the travel speed and the truck GVW. The analysis of variance (ANOVA) provides a statistical test (usually the F-test) for the significance of the regression model (at least one independent variable affects the dependent variable) and for the significance of each independent variable on the model (each dependent variable has significant impact on the dependent variable). The significance of the regression is justified by comparing the regression F-value with the predetermined F-value based on the significance level (the 5% significance level was chosen). If the probability of the regression F-value is equal or greater than the predetermined F-value, at least one independent variable contributes to the variation in the dependent variable. When the significance of the regression is justified, a multiple linear regression model relating the variables can be formed and the significance of the each

independent variable assessed by the t-test. The t-value is the ratio of the coefficient of the independent variable to its standard error. Similarly to the F-value, the t-value is used to assess the significance of each independent variable.

A regression model to estimate axle loads was obtained for each axle of the simulated trucks. To illustrate, Figure 5.22 shows the ANOVA's summary output for the axle 1 of the 'H5-Truck'. The travel speed (V) is the least significant variable. Every regression and independent variable passes the respective significance test. Table 5.16 presents the regression models. The trucks' GVW values for the considered payloads are defined in Table 5.17.



Regression Statistics	
Multiple R	1.00
R Square	1.00
Adjusted R Square	0.9972
Standard Error	0.0482
Observations	192

ANOVA					
	DOF	Sum of Squares	Mean Square	F	Significance F
Regression	3	159.7066	53.2355	22868.56793	1.2062E-240
Residual	188	0.4376	0.0023		
Total	191	160.1442			

	Coefficients	Standard Error	t Stat	P-value	Lower 95%	Upper 95%	Lower 95.0%	Upper 95.0%
Intercept	3.376E+00	1.68E-02	200.76	2.7798E-221	3.34E+00	3.41E+00	3.34E+00	3.41E+00
IRI	1.352E-01	2.04E-03	66.30	2.4333E-132	1.31E-01	1.39E-01	1.31E-01	1.39E-01
V	8.244E-04	1.56E-04	5.29	3.31411E-07	5.17E-04	1.13E-03	5.17E-04	1.13E-03
GVW	7.740E-02	3.06E-04	253.34	3.3096E-240	7.68E-02	7.80E-02	7.68E-02	7.80E-02


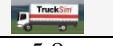
Figure 5.22 – ANOVA's summary output for the axle 1 of the 'H5-Truck'

Table 5.16 – Regression models for the axle loads

Truck	Axle	Regression model	R ²
	1	Axle Load = $3.376 + 1.352 \times 10^{-1} \cdot \text{IRI} + 8.244 \times 10^{-4} \cdot V + 7.740 \times 10^{-2} \cdot \text{GVW}$	1.00
	2	Axle Load = $4.764 \times 10^{-1} + 2.866 \times 10^{-1} \cdot \text{IRI} + 7.999 \times 10^{-3} \cdot V + 2.686 \times 10^{-1} \cdot \text{GVW}$	1.00
	3	Axle Load = $-1.587 + 1.707 \times 10^{-1} \cdot \text{IRI} + 3.711 \times 10^{-3} \cdot V + 2.266 \times 10^{-1} \cdot \text{GVW}$	1.00
	4	Axle Load = $-1.892 + 1.760 \times 10^{-1} \cdot \text{IRI} + 4.821 \times 10^{-3} \cdot V + 2.219 \times 10^{-1} \cdot \text{GVW}$	1.00
	5	Axle Load = $-2.007 + 1.651 \times 10^{-1} \cdot \text{IRI} + 4.201 \times 10^{-3} \cdot V + 2.152 \times 10^{-1} \cdot \text{GVW}$	1.00
	1	Axle Load = $1.505 + 1.465 \times 10^{-1} \cdot \text{IRI} + 1.394 \times 10^{-3} \cdot V + 3.181 \times 10^{-1} \cdot \text{GVW}$	0.96
	2	Axle Load = $-1.599 + 2.404 \times 10^{-1} \cdot \text{IRI} + 4.219 \times 10^{-3} \cdot V + 6.710 \times 10^{-1} \cdot \text{GVW}$	0.99

Axle load in tonnes, IRI in m/km, V in km/h and GVW in tonnes.

Table 5.17 – Trucks' GVW values in tonnes

Payload		
Empty	14.0	5.8
Underloaded by 30%	28.0	13.3
Underloaded by 20%	32.0	15.2
Underloaded by 10%	36.0	17.1
Fully loaded	40.0	19.0
Overloaded by 10%	44.0	20.9
Overloaded by 20%	48.0	22.8
Overloaded by 30%	52.0	24.7

In order to characterize the simulated dynamic axle loads, DLCs were calculated. Figure 5.23, Figure 5.24 and Figure 5.25 present the variation of the DLCs as a function of the travel speed, the IRI-value and the truck's GVW, respectively, for the axles of the H5-Truck's tractor, the

axles of the H5-Truck's semi-trailer and the axles of the F1-Truck. DLCs increase with travel speed and road roughness and decrease with the truck's GVW.

Despite the empty trucks have the smallest GVW, the variation in the dynamic load of them is the largest, except for the first axle of both trucks, which can be explained by the location of the first axle, it carries mainly the tractor weight (constant) instead of the semi-trailer weight (variable with the payload weight). However, although heavier trucks present less variation in the dynamic load, they have higher dynamic loads.

These results are in agreement with results from the literature. For example, the Dynamic Interaction between Vehicles and Infrastructure Experiment (DIVINE) Project (OECD, 1998) refers that when a truck moves along a pavement its load is not steady but can vary between 10 and 40 per cent above or below the static load, depending on the type of suspension, GVW, travel speed and road profile.

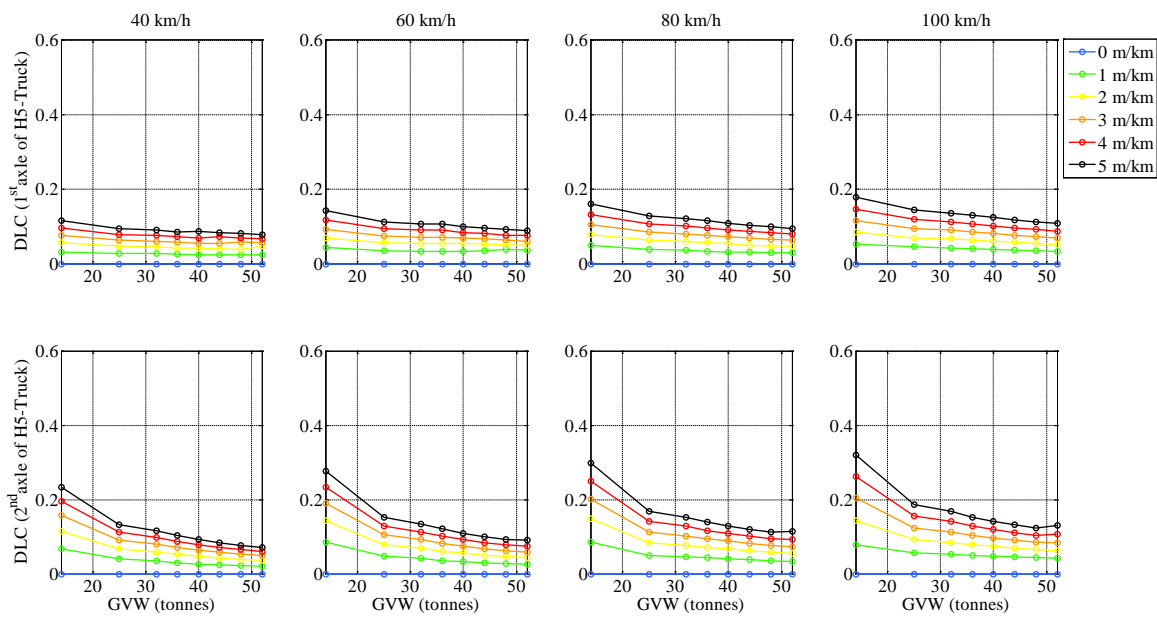


Figure 5.23 - DLCs for the axles of the H5-Truck's tractor

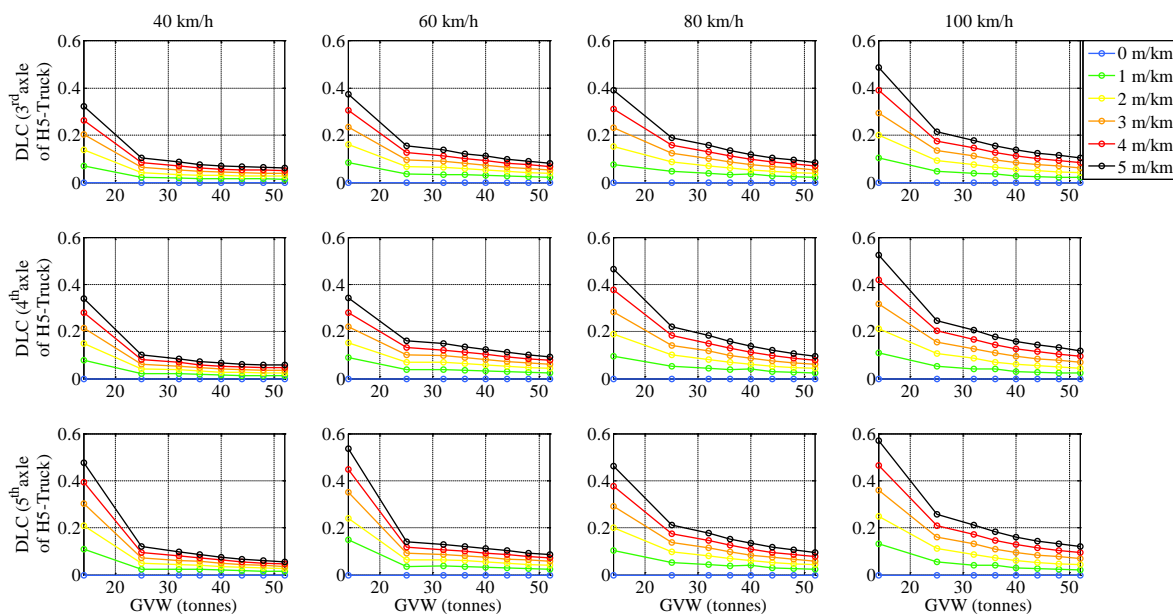


Figure 5.24 - DLCs for the axles of the H5-Truck's semi-trailer

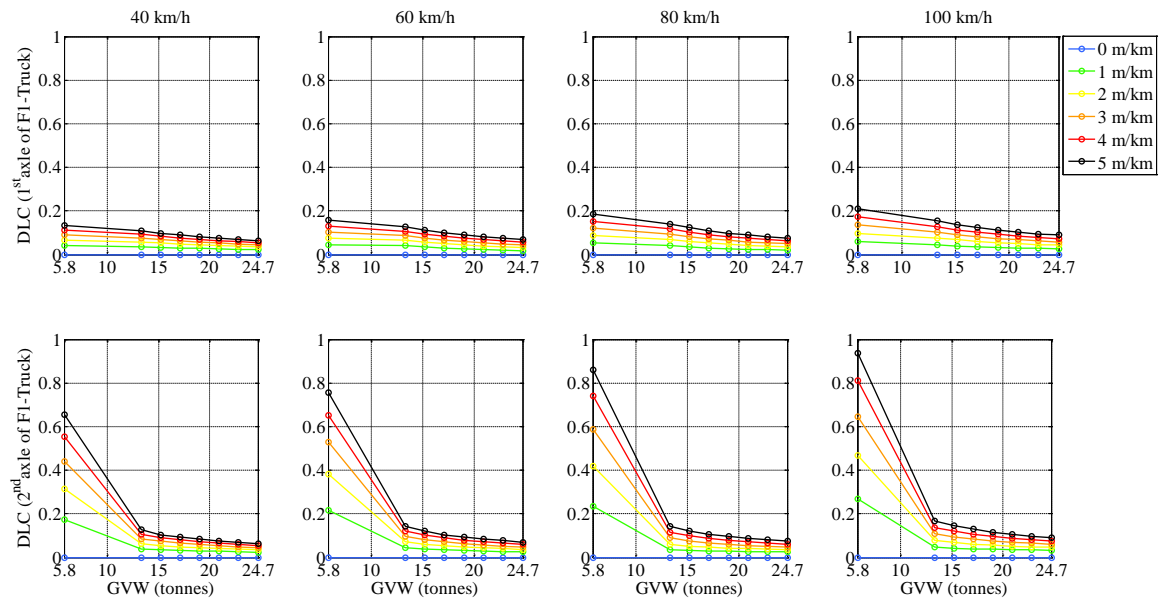


Figure 5.25 – DLCs for the axles of the F1-Truck

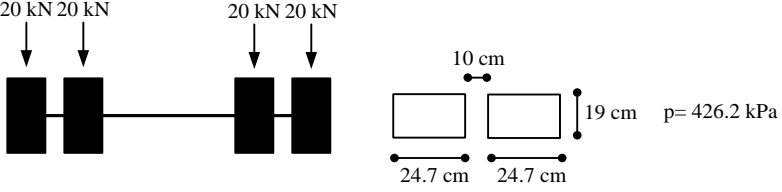
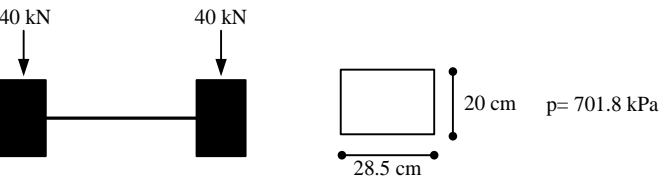
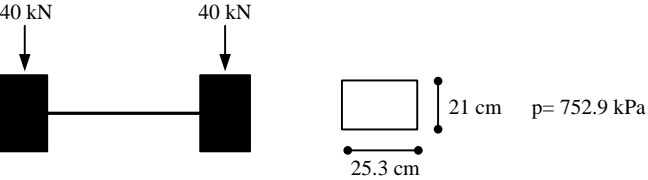
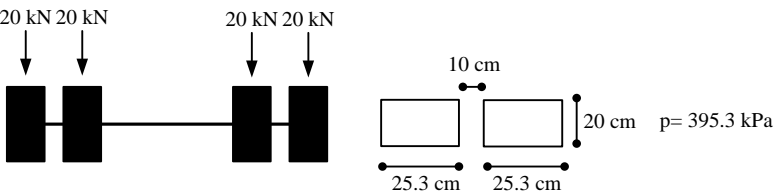
5.6 EALFs OF THE SIMULATED TRUCKS' AXLES

The EALFs are calculated theoretically by using equations (2.23) and (2.24), respectively, for the fatigue design criterion and for the rutting design criterion. They depend on the axle load, the pavement structure and the AC modulus (travel speed).

In order to understand how the tyre-pavement contact area, both the shape and the dimension, affects EALFs, EALFs were calculated for the simulated trucks' axles considering an 80-kN axle load. Table 5.18 depicts these tyre-pavement contact areas as well as the tyre-pavement contact area of the ESAL. Figure 5.26 presents the calculated EALFs.

Table 5.18 - Tyre-pavement contact area for the simulated trucks' axles considering an 80-kN axle load

<p>ESAL</p>	<p>20 kN 20 kN 20 kN 20 kN</p> <p>$R = 0.1050 \text{ m}$ $L = 0.105 \text{ m}$ $p = 577.4 \text{ kPa}$</p>
<p>H5-Truck Axle 1 315/80R22.5 single</p>	<p>40 kN 40 kN</p> <p>23 cm $p = 704.1 \text{ kPa}$ 24.7 cm</p>

<p>H5-Truck Axle 2 315/80R22.5 dual</p>	
<p>H5-Truck Axle 3, 4 or 5 385/65R22.5 single</p>	
<p>F1-Truck Axle 1 315/70R22.5 single</p>	
<p>F1-Truck Axle 2 315/70R22.5 dual</p>	

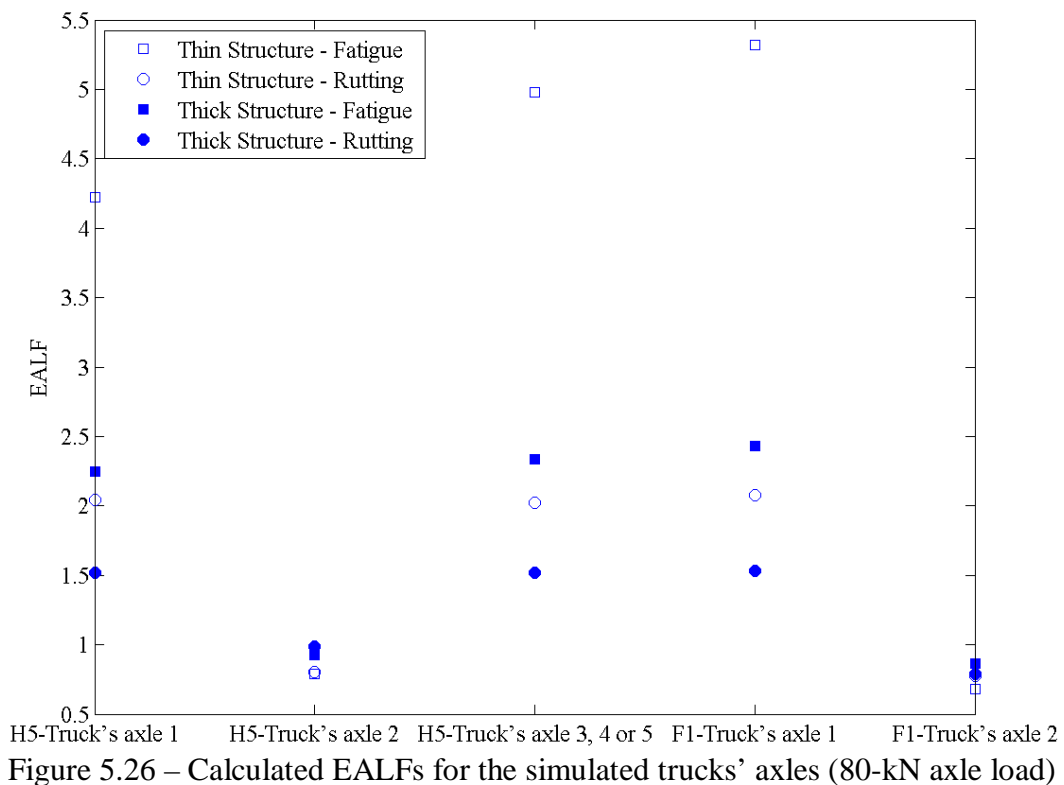


Figure 5.26 shows that EALFs are greatly influenced by the tyre type. The axles equipped with dual tyres have much lower EALFs than the axles equipped with single tyres. The location of the critical pavement response has also a great influence. There is a greater EALFs dispersion for the fatigue design criterion, because, as it is a distress closer pavement surface, it is more influenced by the tyre-pavement contact area. When the critical pavement response is far from the axle load application, as happens in the rutting design criterion, there is a prevalence of the magnitude of the axle load in detriment of the tyre-pavement contact area. Finally, the pavement structure and the characteristics of its materials also influence EALFs. For the thin structure, the AC modulus corresponding to a travel speed equal to 60 km/h was considered (4942 MPa). While for the thick structure, the AC modulus corresponding to a travel speed equal to 80 km/h was considered (6229 MPa). These two travel speeds were defined to consider two roads with different categories, i.e. the thin structure corresponds to a road with lower category than the road corresponding to the thick structure. Consequently, the travel speeds were chosen to match the current average speed for the two types of roads.

In order to better understand the effect of single or dual tyres on EALFs, an 80-kN non-standard axle load (single tyre) was considered. It has the same contact pressure as the 80-kN standard axle load (dual tyre) (or ESAL) (Figure 5.27). The EALFs for this axle are the following: 2.1 for both the thin structure and the fatigue design criterion, 1.6 for both the thin structure and the rutting design criterion, 2.0 for both the thick structure and the fatigue design criterion and 1.4 for both the thick structure and the rutting design criterion.

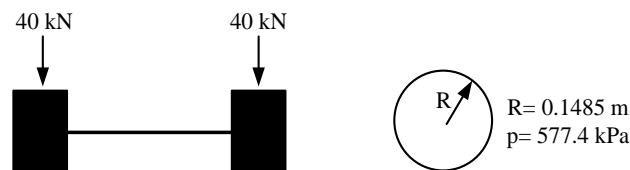


Figure 5.27 - 80-kN non-standard axle load

5.7 AGGRESSIVENESS FACTORS (AFs)

As previously stated, the MACOPAV (JAE, 1995) presents AFs for different traffic classes (Table 2.6) which are used to estimate the expected number of ESAL applications over the pavement design period. Then, the pavement damage is calculated by dividing the expected number of ESAL applications by the allowable number of ESAL applications. The allowable numbers of ESAL applications are calculated by using the transfer functions (2.11) and (2.14), for the fatigue design criterion and the rutting design criterion, respectively. Table 5.19 presents both the fatigue pavement damage and the rutting pavement damage calculated considering the MACOPAV's AFs.

The damage values are lower than one, essentially in the thick structure, suggesting that the MACOPAV overdesigns the pavement structures. However, this is not true as the used AC moduli are higher than the AC modulus indicated in the MACOPAV (4000 MPa). Using the AC modulus of 4000 MPa, the pavement damage is one (see Table 5.20).

Table 5.19 – Pavement damage

Pavement structure	Travel speed (km/h)	AC modulus (MPa)	Allowable number of ESAL applications to prevent fatigue	Allowable number of ESAL applications to prevent rutting	Expected number of ESAL applications	Fatigue damage	Rutting damage
Thin	40	4470	3,151,410	2,093,684	1,961,537	0.622	0.937
	60	4942	3,499,056	2,379,527		0.561	0.824
	80	5306	3,784,787	2,615,349		0.518	0.750
	100	5606	4,028,293	2,816,111		0.487	0.697
Thick	40	5327	225,524,283	193,078,480	106,207,845	0.471	0.550
	60	5837	264,998,271	234,227,588		0.401	0.453
	80	6229	298,304,514	269,392,018		0.356	0.394
	100	6550	327,211,849	299,740,640		0.325	0.354

Table 5.20 – Pavement damage (AC modulus equal to 4000 MPa)

Pavement structure	Allowable number of ESAL applications to prevent fatigue	Allowable number of ESAL applications to prevent rutting	Expected number of ESAL applications	Fatigue damage	Rutting damage
Thin	2,831,623	3,381,869	2,942,306	1.039	0.870
Thick	139,045,214	198,593,874	132,759,806	0.955	0.668

The pavement damage is closely related to the expected number of ESAL applications which in turn it is closely related to the AF. A 20 per cent variation (above and below) in the AF leads with variations of the pavement damage in the range of 0.83 to 1.25. Since this variation affects pavement life, a better definition of AFs is extremely important for pavement design.

The MACOPAV’s AFs represent the aggressiveness of a mixed truck traffic flow. This aggressiveness can be calculated from the knowledge of the AFs of each truck in the mixed truck traffic flow.

This work uses vehicle simulation (TruckSIM[®]) to calculate the AFs of the trucks. From vehicle simulation, axle load profiles are obtained which are then used to calculate theoretical EALFs. By summing all the EALFs of each simulated truck, trucks’ AFs are determined.

Trucks’ AFs are calculated for two pavement structures (thin and thick), two design criteria (fatigue and rutting), two trucks (F1 and H5), four travel speeds (40, 60, 80 and 100 km/h), six road profiles (0, 1, 2, 3, 4 and 5 m/km) and eight payload weights (fully loaded; empty; underloaded by 10, 20 and 30%; and, overloaded by 10, 20 and 30%). Therefore, a total of 1536 AFs were calculated.

Figure 5.28 and Figure 5.29 show the F1-Truck’s AFs and the H5-Truck’s AFs, respectively, for the thin structure. Figure 5.30 and Figure 5.31 show the same but for the thick structure.

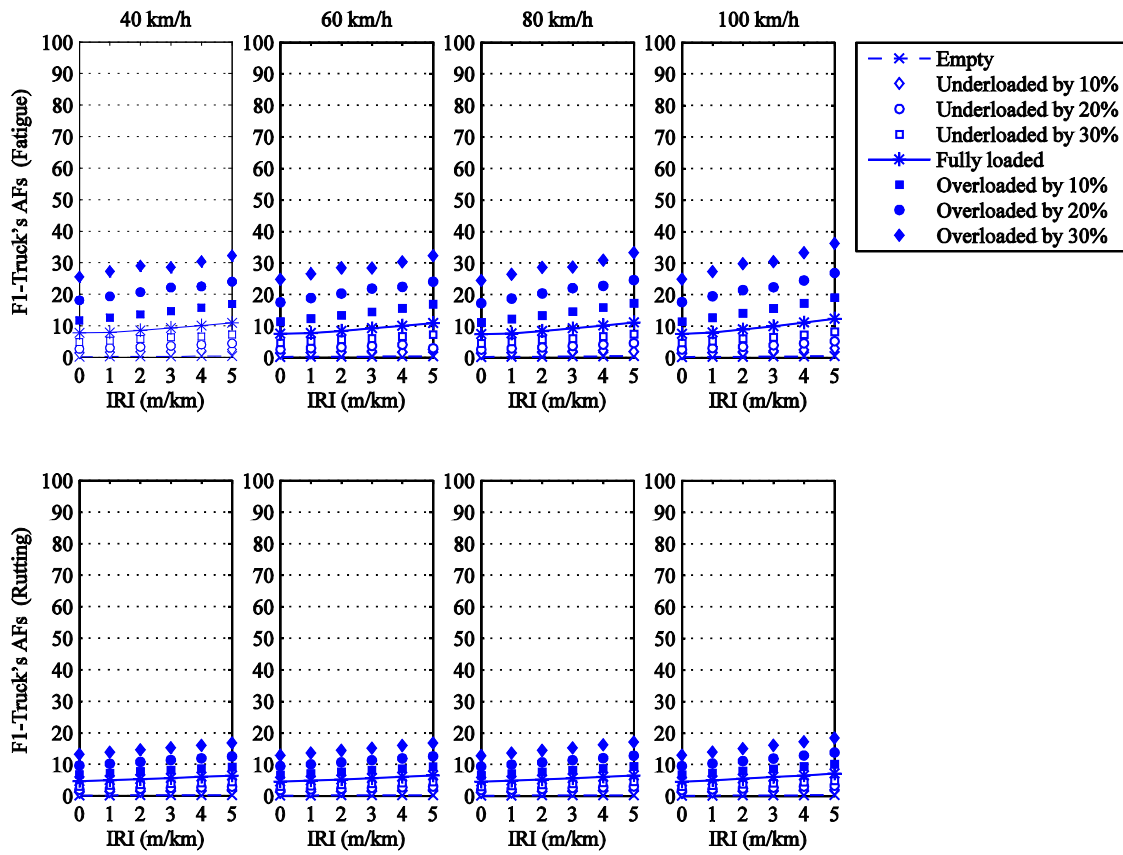


Figure 5.28 – F1-Truck’s AFs for the thin structure

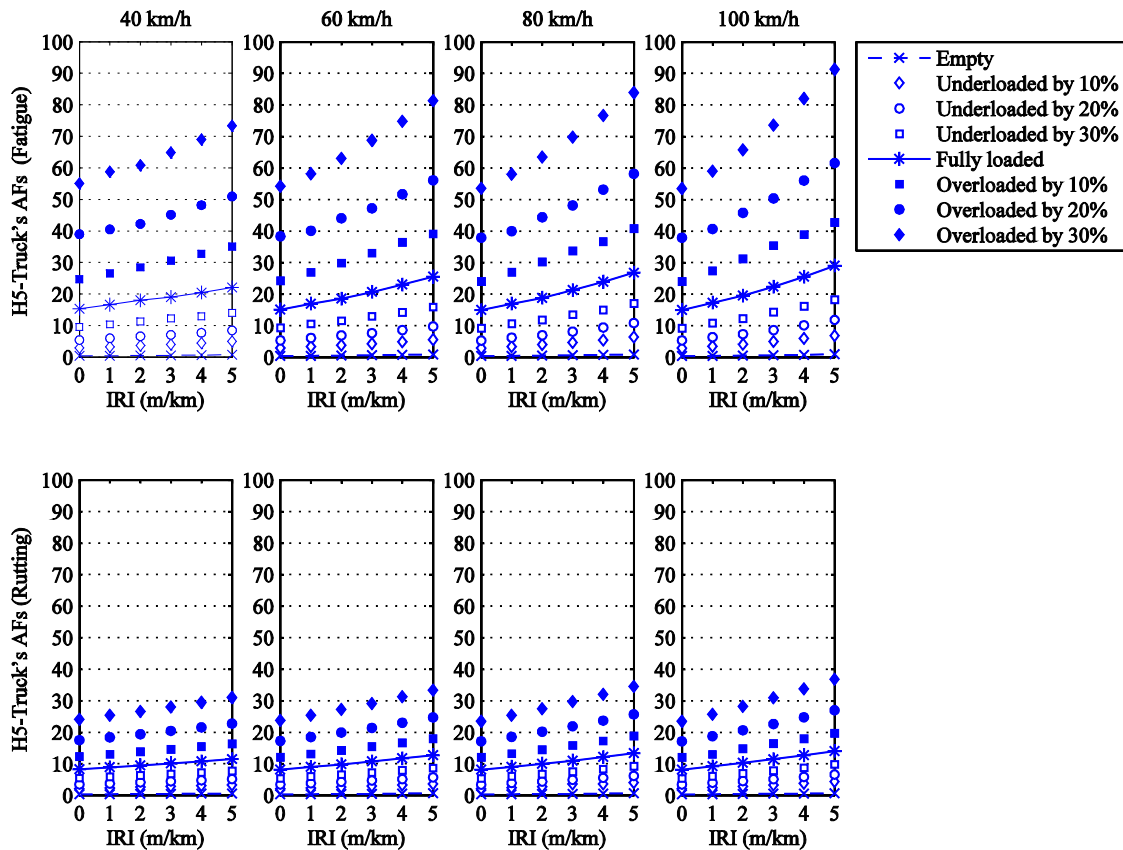


Figure 5.29 – H5-Truck’s AFs for the thin structure

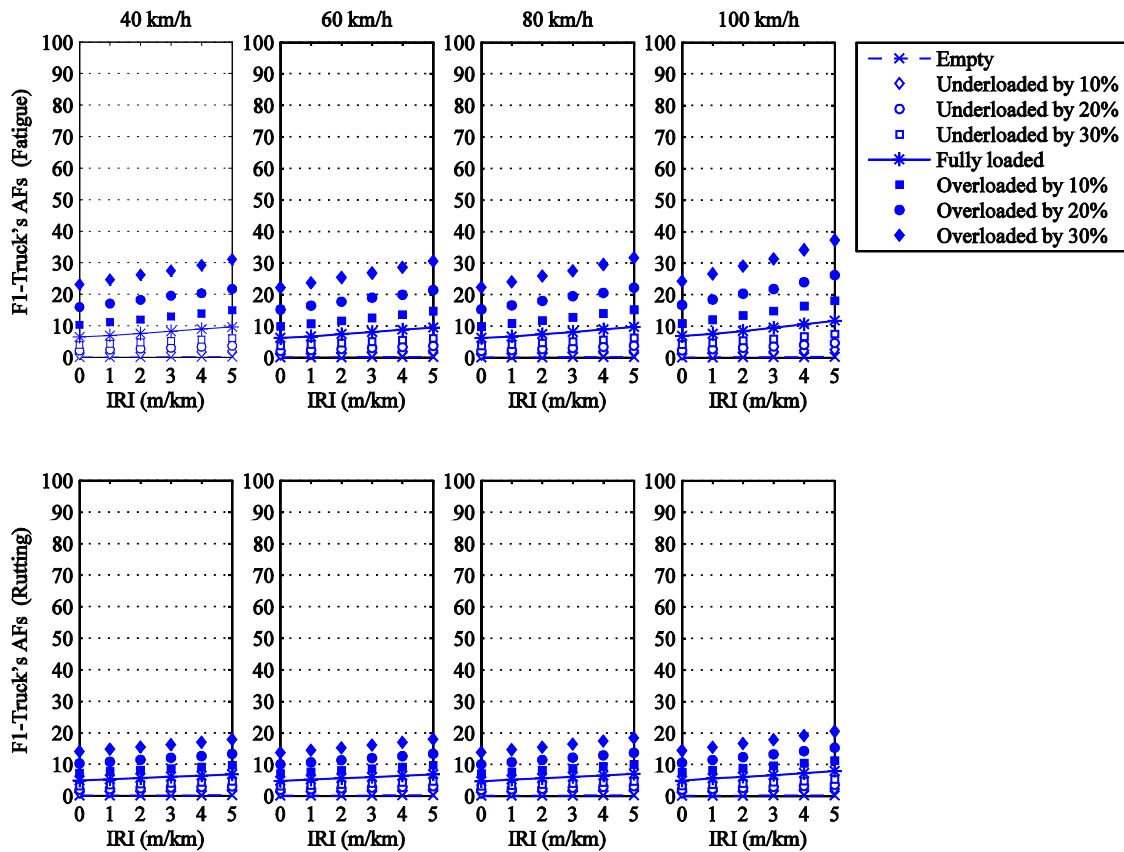


Figure 5.30 – F1-Truck's AFs for the thick structure

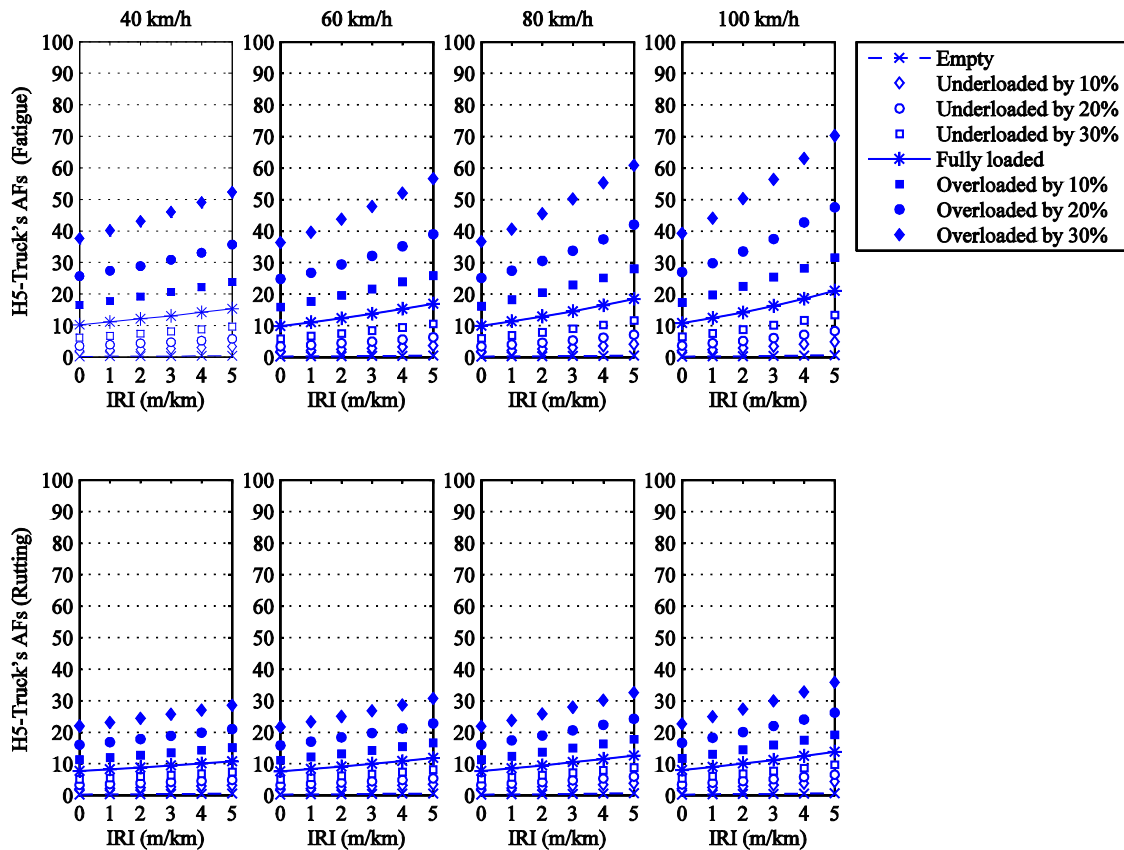


Figure 5.31 – H5-Truck's AFs for the thick structure

It is clear from Figure 5.28 to Figure 5.31 that AFs increases with increases in the IRI value and in the truck's GVW. The travel speed has a lower effect on the AFs. In terms of design criteria, the AFs for the fatigue criterion are greater than those for the rutting criteria, in average 1.8 times for the thin structure and 1.3 times for the thick structure. These differences can be explained by the location of the critical pavement responses, nearer the pavement surface for the fatigue criteria. However, despite those differences, the determining design criterion can be either the rutting criterion or the fatigue criterion, depending on the allowable number of ESAL applications to prevent rutting and to prevent fatigue. The allowable number of ESAL applications to prevent rutting is lower than that the one to prevent fatigue, about 1.5 times for the thin structure and 1.1 times for the thick structure.

If all axles had the same tyre-pavement contact area, which implied that all the axles in a truck were equipped with the same tyre and that the tyre-pavement contact area length was always the same, the ratio of the AF for a GVW_1 to the AF for a GVW_2 would be equal to the ratio of the GVW_1 to the GVW_2 powered to the transfer function exponent (equal to 5 for fatigue design criterion (equation (2.11)) and equal to 4 for the rutting design criterion (equation (2.14))). As the axles in a truck are not equipped with the same tyre and the tyre-pavement contact area length depends on the axle load, the ratio of the AF for a GVW_1 to the AF for a GVW_2 is only roughly equal to the ratio of the GVW_1 to the GVW_2 powered to the transfer function exponent. Nevertheless, the magnitude of the AFs is greatly influenced by the truck configuration and the design criterion.

As the knowledge of AFs allows pavement damage calculations, regression analysis were performed. Nonlinear regression analysis was selected because AFs vary linearly with IRI-value and exponentially with truck's GVW. To perform this type of analysis, the Statistic Package for Social Science (SPSS) was employed (IBM, 2012). Equation (5.4) was achieved with good R-squared values. Although nonlinear, it is a simple equation.

Table 5.21 presents the regression coefficients and the R-squared values for the thin structure while Figure 5.32 depicts the calculated versus the predicted values. Since the effect of travel speed on AFs is lower than the effect of the other variables, regression coefficients are calculated as the average of the four travel speeds. Table 5.22 and Figure 5.33 show the same but for the thick structure.

$$AF = (a + b \cdot IRI) \cdot e^{c \cdot GVW} \quad (5.4)$$

where

- AF = aggressiveness factor of the truck (no dimensional)
- IRI = international roughness index of the road (m/km)
- GVW = gross vehicle weight of the truck (tonnes) (defined in Table 5.17)
- a, b and c = model parameters

From the results, the '(a and c)-regression coefficients' are only slightly affected by the truck speed. In turn, the truck speed affects the '(b)-regression coefficient' which, as expected, increases with increases in the truck speed.

Up to this point, AFs have been calculated considering both the initial AC modulus and the initial IRI value during the pavement design period. However, AFs can be influenced by the AC modulus degradation and the roughness growth during the pavement design period.

Since the AFs are calculated as a ratio of strains, the calculated ones considering the AC modulus degradation during the design period are similar to those calculated considering the initial AC modulus during the design period. Nevertheless, this is not the case with the damage. The consideration of AC modulus degradation during the pavement design period leads to an increase in damage because the maximum number of ESAL applications decreases although the expected number of ESAL applications is more or less the same.

Table 5.21 – Regression coefficients and R-squared values for the thin structure

Truck speed	Regression data	F1-Truck		H5-Truck	
		Fatigue	Rutting	Fatigue	Rutting
40 km/h	a	0.165	0.147	0.254	0.241
	b	0.010	0.009	0.018	0.015
	c	0.204	0.182	0.104	0.089
	R ²	0.993	0.996	0.997	0.997
60 km/h	a	0.157	0.147	0.264	0.252
	b	0.011	0.010	0.028	0.023
	c	0.205	0.181	0.102	0.087
	R ²	0.993	0.996	0.996	0.996
80 km/h	a	0.154	0.144	0.275	0.265
	b	0.012	0.010	0.034	0.028
	c	0.205	0.182	0.101	0.086
	R ²	0.993	0.996	0.997	0.997
100 km/h	a	0.166	0.151	0.270	0.261
	b	0.017	0.014	0.040	0.032
	c	0.203	0.180	0.101	0.086
	R ²	0.994	0.996	0.997	0.997
All travel speeds	a	0.160	0.148	0.266	0.254
	b	0.012	0.010	0.030	0.025
	c	0.204	0.181	0.102	0.087
	R ²	0.991	0.992	0.991	0.991

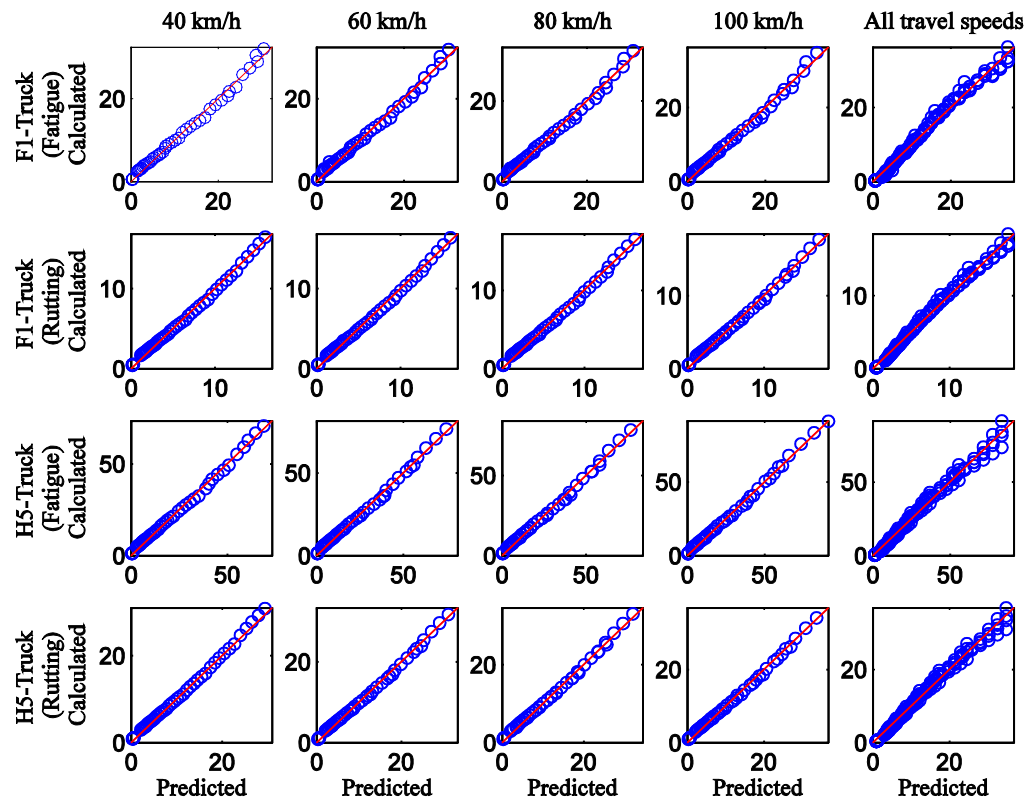


Figure 5.32 – Calculated versus predicted AFs for the thin structure

Table 5.22 – Regression coefficients and R-squared values for the thick structure

Truck speed	Regression data	F1-Truck		H5-Truck	
		Fatigue	Rutting	Fatigue	Rutting
40 km/h	a	0.108	0.150	0.147	0.235
	b	0.008	0.009	0.012	0.015
	c	0.217	0.184	0.107	0.087
	R ²	0.996	0.996	0.998	0.997
60 km/h	a	0.107	0.15	0.147	0.243
	b	0.009	0.01	0.017	0.022
	c	0.216	0.183	0.106	0.086
	R ²	0.996	0.993	0.998	0.997
80 km/h	a	0.103	0.144	0.154	0.257
	b	0.009	0.011	0.022	0.027
	c	0.217	0.185	0.105	0.085
	R ²	0.997	0.996	0.998	0.996
100 km/h	a	0.12	0.157	0.162	0.261
	b	0.014	0.015	0.027	0.033
	c	0.215	0.183	0.105	0.085
	R ²	0.996	0.996	0.998	0.997
All travel speeds	a	0.111	0.151	0.152	0.249
	b	0.010	0.010	0.020	0.025
	c	0.216	0.184	0.106	0.086
	R ²	0.190	0.191	0.191	0.192

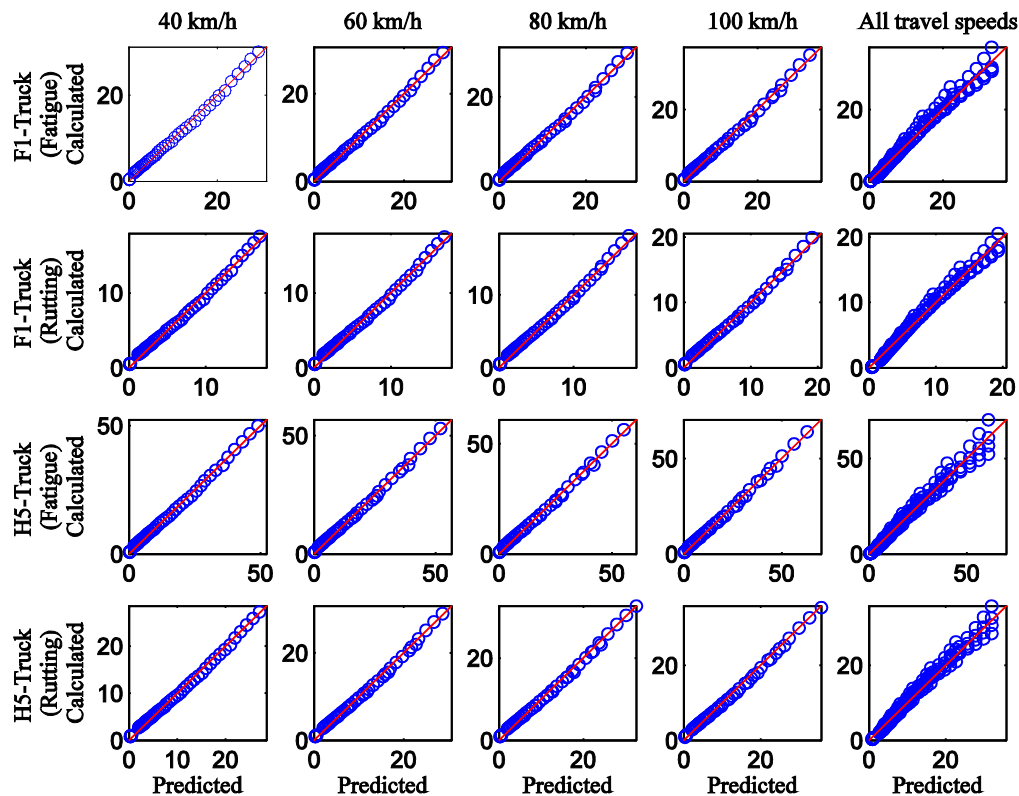


Figure 5.33 – Calculated versus predicted AFs for the thick structure

To consider roughness growth according to Figure 5.20, new simulations were carried out since rougher profiles lead to higher (dynamic) axle loads. Figure 5.34 and Figure 5.35 show the resulting AFs for the thin structure and for the thick structure, respectively. In addition, the AFs calculated considering the initial IRI value during the pavement design period are illustrated. To distinguish the roughness growth situation, the term '(G)' is used.

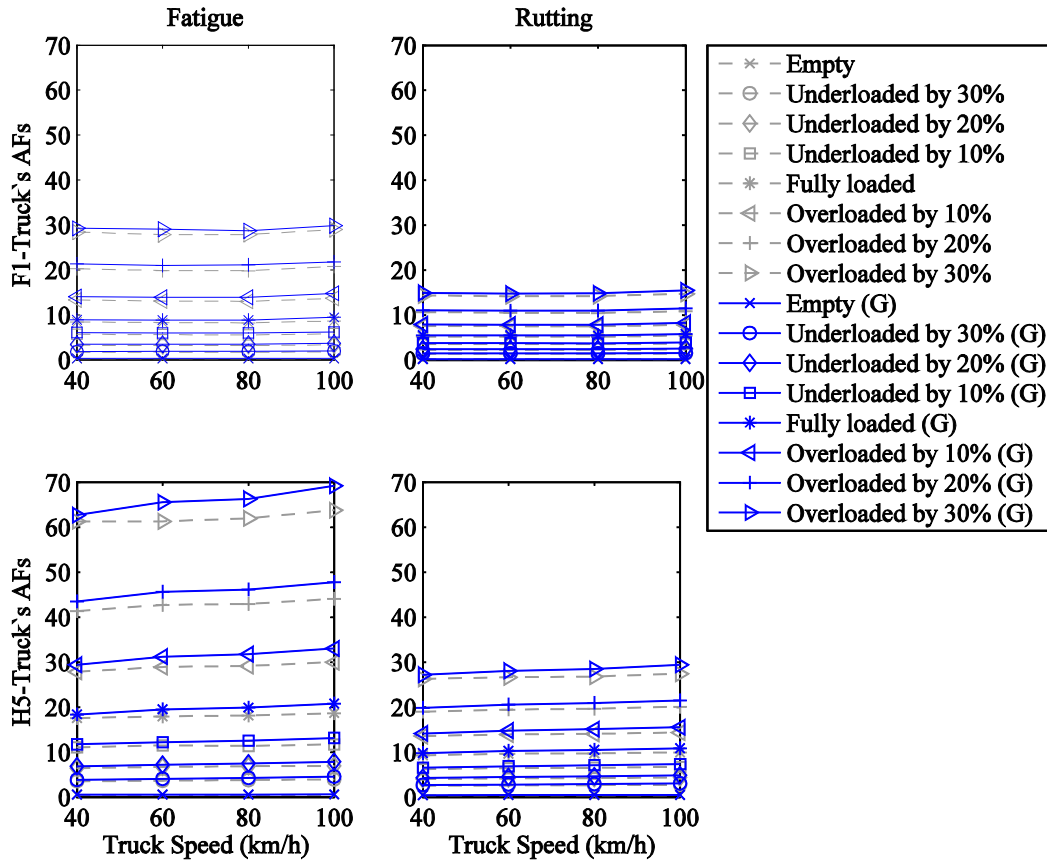


Figure 5.34 – AFs for the thin structure considering roughness growth

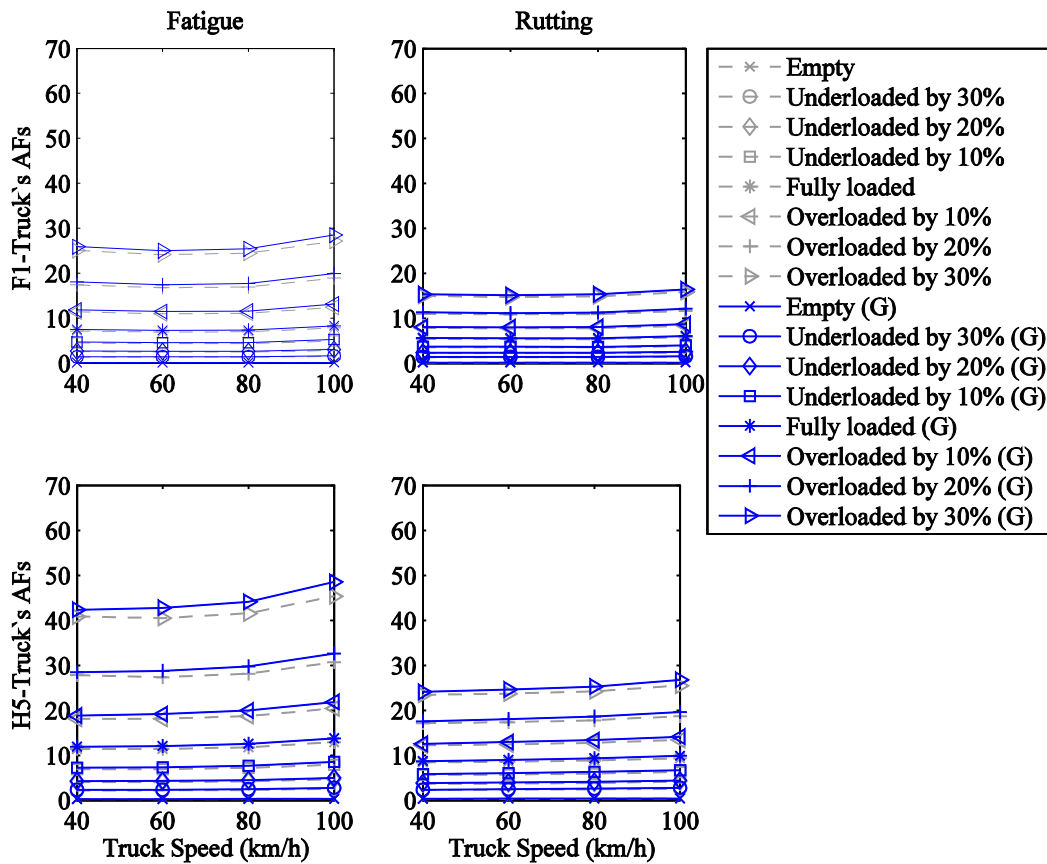


Figure 5.35 – AFs for the thick structure considering roughness growth

Similarly, regression analyses were performed using SPSS. As in this situation just one IRI value is considered (1.67 m/km for the thin structure and 1.24 m/km for the thick structure), the equation (5.5) was considered. Table 5.23 presents the regression coefficients and the R-squared values for the thin structure while the Figure 5.36 depicts the calculated versus the predicted values. Since the effect of travel speed on AFs is less important, regression coefficients are again calculated as the average of the four travel speeds. Table 5.24 and Figure 5.37 show the same but for the thick structure.

$$AF = a \cdot e^{b \cdot GVW} \quad (5.5)$$

where

- AF = aggressiveness factor of the truck (no dimensional)
- GVW = gross vehicle weight of the truck (tonnes) (defined in Table 5.17)
- a and b = model parameters

The IRI growth can increase the AFs up to 19%. The highest AF values correspond to both the highest truck speed and to the lowest truck's GVW, and it decreases with decreases in truck speed and increases in truck's GVW.

Table 5.23 – Regression coefficients and the R-squared values for the thin structure considering IRI growth

Truck speed	Regression data	F1-Truck		H5-Truck	
		Fatigue	Rutting	Fatigue	Rutting
40 km/h	a	0.172	0.164	0.295	0.272
	b	0.209	0.183	0.103	0.089
	R ²	0.995	0.996	0.997	0.997
60 km/h	a	0.168	0.167	0.322	0.297
	b	0.21	0.182	0.103	0.088
	R ²	0.996	0.996	0.997	0.997
80 km/h	a	0.174	0.163	0.341	0.315
	b	0.208	0.183	0.102	0.087
	R ²	0.995	0.996	0.997	0.997
100 km/h	a	0.193	0.177	0.354	0.325
	b	0.205	0.182	0.102	0.087
	R ²	0.998	0.996	0.997	0.997
All travel speeds	a	0.176	0.167	0.327	0.302
	b	0.208	0.183	0.102	0.088
	R ²	0.993	0.992	0.992	0.991

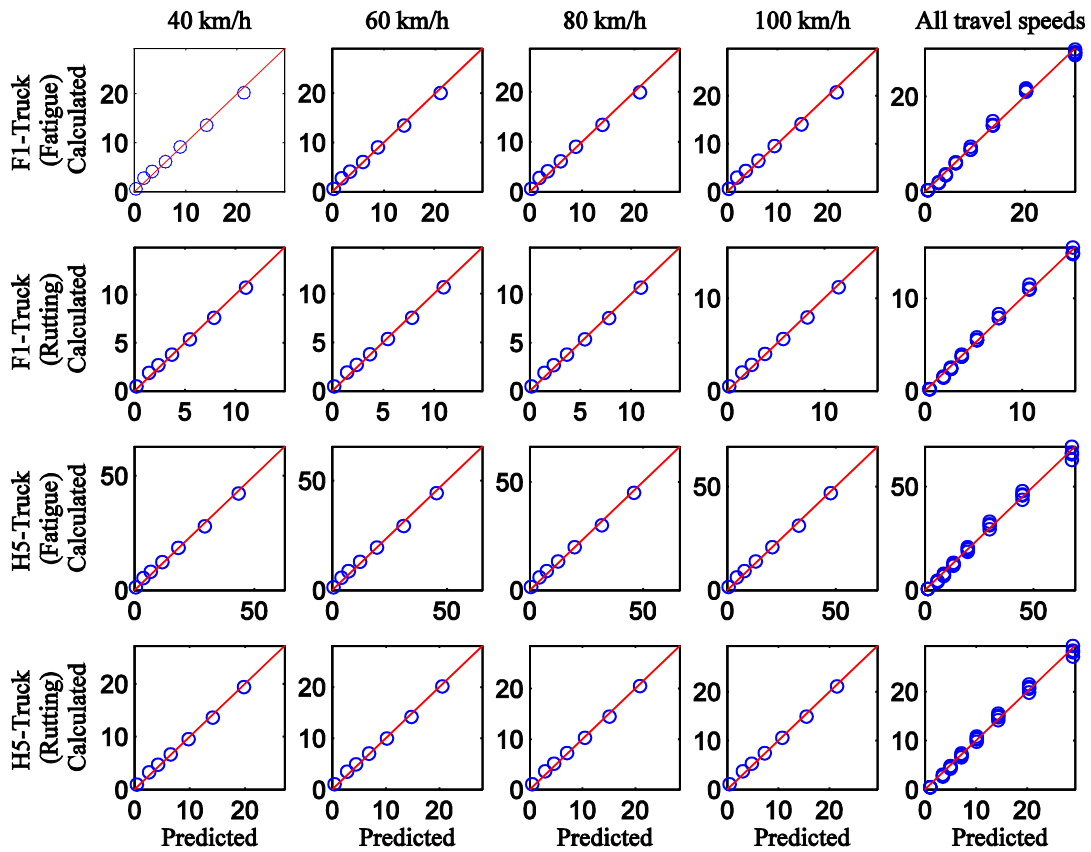


Figure 5.36 – Calculated versus predicted AFs for the thin structure (IRI growth)

Table 5.24 – Regression coefficients and the R-squared values for the thick structure considering IRI growth

Truck speed	Regression data	F1-Truck		H5-Truck	
		Fatigue	Rutting	Fatigue	Rutting
40 km/h	A	0.110	0.155	0.157	0.246
	b	0.222	0.187	0.108	0.088
	R ²	0.997	0.996	0.998	0.997
60 km/h	a	0.110	0.156	0.161	0.261
	b	0.221	0.186	0.108	0.088
	R ²	0.997	0.996	0.998	0.997
80 km/h	a	0.107	0.152	0.174	0.279
	b	0.222	0.188	0.107	0.087
	R ²	0.997	0.996	0.998	0.997
100 km/h	a	0.127	0.169	0.191	0.297
	b	0.220	0.186	0.107	0.087
	R ²	0.997	0.996	0.998	0.997
All travel speeds	a	0.113	0.159	0.172	0.272
	b	0.222	0.187	0.108	0.088
	R ²	0.991	0.992	0.991	0.992

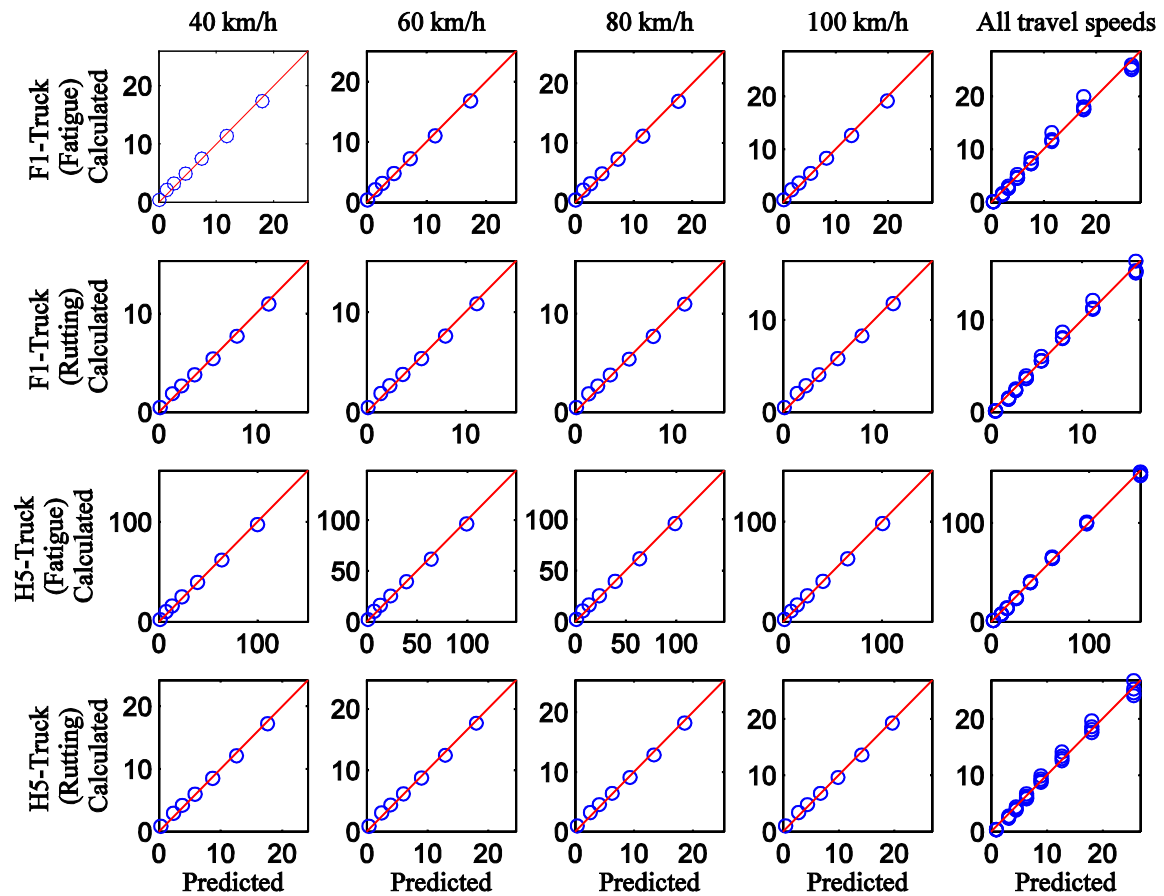


Figure 5.37 – Calculated versus predicted AFs for the thick structure (IRI growth)

5.8 THE THREE LEVELS OF THE STUDY APPROACH

5.8.1 Introduction

Once the load profiles and the AFs are defined, the steps of each one of the three levels of the study approach are described. As has already been mentioned, depending on the level, the pavement designers have more or less flexibility in the pavement design. From level (1) to (3) the pavement design becomes easier although less flexible.

5.8.2 Loads per axle

In this level (level (1) of page 135), the pavement designers use regression models like the presented in Table 5.16. Then, knowing the loads per axle, the following calculations are carried out:

- i. Calculation of the critical pavement response for each design criterion;
- ii. Calculation of the EALF of each axle for each design criterion;
- iii. Calculation of the expected number of passes of each axle;
- iv. Calculation of the expected number of ESAL applications for each design criterion;
- v. Calculation of the allowable number of ESAL applications for each design criterion;
- vi. Calculation of pavement damage for each design criterion.

This level can be applied to any pavement structure and any design criterion.

5.8.3 AFs of the trucks

In this level (level (2) of page 136), the pavement designers use regression models like the expressed by the equation (5.4) or the equation(5.5). Then, knowing the AFs of the trucks, the following calculations are carried out:

- i. Calculation of the expected number of passes of each truck;
- ii. Calculation of the expected number of ESAL applications for each design criterion;
- iii. Calculation of the allowable number of ESAL applications for each design criterion;
- iv. Calculation of pavement damage for each design criterion.

This level can only be applied to the pavement structures and the design criteria considered in the definition of the regression models.

5.8.4 'Damage' Application

In order to account for the AC modulus degradation and the roughness growth over the pavement design period, an incremental procedure was implemented, (level (3) of page 136), using the Visual Basic computer program (VB.NET[®]). This procedure divides the pavement design period (20 years) into a number of time increments (1 year).

For each time increment, a road profile is generated. The road profile is then used as input in the TruckSIM[®] software, obtaining hence load profiles for each axle of each truck. After that, the critical pavement responses are calculated by the Boundary Element Method (BEM) for each axle load, considering the respective tyre-pavement contact area. Next, a theoretical EALF is calculated for each axle load, each pavement structure and each design criterion.

Knowing the EALFs and the expected number of passes of each axle, the number of ESAL applications is calculated for each design criterion. At the end of each time increment, the pavement damage is calculated for each design criterion and subsequently both the AC modulus and IRI-value are updated.

This process goes on until the end of the pavement design period. In addition, this procedure must be able to consider different percentages of trucks on truck traffic flow as well as different payload weights and travel speeds. Figure 5.38 shows the interface of the 'Damage' Application and Figure 5.39 shows the flowchart of this incremental procedure.

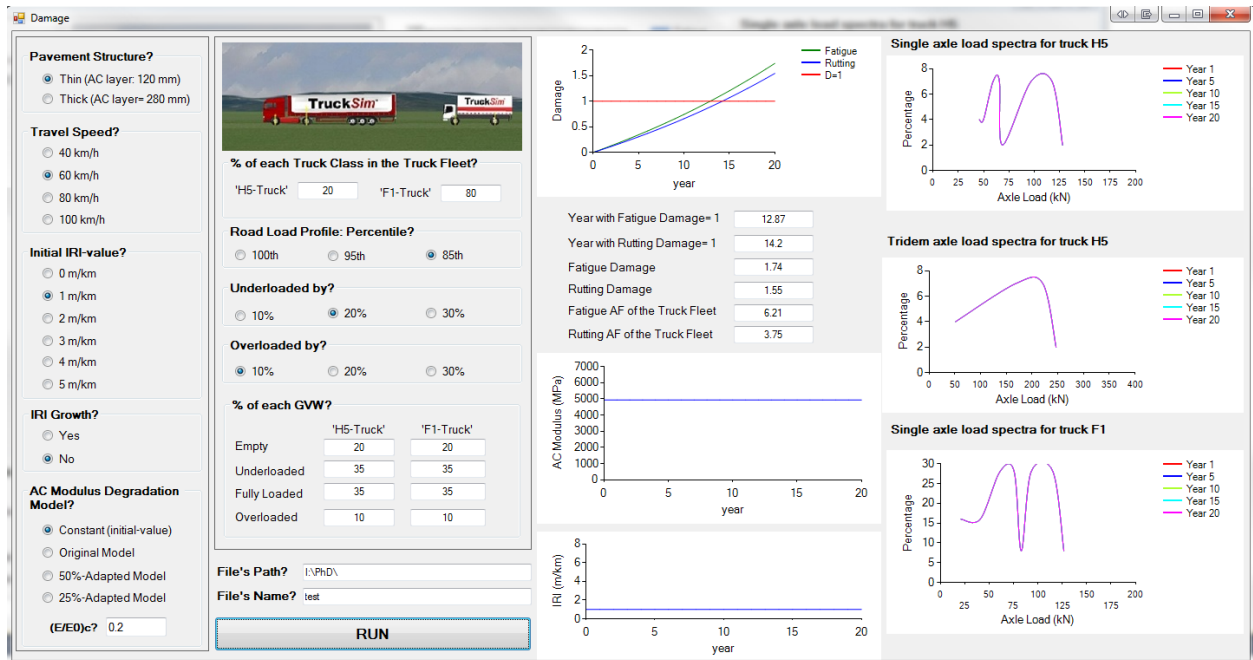


Figure 5.38 - Interface of the 'Damage' application

As can be seen, the interface shows the progression of the pavement damage (both fatigue and rutting), the degradation of the AC modulus and IRI growth over the pavement design period. The axle load spectra of the considered truck traffic flow are also illustrated.

This application can be easily extended to other truck classes (configurations), to other pavement structures and to other design criteria.

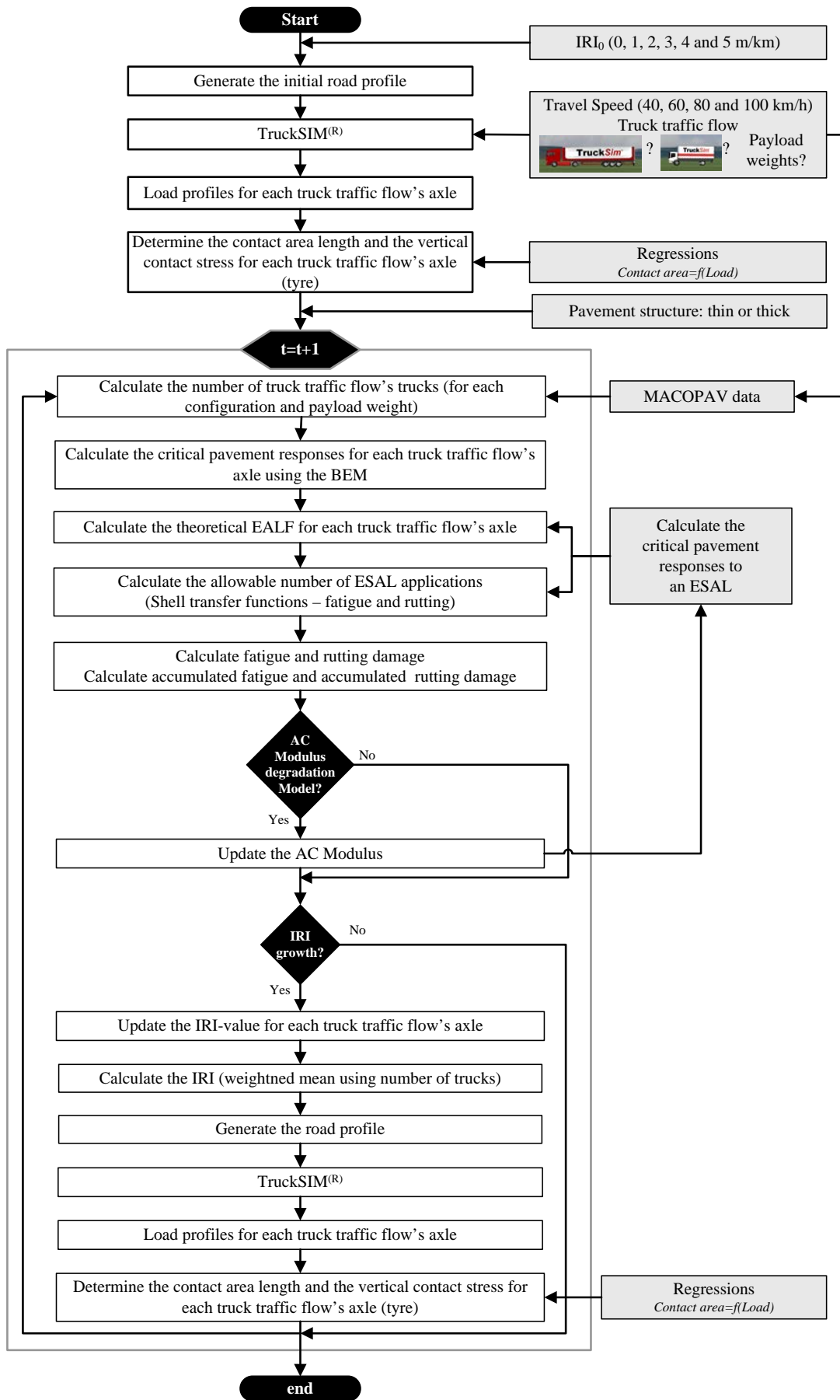


Figure 5.39 – Flowchart of the incremental procedure

5.9 REFERENCES

- Cebon, D. (1999). *Handbook of Vehicle-Road Interaction*. Taylor & Francis.
- Collop, A. C. and Cebon, D. (1996). Stiffness Reductions of Flexible Pavements due to Cumulative Fatigue Damage. *Journal of Transportation Engineering*, 122, 131-139.
- COST 334 (2001). *Effects of Wide Single Tyres and Dual Tyres (Final report of the Action - version 29 November 2001 Taskgroup 3 Final Report)*. European Commission, Directorate General Transport. Belgium.
- ERD@ (2011). ERD file format. <http://www.umtri.umich.edu/divisionPage.php?pageID=118>. Access date: 27 June 2011.
- Glaeser, K.-P. (2010). Performance of Articulated Vehicles and Road Trains Regarding Road Damage and Load Capacity. *11th International Symposium on Heavy Vehicle Transportation Technology*, Australia.
- Harris, N. K., Gonzalez, A., Obrien, E. J. and McGetrick, P. (2010). Characterisation of pavement profile heights using accelerometer readings and a combinatorial optimisation technique. *Journal of Sound and Vibration*, 329, 497-508.
- IBM (2012). SPSS Statistics. <http://www-01.ibm.com/software/analytics/spss/products/statistics/>. Access date: April 12, 2013.
- ISO 8608 (1995). Mechanical vibration - Road surface profiles - Reporting of measured data. International Organization for Standardization (ISO).
- JAE (1995). *Manual de Concepção de Pavimentos para a Rede Rodoviária Nacional (Pavement Design Manual for the Portuguese Road Network)*. JAE (Junta Autónoma de Estradas). In Portuguese.
- Lang, J. M. (2001). Prediction Model in Swedish PMS. *5th International Conference on Managing Pavements*, Seattle, Washington, USA.
- Luz, S. d. S. (2011). Contribuição para a Modelação do Índice de Qualidade na Caracterização da Rede Rodoviária Nacional (Contribution to the Quality Index Model in the Description of the National Road Network). Master Thesis, Universidade Técnica de Lisboa. In Portuguese.
- MATLAB@ (2012). MATLAB - The Language Of Technical Computing. <http://www.mathworks.com/products/matlab/>. Access date: 25 January 2012.
- NCHRP (2004). *MEPDG - Guide for Mechanistic-Empirical Design of New and Rehabilitated Pavement Structures*. NCHRP (National Cooperative Highway Research Program), Transportation Research Board, National Research Council.
- Ngwangwa, H. M., Heyns, P. S., Labuschagne, F. J. J. and Kululanga, G. K. (2010). Reconstruction of road defects and road roughness classification using vehicle responses with artificial neural networks simulation. *Journal of Terramechanics*, 47, 97-111.
- OECD (1998). *Dynamic Interaction between Vehicles and Infrastructure Experiment (DIVINE)*. Organisation for Economic Co-operation and Development (OECD). Paris, France. DSTI/DOT/RTR/IR6(98)1/FINAL.

ProVAL@ (2011). <http://www.roadprofile.com/>. Access date: 27 June 2011.

Shell (1988). *Shell pavement design method, BISAR-PC user manual*. Shell International Petroleum Company Limited.

6 CASE STUDIES AND RESULTS

6.1 INTRODUCTION

The application of the three level-hierarchical study approach, described in the previous chapter, requires the definition of the mixed truck traffic flow over the pavement design period. This implies the specification of the truck configurations, the percentage of each truck configuration, and the Gross Vehicle Weights (GVW) in each truck configuration. This work considers the two truck configurations defined in the previous chapter. They are the ‘H5-Truck’ and the ‘F1-Truck’.

Since the percentage of each truck configuration depends on the road category, different percentages are considered for the thin and the thick structure. The payload weights were established taking into account both the European empty running values and the European load factor values presented in Chapter 2, Figure 2.22 and Figure 2.23, respectively.

Further to the definition of a representative mixed truck traffic flow for Portugal (‘baseline’ case study), another mixed truck traffic flow was defined with the intention of quantify the impact of some transport policies on the pavement damage. Attending to the efficiency of freight transport as answer to the environmental pressures, this works shows the effect of the reduction in empty running on the pavement damage (‘empty running’ case study).

Once the case studies were defined, the calculation of the pavement damage is exemplified for each level of the study approach. This exemplification is only done for the ‘baseline’ case study and when both the initial Asphalt Concrete (AC) modulus and the initial IRI-value are constant over the entire pavement design period.

After that, the third level of the three level-study approach (‘Damage’ application) is applied to analyse pavement damage evolution over the pavement design period, quantifying hence the effect of AC modulus degradation, roughness growth and empty running reduction on pavement damage.

The pavement damage is quantified for both pavement structures (thin and thick) and for both design criteria (fatigue and rutting).

6.2 DEFINITION OF THE CASE STUDIES

6.2.1 Introduction

As had already been mentioned, two case studies are defined. One of them, called ‘baseline’ case study, aims to represent a Portuguese mixed truck traffic flow while the other one, called ‘empty running’ case study, aims to illustrate how the study approach can be applied to analyse the effects of some transport policies on pavement damage.

The ‘empty running’ case study was chosen because nowadays there is a growing concern about environmental issues where truck traffic plays an important role. A more efficient transport

system can be achieved, for example, by increasing the load factors and decreasing the empty running. This has impacts on the pavement damage which ought to be quantified.

6.2.2 ‘Baseline’ case study

As the percentage of truck configurations (classes - Table 2.1) differs between roads, depending on its road category (main road, secondary road, national road and so on), a ‘baseline’ case study is defined for each pavement structure.

Table 6.1 lists the percentage of different classes (configurations) of trucks for two roads, a national road in the Viseu region and a main road in the Lisbon region. These percentages were obtained from five-yearly traffic data (2005- Annual Average Daily Traffic (AADT)).

Table 6.1 - Percentage of different classes of trucks for two roads with different category

Class	National Road	Main Road
F	63%	27%
G	11%	2%
H	7%	66%
I	8%	5%
J+K	10%	0%

Consequently, in addition to consider a different number of trucks for each pavement structure, different percentages for each truck configuration are also considered. For instance, the thin structure is subjected to fewer ‘H5-Trucks’ than the thick structure. Moreover, the trucks on the thin structure, associated to a road with lower speed limit, run slower than the trucks on the thick structure.

Therefore, the thin structure is subjected to a number of trucks corresponding to the T6-traffic class of the MACOPAV (JAE, 1995) while the thick structure is subjected to a number of trucks corresponding to the T1-traffic class. On the other hand, the trucks on the thin structure run at a travel speed equal to 60 km/h while the trucks on the thick structure run at a travel speed equal to 80 km/h.

Within each truck configuration percentage, the same distribution was considered: 20% of empty trucks, 35% of underloaded by 20% trucks, 35% of fully loaded trucks and 10% of overloaded by 10% trucks.

Figure 6.1 and Figure 6.2 illustrate the ‘baseline’ case study for the thin structure and for the thick structure, respectively.

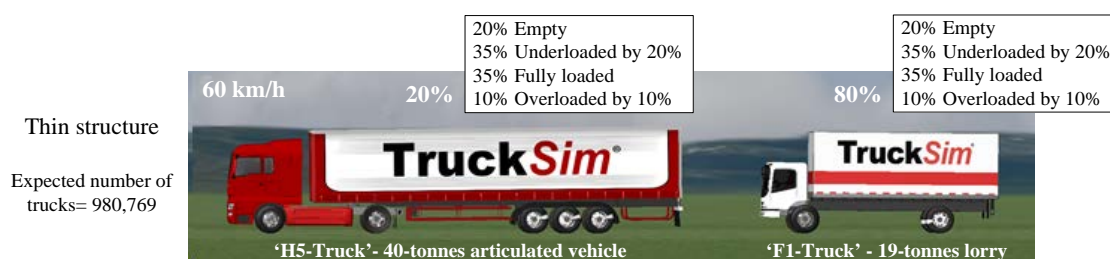


Figure 6.1 – ‘Baseline’ case study for the thin structure

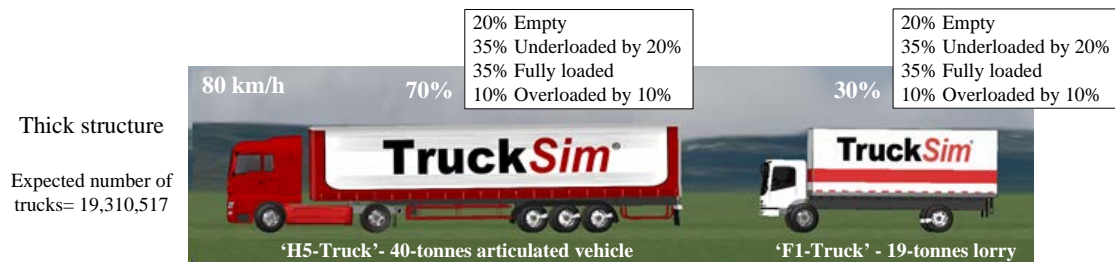


Figure 6.2 – ‘Baseline’ case study for the thick structure

The load factors of the ‘baseline’ case studies were calculated. Table 6.2 and Table 6.3 present these loads factors, for the ‘baseline’ case study of the thin structure and for the ‘baseline’ case study of the thick structure, respectively.

Table 6.2 – Load factor for the thin structure

		Payload weights				Load factor (in mass)
		Empty	Underloaded by 20%	Fully loaded	Overloaded by 10%	
		20%	35%	35%	10%	
H5-Truck	20%	0.0	18.0	26.0	30.0	0.712
F1-Truck	80%	0.0	9.4	13.2	15.1	

Table 6.3 - Load factor for the thick structure

		Payload weights				Load factor (in mass)
		Empty	Underloaded by 20%	Fully loaded	Overloaded by 10%	
		20%	35%	35%	10%	
H5-Truck	70%	0.0	18.0	26.0	30.0	0.709
F1-Truck	30%	0.0	9.4	13.2	15.1	

The defined percentages result in load factors which are in accordance with the European average load factor (0.70) – see Figure 2.23.

6.2.3 ‘Empty running’ case study

In order to quantify the effect of the reduction in empty running on pavement damage, six empty percentages were considered (25%, 20%, 15%, 10%, 5% and 0%). Some of these percentages, the lowest ones, are theoretical because there are situations where it is impossible to find a return load. It is particularly difficult for tank trucks.

The percentage of ‘H5-Trucks’ and ‘F1-Trucks’ is the same as the defined in the ‘baseline’ case study, only varying the percentage of underloaded trucks and fully loaded trucks. Table 6.4 defines the empty running percentages as well as the corresponding load factors.

Table 6.4 – Definition of the empty running percentages and corresponding load factors

No.	Empty	Underloaded by 20%	Fully loaded	Overloaded by 10%	Thin structure’s load factor	Thick structure’s load factor
1	25.0%	32.5%	32.5%	10.0%	0.670	0.667
2	20.0%	35.0%	35.0%	10.0%	0.712	0.709
3	15.0%	37.5%	37.5%	10.0%	0.755	0.752
4	10.0%	40.0%	40.0%	10.0%	0.798	0.794
5	5.0%	42.5%	42.5%	10.0%	0.841	0.837
6	0.0%	45.0%	45.0%	10.0%	0.883	0.879

6.3 AGGRESSIVENESS FACTORS (AFs) AND PAVEMENT DAMAGE CALCULATION USING THE THREE LEVEL-STUDY APPROACH

6.3.1 Introduction

In this section, AFs of the mixed truck traffic flow and pavement damage are calculated using the three level-study approach. For that, the regression models developed in the previous chapter as well as the developed application ('Damage' application) are used.

6.3.2 Level 1 – Study approach (Loads per axle)

The axle loads are calculated by using the regression models presented in Table 5.16. Table 6.5 presents the resulting axle loads.

Table 6.5 – Calculated axle loads

IRI (m/km)	Thin structure (60 km/h)							Thick structure (80 km/h)						
	Empty							Empty						
	H5-Truck					F1-Truck		H5-Truck					F1-Truck	
	axle 1	axle 2	axle 3	axle 4	axle 5	axle 1	axle 2	axle 1	axle 2	axle 3	axle 4	axle 5	axle 1	axle 2
0	4.51	4.72	1.81	1.50	1.26	3.43	2.55	4.53	4.88	1.88	1.60	1.34	3.46	2.63
1	4.64	5.00	1.98	1.68	1.42	3.58	2.79	4.66	5.16	2.05	1.78	1.51	3.61	2.87
2	4.78	5.29	2.15	1.86	1.59	3.73	3.03	4.80	5.45	2.22	1.95	1.67	3.75	3.11
3	4.91	5.58	2.32	2.03	1.75	3.87	3.27	4.93	5.74	2.39	2.13	1.84	3.90	3.35
4	5.05	5.86	2.49	2.21	1.92	4.02	3.51	5.07	6.02	2.57	2.30	2.00	4.05	3.59
5	5.19	6.15	2.66	2.38	2.08	4.17	3.75	5.20	6.31	2.74	2.48	2.17	4.19	3.83
IRI (m/km)	Underloaded by 20%							Underloaded by 20%						
	H5-Truck					F1-Truck		H5-Truck					F1-Truck	
	axle 1	axle 2	axle 3	axle 4	axle 5	axle 1	axle 2	axle 1	axle 2	axle 3	axle 4	axle 5	axle 1	axle 2
0	5.90	9.55	5.89	5.50	5.13	6.42	8.85	5.92	9.71	5.96	5.59	5.22	6.45	8.94
1	6.04	9.84	6.06	5.67	5.30	6.57	9.09	6.05	10.00	6.13	5.77	5.38	6.60	9.18
2	6.17	10.12	6.23	5.85	5.46	6.72	9.33	6.19	10.28	6.30	5.95	5.55	6.74	9.42
3	6.31	10.41	6.40	6.03	5.63	6.86	9.57	6.32	10.57	6.47	6.12	5.71	6.89	9.66
4	6.44	10.70	6.57	6.20	5.79	7.01	9.81	6.46	10.86	6.64	6.30	5.88	7.04	9.90
5	6.58	10.98	6.74	6.38	5.96	7.16	10.06	6.59	11.14	6.81	6.47	6.04	7.18	10.14
IRI (m/km)	Fully loaded							Fully loaded						
	H5-Truck					F1-Truck		H5-Truck					F1-Truck	
	axle 1	axle 2	axle 3	axle 4	axle 5	axle 1	axle 2	axle 1	axle 2	axle 3	axle 4	axle 5	axle 1	axle 2
0	6.52	11.70	7.70	7.27	6.85	7.63	11.40	6.54	11.86	7.77	7.37	6.94	7.66	11.49
1	6.66	11.99	7.87	7.45	7.02	7.78	11.64	6.67	12.15	7.94	7.55	7.10	7.81	11.73
2	6.79	12.27	8.04	7.63	7.18	7.93	11.88	6.81	12.43	8.12	7.72	7.27	7.95	11.97
3	6.93	12.56	8.21	7.80	7.35	8.07	12.12	6.94	12.72	8.29	7.90	7.43	8.10	12.21
4	7.06	12.85	8.38	7.98	7.51	8.22	12.36	7.08	13.01	8.46	8.07	7.60	8.25	12.45
5	7.20	13.13	8.55	8.15	7.68	8.37	12.61	7.21	13.29	8.63	8.25	7.76	8.39	12.69
IRI (m/km)	Overloaded by 10%							Overloaded by 10%						
	H5-Truck					F1-Truck		H5-Truck					F1-Truck	
	axle 1	axle 2	axle 3	axle 4	axle 5	axle 1	axle 2	axle 1	axle 2	axle 3	axle 4	axle 5	axle 1	axle 2
0	6.83	12.77	8.61	8.16	7.71	8.24	12.68	6.85	12.93	8.68	8.26	7.80	8.26	12.76
1	6.97	13.06	8.78	8.34	7.88	8.38	12.92	6.98	13.22	8.85	8.43	7.96	8.41	13.00
2	7.10	13.35	8.95	8.51	8.04	8.53	13.16	7.12	13.51	9.02	8.61	8.13	8.56	13.24
3	7.24	13.63	9.12	8.69	8.21	8.68	13.40	7.25	13.79	9.19	8.79	8.29	8.70	13.48
4	7.37	13.92	9.29	8.86	8.37	8.82	13.64	7.39	14.08	9.36	8.96	8.46	8.85	13.72
5	7.51	14.21	9.46	9.04	8.54	8.97	13.88	7.52	14.37	9.53	9.14	8.62	9.00	13.96

Then, the critical pavement responses are calculated for each axle load as well as for an Equivalent Standard Axle Load (ESAL). From these critical pavement responses, theoretical Equivalent Axle Load Factors (EALFs) are calculated for each axle, each pavement structure and

for design criterion. Table 6.6 and Table 6.7 present the obtained results, respectively for the fatigue design criterion and for the rutting design criterion. To simplify, the lengths of the tyre-pavement contact areas were kept constant. They correspond to an axle load of 80 kN. The variation of the tyre-pavement contact area length was only considered with the ‘Damage’ application.

Table 6.6 – Theoretical EALFs for the fatigue design criterion

IRI (m/km)	Thin structure (60 km/h)							Thick structure (80 km/h)						
	Empty							Empty						
	H5-Truck					F1-Truck		H5-Truck					F1-Truck	
	axle 1	axle 2	axle 3	axle 4	axle 5	axle 1	axle 2	axle 1	axle 2	axle 3	axle 4	axle 5	axle 1	axle 2
0	0.22	0.05	0.00	0.00	0.00	0.07	0.00	0.12	0.07	0.00	0.00	0.00	0.03	0.00
1	0.25	0.07	0.00	0.00	0.00	0.09	0.00	0.14	0.09	0.00	0.00	0.00	0.04	0.00
2	0.29	0.09	0.01	0.00	0.00	0.11	0.00	0.16	0.12	0.00	0.00	0.00	0.05	0.01
3	0.34	0.12	0.01	0.00	0.00	0.13	0.01	0.18	0.16	0.01	0.00	0.00	0.06	0.01
4	0.38	0.15	0.01	0.01	0.00	0.15	0.01	0.21	0.20	0.01	0.00	0.00	0.07	0.01
5	0.44	0.19	0.02	0.01	0.01	0.19	0.01	0.24	0.26	0.01	0.01	0.00	0.09	0.02
IRI (m/km)	Underloaded by 20%							Underloaded by 20%						
	H5-Truck					F1-Truck		H5-Truck					F1-Truck	
	axle 1	axle 2	axle 3	axle 4	axle 5	axle 1	axle 2	axle 1	axle 2	axle 3	axle 4	axle 5	axle 1	axle 2
0	0.84	1.74	0.98	0.69	0.49	1.61	1.03	0.45	2.21	0.49	0.35	0.25	0.75	1.36
1	0.94	2.02	1.13	0.81	0.58	1.81	1.17	0.51	2.56	0.56	0.41	0.29	0.84	1.56
2	1.05	2.33	1.29	0.95	0.67	2.02	1.34	0.57	2.94	0.64	0.48	0.34	0.94	1.77
3	1.17	2.68	1.48	1.10	0.78	2.25	1.52	0.63	3.38	0.74	0.56	0.39	1.05	2.01
4	1.30	3.07	1.69	1.27	0.90	2.50	1.72	0.70	3.86	0.84	0.64	0.45	1.17	2.27
5	1.44	3.50	1.92	1.46	1.04	2.77	1.94	0.78	4.40	0.95	0.74	0.52	1.29	2.56
IRI (m/km)	Fully loaded							Fully loaded						
	H5-Truck					F1-Truck		H5-Truck					F1-Truck	
	axle 1	axle 2	axle 3	axle 4	axle 5	axle 1	axle 2	axle 1	axle 2	axle 3	axle 4	axle 5	axle 1	axle 2
0	1.38	4.80	3.74	2.81	2.09	3.82	3.64	0.75	6.01	1.84	1.41	1.04	1.78	4.79
1	1.53	5.42	4.17	3.17	2.35	4.20	4.04	0.83	6.77	2.05	1.58	1.17	1.96	5.31
2	1.69	6.10	4.64	3.56	2.64	4.61	4.48	0.91	7.60	2.28	1.78	1.31	2.15	5.88
3	1.87	6.84	5.15	3.99	2.96	5.05	4.95	1.01	8.52	2.53	1.99	1.47	2.35	6.49
4	2.06	7.66	5.71	4.46	3.31	5.53	5.46	1.11	9.53	2.80	2.22	1.64	2.57	7.15
5	2.26	8.55	6.32	4.97	3.68	6.04	6.01	1.22	10.62	3.09	2.47	1.83	2.81	7.87
IRI (m/km)	Overloaded by 10%							Overloaded by 10%						
	H5-Truck					F1-Truck		H5-Truck					F1-Truck	
	axle 1	axle 2	axle 3	axle 4	axle 5	axle 1	axle 2	axle 1	axle 2	axle 3	axle 4	axle 5	axle 1	axle 2
0	1.74	7.45	6.52	5.00	3.77	5.59	6.19	0.94	9.27	3.19	2.49	1.87	2.60	8.10
1	1.92	8.32	7.19	5.56	4.19	6.11	6.80	1.04	10.34	3.52	2.76	2.07	2.84	8.89
2	2.11	9.27	7.92	6.17	4.65	6.66	7.45	1.14	11.51	3.87	3.06	2.30	3.10	9.75
3	2.32	10.31	8.70	6.84	5.15	7.25	8.16	1.25	12.78	4.25	3.39	2.54	3.37	10.66
4	2.55	11.44	9.55	7.56	5.69	7.88	8.92	1.37	14.17	4.66	3.74	2.80	3.67	11.65
5	2.79	12.67	10.46	8.34	6.27	8.56	9.73	1.50	15.67	5.10	4.12	3.09	3.98	12.70

Table 6.7 – Theoretical EALFs for the rutting design criterion

IRI (m/km)	Thin structure (60 km/h)							Thick structure (80 km/h)						
	Empty							Empty						
	H5-Truck					F1-Truck		H5-Truck					F1-Truck	
	axle 1	axle 2	axle 3	axle 4	axle 5	axle 1	axle 2	axle 1	axle 2	axle 3	axle 4	axle 5	axle 1	axle 2
0	0.19	0.09	0.00	0.00	0.00	0.07	0.01	0.15	0.13	0.00	0.00	0.00	0.05	0.01
1	0.22	0.12	0.01	0.00	0.00	0.08	0.01	0.16	0.16	0.01	0.00	0.00	0.06	0.01
2	0.24	0.14	0.01	0.01	0.00	0.09	0.01	0.18	0.20	0.01	0.01	0.00	0.07	0.02
3	0.27	0.18	0.01	0.01	0.00	0.11	0.02	0.21	0.25	0.01	0.01	0.00	0.08	0.03
4	0.30	0.22	0.02	0.01	0.01	0.12	0.03	0.23	0.30	0.02	0.01	0.01	0.09	0.04
5	0.33	0.26	0.02	0.01	0.01	0.14	0.03	0.25	0.36	0.02	0.01	0.01	0.11	0.05

IRI (m/km)	Underloaded by 20%							Underloaded by 20%						
	H5-Truck					F1-Truck		H5-Truck					F1-Truck	
	axle 1	axle 2	axle 3	axle 4	axle 5	axle 1	axle 2	axle 1	axle 2	axle 3	axle 4	axle 5	axle 1	axle 2
0	0.56	1.53	0.55	0.42	0.32	0.80	1.07	0.43	2.02	0.44	0.34	0.26	0.61	1.41
1	0.61	1.72	0.62	0.47	0.36	0.88	1.20	0.47	2.27	0.49	0.39	0.29	0.66	1.57
2	0.67	1.93	0.69	0.54	0.41	0.96	1.33	0.51	2.54	0.55	0.43	0.33	0.73	1.74
3	0.73	2.16	0.77	0.60	0.46	1.04	1.47	0.56	2.84	0.61	0.49	0.37	0.79	1.92
4	0.80	2.41	0.85	0.68	0.52	1.13	1.62	0.60	3.16	0.68	0.55	0.41	0.86	2.12
5	0.87	2.68	0.95	0.76	0.58	1.23	1.79	0.66	3.51	0.75	0.61	0.46	0.93	2.33
IRI (m/km)	Fully loaded							Fully loaded						
	H5-Truck					F1-Truck		H5-Truck					F1-Truck	
	axle 1	axle 2	axle 3	axle 4	axle 5	axle 1	axle 2	axle 1	axle 2	axle 3	axle 4	axle 5	axle 1	axle 2
0	0.84	3.45	1.61	1.28	1.01	1.59	2.96	0.63	4.50	1.27	1.02	0.80	1.21	3.84
1	0.91	3.80	1.76	1.41	1.11	1.72	3.21	0.69	4.95	1.38	1.13	0.88	1.30	4.17
2	0.98	4.18	1.91	1.55	1.22	1.85	3.49	0.75	5.43	1.51	1.23	0.97	1.40	4.53
3	1.07	4.58	2.08	1.70	1.34	1.99	3.78	0.81	5.95	1.64	1.35	1.06	1.51	4.90
4	1.15	5.01	2.26	1.85	1.46	2.14	4.09	0.87	6.51	1.78	1.48	1.16	1.62	5.30
5	1.24	5.47	2.45	2.02	1.59	2.30	4.41	0.94	7.10	1.92	1.61	1.26	1.74	5.72
IRI (m/km)	Overloaded by 10%							Overloaded by 10%						
	H5-Truck					F1-Truck		H5-Truck					F1-Truck	
	axle 1	axle 2	axle 3	axle 4	axle 5	axle 1	axle 2	axle 1	axle 2	axle 3	axle 4	axle 5	axle 1	axle 2
0	1.01	4.90	2.51	2.03	1.62	2.16	4.52	0.76	6.37	1.97	1.61	1.28	1.64	5.85
1	1.09	5.35	2.72	2.21	1.76	2.32	4.87	0.83	6.95	2.13	1.76	1.40	1.75	6.31
2	1.18	5.84	2.93	2.40	1.92	2.49	5.24	0.89	7.57	2.30	1.91	1.52	1.88	6.79
3	1.27	6.36	3.17	2.61	2.08	2.66	5.64	0.96	8.23	2.48	2.07	1.64	2.01	7.29
4	1.37	6.91	3.41	2.83	2.25	2.85	6.05	1.04	8.94	2.67	2.24	1.78	2.15	7.83
5	1.47	7.50	3.67	3.06	2.43	3.04	6.49	1.11	9.69	2.87	2.42	1.92	2.30	8.39

Afterwards, the expected number of ESAL applications is calculated by multiplying the EALFs by the number of passes of each truck (Table 6.8). Lastly, the AFs of the mixed truck traffic flow are calculated by dividing the total number of expected ESAL applications by the total number of trucks, and the pavement damage values are calculated by dividing the expected number of ESAL applications by the allowable number of ESAL applications (defined in Table 5.19). Table 6.9 presents the AFs of the mixed truck traffic flow and Table 6.10 presents the pavement damage values at the end of the pavement design period (20 years).

Table 6.8 – Number of truck passes

		Empty	Underloaded by 20%	Fully loaded	Overloaded by 10%	Total number of trucks
Thin structure	H5-Truck	39,231	68,654	68,654	19,615	980,769
	F1-Truck	156,923	274,615	274,615	78,461	
Thick structure	H5-Truck	2,703,472	4,731,077	4,731,077	1,351,736	19,310,517
	F1-Truck	1,158,631	2,027,604	2,027,604	579,316	

Table 6.9 – AFs of the mixed truck traffic flow for Level 1 - Study approach

IRI (m/km)	Thin structure		Thick structure	
	Fatigue damage	Rutting damage	Fatigue damage	Rutting damage
0	5.7	3.4	6.1	4.7
1	6.3	3.7	6.9	5.2
2	7.0	4.1	7.7	5.7
3	7.8	4.4	8.6	6.2
4	8.6	4.8	9.6	6.8
5	9.5	5.2	10.7	7.4
MACOPAV	2		5.5	

Table 6.10 – Pavement damage for Level 1 - Study approach

IRI (m/km)	Thin structure		Thick structure	
	Fatigue damage	Rutting damage	Fatigue damage	Rutting damage
0	1.58	1.40	0.40	0.34
1	1.76	1.53	0.45	0.37
2	1.96	1.67	0.50	0.41
3	2.17	1.82	0.56	0.45
4	2.41	1.98	0.62	0.49
5	2.66	2.15	0.69	0.53

6.3.3 Level 2 – Study approach (AFs of the trucks)

The AFs of trucks were predicted using equation (5.4) with the regression coefficients of Table 5.21 and Table 5.22 for the thin and thick structure, respectively.

Table 6.10 and Table 6.11 present the resulting AFs for the thin structure, respectively for the fatigue design criterion and for the rutting design criterion. Table 6.12 and Table 6.13 present the same but for the thick structure.

Table 6.11 – Fatigue AFs for the thin structure

IRI (m/km)	H5-Truck				F1-Truck			
	Empty	Underloaded by 20%	Fully loaded	Overloaded by 10%	Empty	Underloaded by 20%	Fully loaded	Overloaded by 10%
0	1.10	6.90	15.61	23.48	0.52	3.54	7.72	11.39
1	1.22	7.64	17.27	25.97	0.55	3.79	8.26	12.19
2	1.33	8.37	18.93	28.46	0.59	4.04	8.80	12.99
3	1.45	9.10	20.58	30.95	0.62	4.29	9.34	13.79
4	1.57	9.83	22.24	33.44	0.66	4.53	9.88	14.59
5	1.68	10.57	23.89	35.93	0.70	4.78	10.42	15.38

Table 6.12 –Rutting AFs for the thin structure

IRI (m/km)	H5-Truck				F1-Truck			
	Empty	Underloaded by 20%	Fully loaded	Overloaded by 10%	Empty	Underloaded by 20%	Fully loaded	Overloaded by 10%
0	0.85	4.08	8.18	11.58	0.42	2.30	4.58	6.46
1	0.93	4.45	8.93	12.64	0.45	2.46	4.89	6.90
2	1.01	4.82	9.67	13.70	0.48	2.62	5.20	7.34
3	1.09	5.19	10.42	14.76	0.51	2.77	5.51	7.78
4	1.16	5.57	11.17	15.81	0.53	2.93	5.83	8.22
5	1.24	5.94	11.91	16.87	0.56	3.09	6.14	8.66

Table 6.13 – Fatigue AFs for the thick structure

IRI (m/km)	H5-Truck				F1-Truck			
	Empty	Underloaded by 20%	Fully loaded	Overloaded by 10%	Empty	Underloaded by 20%	Fully loaded	Overloaded by 10%
0	0.67	4.43	10.27	15.63	0.36	2.79	6.36	9.60
1	0.77	5.07	11.74	17.86	0.39	3.03	6.92	10.44
2	0.86	5.70	13.20	20.10	0.43	3.28	7.47	11.28
3	0.96	6.33	14.67	22.33	0.46	3.52	8.03	12.12
4	1.05	6.97	16.14	24.56	0.49	3.76	8.58	12.96
5	1.15	7.60	17.61	26.79	0.52	4.01	9.14	13.80

Table 6.14 – Rutting AFs for the thick structure

IRI (m/km)	H5-Truck				F1-Truck			
	Empty	Underloaded by 20%	Fully loaded	Overloaded by 10%	Empty	Underloaded by 20%	Fully loaded	Overloaded by 10%
0	0.84	3.90	7.70	10.82	0.42	2.40	4.84	6.88
1	0.93	4.31	8.51	11.96	0.45	2.58	5.21	7.41
2	1.02	4.72	9.32	13.09	0.49	2.76	5.58	7.93
3	1.11	5.13	10.13	14.23	0.52	2.95	5.95	8.46
4	1.20	5.54	10.94	15.37	0.55	3.13	6.32	8.98
5	1.29	5.95	11.75	16.50	0.58	3.31	6.69	9.51

Knowing the AFs of the trucks, the expected number of ESAL applications during the pavement design period is calculated by multiplying these AFs by the number of passes of each truck (defined in Table 6.8). Then, the AFs of the mixed truck traffic flow and the pavement damage values are calculated as in the previous level. Table 6.15 presents the AFs of the mixed truck traffic flow and Table 6.16 presents the pavement damage values at the end of the pavement design period (20 years).

Table 6.15 – AFs of the mixed truck traffic flow for Level 2 - Study approach

IRI (m/km)	Thin structure		Thick structure	
	Fatigue damage	Rutting damage	Fatigue damage	Rutting damage
0	6.2	3.6	6.1	4.7
1	6.7	3.9	6.9	5.2
2	7.3	4.2	7.7	5.6
3	7.8	4.5	8.4	6.1
4	8.3	4.7	9.2	6.6
5	8.8	5.0	10.0	7.0
MACOPAV	2		5.5	

Table 6.16 - Pavement damage for Level 2 - Study approach

IRI (m/km)	Thin structure		Thick structure	
	Fatigue damage	Rutting damage	Fatigue damage	Rutting damage
0	1.75	1.50	0.39	0.34
1	1.89	1.61	0.44	0.37
2	2.04	1.72	0.50	0.40
3	2.18	1.84	0.55	0.44
4	2.32	1.95	0.60	0.47
5	2.47	2.06	0.65	0.50

6.3.4 Level 3 – Study approach ('Damage' application)

This level uses the developed application for the calculation of both the AFs of the mixed truck traffic flow and the pavement damage values. Figure 5.38 showed (page 169) the interface of the 'Damage' application. The results presented in Figure 5.38 are for the thin structure when the initial IRI-value is 0 m/km. The other results are presented in Table 6.15.

Table 6.17 – AFs of the mixed truck traffic flow for Level 3 - Study approach

IRI (m/km)	Thin structure		Thick structure	
	Fatigue damage	Rutting damage	Fatigue damage	Rutting damage
0	5.8	3.5	5.6	4.5
1	6.2	3.8	6.4	5.0
2	6.8	4.1	7.2	5.5
3	7.5	4.4	8.1	6.0
4	8.3	4.7	9.1	6.6
5	9.1	5.1	10.2	7.3
MACOPAV	2		5.5	

Table 6.18 – Pavement damage for Level 3 - Study approach

IRI (m/km)	Thin structure		Thick structure	
	Fatigue damage	Rutting damage	Fatigue damage	Rutting damage
0	1.61	1.43	0.37	0.32
1	1.74	1.55	0.41	0.36
2	1.91	1.67	0.47	0.39
3	2.11	1.81	0.53	0.43
4	2.32	1.95	0.59	0.48
5	2.54	2.11	0.66	0.52

6.3.5 Comparison

From the application of the three levels of the study approach, it is possible to realise the flexibility of each one. The level (1) is the most flexible. It can be applied to any pavement structure and can consider any design criterion. However, it is the level that requires more calculations from the pavement designers. On the other hand, the level (3) is least flexible. It can only be applied to pavement structures considered in the 'Damage' application. However, the pavement damage estimation is automatic.

The AFs of the mixed truck traffic flow considered are in almost all cases higher than the MACOPAV ones. Only the rutting AF of the mixed truck traffic flow running over the even surface of the thick structure (IRI equal to 0 m/km) is slightly lower than the corresponding MACOPAV one. When the IRI of the pavement surface increases in 1 m/km, there is an increase of about 10% in the AF of the mixed truck traffic flow.

Just to have an average insight of what happen when a pavement with an expectable initial IRI of 2 m/km and just for the fatigue damage once the MACOPAV's AF were established for this damage condition, it can be said, only taking into account the vehicles' suspension excitation, that the AF for the thin structure is currently underestimated in about 240% and for the thick structure in about 30%. This is for the Level 3 approach.

As the variations in the pavement damage values are equal to the variations in the AFs, henceforward only pavement damage values will be presented.

Figure 6.3 depicts the pavement damage results from the three levels of the study approach when applied to the same pavement structures and design criteria.

As seen, there is a good agreement between the three levels. Therefore, if the level (3) is extended to a broader number of situations, it can be easily used by the pavement designers. Otherwise, the lowest level is used.

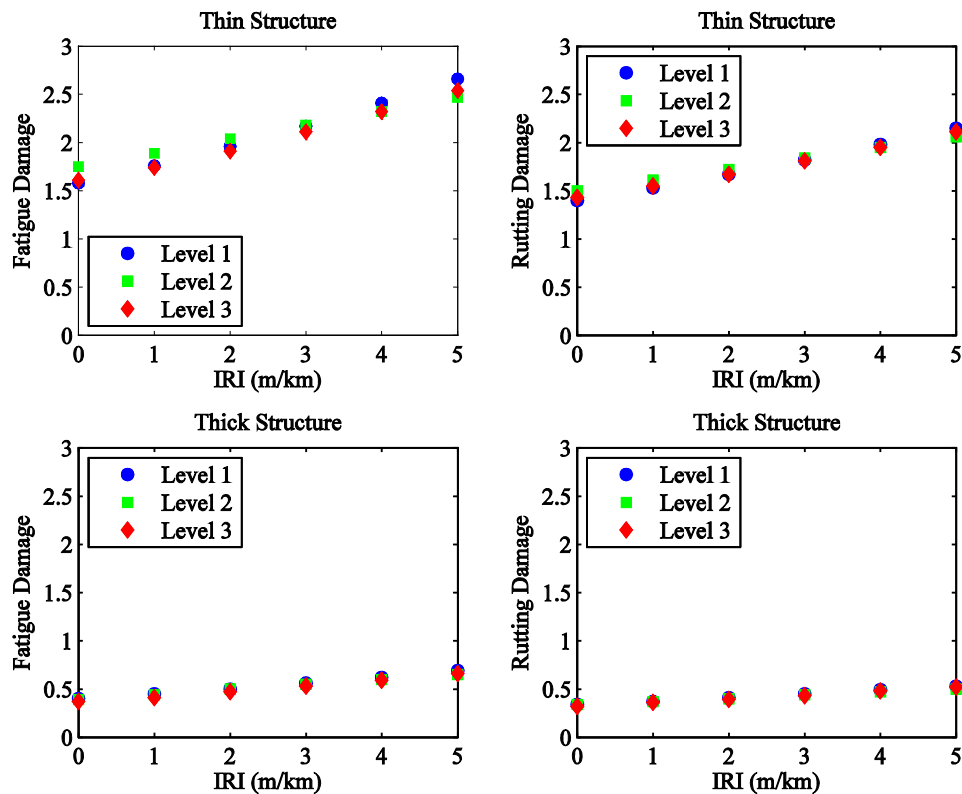


Figure 6.3 – Comparison of the results from the three levels of the hierarchical study approach

6.4 PAVEMENT DAMAGE CALCULATION USING THE ‘DAMAGE’ APPLICATION

6.4.1 Introduction

In this section, only the level (3) of the study approach is used (‘Damage’ application). It is going to be applied to the both case studies, the ‘baseline’ case study and the ‘empty running’ case study. This level has the advantage of considering the degradation of the AC modulus and the roughness growth along the pavement design period.

6.4.2 ‘Baseline’ case study

The pavement damage is calculated for the following situations:

- Constant AC modulus and IRI-value (both equal to its initial value) during the pavement design period. Only the effect of the initial roughness on the pavement damage is quantified.
- Variable AC modulus according to each one of the three degradation models (‘Original Model’, ‘50%-Adapted Model’ and ‘25%-Adapted Model’). First, only the effect of the AC modulus degradation (without roughness) on the pavement damage is quantified. Then, both effects (the AC modulus degradation and the initial roughness) on the pavement damage are quantified.
- Roughness growth according to the prediction model of the Swedish Pavement management System (PMS). First, only the effect of roughness growth on the pavement damage is quantified. Then, this effect associated with the effect of AC modulus degradation on the pavement damage is quantified.

Effect of initial roughness on pavement damage

Figure 6.4 and Figure 6.5 show the effect of the initial IRI value on the pavement damage, respectively, for the thin and for the thick structure.

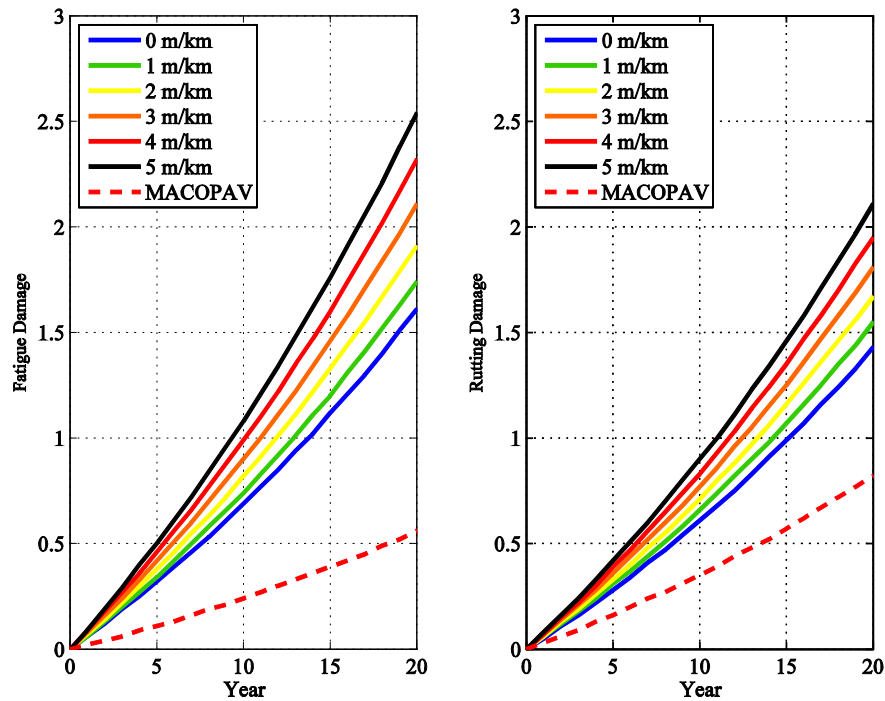


Figure 6.4 – Effect of initial roughness on the damage of the thin structure ($E=E_0$ and IRI does not grow)

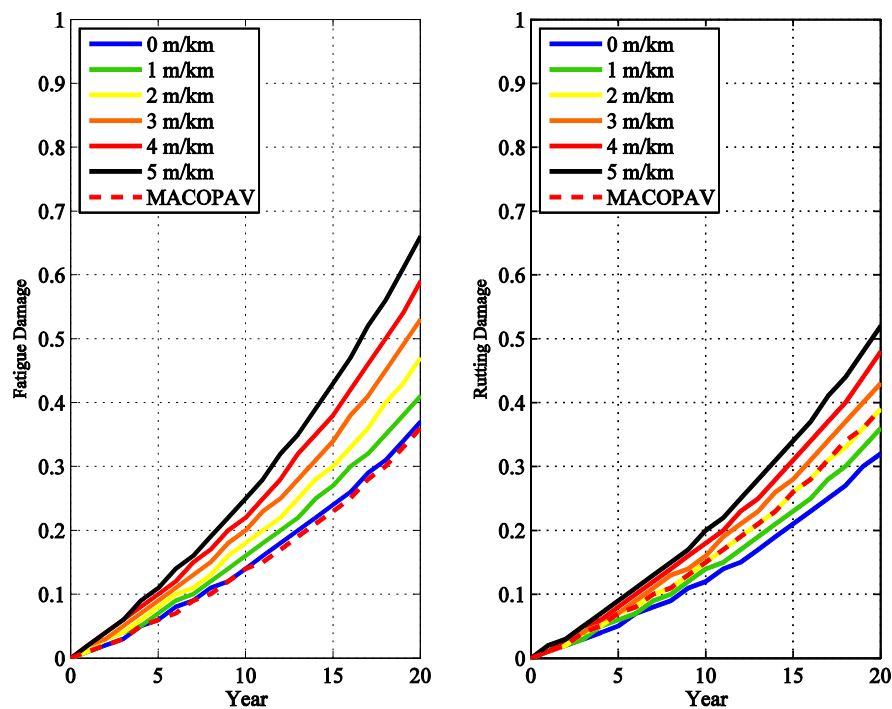


Figure 6.5 - Effect of initial roughness on the damage of the thick structure ($E=E_0$ and IRI does not grow)

As expected, the higher the initial IRI value, the higher the pavement damage is. The pavement damage (fatigue and rutting) appear to be low, only the thin structure has damage values higher

than one at the end of the pavement design period. For that reason, the pavement damage calculated considering the MACOPAV’s AFs is also illustrated. This damage also appears to be low which can be explained by the AC modulus value considered. If the MACOPAV’s AC modulus is used (4000 MPa), the pavement damage will be about one at the end of the pavement design period (see Table 5.19 and Table 5.20).

When the initial IRI-value grows from 0 to 5 m/km, the pavement damage of the thin structure increases 58% (fatigue criterion) and 48% (rutting criterion). For the thick structure the corresponding values are 81% and 63%.

The pavement damage values of the thin structure are significantly higher than those of the thick structure. This may be due to a higher aggressiveness of the mixed truck traffic flow in relation to the bearing capacity of the thin structure compared to the thick structure. However, considering only ‘F1-Trucks’ (zero per cent of ‘H5-Trucks’) in the truck traffic flow in the ‘baseline’ scenario of the thin structure, the fatigue damage is 1.34 (0 m/km) and 2.03 (5 m/km), and the rutting damage is 1.23 (0 m/km) and 1.77 (5 m/km).

Effect of AC modulus degradation on pavement damage

Figure 6.6 and Figure 6.7 show the isolated effect of the AC modulus degradation ($IRI_0 = 0$ m/km) on the pavement damage for the thin and for the thick structure, respectively. The three AC modulus degradation models were considered.

The results show that the used AC modulus degradation model influences greatly the pavement damage. Table 6.16 presents the increases in the pavement damage considering each one of the three AC modulus degradation models. These increases are in relation to situation of constant AC modulus over the pavement design period (equal to initial value) and are closely related to the corresponding AC modulus degradations shown in Figure 6.8.

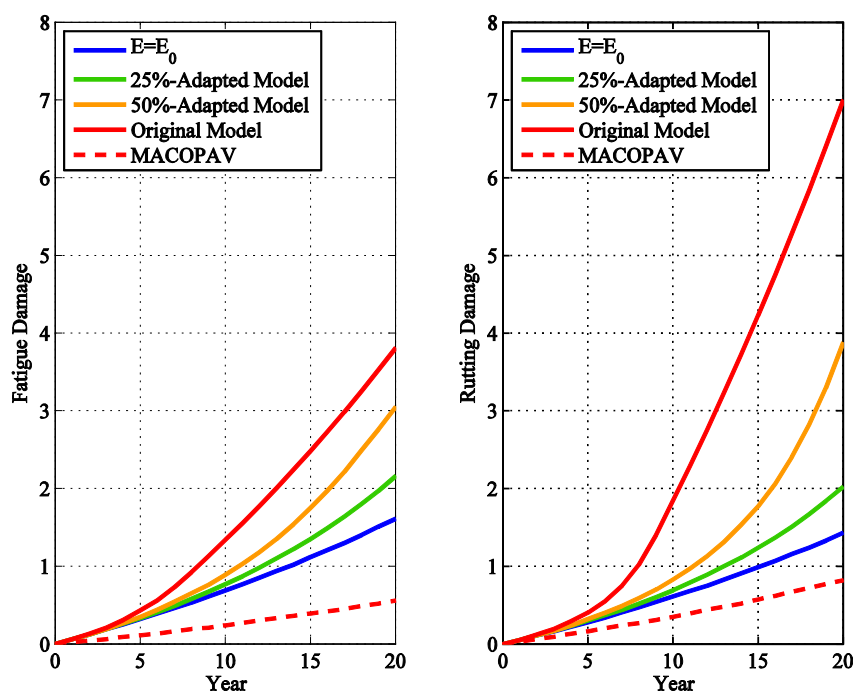


Figure 6.6 – Isolated effect of the AC modulus degradation models on the damage of thin structure ($IRI=0$ m/km)

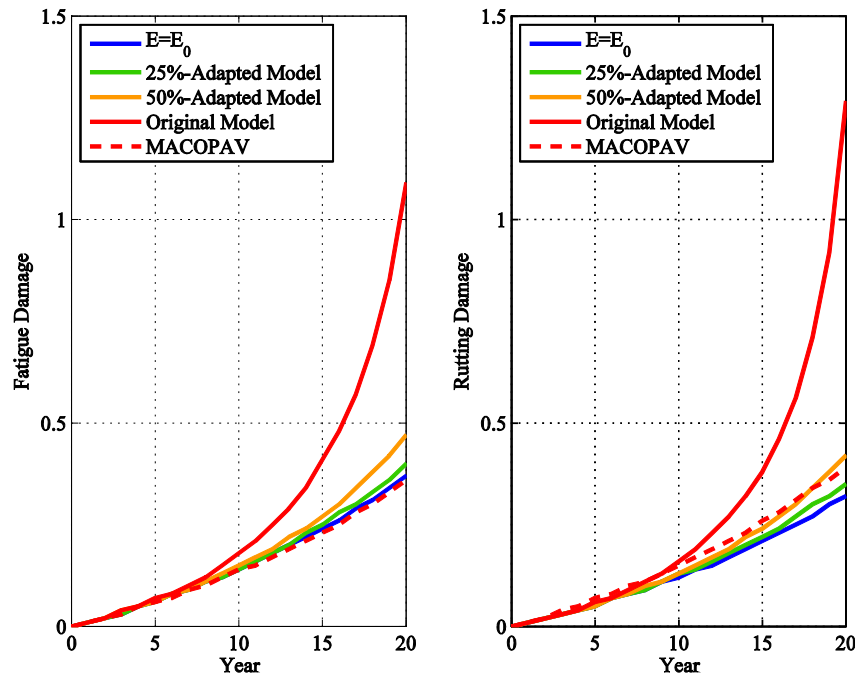


Figure 6.7 - Isolated effect of the AC modulus degradation models on the damage of the thick structure (IRI= 0 m/km)

Table 6.19 – Increases in the pavement damage with the AC modulus degradation

	Thin structure		Thick structure	
	Fatigue	Rutting	Fatigue	Rutting
25% -Adapted Model	34%	42%	9%	10%
50% -Adapted Model	89%	172%	28%	31%
Original Model	136%	391%	197%	304%

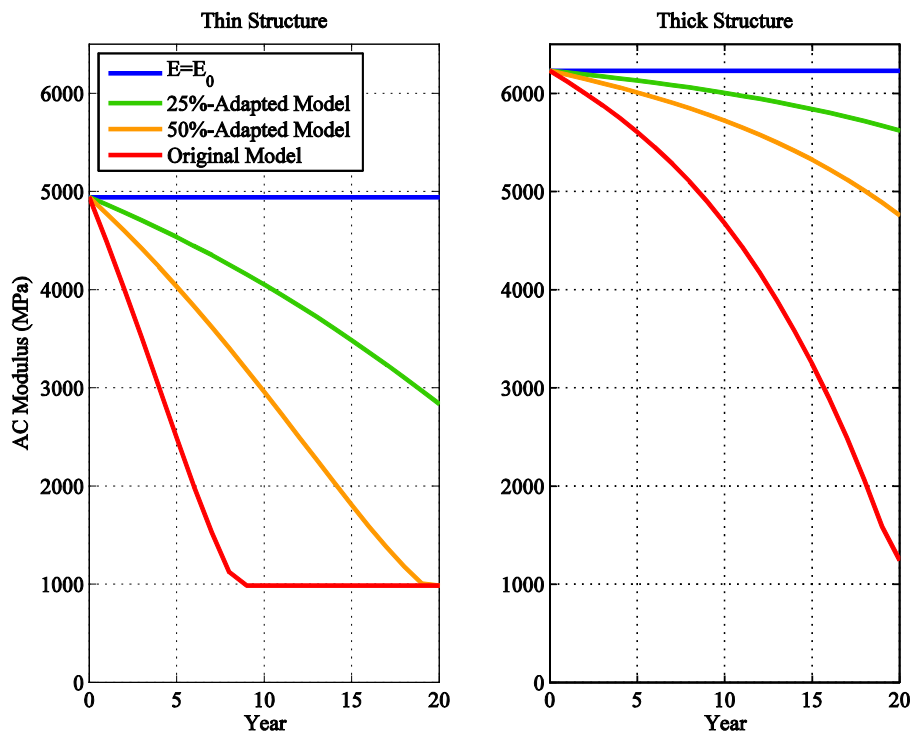


Figure 6.8 – Degradation of the AC modulus for both structures

Combined effect of both AC modulus degradation and initial roughness on pavement damage

Figure 6.9 and Figure 6.10 show the combined effect of both the AC modulus degradation models and the initial roughness on the damage of the thin structure and on the damage of the thick structure, respectively.

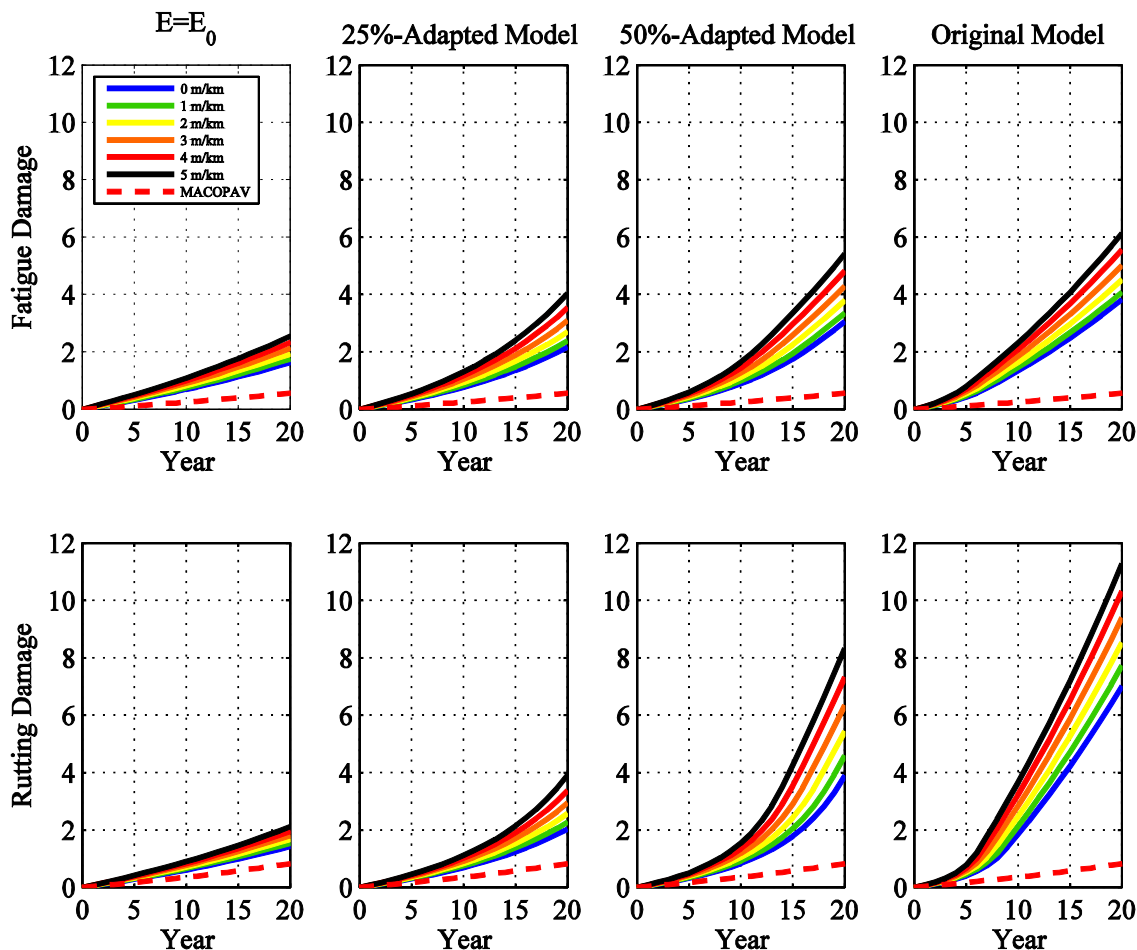


Figure 6.9 – Combined effect of both AC modulus degradation and initial roughness on the damage of the thin structure

The pavement damage, at the end of the pavement design period, increases in the ranges of Table 6.17 when initial IRI value rises from 0 to 5 m/km (in relation to constant AC modulus and equal to its initial value).

Table 6.20 – Increase ranges in the pavement damage when initial IRI value rises from 0 to 5 m/km

	Thin structure		Thick structure	
	Fatigue	Rutting	Fatigue	Rutting
25%-Adapted Model	34-59% (↑74%)	42-85% (↑103%)	9-20% (↑132%)	10-23% (↑117%)
50%-Adapted Model	89-112% (↑26%)	172-295% (↑71%)	28-72% (↑157%)	31-84% (↑173%)
Original Model	136-141% (↑3%)	391-434% (↑11%)	197-514% (↑161%)	304-1086% (↑258%)

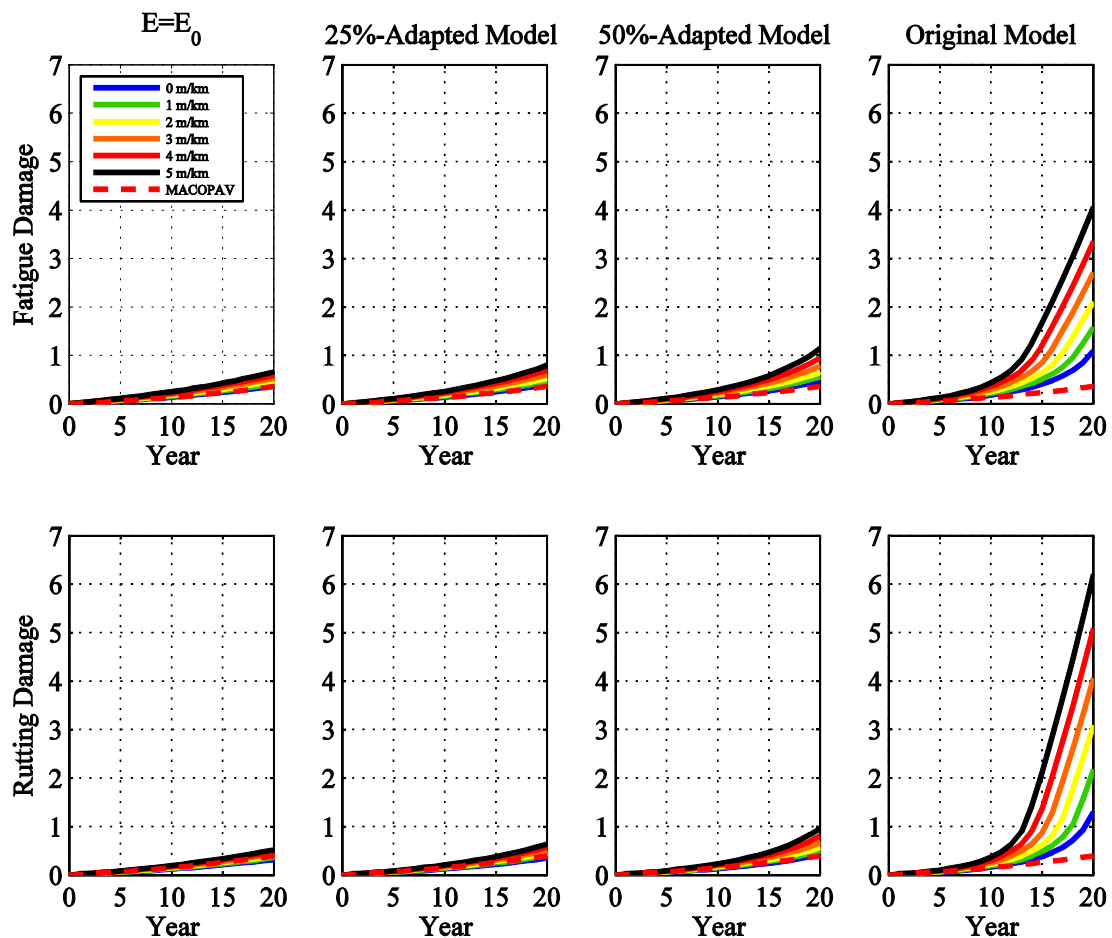


Figure 6.10 – Combined effect of both AC modulus degradation and initial roughness on the damage of the thick structure

When the combined effect of both the AC modulus degradation, over the pavement design period, and the initial IRI value of the road profile on the pavement damage is considered, the damage can increase in the range 74-132% with the ‘25%-Adapted Model’, in the range 26-173% with the ‘50%-Adapted Model’ and in the range 3-256% with the ‘Original Model’. These increase ranges are in relation to the situation of the isolated effect of the AC modulus degradation (IRI equal to 0 m/km).

For example, the range with the highest variation, referred in the previous paragraph (3-256%), may be explained by the AC modulus values, the percentage of 3% happened in the thin structure where the AC modulus achieved its critical value in the year 9 (when initial IRI value is equal to 0 m/km) and in the year 6 (when initial IRI value is equal to 5 m/km). As the critical AC modulus was achieved so early in both situations, 0 and 5 m/km, the variation in the pavement damage was only 3%. The AC modulus was the same in the majority of the pavement design period. On the other hand, the percentage of 256% happened in the thick structure where the AC modulus achieved its critical value in the year 20 (when initial IRI value is equal to 0 m/km) and in the year 14 (when initial IRI value is equal to 5 m/km), resulting a higher variation in the AC modulus values and consequently in the pavement damage.

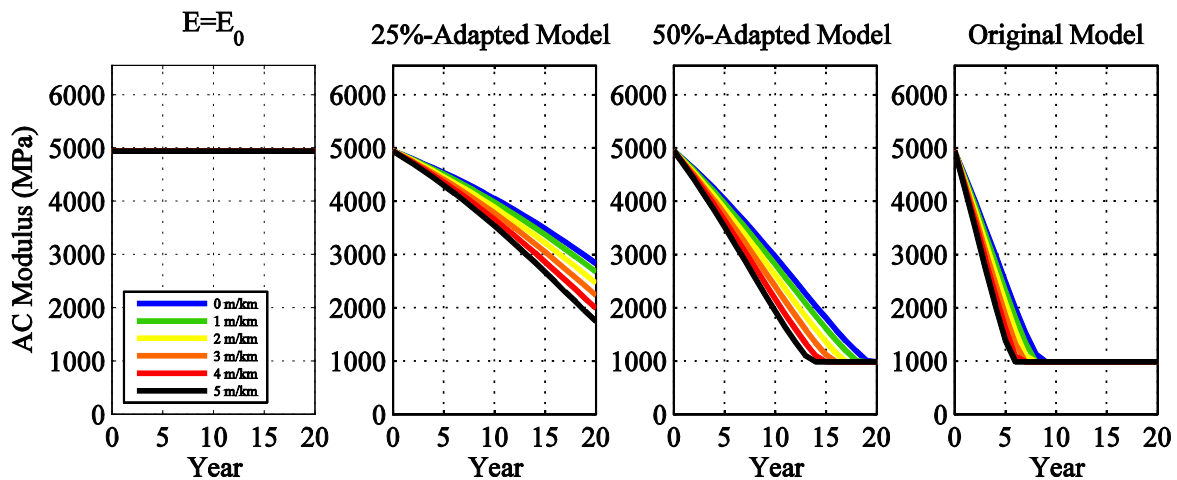


Figure 6.11 – Degradation of the AC modulus for the thin structure

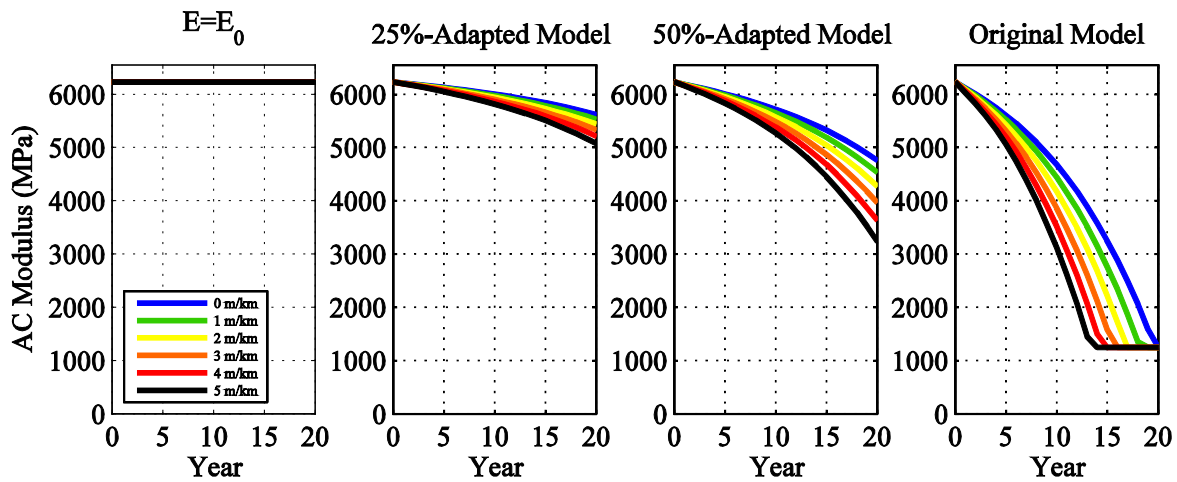


Figure 6.12 - Degradation of the AC modulus for the thick structure

Effect of roughness growth on pavement damage

Finally, Figure 6.13 and Figure 6.14 show the effect of the roughness growth, during the pavement design period, on the pavement damage for the thin and for the thick structure, respectively.

The IRI growth during the pavement design period can increase the pavement damage from 5% to 18%. The minimum percentage occurs in the rutting damage of the thick structure without AC modulus degradation while the maximum percentage occurs in rutting damage of the thick structure with AC modulus degradation according to the ‘Original Model’.

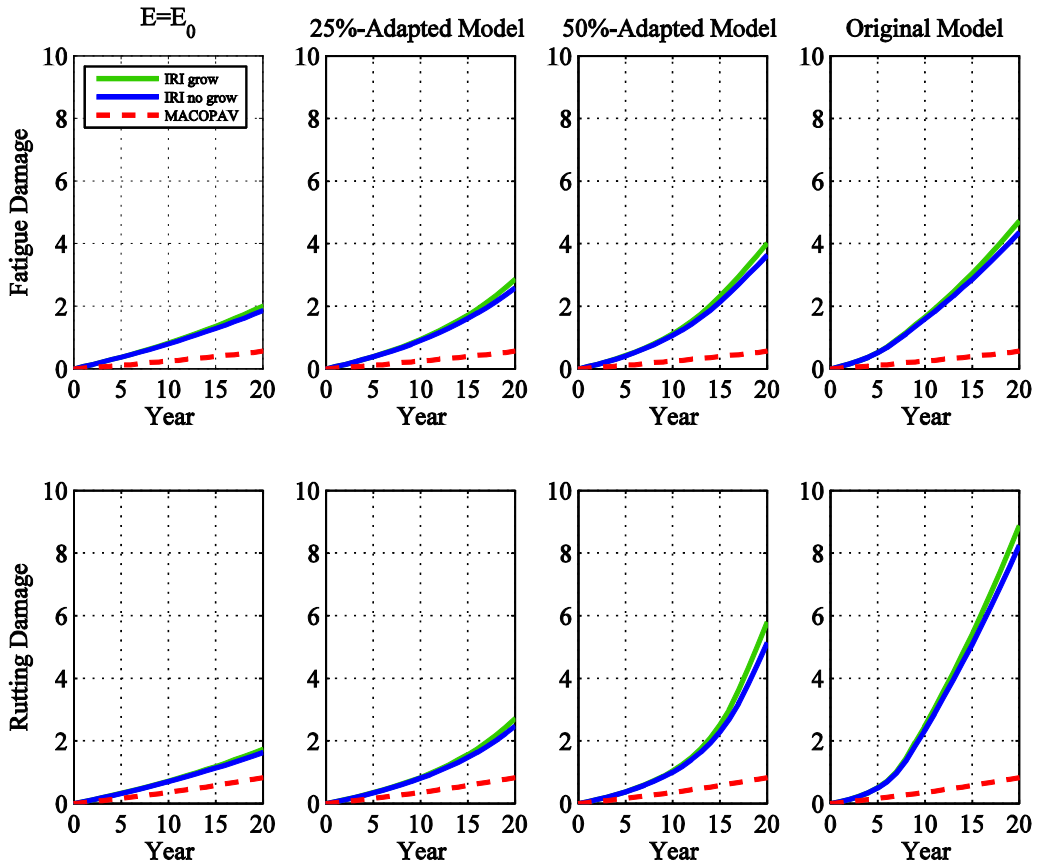


Figure 6.13 – Effect of roughness growth on the damage of the thin structure

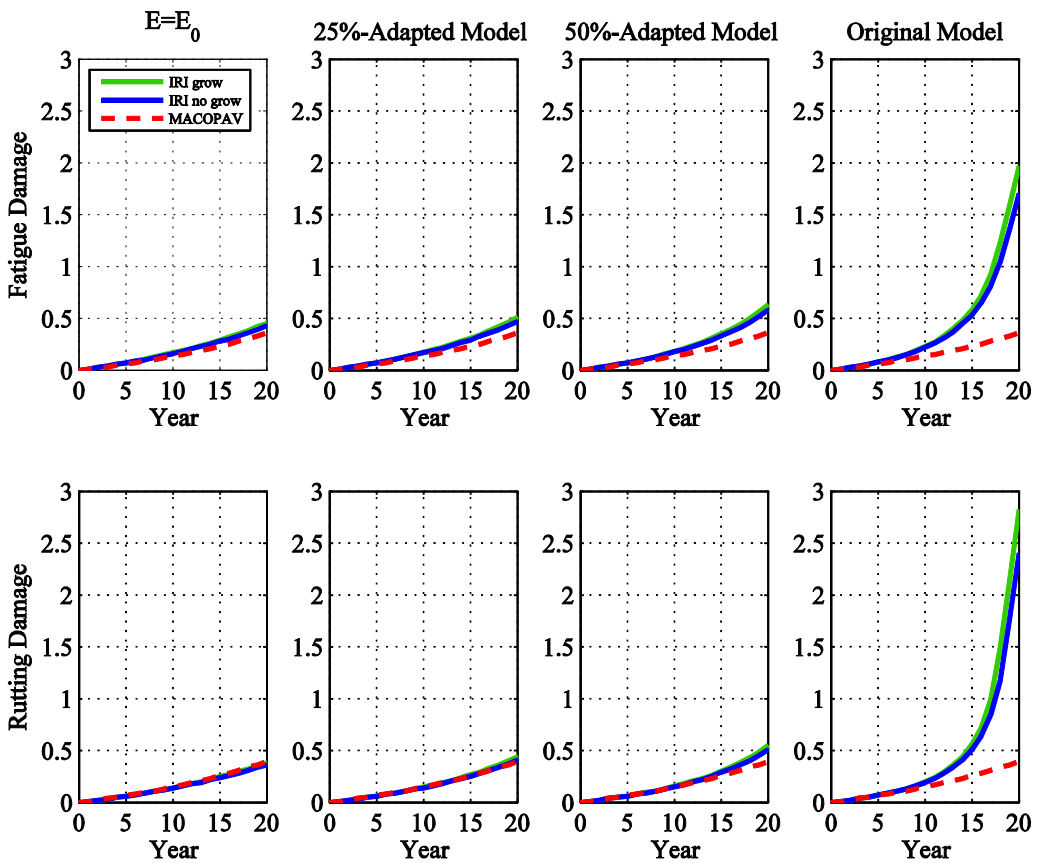


Figure 6.14 – Effect of roughness growth on the damage of the thick structure

6.4.3 'Empty running' case study

Figure 6.15 and Figure 6.16 show the effect of the reduction in the empty running percentage on the pavement damage at the end of the design period, for the thin and for the thick structure, respectively.

Based on these results, the following conclusions can be drawn:

- A reduction in the empty running percentage from 25% to 0% increases the pavement damage, at the end of its design period, by more than 26% whichever case is analysed;
- The pavement damage increases linearly with the reduction in the empty running percentage;
- When the empty running percentage reduces from 25% to 0%, the highest increase in the pavement damage of the thin structure was 66% and the highest increase in the pavement damage of the thick structure was 164%.

Ten percent of overloaded trucks were considered. However, in future, better enforcement systems to ensure compliance can cancel out overloaded trucks reducing pavement damage. In order to quantify this reduction amount, new simulations were carried out. Table 6.18 defines the new percentages as well as the new respective load factors.

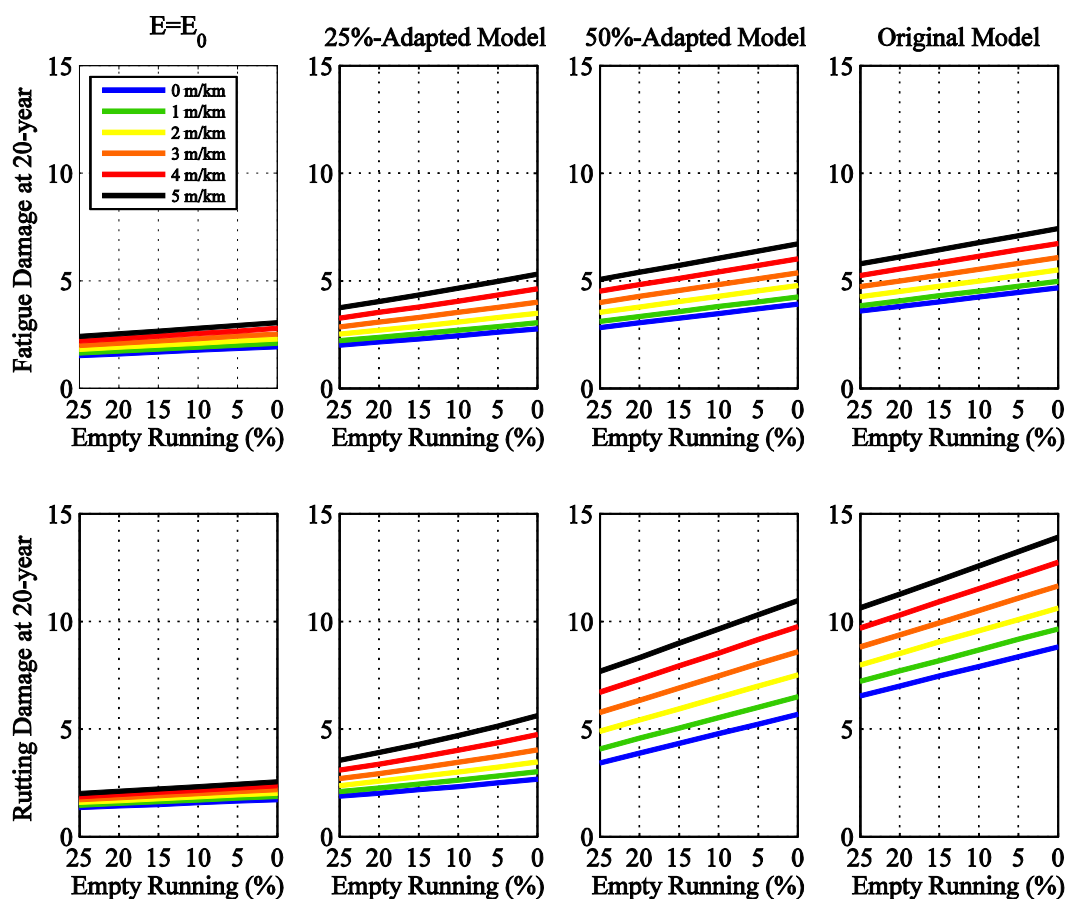


Figure 6.15 – Effect of reduction in empty running percentage on the damage of the thin structure

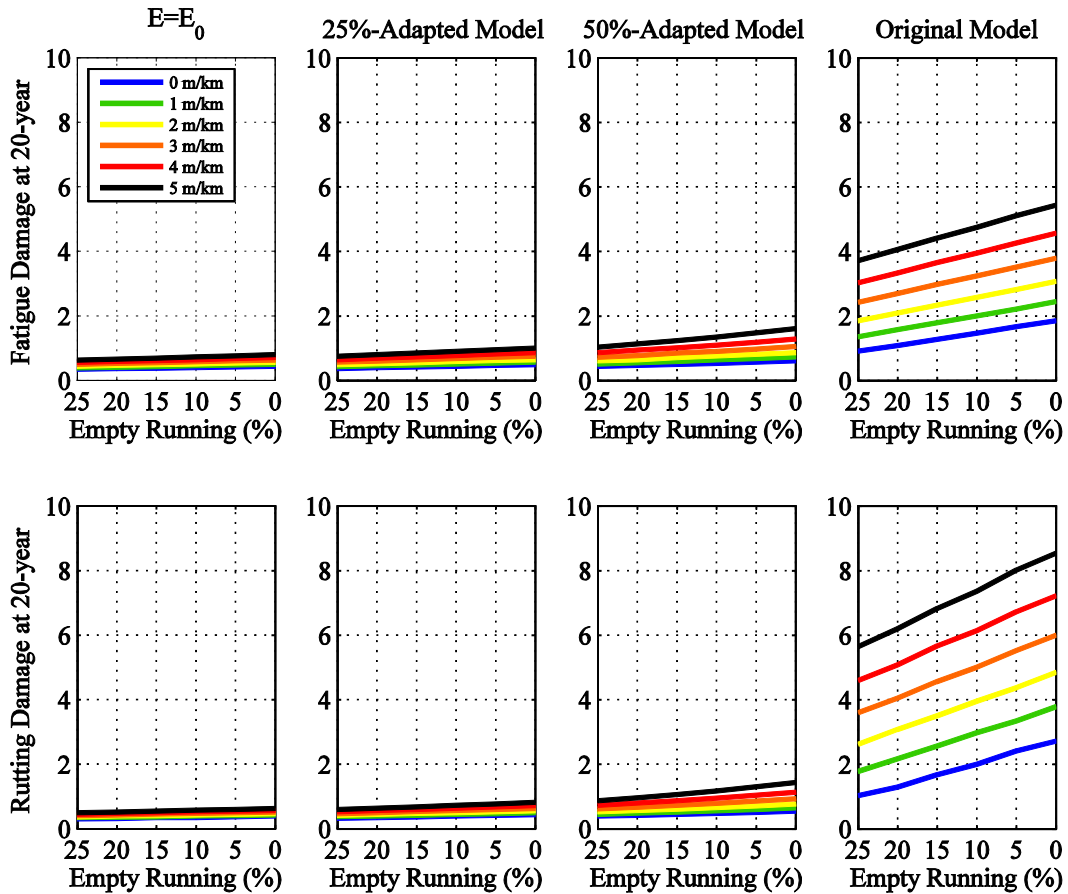


Figure 6.16 –Effect of reduction in empty running percentage on the damage of the thick structure

Table 6.21 – Definition of the empty running percentage without overloaded trucks and respective load factors

No.	Empty	Underloaded by 20%	Fully loaded	Overloaded by 10%	Thin structure's load factor	Thick structure's load factor
1	25.0%	37.5%	37.5%	0.0%	0.641	0.637
2	20.0%	40.0%	40.0%	0.0%	0.683	0.679
3	15.0%	42.5%	42.5%	0.0%	0.726	0.722
4	10.0%	45.0%	45.0%	0.0%	0.769	0.764
5	5.0%	47.5%	47.5%	0.0%	0.811	0.807
6	0.0%	50.0%	50.0%	0.0%	0.854	0.849

Figure 6.17 and Figure 6.17 present the results of those new simulations. Obviously, the pavement damage is lower when there is a reduction in the trucks' GVW. This reduction is in the range of 9-28% for the thin structure and in the range 7-49% for the thick structure.

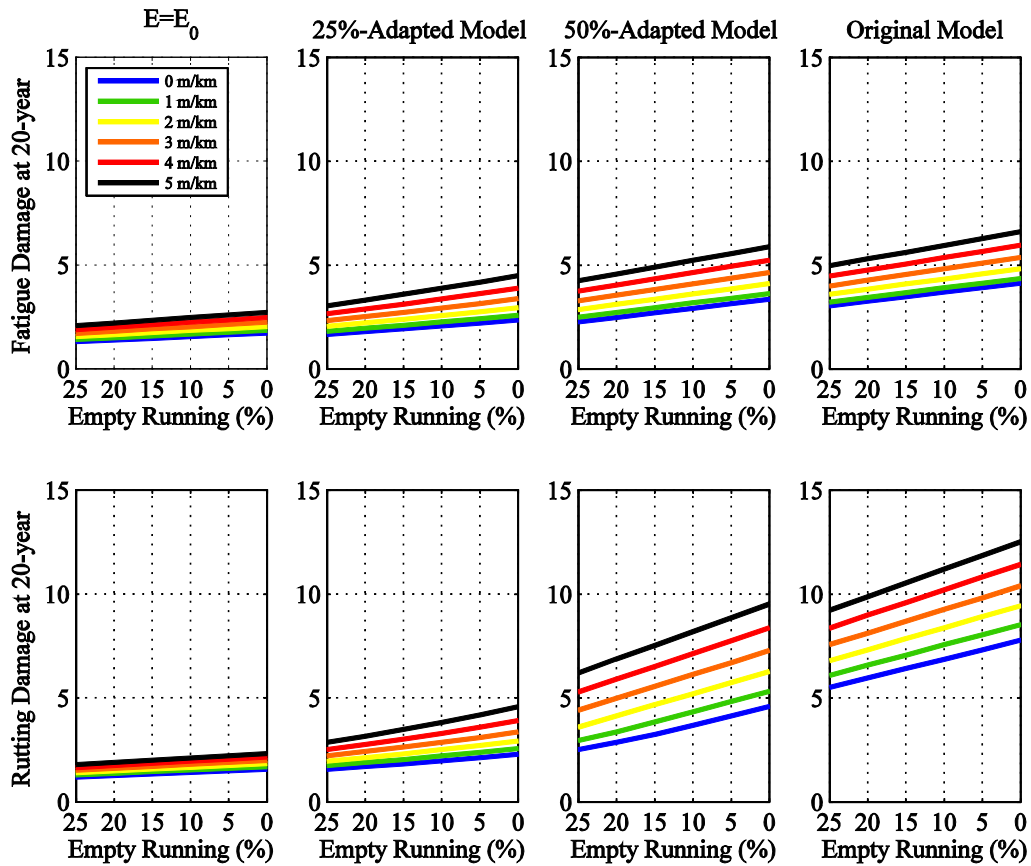


Figure 6.17 - Effect of reduction in empty running percentage on the pavement damage of the thin structure (0 % of overloaded trucks)

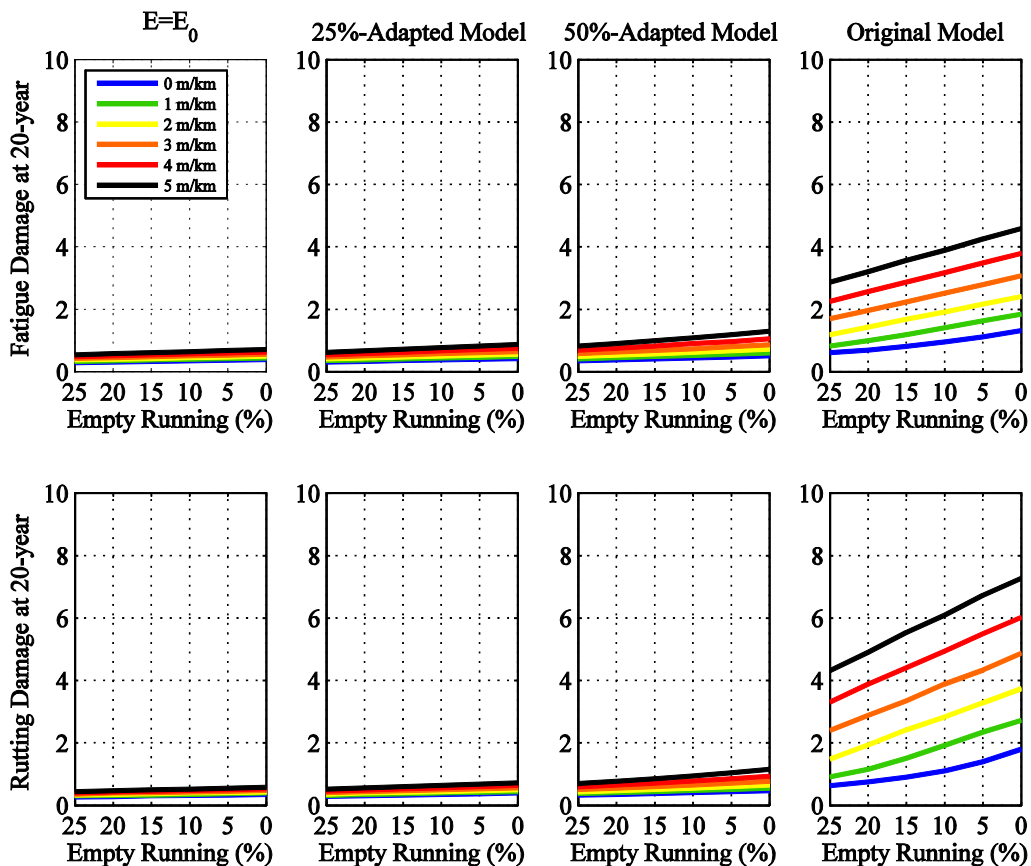


Figure 6.18 - Effect of reduction in empty running percentage on the pavement damage of the thick structure (0 % of overloaded trucks)

6.5 CONCLUDING REMARKS

This section aims to present a summary of the main results found in this chapter. Since two case studies were considered, the ‘baseline’ case study and the ‘empty running’ case study, this section encompasses two subsections, one for each of the case studies.

6.5.1 ‘Baseline’ case study

The pavement damage along the pavement design period was calculated for different situations in order to quantify (1) the effect of the initial roughness on the pavement damage, (2) the effect of the AC modulus degradation on the pavement damage and (3) the effect of the roughness growth on the pavement damage. For that, the developed application (‘Damage’ application) was used. Although it had allowed obtaining the pavement damage along the pavement design period, only the pavement damage at the end of the pavement design period is summarized here.

Figure 6.19 presents the pavement damage at the end of the pavement design period considering different initial roughness values and different AC modulus degradation models.

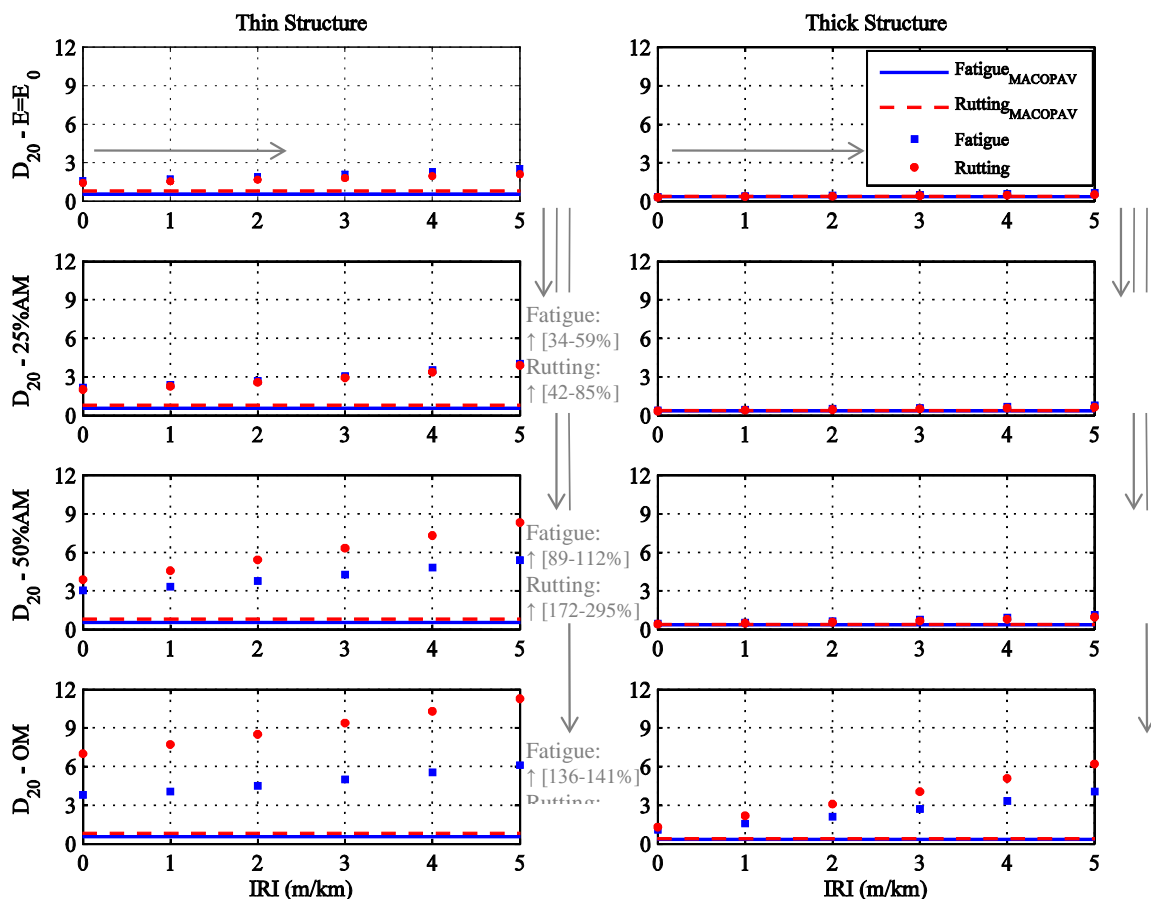


Figure 6.19 - Pavement damage at the end of the pavement design period considering the effect of different initial roughness values and different AC modulus degradation models

Figure 6.19 shows that the pavement damage at the end of the pavement design period varies linearly with the initial IRI value, whichever the AC modulus degradation model used.

In addition, the effect of the roughness growth (depicted in Figure 5.20 on page 151), during the pavement design period, on the pavement damage was quantified. Once again, only the

pavement damage at the end of the pavement design period is summarized here (see Figure 6.20).

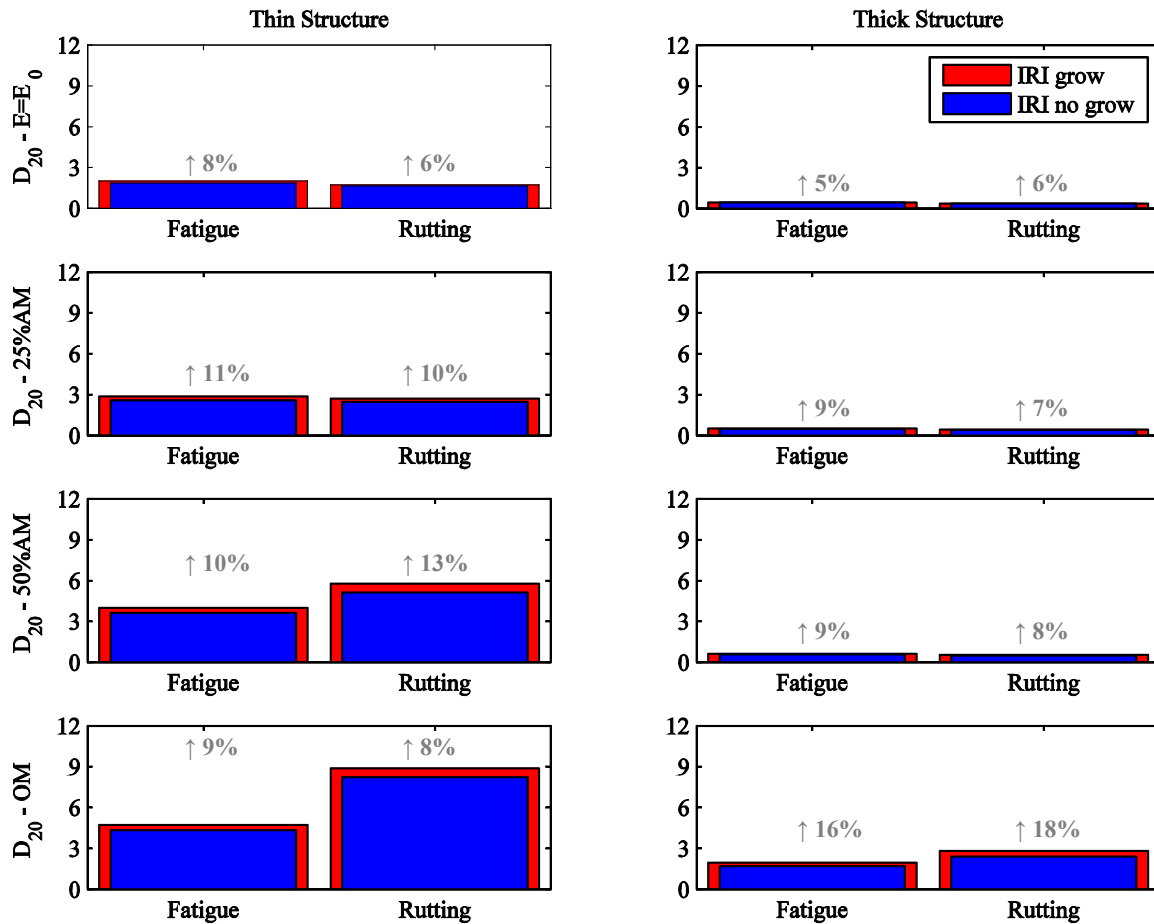


Figure 6.20 - Pavement damage at the end of the pavement design period considering the effect of roughness growth during the pavement design period

6.5.2 'Empty running' case study

In relation to the 'baseline' case study, only the pavement damage values at the end of the pavement design period for the limit situations (IRI equal to 0 and 5 m/km; empty running percentage equal to 0 and 25%) are summarized here (see Figure 6.21).

These results are for the 'empty running' case study with 10% of overloaded trucks, which is a feasible figure to represent the Portuguese reality according to some previous findings (OTEP (2004) and Lima and Quaresma (1999)).

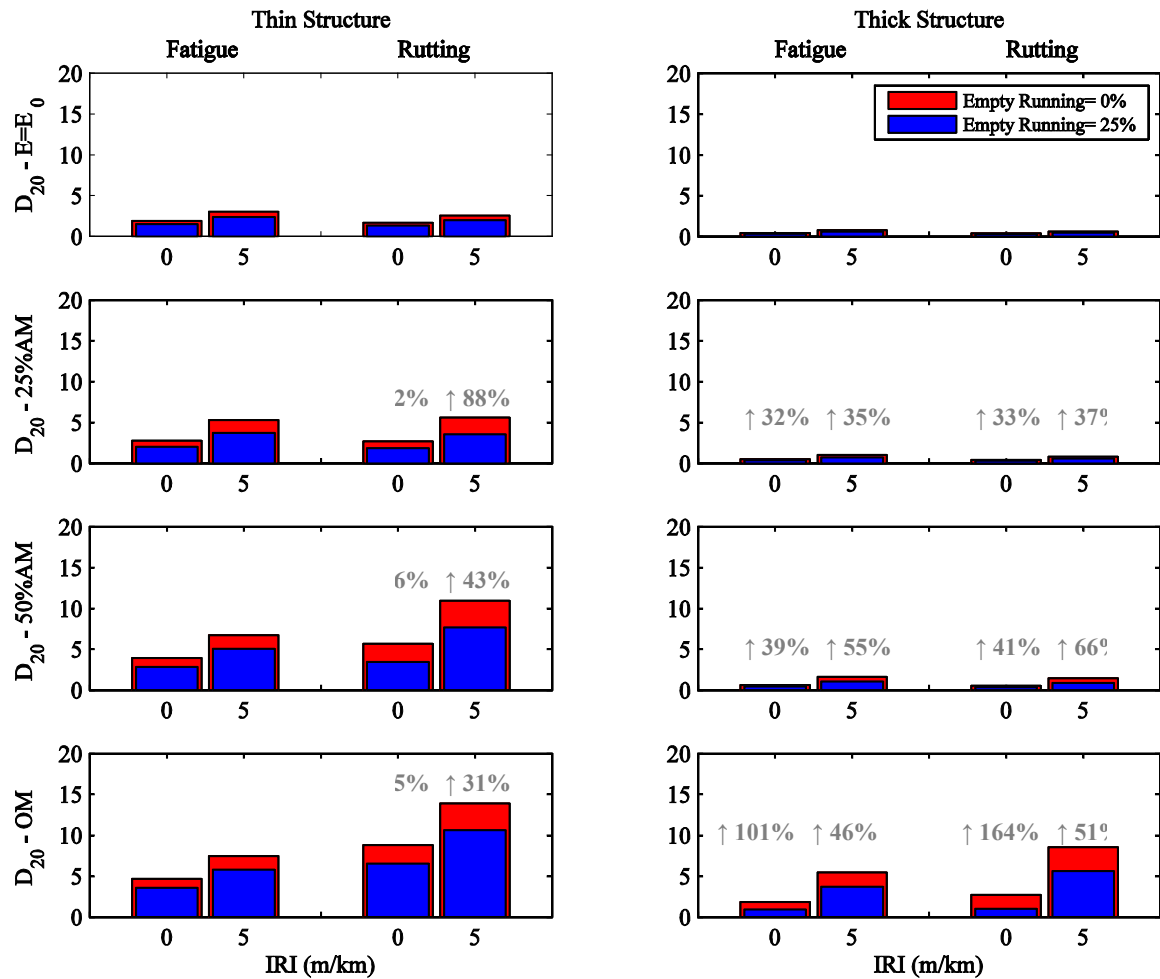


Figure 6.21 - Pavement damage at the end of the pavement design period considering the effect of reduction in empty running percentage

6.6 REFERENCES

JAE (1995). *Manual de Concepção de Pavimentos para a Rede Rodoviária Nacional (Pavement Design Manual for the Portuguese Road Network)*. JAE (Junta Autónoma de Estradas). In Portuguese.

Lima, H. and Quaresma, L. (1999). *Caracterização do factor de agressividade do tráfego de veículos pesados em Portugal (Characterization of the aggressiveness of heavy-vehicle traffic in Portugal)*. JAE (Junta Autónoma de Estradas) and LNEC (Laboratório Nacional de Engenharia Civil). Lisboa. In Portuguese.

OPEP (2004). *Estudo Piloto de Pesagem de Veículos Pesados de Mercadorias nas Fronteiras entre Portugal e Espanha (Pilot Study of Weight Measurement of heavy-goods vehicles at the borders between Portugal and Spain)*. OPEP (Observatório Transfronteiriço Espanha/Portugal). In Portuguese.

7 CONCLUSIONS AND FURTHER DEVELOPMENTS

7.1 INTRODUCTION

This thesis attempted to develop a methodological framework for Aggressiveness Factors (AFs) estimation and pavement damage calculation considering simulated axle load spectra (vehicle-pavement interaction).

In order to achieve this main objective, the following specific objectives were pursued:

- (1) 3D-implementation and validation of the Boundary Element Method (BEM) (pavement response model used);
- (2) Generation of road surface profiles for specific International Roughness Index (IRI) values;
- (3) Simulation of dynamic axle load profiles for different heavy vehicles by using a commercial software (TruckSIM[®]);
- (4) Creation of a methodological framework to calculate mechanical-empirical AFs from pavement damage along the pavement design period and this specifying the heavy traffic flow, the travel speed of the heavy vehicles, the flexible pavement structure and the initial IRI value. The methodology should also be able to consider the roughness growth and/or the degradation of the AC modulus;
- (5) Application of the methodological framework to a ‘baseline’ case study and to a case study that shows the effects of an increase of road freight transport efficiency, translated by a reduction of empty running trips, on pavement damage (‘empty running’ case study).

Once the two first specific objectives have been achieved, the methodological framework was created. It consisted essentially in the following steps:

- (a) Definition of a mixed truck traffic flow;
- (b) Calculation of AFs for the trucks of the mixed truck traffic flow;
- (c) Calculation of the AF of the mixed truck traffic flow;
- (d) Calculation of the number of Equivalent Standard Axle Load (ESAL) applications;
- (e) Calculation of the allowable number of ESAL applications;
- (f) Calculation of the pavement damage.

As some pavement designers may not have the necessary resources to apply this methodological framework, a hierarchical approach was defined to facilitate its application. It encompasses three levels, representing different levels of flexibility for the pavement designers. The three levels comprise the following

- (1) The knowledge of the axle loads for each simulated truck as a function of the initial IRI value of the road profile, the travel speed and the truck’s Gross Vehicle Weight (GVW);
- (2) The knowledge of the AFs for each simulated truck as a function of the initial IRI value of the road profile, the travel speed and the truck’s GVW. These AFs are both design criterion-specific and pavement structure-specific;

- (3) The use of an application to calculate the AFs for the mixed truck traffic flow and the pavement damage through the pavement design period.

The development of the first level implied the definition of regression models to calculate axle loads (from the simulated ones) as a function of the initial IRI value of the road profile, the travel speed and the truck's GVW. In its turn, the development of the second level implied the definition of regression models for the AFs of the trucks (from the simulated ones) as a function of the initial IRI value of the road profile and the truck's GVW. Regression coefficients were defined for each truck type, each pavement structure, each travel speed and each design criterion. Lastly, the development of the third level implied the creation of an application ('Damage' application). This application allows roughness growth and AC modulus degradation over the pavement design period.

From level (1) to (3) the pavement design becomes easier although less flexible. That is, the level (3) is the least flexible since it can only be applied to the situations considered in the development of the 'Damage' application, while the level (1) can be applied to any pavement structure and any design criterion (only the axle load spectrum is available). Notwithstanding this, however, the pavement damage estimation with the level (3) is automatic while it requires several calculations with the level (1), such as the pavement structural responses.

Two case studies were defined for applying the methodological framework, a 'baseline' case study and an 'empty running' case study.

The 'baseline' case study without changes over the pavement design period was used to show the agreement between the three levels of the study approach. Then, the third level of the approach ('Damage' application) was used for several pavement damage calculations. This level was applied to both case studies. The following effects were analysed:

- Effect of the initial IRI value of the road profile on the pavement damage;
- Effect of the AC modulus degradation over the pavement design period on the pavement damage;
- Combined effect of both the AC modulus degradation over the pavement design period and the initial IRI value of the road profile on the pavement damage;
- Effect of the IRI growth over the pavement design period on the pavement damage;
- Effect of the reduction in the empty running percentage on the pavement damage.

7.2 CONCLUSIONS

The proposed objectives were achieved successfully. A methodological framework was created in a hierarchical approach to facilitate its application. The application of the three levels of the study approach to the 'baseline' case study shows a good agreement between them. The pavement damage differences between the three levels were lower than 10%. The third level is the easiest to apply (the pavement damage estimation is automatic with it) despite being the less flexible (it can only be applied to the situations considered in the development of the 'Damage' application). However, its lack of flexibility can be overcome by extending it to a broader number of situations, allowing its widespread use by pavement designers.

In relation to the other levels, the third level has also the advantage of incorporating changes along the pavement design period such as the degradation of the AC modulus and the roughness growth. Therefore, it was used to quantify (1) the effect of the initial IRI value of the road profile

on the pavement damage, (2) the effect of the AC modulus degradation on the pavement damage and (3) the effect of the roughness growth on the pavement damage.

As expected, the higher the initial IRI value of the road profile, the higher the pavement damage is. When the initial IRI value goes from 0 to 5 m/km, the damage of the thin structure, at the end of the pavement design period, increases 58% (fatigue criterion) and 48% (rutting criterion), while the damage of the thick structure, at the same time, increases 81% (fatigue criterion) and 63% (rutting criterion) (see Figure 6.19). Even not considering the variation 0 to 5 m/km, but just an increase of 1 m/km in the IRI value, the pavement damage increases in the range 8-13%.

Just to have an average insight of what happens when a pavement with an expectable initial IRI of 2 m/km and just for the fatigue damage once the MACOPAV's AF were established for this damage condition, it can be said, only taking into account the vehicles' suspension excitation, that the AF for the thin structure is currently underestimated in about 240% and for the thick structure in about 30%. This is for the Level 3 approach.

These results underline the importance of considering the dynamic behaviour of the loads in the pavement damage.

The pavement damage values of the thin structure are significantly higher than those of the thick structure. This may be due, as already mentioned, to a higher aggressiveness of the mixed truck traffic flow in relation to the bearing capacity of the thin structure compared to the thick structure.

In order to a better understanding of the effect of the AC modulus degradation over the pavement design period on the pavement damage, three AC modulus degradation models were considered. An original model as was found in the literature ('Original Model') and two other models developed from the original one ('25%-Adapted Model' and '50%-Adapted Model'). The developed models conduct to lower degradations of the AC modulus. When the AC modulus degrades according to the 'Original Model', the pavement damage, at the end of the pavement design period, can increase in the range 136% to 391%. As expected these increases are lower when the other two models are considered (see Figure 6.19). Therefore, the amount of AC modulus degradation influences greatly the pavement damage, underlining the importance of considering the AC modulus degradation over the pavement design period in the pavement damage.

When the combined effect of both the AC modulus degradation, over the pavement design period, and the initial IRI value of the road profile on the pavement damage is considered, the damage can increase in the range 74-132% with the '25%-Adapted Model', in the range 26-173% with the '50%-Adapted Model' and in the range 3-256% with the 'Original Model' (see Table 6.17). These increase ranges are in relation to the situation of the isolated effect of the AC modulus degradation (IRI equal to 0 m/km). These ranges are closely related to the corresponding AC modulus degradations shown in Figure 6.11 and Figure 6.12 for the thin and thick structure, respectively.

The IRI growth during the pavement design period can increase the pavement damage from 5% to 18% (see Figure 6.20). The minimum percentage occurs in the rutting damage of the thick structure without AC modulus degradation while the maximum percentage occurs in rutting damage of the thick structure with AC modulus degradation according to the 'Original Model'.

A reduction in the empty running percentage from 25% to 0% increases the pavement damage at the end of the design period by more than 26%, whichever case is analysed (see Figure 6.21).

The highest increase in the pavement damage of the thin structure was 66% and the highest increase in the pavement damage of the thick structure was 164%.

The mixed truck traffic flow of the 'empty running' case study was defined considering 10% of overloaded trucks. However, since better enforcement systems to ensure compliance can cancel out the overloaded trucks reducing the pavement damage, new simulations were carried out. As expected, the pavement damage is lower when there is a reduction in the trucks' GVW. This reduction is in the range of 9-28% for the thin structure and in the range 7-49% for the thick structure.

Obviously, the presented results are closely related to both the mixed truck traffic flows and the flexible pavement structures considered in the analysis. Either the mixed truck traffic flows or the flexible pavement structures were defined to have a reasonable representation of real situations. It should be emphasized again that the two considered trucks represented 75% of the Portuguese truck traffic fleet in 2011.

However, a methodology like the developed one has the advantage of being easily extended to other trucks, to other flexible pavement structures and to other failure criteria. In addition, it has the advantage of keeping up with the road freight industry, truck industry and transport policies which have been evolving over time to achieve a compromise between greater efficiency, higher productivity and lower environmental impacts, by incorporating future trucks such as the Longer and Heavier Vehicles (LHVs) (available from the TruckSIM[®] library).

If the pavement designers have regression coefficients for both the truck configurations and the pavement structures used in Portugal or, even better, a methodology with the presented framework extended to a broader number of situations, the pavement design can be more realistic. They only need to define the mixed truck traffic flow which can be based, for example, on traffic measurements and statistical data.

To conclude, this thesis underlines the importance of a good definition for the traffic load action. This definition is currently based on AFs which are extremely influenced by the type of truck, its payload, the pavement structure and its properties, the design criterion and the roughness level of the road profile. The Portuguese pavement design procedure uses AFs that have remained unchanged since at least 1995 and subsequently they are not keeping up with road freight industry, truck industry and transport policies. It is hence crucial to have methodologies that can help pavement designers to use more current AFs (and consequently better damage estimations) mainly in a situation with limited resources.

7.3 FURTHER DEVELOPMENTS

The methodological framework was applied to two trucks and two flexible pavement structures. Therefore, it should be extended to other situations creating a database allowing the application of the third level of the hierarchical study approach over a greater range of real applications. The extension of the methodology should also consider Portugal areas with different climatic conditions and formation levels with different strengths.

This extension encompasses the following steps:

- (1) Simulation of the current trucks of the Portuguese truck traffic fleet with different payloads, different truck speeds running over surface profiles with different IRI values;

- (2) Definition of the bituminous layers moduli as a function of both the trucks speed and the Portuguese climatic area;
- (3) Definition of the formation level classes by specifying ranges for the subgrade moduli.

In terms of trucks, although the simulated trucks (the lorry/truck and the articulated vehicle) are the predominant ones in the Portuguese truck traffic fleet, their axle configurations (Figure 2.11) and load capacity ranges (Figure 2.12) can vary. For example, in 2011 the percentage of lorries/trucks with 2 axles was approximately 70%, with 3 axles was 20% and with 4 axles was 10% (see Figure 2.11). Therefore, the truck simulations should be extended to consider other axle configurations and load capacity ranges. In addition, LHVs should be simulated to analyse the impact of its use in Portugal.

The truck simulations should be validated mainly for trucks not found in the literature. Therefore, an effort would be made to include obtainable Weight-In-Motion (WIM) data.

In terms of Portuguese climatic areas, three areas are suggested: (1) a hot area, (2) a warm area, and (3) a coastal area, in line with some previous works (JAE (1995) and Picado Santos (2000)) and admitting some simplification.

In terms of the formation level classes, three classes are suggested: (1) a poor formation level with subgrade modulus lower than 80 MPa, (2) a fair formation level with subgrade modulus between 80 and 120 MPa, and (3) a very good formation level with subgrade modulus greater than 120 MPa. This will cover, for sure, all the situations for which meaningful heavy traffic should be considered.

This suggestion is only to underline that even with a catalogue of structures not so detailed, it is possible without a huge operation to cover the needs of characterization of the situations that lead to a much proper flexible pavement designs than the one that is in general followed up nowadays.

7.4 REFERENCES

JAE (1995). *Manual de Concepção de Pavimentos para a Rede Rodoviária Nacional (Pavement Design Manual for the Portuguese Road Network)*. JAE (Junta Autónoma de Estradas). In Portuguese.

Picado Santos, L. (2000). Design Temperature on Flexible Pavements: Methodology for Calculation. *International Journal of Road Materials and Pavement Design*, 1, 355-371.